Spatial Modelling of Blue Whiting Population Dynamics in the North-East Atlantic

Emma Dolmaire

September 2022

This thesis is submitted to the University of Strathclyde for the degree of
Doctor of Philosophy in the Faculty of Science.

Department of Mathematics and Statistics
University of Strathclyde
Glasgow, Scotland

Copyright Declaration

This thesis is the result of the author's original research. It has been composed by the author and has not been previously submitted for examination which has led to the award of a degree.

The copyright of this thesis belongs to the author under the terms of the United Kingdom Copyright Acts as qualified by University of Strathclyde Regulation 3.50. Due acknowledgement must always be made of the use of any material contained in, or derived from, this thesis.

Signed:

Date: 17/10/2022

Abstract

For this thesis project, a spatial model of the population dynamics of blue whiting, *Micromesistius poutassou*, in the North-East Atlantic has been developed. Since stock biomass fluctuations recorded in the past decades have raised concerns for the stock sustainability, improving our understanding of blue whiting population dynamics has become necessary for developing better fishery management strategies. Observations suggest that changes in recruitment and/or population distributions might be explained by environmental factors and spatial processes. However, it is unclear how these drivers directly affect the population, and how they might be used to predict future changes. Here I propose a spatial population model, which is essentially driven by bio-geophysical factors, and which describes the entire life cycle of blue whiting, allowing us to study the importance of different drivers and to produce long-term predictions of the population in a context of fishery and climate change.

The model includes two components, one focusing on the population and individual growth, the other on behaviours and movements. For the first time, environmental gradients are explicitly used as drivers to movement direction of long-distance migratory fish, and individual growth depends on the spatial distribution of a food variable representative of the fish diet. I found that successful feeding migrations are driven by currents, food and temperature, while successful spawning migrations are mainly affected by local values and gradients of temperature and salinity. Simulations revealed emergent model properties which agree with the empirical story: (1) feeding migration pathways varied with both climate and the initial position of individuals on spawning grounds, (2) spawning location of an individual was influenced by both climate and the location of its feeding area, (3) migration timing was important for both spawning and feeding success, (4) juvenile and adult recruitment took place in areas formerly identified as nursery habitats, and (5) juvenile recruitment depended on spawning distri-

bution and larval drift. In the model, the population response to varying fishing pressure was significantly affected by both recruitment and individual growth. I suggest this model as a tool to test and study different fishing behaviours or fishery management strategies over the long term and in a climate change context.

Acknowledgements

First, I would like to thank both my supervisors, Dougie Speirs and Mike Heath, for their constant help and support throughout my PhD. Although the last two years were particularly tough, you were always there to encourage me, to believe in me and to make me see things positively. Thank you.

I thank Martin Edwards and David Johns from the Marine Biological Association for giving me access to the CPR dataset used in this work. Thank you, as well as Alistair Lindlay, for helping me out with the dry weight estimates for euphausiids, hyperiids and *C. finmarchicus*.

I thank Andrew Yool from the National Oceanography Centre (Southampton) for the access to their NEMO-Medusa outputs and for answering our questions about the dataset.

Around the start of my PhD, when my knowledge on the blue whiting population was still very limited, I solicited the help from Verena Trenkel from IFRE-MER (Nantes). Thank you Verena for sharing your thoughts about the blue whiting population structure with us.

Thank you John Pinnegar for giving me access to the full raw dataset of blue whiting stomach records from DAPSTOM (Cefas - Centre for Environment, Fisheries, and Aquaculture Science).

I would like to thank the whole marine group of the mathematics and statistics department for their enthusiasm at sharing their work as well as at showing interest for other people's work. Thank you Dougie for organising marine group excursions to the Isle of May, to Cumbrae and to the Bass Rock, which were all beautiful and fun, and let me with very nice memories.

Thank you Irene, Sandra and Mary from the department administration for your welcoming presence and for all the support you give to us, PG students.

Finally, a special thank you goes to Ian Thurlbeck and Ronnie Wallace, our department IT staff during the time of my PhD. Thank you Ian for always help-

ing me out and for your enthusiasm at helping me out with my model codes or any software I needed to use for my project. I really missed you after your departure from the department in 2020. Thank you Ronnie for helping me whenever I had an issue with my office computer, which became quite numerous in the last two years because of the new imposed working conditions. Thank you also for making me smile by sending me occasionally pictures of HTTYD-fan arts, after accidentally discovering this side of me from my personal computer's background.

To my postgraduate friends:

First, I want to thank Hazel and Hoa for your kindness and friendship. I enjoyed our lunch break together, as well as our small outings to visit Scotland.

Thank you Agnes and Euan, who started their PhD around the same time than me. Our mutual support was always welcome, especially in dealing with the PG certificate.

I also want to thank all the regular players of my board game nights and those who came to celebrate my 25th birthday. I have always greatly enjoyed spending time with you and I hope you had fun too.

Thank you Jeremy for the wonderful moments we spent together during these coach trips. I had so much fun! I am glad we got to know each other and became friends.

I would like to thank Luce for the few times we got to share an office together. I loved talking with you (in French) about anything and everything. Your friendship is very precious to me.

Finally, to Trevor, my favourite office mate, a big thank you! It was always fun to chat with you, especially about movies! I also enjoyed seeing your thesis stand-up performances with the Bright Club. Also thank you for being almost always present to any board game nights I organised.

To these special friends who keep inspiring me:

Thank you Clara for this wonderful friendship we have since my time in Hamburg. I was so happy for you when I learned that you passed your thesis viva and you were now a doctor. I was also happy to see you again twice during my PhD, once to your place and once to mine. And I am looking forward to see you again soon!

Thank you Cyril, one of my dearest friend since my first year at the uni in 2011. You always showed me what amazing things we could accomplish when we put our heart into it. I was so happy to finally see you again three years ago. I will always keep the nickname you gave me in Marseilles close to my heart!

Thank you Margot, Morane and Anaïs for your kind messages. I am always happy to receive news from you. Also thank you Margot for your visit in Scotland!

Thank you João for your friendship and support, especially during the pandemic. You made me believe in my dreams during a difficult time, and I hope I was able to do the same for you. I hope to be able to go to Brazil one day and visit you!

To all my Abibac friends from high school:

Thank you Marie for your words of support and encouragement these special times I came to Nantes to see you. I would like to thank you and Clément as well for inviting me several times, in particular for New Year's Eve. I had a lot of fun each time. And I hope I will be able to celebrate my PhD with you too.

Thank you Claire, Antonine, Eve and Fabien for all these beautiful moments we shared together. I am always so happy to see all of you again, and I know I can always count on you.

Thank you Floriane and Sébastien for your two visits to Scotland. I enjoyed the short times we spent together, wandering around Edinburgh, or hiking in the Highlands.

And last but not least, I want to thank Simon for the continuous and incredible friendship you gave me since high school. You were always there, when I needed you. You always came for a visit when I was studying far away. You gave me strength to carry on when I was down. And above all, I enjoyed every single moment we spent together!

To my family:

First, I would like to thank my parents for your love and also for your worries. For your constant support towards my studies. For believing in me and for pushing me forward when I needed to. I wish you will be able to travel to Scotland and celebrate this big accomplishment with me!

Contents

List of Figures

List of Tables

Part I

Introduction

Thesis overview

Industrial exploitation of blue whiting, *Micromesistius poutassou*, started in the 1970s in the North-East Atlantic. The high stock fluctuations observed in the 1990s raised strong economical concerns for the sustainability of the stock. It also caused a rising interest for the blue whiting spatial population dynamics among the scientific community. What is driving this important fluctuation in recruitment? Can it be related to changes in the spatial distribution of the population? Can it be explained by changes in the environmental conditions experienced? Does climate change affect the stock sustainability and its response to fishing pressure? In this context, the following modelling project can be considered as a milestone towards improving our understanding of the stock dynamics and helping improve fishery management strategies.

Several stages were involved in the building of the spatial model of the blue whiting population dynamics (Fig. 1). First, a thorough review of the current knowledge base on the species ecology in the North-East Atlantic was performed to help target the model needs. In parallel, the knowledge base for modelling population dynamics was studied using the book 'Ecological Dynamics' by Gurney & Nisbet (1998) and helped in the writing of the model equations for individual and population growth. Then, spatial properties of the model were investigated, starting with exploring the biogeophysical input data and followed with population movements. The NEMO-Medusa outputs with forecasts available from 1988 to the end of this century (Yool et al., 2013b) were chosen as main input data, and population migrations were implemented and modelled with the help of `Ichthyop`, a particle tracking model (Lett et al., 2008). Stomach records from DAPSTOM (Pinnegar, 2014) and plankton abundance observations from CPR surveys (Edwards, 2018) were also used to develop a spatial food variable adapted to the blue whiting diet. At last, the final model was tested with varying

settings, and then fitted to catch records from ICES (2019b) for studying long-term predictions of the blue whiting population.

The blue whiting population model was written in `C`, while migratory behaviours were implemented in `R`. The current version of the codes for the blue whiting model and for computing migration fields are available on the GitLab platform, through the following links:

blue whiting model https://gitlab.cis.strath.ac.uk/marinemodelling/blue-whiting-model-edthesis/blue-whiting-model-codes.git

migration https://gitlab.cis.strath.ac.uk/marinemodelling/blue-whiting-model-edthesis/bw-adult-movements.git

model library https://gitlab.cis.strath.ac.uk/marinemodelling/blue-whiting-model-edthesis/bw-model-lib.git

To set the scene, I will start here with the literature review on blue whiting ecology, where some potential candidates of drivers affecting population growth and/or spatial movements will be identified (chapter 1). In the second part, the blue whiting model is described and explained. It is split into two components: (1) the individual and population growth model (chapter 2) and (2) the spatial model including the modelling of migratory behaviours (chapter 3). The third part allows us to study input variables of the blue whiting model and to make early assumptions about their effect on the modelled population dynamics: chapter 4 explores predictions from the NEMO-Medusa outputs, chapter 5 focuses on the modelling and predictions of the blue whiting food variable, and chapter 6 discusses the observed variations of fishing catch in time and space to support the formulation of the fishing models tested here. The fourth part of this thesis presents all the results produced either with just the migration model (chapters 7 and 8) or with the final population model (chapter 9). Finally, in the last part, all the main results of this modelling work are discussed, together with the model performance (chapter 10).
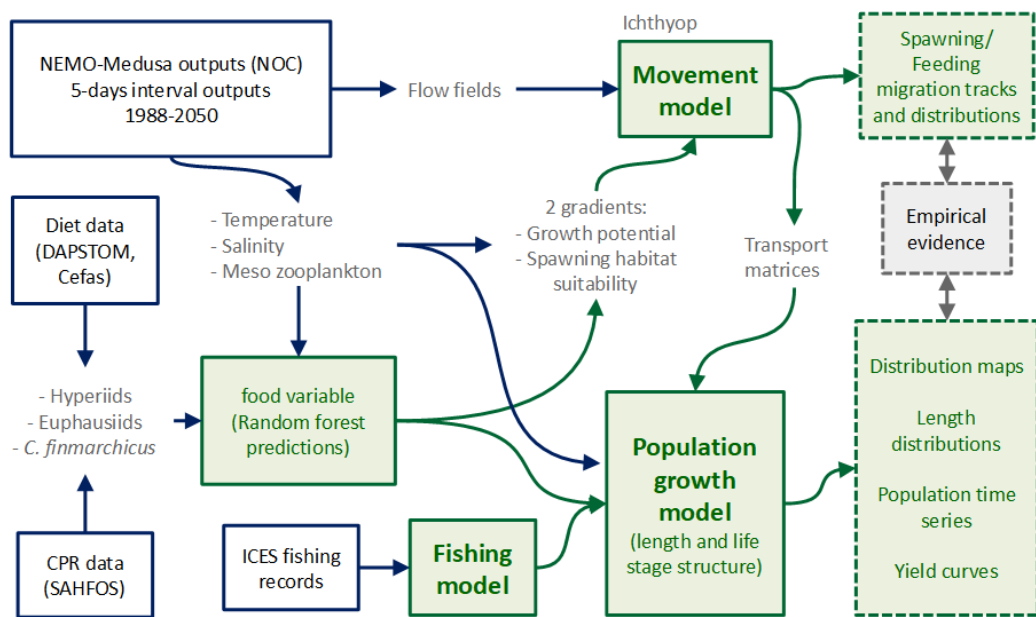
Figure 1: Summary of the building process of the spatial population model for blue whiting, including external input data (white boxes), produced data and models (solid green boxes) and model outputs (dashed green boxes). Extracted or produced output variables from a previous stage to be used in the next stage are written outside the boxes in grey.

Chapter 1

Blue whiting ecology

The largest population of blue whiting, *Micromesistius poutassou*, lives in the north-eastern Atlantic, extending from the Mediterranean and off Portugal in the South, to the Barents Sea in the North (Bailey, 1982). From February to April, mature blue whiting aggregate on the population main spawning grounds west of the British Isles, from the Porcupine Bank area to the Rockall Plateau (Bailey, 1982; Skogen et al., 1999; Payne et al., 2012) (fig. 1.1). Larvae hatch and start to grow in this area, and drift with currents that either lead them to the southern nursery ground in the Bay of Biscay, or to northern continental shelf areas (Svendsen et al., 1996; Bartsch & Coombs, 1997; Skogen et al., 1999). After spawning, it is assumed that most of the adult population undertake a northwards migration to the main feeding grounds in the Norwegian Sea, where they stay during summer (Bailey, 1982).

Juveniles grow on their nursery grounds, and when they reach or are about to reach maturity at age 1, they undertake their first spawning migration (Heino & Godo, 2002; Gastauer et al., 2016). New mature individuals from the Bay of Biscay seem to spawn in the Porcupine Bank area for their first time (Brophy & King, 2007; Trenkel et al., 2014). However, there is a large lack of knowledge about what happens to these southern individuals after their first spawning. Do they migrate northwards to the main spawning grounds like all other individuals? And if this is the case, do they show affinity to their first spawning ground, returning to the Porcupine Bank during the next spawning seasons? Answering these questions may have great implications for our understanding of the population dynamics and structure.

Industrially fished since the 70s (Monstad, 1990), the population is currently
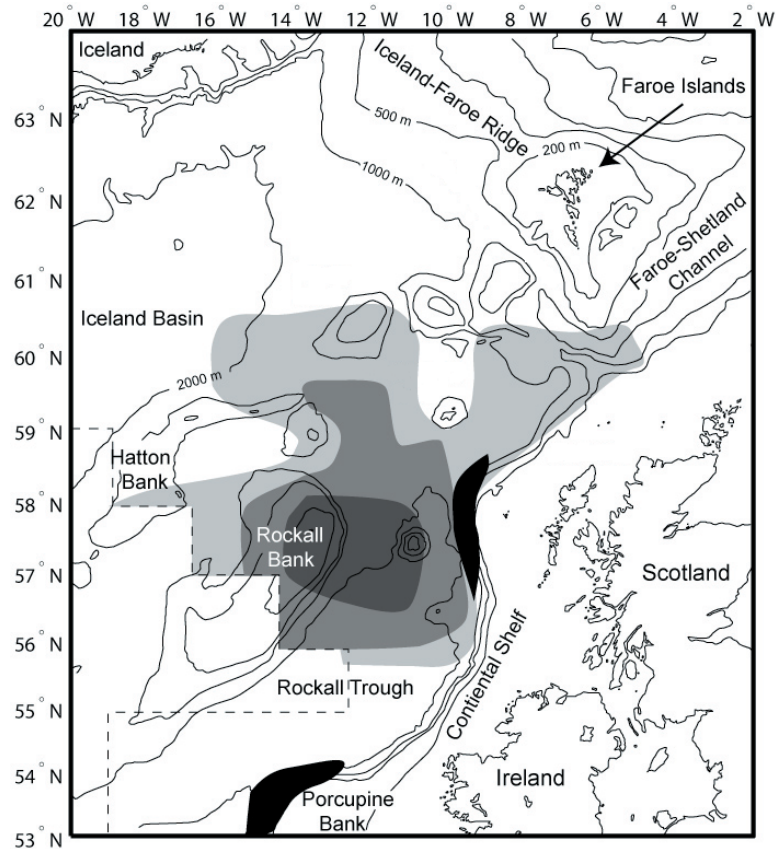
Figure 1.1: Map of the blue whiting spawning region off the British Isles (map made by Hátún et al. (2007)). The gray contours give the qualitative distribution of blue whiting larvae in years 1948-1956 according to Henderson (1961). Areas in black show intensive spawning areas in more recent years, according to Skjoldal et al. (2004).

managed as a single unit (ICES, 2012a). But concerns on the future of blue whiting fishery have been growing because of the large stock abundance fluctuations observed since the 90s (Payne et al., 2012). This has raised important questions about the drivers involved in the population dynamics of blue whiting. The effect of climate processes and hydrodynamics on the population dynamics, including growth and recruitment has been investigated in many studies, especially for the larval stage (Hansen & Jákupsstovu, 1992; Hillgruber et al., 1995; Svendsen et al., 1996; Bartsch & Coombs, 1997; Bailey & Heath, 2001; Kloppmann et al., 2001, 2002; Heino et al., 2003; Hátún et al., 2007; Heino et al., 2008; Lopez-Lopez et al., 2017; Miesner & Payne, 2018). In fact, one of the potential drivers could be related to the dynamics of the subpolar gyre (Hátún et al., 2009b,a; Trenkel et al., 2014). The subpolar gyre is the counter-clockwise circulation in the subpolar region of the Atlantic, and brings cold water from the Labrador Sea into the area between Iceland and the British Isles (Hátún, 2005). Its temporal strength

variations influence temperature regimes west of the British islands, and may affect ecosystem dynamics (Hátún et al., 2009a). Since the spawning grounds of blue whiting are located in this area, the subpolar gyre could have an effect on recruitment in the early life stages.

Another concern for blue whiting fishery management is their population structure: more and more study results give support to the existence of two distinct population units, rather than one single (Brophy & King, 2007; Was et al., 2008; Keating et al., 2014; Pointin & Payne, 2014; Mahe et al., 2016). If the evidence is considered strong enough, then this could partially explain the high stock fluctuations, as a result of potential recruitment imbalance, because one stock could be overexploited without notice. As emphasized by Reiss et al. (2009), mismatches between management units and genetic structure may lead to the weakening of the population ability to adapt to changing environment because of genetic diversity loss. They firmly advised to consider genetic evidence for different population units as minimum to define management units.

Modelling the spatial dynamics of the blue whiting population may provide new answers to these questions. A spatial length-structured population model would be well adapted for this task, as the size determine a lot of individual and population dynamics in marine ecosystems, like the place in the food chain combined with survival and feeding strategies (Ware, 1975; Gislason et al., 2010), or the influence of currents on movement (Nøttestad et al., 1999). This type of model should then enable to describe dynamics of growth, recruitment, and migrations, taking into account the biological and physical changes of environment encountered along their life. The main objective of this review is to bring together all blue whiting studies relevant to their population dynamics, by discussing the current assumptions made and suggesting some new ones, and to give a reliable basis for modelling. In that way, quantifying growth should be the first focus of this work, since this knowledge will be essential to build the length-structured model. Reproduction and mortality of blue whiting will also be discussed. Some population dynamics are highly influenced by spatial processes, which will be identified, and as well as their potential involvement for the model. Finally, the population structure will be discussed, together with the question on whether or not two distinct blue whiting stocks should be considered.

1.1 Individual growth

Individual growth is mainly affected by the energy balance between gains through feeding, and costs from metabolism and movement. Thus, growth rates reflect environmental conditions experienced by individuals along their life, especially during the early life stages. In the process of building a length-structured model for the blue whiting population, it is essential to be able to estimate the individual growth rates, and to do that, we need to know the potential drivers affecting it. In the following parts, I looked for these drivers in the literature.

1.1.1 Larval diet and growth

Before hatching, eggs are found mainly between 250 and 450 m depth (Coombs et al., 1981). Observations showed a relationship between the size of the larvae and their vertical distribution, with larger larvae found closer to the surface (Coombs et al., 1981; Ådlandsvik et al., 2001). One possible explanation for this depth distribution may be the buoyancy increasing through larval development, showed in the model by Ådlandsvik et al. (2001). Although they were not able to verify this theory because of lack of buoyancy measurement for larvae, they justly underlined the advantage of reaching the surface by passive rising for larvae, which limits energy costs, and predator detection. However, if the passive rising theory is true, blue whiting larvae may still use locomotion to accelerate this rising process, or on the contrary to stay longer at some depths, so that they can quickly reach highly productive areas, or adapt to fast changing environments. In fact, Hillgruber & Kloppmann (2000) argued that food abundance, light intensity and turbulence may together influence the depth distribution of larvae, by affecting food availability, and thus their feeding success. Larvae would then most likely move actively to depths whose environment conditions maximize feeding success.

Blue whiting larvae feed mostly on developmental stages of Copepods, with nauplii as the most abundant one (Hillgruber et al., 1995). Studies showed an onto-genetic shift in the diet of larvae (Hillgruber et al., 1997; Hillgruber & Kloppmann, 1999, 2000): whereas the smallest larvae largely prefer to feed on tintinnids and cyclopoid nauplii, they gradually shift their diet to larger prey items,

mostly calanoid nauplii and copepodite stages, when their size increases. Copepod eggs are also often found in their stomach and gut, but the ingested weight remains relatively low, and no strong shift is observed with increasing larval size (González-Quirós & Anadón, 2001). González-Quirós & Anadón (2001) argued that ingestion of copepod eggs is more related to accidental ingestion of free eggs, or ingestion of copepod females bearing eggs, rather than to be a target prey of blue whiting larvae.

Growth rates of fish larvae are often correlated positively with feeding success (Pepin et al., 2015). Thus, by investigating the driver affecting feeding success, we can potentially highlight drivers affecting larval growth. Many studies assessed the feeding success of blue whiting larvae by measuring the feeding incidence (the proportion of feeding individual), and the feeding intensities by weight or by number of items ingested. Kloppmann et al. (2002) observed a decrease of the feeding success during strong wind events, which also went along with an increasing production of proteins, and lower condition of the larvae. This suggested that the high turbulences caused by these wind events forced the larvae to spend a lot of energy in maintaining themselves in the water column, and decreased the prey capture rate. However, since turbulence also increase the prey encounter rate, there must be an optimal turbulent state resulting from moderate wind (Hillgruber & Kloppmann, 2000).

Diel variations in feeding incidence and intensities were also reported. It seems that larvae have higher feeding success during daylight (Hillgruber & Kloppmann, 1999). They also tend to eat larger prey by day (Hillgruber & Kloppmann, 2000), which shows that light also affect feeding success, most likely by enhancing visibility of prey. However, in the context of modelling population dynamics, the effect of light can be ignored since the time scale used for such models is usually greater than one day, and so observations of diel variations are impossible.

Different water masses are present on the spawning grounds. In the Porcupine area, warm and saline waters are brought by the secondary shelf edge current (sSEC), directed northwards and longing the continental shelf, while the anticyclonic circulation present around Porcupine Bank allows for the retention of cooler and less saline waters above the area. Different feeding success were reported between both water masses, with very low feeding incidence but very high feeding intensities in the cool waters above Porcupine Bank, and better feeding incidence

but low feeding intensities in the sSEC (Hillgruber & Kloppmann, 1999). These observations went along with a change in larval size, with mostly large larvae above Porcupine Bank, and small larvae in the sSEC. Moreover, Bailey & Heath (2001) observed that most larvae were distributed in waters with temperature of 9-10°C, and with salinity around 35.3, which are the characteristics of the shelf edge current (SEC). Thus, the larval development seems to require particular environmental conditions, and these requirements may shift throughout their growth.

1.1.2 Adult growth: food availability and density dependence

As for the larval stages, a few studies investigated the diet (tab. 1.1) and feeding success of blue whiting juveniles and adults. Again, a shift in diet seems to occur with increasing size (Cabral & Murta, 2002; Dolgov et al., 2010; Bachiller et al., 2016). In all these studies, the size of ingested prey tended to increase with blue whiting size. Especially, fish occurred more frequently in the stomach of larger blue whiting (Dolgov et al., 2010). Cabral & Murta (2002) also observed diet variations with depth, which were correlated with the diet variations as a function of blue whiting length. Since indices for the stomach fullness were calculated differently between studies, we can not accurately compare their results. Nevertheless, considering analyses of the Total Fullness Index (TFI) values from Dolgov et al. (2010), and of the Stomach Fullness Degree (SFD) values from Bachiller et al. (2016), both suggested that feeding intensities also increase with size. But while Bachiller et al. observed an increase in feeding incidence with increasing length, Dolgov et al. found no size effect on the proportion of empty stomachs. This might be explained by the potential difference in food availability between the Barents Sea and the Norwegian Sea. In fact, the average feeding incidences from the Arctic and coastal areas of the Norwegian Sea are highly variable between years, compared to the more central area, and suggested that these areas are located at the edge of the ideal feeding habitat. In the Barents Sea, since fish is an important prey in blue whiting diet (60% of total stomach content weight), intra-species competition for smaller prey items is minimized (Dolgov et al., 2010). Larger individuals seem to prey preferentially on fish, leaving the

Table 1.1: Preys found in the diet of *M. poutassou* as reported from studies overall its distribution range.

Area	Period	Mean length (cm)	Diet	Reference
Barents Sea	All along the year	27 (range: 13.7-45)	Euphausiids (krill, *Meganyctiphanes norvegica*), amphipods (pelagic hyperiids), copepods, other invertebrates, fish (polar cod)	Dolgov et al., 2010
Norwegian Sea	June-July	25	Amphipods (hyperiids), appendicularians, euphausiids, copepods	Prokopchuk & Sentyabov, 2006
Norwegian Sea	May, July	27	Euphausiids, amphipods, copepods	Bachiller et al., 2016
Northwest of the Iberian Peninsula	September-October	(range: 12-21)	Euphausiids (*Meganyctiphanes norvegica*), amphipods (Hyperiids), fish	Lopez-Lopez et al., 2017
Portuguese coast	July, October, February	23 (range: 14-35)	Copepods, larvae of decapods, decapods (*Pasiphae sivado*), and Euphausids (*Meganyctiphanes norvegica*)	Cabral & Murta, 2002

crustaceans for smaller individuals, and resulting in a lack of variation of feeding incidence with size.

Seasonal variations in feeding were also observed (Cabral & Murta, 2002; Dolgov et al., 2010; Bachiller et al., 2016). From summer to winter, the predominant prey in the diet may shift from decapods to euphausiids (Cabral & Murta, 2002). Dolgov et al. (2010) also reported higher proportions of fish ingested from late summer to early winter. Both diet variations suggested blue whiting tend to feed progressively on larger prey from summer to winter. However, Dolgov et al. noted that these seasonal diet variations might be more a reflection of geographic variations, in particular those caused by changes in the sampling cover between seasons. Feeding success seems globally maximal during summer. Dolgov et al. observed significant seasonal variations of feeding incidence, which was the lowest during late spring, and the highest during late summer. The low feeding incidences reported in late spring are most likely due to the feeding migration which blue whiting undertake at this time of the year, and during which they would barely feed. However, Bachiller et al. (2016) showed that feeding intensity tends to decrease from May to July, which may reflect the decreasing food availability in the Norwegian Sea as it is progressively consumed during the season.

Food availability may highly affect feeding success and thus growth as well. One important driver that may decrease food availability is the density of pop-

ulation present in the feeding area. For example, lower feeding intensities and a diet shift to smaller and more abundant preys were observed in the Norwegian Sea in areas where the blue whiting population was highly concentrated (Dolgov et al., 2010). In fact, in a study which focused on potential drivers affecting blue whiting growth using a modified von Bertalanffy model, variations in mean length at age and mean mass at age seemed to be best explained by the density dependence effect (Trenkel et al., 2015).

1.2 Reproduction, mortality, and inter-species interactions

Building a population dynamic model requires to understand essential biological processes for population growth, such as fecundity and mortality. the following sections review past studies which proposed functions and/or parameter estimates for fecundity or mortality. Since inter-species interactions may affect mortality, they will also be discussed here.

1.2.1 Maturity age and fecundity

Since the review from Bailey (1982), no published study has focused on maturity and fecundity of blue whiting. Thus, our current knowledge is essentially based on the assumptions made by Bailey (1982), and the observations of mature and immature individuals on the spawning grounds. By investigating results from studies issued before 1982, Bailey estimated the average length of first maturity between 18 and 20 cm. As part of the ICES annual assessment of the blue whiting population in the north-eastern Atlantic, results of surveys suggested similar values for length (19-24 cm) at first maturity (Trenkel et al., 2014; ICES, 2005, 2007). Figure 1.2 shows the proportions of mature by length class, caught during different years, according to ICES. This data will be useful to find the right parameter estimates and simulate the maturing process of the blue whiting population in the length-structured growth model developed here.

Other models used age to describe maturity. It is the case for stock assessment models developed by the ICES Working Group on Northern Pelagic and Blue

Whiting Fisheries (WGNPBW) (ICES, 2007, 2016a) which have been considering the same proportions of mature at age since 1994 (Fig. 1.2). They suggested that most individuals become mature around 2-3 years old.

Fecundity of northern blue whiting is scarcely documented. Based only on two
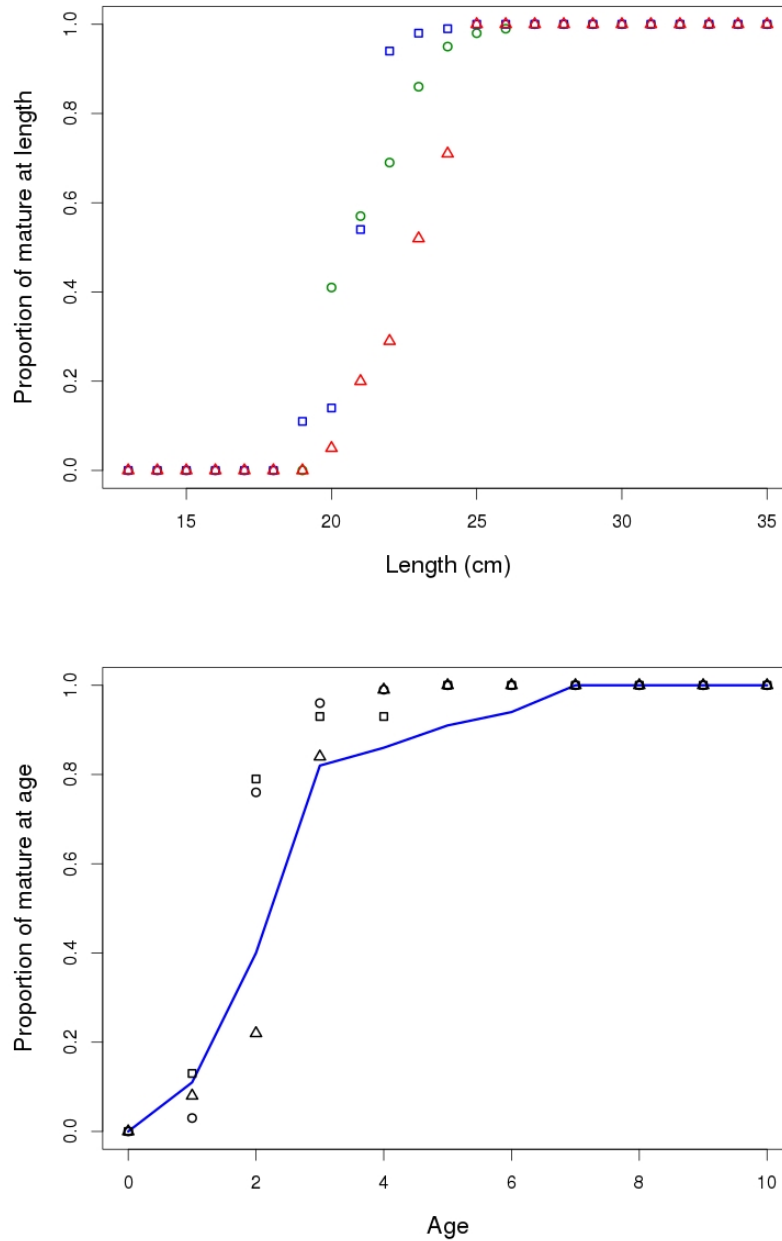
Figure 1.2: Proportions of mature blue whiting in each length class (top) and age class (bottom) in catch samples (ICES, 2004, 2005, 2011a). Estimated proportions represented here are from years 2004 (circles), 2005 (squares) and 2011 (triangles). The blue line (bottom figure) corresponds to proportion of mature at age considered in ICES's stock assessment models used for blue whiting (ICES, 2007, 2019b).

studies at Porcupine Bank (Polonsky, 1968, 1969) and his own observations at Rockall Bank in 1968 and 1969, Bailey (1982) proposed the following relationship between the fish length and the number of eggs released during spawning:

$$e = 0.142\ L^{3.742} \tag{1.1}$$

where e is total fecundity and L is length. Thus, according to this relationship, a female of 40 cm should be able to produce around $140,345$ eggs (Fig. 1.3). More fecundity studies are available for the southern species of blue whiting (*M. australis*), and fecundity seems to have always the same kind of relationship with fish length (Pájaro & Macchi, 2001). Moreover, even if both species do not share the same average size at maturity (30-40 cm for *M. australis*), the number of eggs potentially produced by a 45 cm female is very similar between both species (around $200,000$). This suggests that the relationship given by Bailey (1982) may be a good first estimation for fecundity to use in a blue whiting population model.
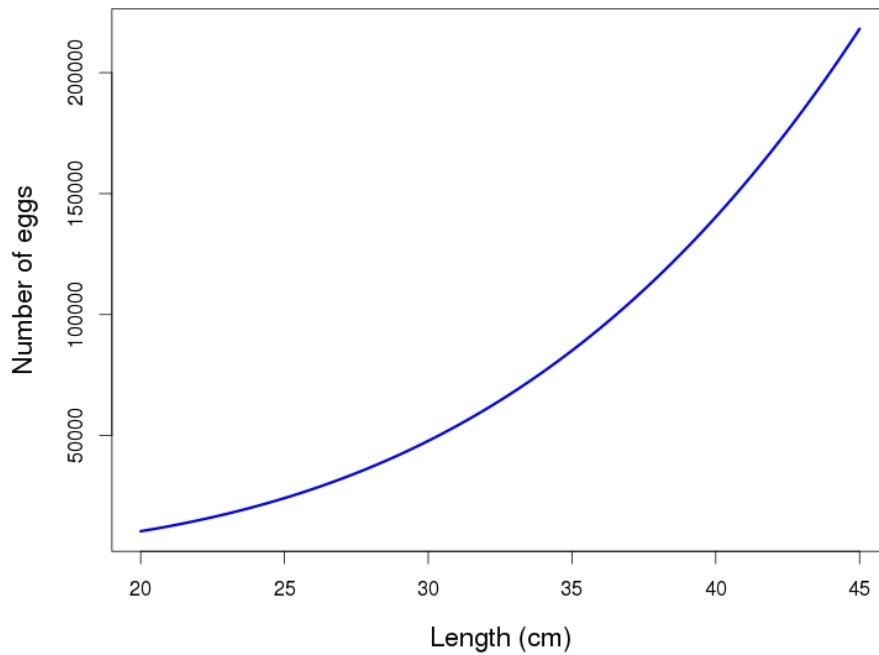
Figure 1.3: Relationship between *M. poutassou* length and number of eggs spawned per individual according to Bailey (1982) (equation 1.1).

1.2.2 Natural mortality: inter-species interactions

Mortality is very difficult to assess in the marine environment, because many potential drivers exist but it is often difficult to study and quantify their effect on population. Thus, ICES still considers a constant natural mortality rate over the blue whiting lifespan, though they are aware that this might not reflect the reality (ICES, 2007, 2016a). In these fish population assessments, natural mortality means mortality that is not induced by human activities (fishery). This includes mortality caused by predators, parasites, competition, and senescence.

In the Norwegian and the Barents Sea, blue whiting constitute an important prey for piscivores like cod, swordfish, Greenland halibut, and long-finned pilot whale (Dolgov et al., 2010; Heino & Godo, 2002), while hake, mackerel, and horse mackerel are some of the predators reported in the southern waters of its distribution range (Silva et al., 1997). Therefore, the blue whiting mortality rate induced by predation would be difficult to estimate, because of the large number of potential predator species, and because these predators eventually vary over the blue whiting lifespan.

An other potential mortality source in blue whiting population is parasitism. According to several studies, infection by the coccidian *Goussia* sp. (formerly identified as *Eimeria* sp.) tends to highly decrease the condition of blue whiting adults by damaging their liver (Abollo et al., 2001; MacKenzie, 1981). A relationship between infection intensity and fish age seems to exist, most likely because of the parasite accumulation through the consumption of crustaceans, its former hosts, over the fish lifetime (Abollo et al., 2001; MacKenzie, 1978). Abollo et al. also reported a host response in infected blue whiting, but suggested that the energy costs of this response may be so high for heavily infected individuals, that this would ultimately lead to their condition decline.

Competition for same food resources may also increase mortality in a population. There is currently no strong evidence for inter-species competition in the blue whiting population. However, some recent studies suggested that herring, *Clupea harengus*, might be a potential competitor for blue whiting, because of their horizontal distribution overlap in the Norwegian Sea (Utne et al., 2012b; Langøy et al., 2012; Utne & Huse, 2012), and some similarities and overlap found in diet of both species (Bachiller et al., 2016; Langøy et al., 2012). Utne et al.

(2012b) suggested interactions between blue whiting and herring might be more likely during years of high stock abundances, since horizontal distribution overlap increase. But blue whiting tend to occupy deeper layers of the water column than herring (Huse et al., 2012), and then competition between both seems very limited. However, Huse et al. (2012) suggested that, if competition exists, this most likely happens between herring and blue whiting juveniles. In fact, the younger individuals of blue whiting seem to have shallower distribution, which may affect herring population in years of high blue whiting recruitment: Huse et al. (2012) observed that herring tended to be more confined to the surface layer during peaks of blue whiting biomass. Huse et al. explained that a niche overlap might exist between blue whiting juveniles and herring, and years of high blue whiting recruitment may lead to competition between both, resulting in the vertical shift of herring.

While inter-species competition seems most likely to affect blue whiting population dynamics during years of high abundance, increasing in abundance also leads to more intra-species competition. Then inter- or intra-species competition effect on mortality can be simplified by a density-dependence effect. Powers's investigation (2014) on modelling natural mortality rates in fish population suggested that using a population model with density-dependent mortality may be relevant for population that endure high recruitment variations and that may be affected by density-dependence. Since this seems to be the case for the northern blue whiting, density-dependent mortality should be considered in their future population models.

1.2.3 Fishery and stock fluctuations

Blue whiting fishery takes place overall its distribution range, from off Portugal to the Barents Sea, but is most important in term of catches along the continental shelf edge of the spawning grounds west of the British Isles to the Faroe Islands, and during the spawning season (ICES, 2016a). According to fishing mortalities estimated from 1981 to 2016 (ICES, 2016a), the average fishing mortality rate of 3-7 year-old fish is around 0.35. Recorded catches of blue whiting fisheries included fish of any age, and the fishing mortality rate was estimated to increase with fish age (Fig. 1.4). Moreover, length-age distributions from surveys (ICES,

2004) suggested that fish start to be targeted by the fishing trawls around a length of 25 cm.

The official total catch biomass (TCB) fluctuated with the total stock biomass (TSB) and spawning stock biomass (SSB) (Fig. 1.5). In fact, high fluctuations of recruitment and stock have been recorded during the past decades. During years of high decreasing stock, fishing rates were adjusted to let the stock recover its sustainable state. As a consequence, estimated fishing mortalities dropped during the stock decline from 2003 to 2011 (Fig. 1.5). The blue whiting fishery had no long-term management plan until 2016, but considering the high stock fluctuations endured, the North East Atlantic Fisheries Commission (NEAFC) recently requested one to ICES, which advised at the end of 2016 to follow a long-term management strategy (LTMS) evaluated as precautionary (ICES, 2016a,b). In the last steps of spatially modelling blue whiting population dynamics, it might be then interesting to include this LTMS, and study its effects.

However, the role that the fishery plays in these high stock fluctuations is unknown. This is the reason why potential drivers that may influence recruitment need to be identified. Several studies suggested that spatial processes are in-
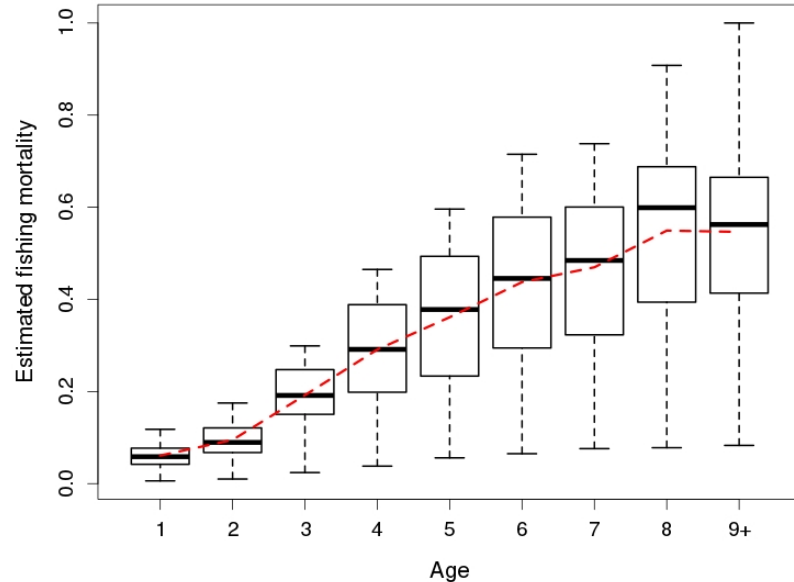
Figure 1.4: Fishing mortality at age estimated by ICES for 1981-2016 (ICES, 2016a). Boxplots show the distribution of annual mortality values (computed with default setting of the R `boxplot` function) and the red dotted line corresponds to the mean fishing mortality at age. Time-series of fishing mortality at age used to produce the box-plots are shown in figure 1.5.
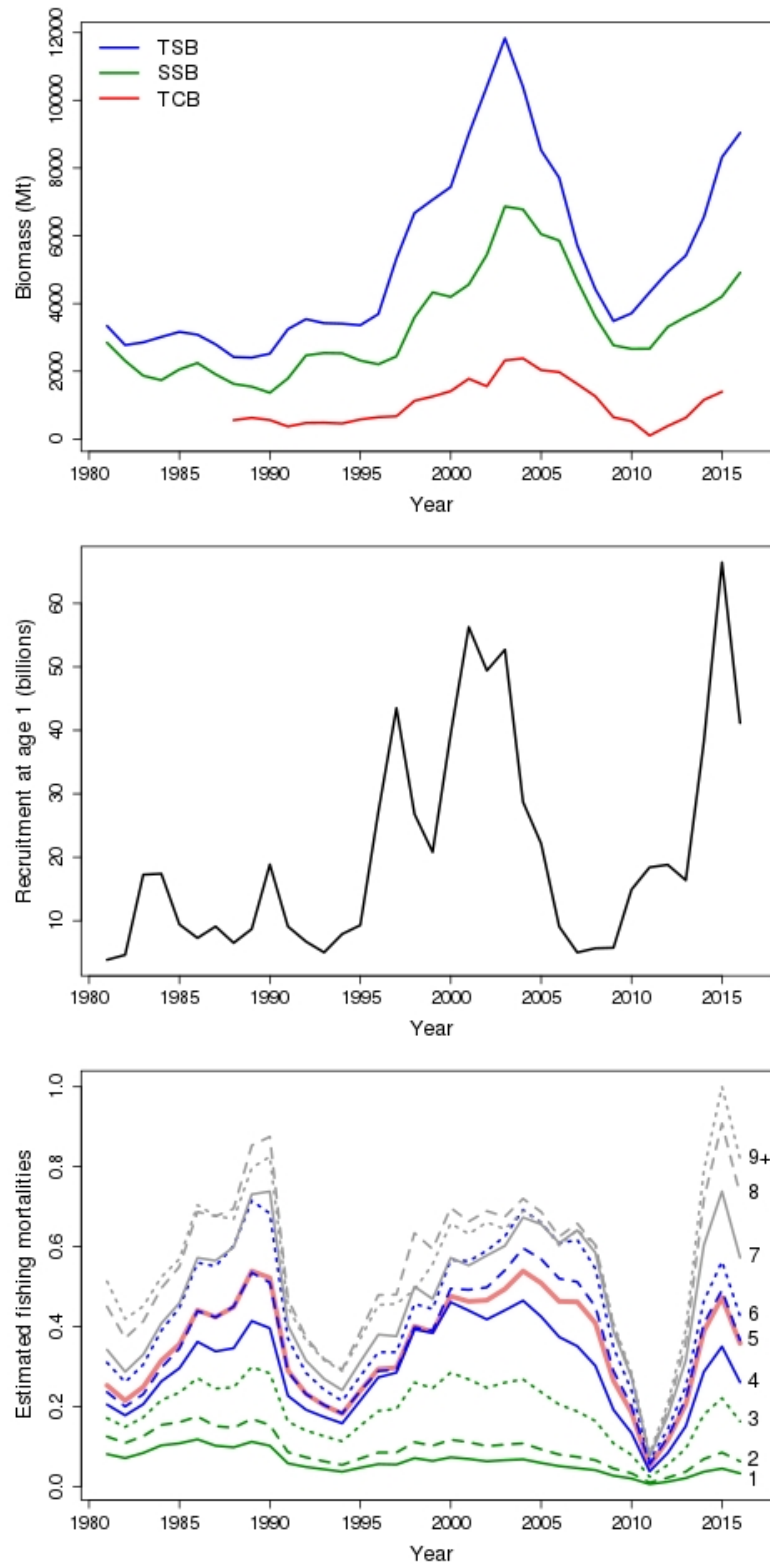
Figure 1.5: Time series of blue whiting stock biomass (top graph), recruitment at age 1 (middle graph) and fishing mortality (bottom graph) for the period 1981-2016 (ICES, 2016a). In the top graph, total stock biomass (TSB) is in blue, spawning stock biomass (SSB) in green, and total catch biomass (TCB) is represented in red from 1988 to 2015. In the bottom graph, time-series of estimated mortality rate for each age class are plotted in green (age 1-3), blue (age 4-6) and grey (7-9+), while the thick red line (mostly following mortality values of 5-year age class) represents average mortality rates for fish aged from 3 to 7 years.

volved. This is the focus of the next section, while spatial properties of the blue whiting fishery will be further described and discussed in chapter 6.

1.3 Spatial dynamics and recruitment

Blue whiting is a migratory fish, travelling between feeding and spawning areas in an annual cycle (fig. 1.6). Early in the history of industrial exploitation of the blue whiting stock, fishing fleets seemed to follow their migration cycle, and monthly mapping of fish catch over the period January-June from 1980 to 1989 suggested variations in spawning distributions and feeding migration pathways (Monstad, 1990). Those variations may affect both recruitment and growth of blue whiting with consequences for fishing. In the following, studies which focused on the spatial dynamics of blue whiting are reviewed and discussed, with the aim of identifying potential drivers to the observed variations in spatial distribution and recruitment.

1.3.1 Larval drift

From the moment eggs are spawned, they are subject to passive transport caused by currents. In the late 90s, a few studies started building and using models to simulate this egg and larval transport (Svendsen et al., 1996; Bartsch & Coombs, 1997; Skogen et al., 1999). They all support the existence of both a southern and northern larval drift which mostly depend on the initial spawning location (fig. 1.6). According to these models, the Porcupine Bank area seems to be roughly separating the two main modes of larval drift, with northward drifting larvae to the North and southward drifting larvae to the South.

Svendsen et al. (1996) showed with their particle tracking model that 10 to 20% of larvae tend to drift southward into the Bay of Biscay and those larvae were all coming from the Porcupine Bank area, while the most southern initial position of northward drifting larvae in the model were recorded in the northern area of Porcupine Bank. Northward drifting larvae ended either in the Norwegian Sea (5-10%), the North Sea (1-5%) or on the shelf from Ireland to the North Sea (15-30%). With Bartsch & Coombs's model of larval drift for blue whiting
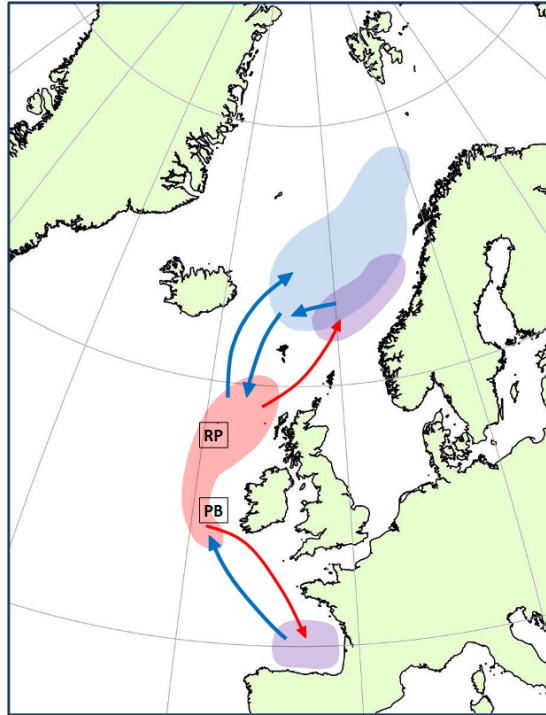
Figure 1.6: Simple representation of the main larval drifts (red arrows) and adult migration routes (blue arrows). Larvae drift either southward or northward from the area west of British Isles (light red area) to nursery areas observed respectively in the Bay of Biscay and along the Norwegian continental edge (purple areas). The Norwegian Sea (light blue area) is considered the main feeding area of blue whiting adults. Location of the Porcupine Bank (PB) and the Rockall Plateau (RP) are also given here.

(1997), the separation between northward and southward drifting larvae for initial hatching position was estimated around latitudes 53-54°N. While estimating a similar average position (54.5°N), Skogen et al.'s model results (1999) suggest high variability for this separation, with some larvae from the Scottish continental shelf also tending to drift southward in some years. However, in Skogen et al.'s study, the two drift patterns were mostly defined as the latitude difference between initial and final positions of larvae, with southward drifting larvae being dominant (71% in average). When they looked at larvae successfully drifting into the Bay of Biscay (18% of total larvae) or North of the Faroe-Orkney section (11% of total larvae), initial positions were much more limited to the Porcupine Bank for southward drifting larvae and quite limited to the northern areas of the spawning grounds for northward drifting larvae. Those results were consistent with past simulations from Svendsen et al. (1996) and Bartsch & Coombs (1997) in which 40 to 60% of larvae remained on the main spawning grounds by the end of summer, especially over Rockall Bank/Trough and Porcupine Bank. Moreover, retention

of large larvae has been observed by Hillgruber et al. (1995) in the Porcupine Bank area and tends to support those model results.

Larval mortality was not included in the models and so the predicted final distributions of larvae in summer do not represent reality, although they give a good idea of the drifting patterns and allows for identification of areas that might fulfil the function of nursery habitat. To understand how larval drifting patterns are related to blue whiting recruitment, Svendsen et al. (1996) compared time-series of the Virtual Population Analysis (VPA) recruitment values from ICES for blue whiting juveniles (0-group) with the proportions of larvae drifting in defined areas (e.g. Bay of Biscay and North Sea) according to their particle tracking model. They observed a positive relationship between high recruitment year-classes and larger drifting events of larvae into northern shelf areas and the North Sea, while there was no clear relationship between southward drifting into the Bay of Biscay and recruitment. Yet the amount of larvae remaining in the Rockall Plateau region seemed to control most juvenile recruitment variations. In fact, after a multiple linear regression analysis, Svendsen et al. (1996) found the following relationship:

$$R_0 = -2.54 + 2.79 * (D_{\mathrm{NS}}(\mathrm{Aug})) + 0.72 * (D_{\mathrm{RP}}(\mathrm{Aug})) \tag{1.2}$$

Where D_{NS} is the proportion of larvae drifting into the North Sea and D_{RP} is the proportion of larvae staying or drifting into the Rockall Plateau area. Their modelled recruitment R_0 could explain 40% of the total variance of ICES VPA recruitment values.

While a lot of larvae tend to drift southward (Svendsen et al., 1996; Bartsch & Coombs, 1997; Skogen et al., 1999), Svendsen suggested that those larvae might be lost to recruitment because of low productivity in offshore areas of the Bay of Biscay. However, some studies showed that phytoplankton bloom events take place around March-April, starting in up-welling coastal regions and spreading offshore in the Bay of Biscay (Varela, 1996; Garcia-Soto & Pingree, 2009), and blue whiting larvae and juveniles have been recorded off the Cantabrian shelf (Varela, 1996; Carrera et al., 2001). This suggests that some larvae may survive the southward drift through the Bay of Biscay to arrive in the southern areas, where productivity could be high enough in March-April to sustain larval growth. In fact, model results from Svendsen et al. (1996) showed that southward drift-

ing larvae managed to reach Spanish coastal areas before the end of April when spawning occurred early in March. Thus, the Bay of Biscay is also considered as a nursery area for blue whiting larvae and juveniles. The reason for the weak relationship between total recruitment and the proportion of larvae drifting in the Bay of Biscay in Svendsen's study could be explained by the existence of two distinct populations defined by the two larval drifting patterns (Skogen et al., 1999), and of which the southern population contribution to total recruitment could have been under-represented in ICES VPA values at the time. VPA numbers are obtained by back calculations from commercial landings and research cruises (Svendsen et al., 1996; Anon, 1990) which took place from the area South of Ireland and Porcupine Bank in the South, to the Norwegian Sea and North Sea in the North (Monstad, 1990). Assumptions on blue whiting population structure are discussed further in section 1.4.

Recruitment seems to be affected by the dynamics of the shelf edge current (SEC) for larvae spawned between Porcupine Bank and the shelf break between Shetland and Faroe. In the Porcupine area, Hillgruber et al. (1995) observed that eggs and larvae were mostly distributed over the western area of the Porcupine Bank where temperatures were between 9 and 10°C and salinity always around 35.4. In the northern areas of the spawning grounds, Bailey & Heath (2001) also found most larvae in waters with temperatures between 9 and 10°C and salinities between 35.25 and 35.4. Those temperature and salinity ranges are characteristic of the SEC and seem to be optimum conditions for larval development (section 1.1.1). A North-East drift seems to be visible in the North-West area of Porcupine Bank (Hillgruber et al., 1995), supporting the northward larval transport by the SEC. Retention of larvae was also observed in shallower areas of Porcupine (Hillgruber et al., 1995) and the high concentrations of larger larvae in those areas support Svendsen et al.'s assumption that retention areas over the shelf might be positive for recruitment.

1.3.2 Feeding migrations and distributions of adults and juveniles

After spawning, most adults leave the spawning grounds and undertake a migration towards the Norwegian Sea (Bailey, 1982). From the fishery in Faroese

waters, we know that migrating adults tend to cross the Iceland-Shetland section between late April and early June (Hansen & Jákupsstovu, 1992) and start entering the Norwegian Sea around the same time. In the Norwegian Sea, blue whiting optimum temperature range seems to be 5-7°C (Monstad & Blindheim, 1986), and some studies showed that they tend to stay in areas warmer than 2°C (Blindheim et al., 1971; Utne et al., 2012b). Acoustic surveys showed that densities of blue whiting tend to be higher in May than later in July-August, and that they are first and mainly concentrated in southern or central areas of the Norwegian Sea before dispersing more uniformly and over larger areas in late summer (Utne et al., 2012b). This migration behaviour was reproduced in an individual-based model (IBM) developed by Utne & Huse (2012), and demonstrated the importance of passive advection by currents for the feeding distribution of blue whiting in the Norwegian Sea. In the model, swimming was determined by three types of movement: directed, stochastic (random, dispersive) and advection (currents). From April to May, swimming was mostly directed by currents, resulting in a very straight migration from the spawning area to the central area of the Norwegian Sea. After May, some directed swimming was still included to avoid areas colder than 2°C, but was mostly less important than stochastic swimming and resulted in individual dispersion and extension of the horizontal distribution. Passive advection affected fish in both periods and Utne & Huse claimed that currents highly influence the spatial distribution in the second period, as they found very low migration speeds.

The biggest limit of the previous model was the initialisation of the feeding migration at a fixed location between Faroe and Shetland Islands, although empirical evidence for pathway variability around Faroe Islands exists (Hansen & Jákupsstovu, 1992): in years of weaker eastward currents at depth −400 m, catches were more important in the Faroe Bank Channel (South-West Faroe Islands) than in the Faroe-Shetland Channel. Like Utne & Huse (2012), Hansen & Jákupsstovu (1992) suggested that blue whiting partly used passive advection to reach the feeding areas. Looking at temperature and salinity distribution in the study area, high abundance of fish seemed to coincide with the mid-water front formed just south of Faroe Plateau (Hansen & Jákupsstovu, 1992).

Hátún et al. (2007) explained that passive advection and changes in the frontal dynamics might be two of the mechanisms involved in the East-West variation of

migration pathways around Faroe Islands, but they are likely not the most important ones. They proposed other mechanisms, such as an hypothetical swimming ability that allows adult to stay in optimum hydrographic conditions, swimming following gradients of increasing food availability, or variations in spawning distribution. Hansen & Jákupsstovu also pointed out the possible need for a swimming ability that would keep them in the frontal area, however Hátún et al. argued that the required level of swimming ability would be too high for blue whiting. According to Chapman et al. (2011), assessing flow direction is very difficult for pelagic fish, which is why the majority of swimming orientation responses observed are the full drift response: fish swim in the direction of their targeted area, disregarding currents entirely, which results in a drift.

Among the last two potential mechanisms affecting migration pathways, a food-gradient directed migration was the less clear (Hátún et al., 2007), although Nøttestad et al. (1999) counted food abundance and distribution as one the main drivers of large-scale migration. The driver may likely affect migration only once fish arrived in the Norwegian Sea where food is more abundant (Nøttestad et al., 1999). While in the early stage of the migration, between the spawning areas and Faroe Islands, it would require adults to be able to detect very light changes in local food availability, and there are currently no evidence for such strong sensing abilities for blue whiting. Therefore Hátún et al. disregarded food availability as a driver for feeding migration. According to them, variable spawning distribution is the most important mechanism. They claimed that a dominant migration to the West of Faroese Islands was caused by a greater number of fish departing from the Rockall Plateau, due to a westward expansion of the spawning grounds.

After the larval stage, the location of freshly recruited juveniles will highly affect their future migratory behaviour. The recent study by Post et al. (2019) has implicitly revealed that larval retention over the Rockall Plateau and recruitment of juveniles in this area may lead to a very different annual migration. Using general additive models (GAMs) on bottom trawl survey data from Greenland waters to understand variations of catch at age in both space and time along the Greenland shelf edge (GSE), they found that age-0 juveniles start to appear east of Greenland around August and seem to migrate westward into the South-western areas of the GSE. Since no spawning event has been yet observed in Greenland

waters (Post et al., 2019), the apparition of juveniles east of Greenland seems to indicate that they came from the main spawning grounds in the East, most likely from the Rockall region or Icelandic waters. Post et al. suggest that blue whiting juveniles use the GSE as a nursery habitat until maturation. According to their models, mature adults were mostly found East Greenland early in summer and then would progressively disappear throughout summer from the region. Their results suggest that after maturation, fish from West Greenland come back to eastern areas. The presence of mature adults east of Greenland every year around June seems to indicate that they too spawn in the main blue whiting spawning area, before migrating back towards Greenland early in summer for feeding.

Recruitment of juveniles in both the Norwegian Sea and North Sea nursery area may have a potential effect on blue whiting total abundance farther North in the Barents Sea. Heino et al. (2008) observed a positive relationship between years of strong first year recruitment and abundance in the Barents Sea the following year, as well as a strong positive correlation between abundance in the Barents Sea and incursion of warmer and more saline waters into the area from the South, mostly with a time lag of 1-2 years. At first, this seems to suggest a northward expansion of the feeding distribution into the Barents Sea due to an increase in population density and competition for food in the Norwegian Sea following years of strong recruitment. In fact, Utne et al. (2012b) showed that the area occupied by blue whiting in the Norwegian Sea could be positively correlated to TSB values. However, length measurements of fish caught in the Barents Sea revealed peaks of juvenile abundance (length under 19 cm) in years of high abundance in the area (Heino et al., 2008), and it seems likely that stronger shelf edge currents might have also favoured transport (and perhaps migration as well) of juveniles into the Barents Sea from the nursery areas in the North Sea and along the shelf, south-west of Norway.

In a survey performed along the French and Spanish continental shelf in March-April by Carrera et al. (2001), trawl samples mostly contained immature individuals. Mature adults caught during the survey were mainly young adults. By the end of March, spawning is supposed to have ended in the southern part of the spawning grounds and adults to have left for their feeding migration (Pointin & Payne, 2014). Compared to the northward feeding migration, the low presence

of mature adults along the shelf in the Bay of Biscay is not a sufficient proof for a southward post-spawning adult migration. However, Carrera et al. suggested that a juvenile migration or passive transport from South of Porcupine Bank or a juvenile recruitment from southward drifting larvae is very likely. Based on this, it was hypothesised that most adults spawning in the Porcupine Bank area, including first spawners from southern nursery areas, would join the northward feeding migration in late March.

1.3.3   Spawning time and distribution

Knowledge on spawning distribution and timing mostly come from the study of larval distribution (e.g. by CPR), acoustic surveys and fishery catch distributions. Concentration of fish along the continental shelf off British Isles seems to start appearing and increasing in January-February, especially in the Porcupine region (Monstad, 1990), and larvae have been sometimes recorded in the Bay of Biscay around the same early period (Bailey, 1982; Pointin & Payne, 2014). The high season for spawning is known to be around March-April (Bailey, 1982; Skogen et al., 1999), with most fish distributed along the continental edge from North Porcupine Bank to Faroe Bank (Bailey, 1982; Pointin & Payne, 2014). Spawning over the Rockall Plateau would take place around the same time, although the presence of spawners in the region fluctuated between years (Hátún et al., 2007). Some spawning events have also been observed south of Iceland and along the Norwegian shelf later around May-June (Bailey, 1982). Recent studies suggest that spawners arriving from the South will spawn in the most southern parts of the spawning grounds, while spawners from the Norwegian Sea will essentially be distributed over the Rockall Plateau and the continental shelf edge between the northern side of Porcupine Bank and Faroe Islands (Keating et al., 2014; Mahe et al., 2016). Thanks to Post et al. (2019), we also know that part of the spawning population over Rockall Plateau might be arriving from Greenland waters.

Many studies investigated the causes of variation in spawning distribution and the consequences for stock recruitment (Hátún et al., 2007, 2009b; Payne et al., 2012; Gastauer et al., 2016; Miesner & Payne, 2018). In some years, the spawning population seemed to have a more western distribution, with fish occupying more of the Rockall Plateau (Hátún et al., 2007; Gastauer et al., 2016). As mentioned

in the last section, this could affect feeding migration pathways (Hátún et al., 2007), but it could also affect recruitment. For example, Payne et al. (2012) suggest that eggs, larvae and/or juveniles around Rockall Plateau might be less affected by mackerel predation, since mackerel distribution seems to stay confined to the shelf during the spawning period. Thus, a westward expansion of the spawning distribution could be beneficial for recruitment.

It seems also possible that recruitment has an effect on the spawning distribution itself. Gastauer et al. (2016) observed a strong positive correlation between the area occupied by the population during the spawning season and the total stock size. In years of high stock values, the area expanded westward over the Rockall Plateau. The average depth of the distribution also increased during those years, while the mean age of the population dropped. Their results also suggested that this westward expansion of the distribution is mainly conducted by fish of 2 years old and older, most likely forced to move farther from the continental shelf edge to make space for 1-year fish, whose densities over the shelf edge would increase in years of strong recruitment.

While variation in stock size may cause variation in total area occupied by spawners, it seems that the optimum physical conditions for spawning are always met in the resulting spawning area. Optimum spawning conditions are defined by a minimum temperature of 9°C (Bailey, 1982; Bailey & Heath, 2001; Hátún et al., 2009a; Miesner & Payne, 2018), a salinity range of 35.3-35.5 (Miesner & Payne, 2018; Hátún et al., 2009a; Bailey & Heath, 2001; Bailey, 1982), and a depth range of 250-600 m (Miesner & Payne, 2018; Gastauer et al., 2016). In their study using an SDM (Species Distribution Model), Miesner & Payne (2018) showed that variation in salinity over the spawning grounds seems to be one of the main factors responsible for spatial shifts observed in the spawning distribution. A westward and northward shift of the spawning area seems to happen in years of warm and saline waters present all over Rockall Plateau (Hátún et al., 2009a; Miesner & Payne, 2018). Those hydrographic changes are strongly linked with climate processes, especially changes in the subpolar gyre strength (Hátún, 2005), which is the focus of the next section.

1.3.4 Effects of the subpolar gyre

Regional oceanography of the North-East Atlantic is mainly defined by the subpolar gyre (SPG) and its anti-clockwise circulation (Hátún, 2005). In the South and in the East, the SPG is bordered by the North Atlantic Current (NAC). The SPG is characterised by colder and fresher waters than the subtropical gyre (STG) waters brought by the Gulf Stream and the NAC into the eastern areas off Europe. The NAC position and the water-mass distribution off the British Isles seem to be controlled by the SPG strength (Hátún, 2005). Häkkinen & Rhines (2004) showed that a strong decline in the subpolar gyre strength took place in the 90s, and according to Hátún (2005), those variations affected distribution of water-masses, with warm and saline water intrusion found farther North along the continental shelf edge and over Rockall Plateau in years of weak SPG than in years of strong SPG (fig. 1.7).

(a) Strong SPG
(b) Weak SPG
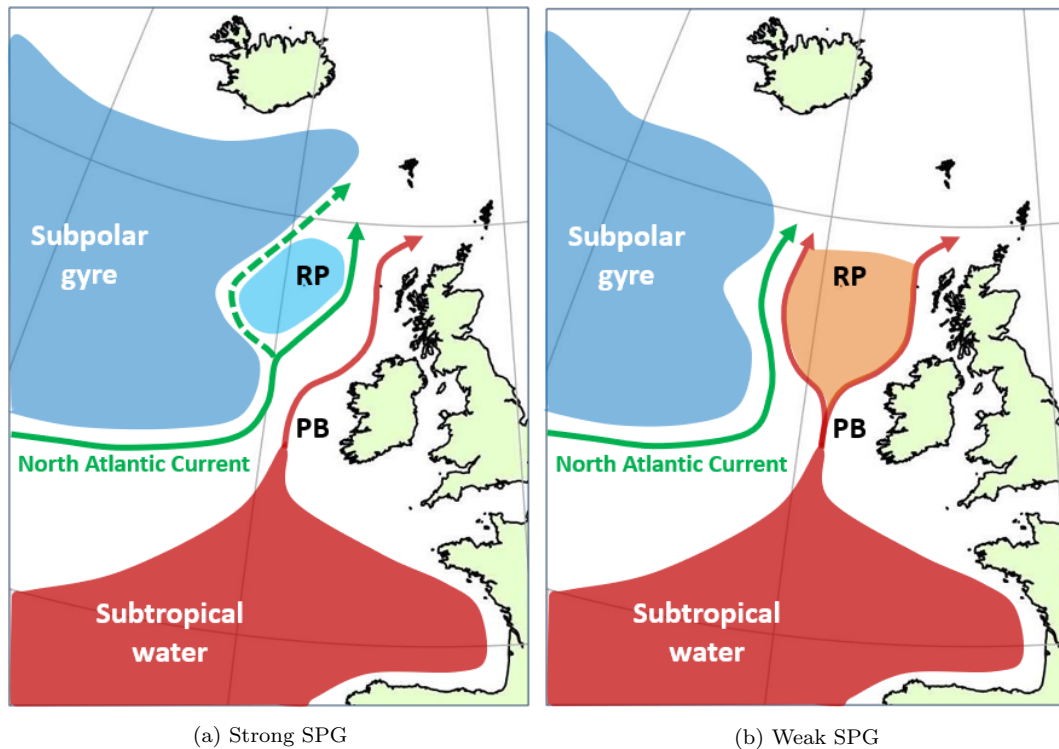
Figure 1.7: Simplified representation of the subpolar gyre dynamics with its anti-clockwise circulation bordered by the North Atlantic Current (NAC) in the South. During years of strong SPG, the NAC brings cold and fresh SPG water into the Rockall Plateau area (a), while the weakening of the SPG may result in the intrusion of warm and saline STG water into that same area (b) (after the figures from Hátún et al. (2007) and from Payne et al. (2012)).

A few studies argue that changes in subpolar gyre dynamics may be responsible for the variations observed in stock abundance and distribution of many species present in the region (Hátún et al., 2009b, 2016; Trenkel et al., 2014). For blue whiting, Payne et al. (2012) suggested that the subpolar gyre strength may have a negative direct and/or indirect effect on recruitment success. Figure 1.8 shows an updated version of the time-series presented in Payne et al.'s paper, using R and SSB values from ICES WGWIDE report (2019b) and available SPG-I values computed by the model from Berx & Payne (2017). We note here that the choice of the subpolar gyre index plays an important role in formulating hypotheses on the relationship between SPG and population dynamics. Payne et al.'s assumption of a relationship between recruitment and the subpolar gyre strength is based on the reversed SPG index computed by Hátún (2005), which
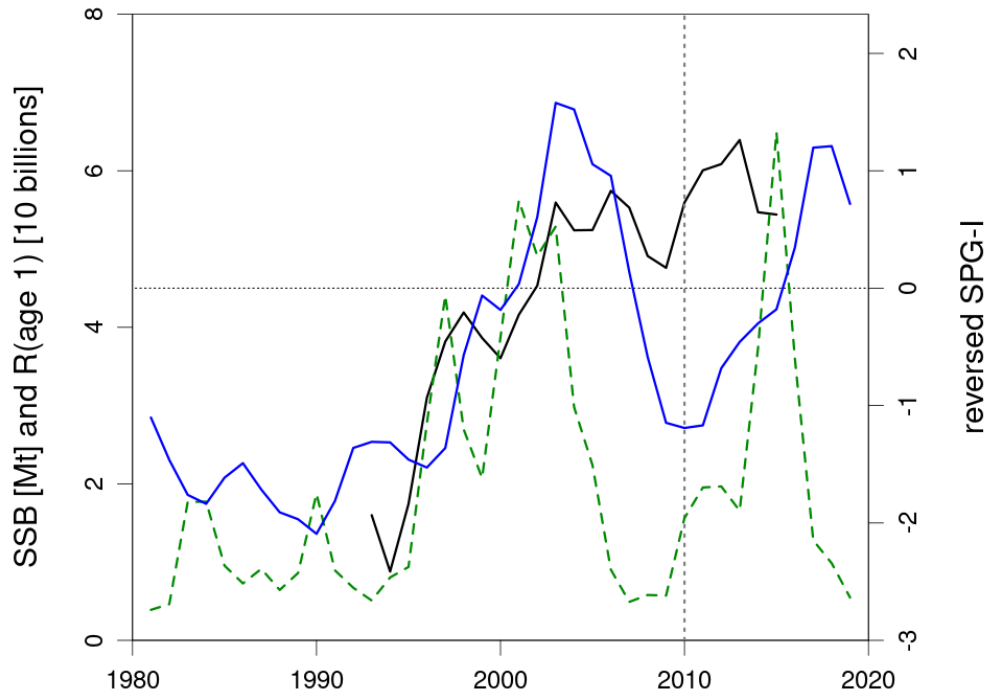
Figure 1.8: Time-series of blue whiting spawning stock biomass [million tonnes] (SSB, solid blue line) and recruitment at age 1 [10 billions] (R(age 1), dashed green line) both estimated by ICES (2019b) and compared here to the reversed subpolar gyre index (reversed SPG-I, solid black line) computed by Berx & Payne (2017) for the period 1993-2015. The reversed SPG-I value decreases with increasing subpolar gyre strength. This plot is based on similar figures in the paper by Payne et al. (2012), although their time-series stopped in 2010 (represented here by the vertical dotted line).

suggested changes of greater amplitude than the SPG-I from Berx & Payne (2017) between some years (e.g. 1998-2000). As a consequence, the relationship between SPG strength and 1-year recruitment becomes insignificant when using SPG-I: it seems unlikely that a decrease in SPG strength might be the direct cause for an increase in first-year recruitment. In the time-series, recruitment tends to start increasing before or in same years as SPG weakening events (e.g. in 1998-2003). However, the time-series present a negative correlation between SSB and SPG strength for the same years, and suggest that the subpolar gyre strength might affect the abundance of spawners off British Isles.

As we saw in the previous section, the spawning area seems to match with a certain range of salinity (Miesner & Payne, 2018). Spatial distribution of salinity in the area is strongly affected by climate dynamics involving both SPG and STG (Hátún, 2005). The optimum salinity range for spawning is associated with STG waters which are warmer and more saline than SPG waters. Thus, more western and northern spawning distribution were observed in years of weak subpolar gyre (Hátún et al., 2007, 2009a). In their study, Hátún et al. (2007) explained that those East-West variations in the spawning distribution are the main direct cause for observed East-West variations in dominant feeding migration pathway around Faroe Islands. This would explain why the feeding migration pass predominantly west of Faroe Islands in years of weak subpolar gyre Hátún et al. (2007, 2009a).

Finally, there are some evidence for climate effects on larval/juvenile drift/migration, mostly visible in areas at the extremities of the population habitat. In the Barents Sea, peaks of population abundance seem to take place 1-2 years after an intrusion event of warm and saline Atlantic waters North of Norway (Heino et al., 2008). This could potentially be caused by changes in SPG dynamics that would result in stronger shelf edge currents. It would then improve success of larvae drifting into suitable nursery habitats in the Norwegian Sea and help juveniles into reaching more northern areas such as the Barents Sea (Heino et al., 2008). In Greenland waters, Post et al. (2021b) found a positive correlation between blue whiting abundance present along the coast and the local temperature average. This seems to indicate that an ocean warming followed by further weakening of the subpolar gyre might increase blue whiting recruitment success in those waters.

1.4 Population structure

Since the 70s, the blue whiting fishery in the North-East Atlantic has always been managed as one single population unit. But the legitimacy of a single blue whiting population in this area started to be questioned by a part of the scientific community in the end of the 70s, when studies started highlighting some phenotypic differences between distinct areas (Bailey, 1982). This raised the question about the potential existence of population subunits that are genetically distinct.

As discussed previously, Skogen et al. (1999) modelled the larval drift in the Porcupine Bank area, and found two drifting directions, one towards the North and one towards the South, and claimed that it could result in population differentiation.

Studies that supports the existence of at least two distinct populations of blue whiting in the North-East Atlantic, are often non-genetic. Thus, Brophy & King (2007) analysed otolith growth histories of adults sampled on both spawning and feeding grounds, and argued that blue whiting growing as larvae in the Bay of Biscay tend to occupy the most southern part of the spawning grounds, and do not migrate to the main feeding ground in the Norwegian Sea. Their study highlighted significantly faster larval growth rates in the Bay of Biscay than in any other regions in the North. On the spawning grounds, except for one case, otolith growth rates seemed to increase from the northern to the southern part, which suggested that fish that grow as larvae in the Bay of Biscay, most likely end up in the southern spawning grounds. The fact that they found no individuals in their samples from the Norwegian feeding ground with growth rates matching those of the Bay of Biscay, would indeed suggest at first that fish from the Bay of Biscay do not migrate into this main feeding ground. However, this observation should be taken with precaution, since this study only considered adults with ages from 1 to 4 years old. These individuals are most likely first-time spawners (Bailey, 1982), and so the former observation is alone insufficient to reject a possible migration towards the Norwegian Sea after their first spawning. Moreover, in Brophy & King's study, the two samples taken in the Norwegian Sea in July/August 2003 could have easily missed individuals coming from the southern parts of the spawning grounds, for spatial or temporal reasons.

Other otolith studies from Keating et al. (2014) and Mahe et al. (2016) analysed

the blue whiting otolith shape, and performed cluster and principal component analyses for identifying potential different populations. Both claimed to have found evidence for two distinct populations of blue whiting in the North-East Atlantic, one based in the northern part of the distribution range, and the other in the South. From their analyses of otolith shapes of individuals between 1 and 13 years old sampled over the whole distribution range, Mahe et al. (2016) split the population in two clusters. While one cluster was only characterized by northern individuals, the second was composed of individuals from every sampled areas. This suggests that although the southern individuals endure an early life history different from the northern individuals, they likely mix with the main population on the main spawning grounds, as well as on Norwegian feeding grounds. Thus, in the absence of genetic evidence for population differentiation or in the absence of evidence for fidelity to spawning areas, this study seems to support the existence of one single blue whiting population unit. Formerly Keating et al. (2014) investigated the population structure specifically from spawning ground samples. They also distinguished two distinct otolith morphotypes, and found that these had different latitudinal distributions, with one cluster occupying preferentially the northern part of the spawning grounds, while the other occupied the southern part. Mixing between both clusters was observed around the Porcupine Bank area. Since this study involved 6 and 7 year-old fish, this could indicate that repeat-spawner with southern early life history show some degree of affinity to their first spawning ground by occupying the most southern part of the spawning distribution. However, these results are also to be interpreted carefully, since one of the two sampling year presented only one otolith morphotype. Moreover, when the average outline of the two otolith shapes identified by Keating et al. (2014) are compared with those from Mahe et al. (2016), we find paradoxically that the larger otolith shape which corresponded to individuals from the southern part of the spawning grounds in the former study, corresponded to northern individuals in the latter. Thus, it seems very difficult to postulate the existence of two distinct blue whiting populations with life history divergence as only evidence.

Genetic studies of the blue whiting population are very scarce (Giæver & Stien, 1998; Ryan et al., 2005; Was et al., 2008). The first one performed by Giæver & Stien (1998), seemed to provide some evidence for genetic differentiation between both extremes of the distribution range. But in this former study, variations

of allele frequencies between regions were rarely significant enough: only two samples in the Barents Sea showed significant differences in allelic proportions with the Norwegian Sea, and for just one locus. Even the genetic differences between the Mediterranean Sea and the main spawning ground were not highly significant. Moreover, differences were detected neither over the main spawning grounds, west of the British Isles, nor between these spawning grounds and the Norwegian Sea, suggesting that all individuals spawning in this area belong to the same population. Since the study was based on only two enzyme loci, the evidence was not sufficiently conclusive.

Using one mini-satellite and five micro-satellite loci, Ryan et al. (2005) gave a stronger evidence for a genetic differentiation between the extremes of blue whiting distribution range. They also highlighted some significant genetic variations on the main spawning grounds, in Porcupine Bank and the Hebridean Sea, especially between the two sampled years in the Hebridean Sea, in 1992 and 1998. According to Hátún (2005), 1992 corresponded to a year with a strong subpolar gyre, whereas the subpolar gyre was weak in 1998. We could then argue that genetic segregation on the spawning grounds may also be affected by the subpolar gyre dynamics. This theory is also supported by the other pairwise FST values and heterogeneity comparisons between samples of the spawning grounds: the genetic differentiation between the Hebridean Sea and the Porcupine Bank, which was significant in 1992 but not in 1998, suggest that a strong gyre would increase the genetic segregation. In a context of two genetically distinct populations, increasing gyre strength could force the southern spawners to stay in the warmer waters of the southern areas of the spawning grounds, while a gyre weakening might improve habitat suitability of western and northern areas (Miesner & Payne, 2018) and cause southern spawners to migrate farther north and mix with northern spawners.

The most recent study in blue whiting genetic structure (Was et al., 2008) provides the strongest evidence for a genetic structuring of the population in the North-East Atlantic, and sections were identified as potential barriers to gene flow between areas. A first identified barrier seems to separate the Bay of Biscay from the rest of the population, a second barrier and third barrier also suggest a strong genetic differentiation between the population residing in the Celtic Sea and the rest. A last barrier was suggested for the north-western part of the Rockall

Plateau. In the light of the study performed by Post et al. (2019) on the Greenland population of blue whiting, the fourth barrier could mark the presence over Rockall Plateau of spawners that migrated from Greenland waters (see section 1.3.2). While other studies supported the existence of two distinct populations, Was et al.'s study suggests a more complex genetic structure of the population with at least three distinct subunits, which presented significant genetic differentiation from the main population distributed between Porcupine Bank and Faroe Islands. These subunits might be the result of larval drift (Bay of Biscay), retention of larvae (Celtic Sea), and passive transport of juveniles to different nursery areas (Greenland waters). However, in the Bay of Biscay, genetic differentiation could be exclusively caused by first-time spawners spawning south of Porcupine and by the subsequent southern drift of larvae from this area. Was et al. (2008) noted that Bay of Biscay samples only included fish of 1-2 years old, suggesting that after their first spawning, fish from this population subunit might be joining and mixing with the main population unit for their annual migration cycle.

1.5 Conclusions

In this review, knowledge was gathered on the blue whiting ecological dynamics, which will be very useful to consider in the building process of the spatial population model (e.g. fecundity function, maturity at length, diet composition, density dependence, spawning optimum conditions). Some other elements will most likely impact the modelling approach, especially with regards to spatial dynamics. For example, we will want to reproduce main migration patterns while avoiding stilted approaches of movement modelling, so that the effects of environmental drivers on migration pathways and success can be studied. Therefore, the following modelling work will first aim at investigating the role of different physical and biological factors in driving blue whiting adults to their main feeding grounds.

The current empirical evidences for a distinct differentiation between a southern stock and a northern stock, roughly separated by Porcupine Bank, were not considered sufficient, and so population structure will not be addressed in the model. Even in the presence of a genetic population structure, it was hypoth-

esised that new mature adults from the Bay of Biscay, once they spawned for their first time, will share the same annual migration cycle than the majority of the population, likely spawning in more northern locations in following years. However, while stock differentiation will not be included in the model building process, southward larval drift is still expected. Thus any emergent properties from the model regarding population recruitment, distribution and movement might give us a new insight for understanding population structure and will be discussed at the end of this work.

Finally, we noticed how it can be difficult and complex to try and explain recruitment variations with bio-geophysical drivers, such as food, temperature and salinity, when spatial processes are also involved. The effect of the subpolar gyre on recruitment is not clear. In fact, the impact of climate changes on larval drift and population recruitment has yet to be properly investigated. Other unknowns concern the return migration to the spawning areas, in particular how it is triggered and how temperature, salinity, topography and currents may affect its success. Since the objective is to study the effect of these drivers on the spatial dynamics of the population, from the larval stage to mature adults, and their subsequent effect on population growth, a spatial model including all blue whiting life stages and describing the full migration cycle will help investigate all these aspects. Furthermore, the question of how fishing pressure may affect the blue whiting population growth is also an other major concern which will be possible to address with this model.

Part II

The Spatial Population Model

Chapter 2

Life stage and length-structured growth model

The first part of the blue whiting model is focused on individual and population dynamics without the spatial dimension. The blue whiting population growth model was built by combining equations for individual growth (von Bertalanffy) and population growth (recruitment/reproduction and survival). As a consequence, the growth model presents a double structure: (1) a length structure which is used for individual growth, and (2) a stage structure which is used for population growth. Most equations used in this chapter can be found in the book 'Ecological Dynamics' written by Gurney & Nisbet (1998), which was the main modelling knowledge source for building this model. The part of the model code (in `C`) describing growth is available on the GitLab platform (links p. 3).

2.1   Model structure

The following section describes both the life-stage and length structures of the model. Splitting the model into life stages allows us to define growth and vital statistics specific to each life stage. It is also necessary for implementing spatial dynamics (chapter 3) which are different between life stages. Adding a length structure to the model will also benefit us for modelling more accurate fishing, by including length selectivity.

2.1.1 Life stages

Transition between life stages are caused by changes in growth, mortality, habitat and/or maturity. The blue whiting population grows through four life stages: eggs (E), larvae (D), juveniles (J) and adults (A). The base model for this system can be first written as a discrete-time model defined by the following recursion equation:

$$\begin{pmatrix} E_{t+\Delta t} \\ D_{t+\Delta t} \\ J_{t+\Delta t} \\ A_{t+\Delta t} \end{pmatrix} = \begin{pmatrix} (1-H)\,S_E & 0 & 0 & \beta/2 \\ H\,S_E & (1-R)\,S_D & 0 & 0 \\ 0 & R\,S_D & (1-M)\,S_J & 0 \\ 0 & 0 & M\,S_J & S_A \end{pmatrix} \begin{pmatrix} E_t \\ D_t \\ J_t \\ A_t \end{pmatrix}$$

$$(2.1)$$

where E, D, J and A are number of individuals at each life stage class and S the corresponding probabilities of staying in the same life stage after one time step ($\Delta t = 5$ days). β is the fecundity of a female adult per time step, which is null outside spawning season. β is divided by two, as we assume that 50% of the adult population is female. Finally H, R and M are proportion of the population in the corresponding life stage hatching, recruiting or maturing into the next life stage during one time step.

We note here that length structure is not yet included in the model and will be added later. This will lead to modifications in how some parameters are written. For example, the fecundity parameter β which is here a constant will become β_l which is dependent on adult length (section 2.2, eq. 2.15 and 2.16).

The probability S of staying in a life stage at next time step is equivalent to a survival probability but considering both mortality rate and rate of being recruited into the upper life stage. We define the natural mortality rate δ_i in life stage i and the fishing mortality rate F. Thus we write the S functions as:

$$S_E = \exp[-\delta_E \Delta t] \qquad\qquad S_D = \exp[-\delta_D \Delta t] \qquad (2.2)$$

$$S_J = \exp[-(\delta_J + F)\Delta t] \qquad\qquad S_A = \exp[-(\delta_A + F)\Delta t] \qquad (2.3)$$

where fishing F is only applied to juveniles and adults. With the exception of δ_D which is density-dependent (see section 2.3.1), all natural mortality rates δ_i are considered constant.

We define h, r and m respectively hatching, recruitment and maturing rates per unit of time. Those three parameters are also considered as loss rates in continuous time and will be used to write the proportions H, R and M in discrete time. We can express the proportions of the population that do not hatch, recruit or mature with the same function used for survival, and thus write the following recruitment functions:

$$H = 1 - \exp[-h\Delta t] \quad R = 1 - \exp[-r\Delta t] \quad M = 1 - \exp[-m\Delta t] \quad (2.4)$$

Parameters h, r and m are constant rates. Once the length structure is added to the model, R and M will be used only in length classes respectively equal to or higher than minimum length for recruitment L_R and for maturing L_M. There will be no length structure for eggs, and new hatched larvae will be directly transferred into the hatching length class L_H.

2.1.2 Length-structured model

In the literature, blue whiting growth is described as following the von Bertalanffy growth equation (Von Bertalanffy, 1951), and related growth parameters are often estimated from length and age data (Bailey, 1982). While the growth model will mainly be using this equation, we need to come back to basic balance equations to properly define processes and parameters.

We first consider the continuous balance equation (2.5) for individual weight (W) where I is the food uptake rate and ε is the assimilation efficiency. Parameter μ is used to describe the cost rate of staying alive, called the basal maintenance rate, which is assumed to be proportional to body weight.

$$\frac{dW}{dt} = \varepsilon\, I - \mu\, W \quad (2.5)$$

In a varying environment, the food uptake rate I depends on food concentration (ρ). To describe this relationship, we use a Holling type II functional response:

$$I \; = \; I_{\mathrm{max}} \left(\frac{\rho}{\rho_H \; + \; \rho} \right) \tag{2.6}$$

where ρ_H is the half-saturation food concentration and I_{max} is the maximum uptake rate.

Ingestion and assimilation of food also depend on the size of individuals. Larger fish tend to ingest greater abundance of food, which means the maximum uptake rate tends to increase with body size. However, we want to avoid exponential growth and therefore for I_{max} to be volume dependent (Gurney & Nisbet, 1998). The cross-section assimilation model, which considers a proportional relationship between I_{max} and L^2, allows for growth to decrease with increasing weight. Assuming blue whiting keep a constant shape throughout their life, the weight-length relationship is defined by $W \; = \; a \; L^3$, where a is a constant of proportionality. This implies that I_{max} also varies proportionally with $W^{2/3}$.

$$I_{\mathrm{max}} \; = \; \xi \; W^{2/3} \tag{2.7}$$

Now we define $\Phi = \varepsilon \; \xi$ to reduce the number of parameters thereafter, and recast equation (2.6) into balance equation (2.5) which gives us:

$$\frac{dW}{dt} \; = \; \frac{\Phi \; \rho}{\rho_H + \rho} \; W^{2/3} \; - \; \mu \; W \tag{2.8}$$

Using the weight-length relationship, we then rewrite equation 2.8 into the balance equation for length:

$$\frac{dL}{dt} \; = \; \frac{\Phi \; \rho}{3 \; a^{1/3} \; (\rho_H + \rho)} \; - \; \frac{\mu}{3} \; L \tag{2.9}$$

This equation has a steady state and implies that individuals stop growing after reaching a maximum length (L_∞). In the following equation, we see that this maximum length depends on the environmental food concentration.

$$L_\infty \;=\; \frac{1}{\mu \; a^{1/3}} \left(\frac{\Phi \; \rho}{\rho_H + \rho} \right) \tag{2.10}$$

With L_∞, we can rewrite equation (2.9) and find its analytic solution, which is none other than the von Bertalanffy growth equation:

$$L_{t+\Delta t} \;=\; L_\infty \;-\; \left[\, L_\infty \;-\; L_t \,\right] \, \exp\left(-\frac{\mu}{3} \, \Delta t \right) \tag{2.11}$$

Growth differences between blue whiting individuals that lived in the Bay of Biscay and those that lived in the Norwegian Sea in their early life stages (Brophy & King, 2007) suggest that growth might also depend on temperature. Temperature is expected to affect the metabolic rate (μ), the food search rate (σ) and food handling time (τ). The food search rate can also be defined as the probability of capturing food per unit of time, while the handling time corresponds to the time needed by the individual to assimilate one unit of food (Gurney & Nisbet, 1998). With those definitions, we rewrite parameters from the functional response in equation (2.8):

$$\Phi \;=\; \frac{1}{\tau} \qquad\qquad \rho_H \;=\; \frac{1}{\tau \; \sigma} \tag{2.12}$$

To simulate temperature-dependent parameters, we use Q_{10} values. A parameter's Q_{10} value describe the parameter's sensitivity to a temperature change of 10°C. We decide to make metabolic rate, food search rate and food handling time all temperature dependent:

$$\mu \;=\; \mu_0 \, (Q_\mu)^{T/10} \qquad \tau \;=\; \tau_0 \, (Q_\tau)^{T/10} \qquad \sigma \;=\; \sigma_0 \, (Q_\sigma)^{T/10} \tag{2.13}$$

In the Q_{10} relationships for μ, τ and σ (2.13), T is the local temperature value and μ_0, τ_0, σ_0, Q_μ, Q_τ and Q_σ are all constants that need to be estimated. We assume that $Q_\sigma = 1/Q_\tau$, which implies a constant half-saturation food concentration (ρ_H). Thus equation (2.10) for L_∞ becomes:

$$L_\infty \;=\; \frac{(Q_\mu\;Q_\tau)^{-T/10}}{\mu_0\;a^{1/3}}\;\left(\frac{\sigma_0\;\rho}{1\;+\;\tau_0\;\sigma_0\;\rho}\right) \tag{2.14}$$

Equations 2.13 along with 2.14 imply that the spatial model will need inputs of temperature and food fields at each time step to calculate local individual growth. Thus, in the spatial model, L_∞ will vary in time and space with the local values of food concentration and temperature. This means that the actual maximum length reached by fish in their lifetime is not equal to the L_∞ experienced at one single time step. L_∞ is then rather a measure of the environmental conditions experienced at a time t, which tell us the maximum length fish would reach if they were to keep experiencing the exact same environmental conditions for the rest of their lifetime. Environmental inputs to the final model are discussed in chapters 4 and 5.

Finally, we need to include some growth variability among individuals of a same length class at a time t, so that over time, the length distribution of these individuals becomes normal (Gaussian). To do that, we used tent distributions with 0.05 cm length increments and a length variance of 0.25 cm^2. The length variance was chosen so that the final tent distribution of one length class after growth was including at least one neighbouring length class besides the length class comprising the new fish length, with length class increments in the model being 0.5 cm. This was done to ensure that a minimum growth variability took place for each length class at each time step.

2.2 Reproduction

We just combined the length-structured model with the life stage model. Length structure is relevant to adult, juvenile and larval life stages. While the egg life stage does not present any length structure, egg production depends on adult length. Considering equation (2.1) combined with a length structured model, we get the following update equation for eggs:

$$E_{t+\Delta t} \;=\; (1-H)\,S_E\,E_t \;+\; \sum_l \frac{\beta_l}{2}\,A_{t,l} \tag{2.15}$$

where $A_{t,l}$ is the number of adults in length class l at time t.

We used the length-fecundity relationship estimated by Bailey (1982) to estimate the number of eggs released during the spawning season whose duration is χ_s. Thus the length-dependent number of spawned eggs per female, β_l from equation (2.15), is defined by:

$$\beta_l \;=\; \begin{cases} \dfrac{\Delta t}{\chi_s}\, e_0\Big(L_l\Big)^{e_1} & \text{if in spawning season} \\[2em] 0 & \text{otherwise} \end{cases} \tag{2.16}$$

where e_0 and e_1 are fecundity parameters, and L_l is average length in length class l. In the model, the spawning duration χ_s is determined by the number of time steps between the defined starting and end dates of the spawning season. Most of the time, spawning was set to start the 30th of January and to end the 16th of March, for a 50 days long spawning season.

2.3 Mortality and survival

2.3.1 Natural mortality

For the model, different survival equations were tested for larvae, while juvenile and adult survival rates were kept constant. After several test simulations, a model which can describe mortality induced either by larval competition or by predation, was retained. It is defined by the following larval density dependent survival equation:

$$C_{D_t} \;=\; 1\Big/\Big(1 \;+\; c_0 \sum_L \big[\,W_l\,D_{t,l}\,\big]\Big) \tag{2.17}$$

where c_0 is a constant parameter, W_l is the average body weight in length class

l and $D_{t,l}$ is the number of larvae at time t in length class l.

However, once implemented in the spatial model (chapter 3), this density-dependent larval survival caused one problem. In every defined cell of the model, when the larval population density becomes very low, survival rate is so close to 1 that some larvae can stay alive for a very long time. This is problematic for larvae that drift in unsuitable habitats and are unable to grow to be juveniles, since low larval density keep them alive longer than if they were in suitable habitats with high larval density. This issue affects the total population of larvae in the model which seems to never decrease to zero. To solve this, we introduce an intrinsic mortality rate δ_{D_0} which can be explained as the minimum rate at which larvae die, with $1/\delta_{D_0}$ being the characteristic life time expected for one larva with no growth. Thus the final mortality rate for larvae is given by:

$$\delta_D \;=\; \delta_{D_0} \;-\; \frac{\ln\left[\, C_{D_t} \,\right]}{\Delta t} \tag{2.18}$$

2.3.2 Fishing mortality

According to ICES reports on blue whiting stock, fishing rates vary from year to year and seem partially correlated with stock fluctuations. In the historical period of the model, we decided to use ICES values of fishing rate for each year, which are available from 1981 to 2019 (ICES, 2019b). For the projection period, different scenarios were tested, either with constant fishing rate calculated from the last year's fishing rate, or modelling it as a response to the precedent year's catch numbers. The later will not be discussed further in this thesis, however the option can now be activated in the model.

Spatially, two models of fishing were tested. Assuming that spatial distribution of catches reflects the entire spatial distribution of the population (chapter 6), the first model considers the fishing pressure uniformly distributed in space and constant over the year. While it is reasonable to suppose that fishing fleets follow the annual migrations of blue whiting, it would be harder to believe that they fish with the same efficiency in areas with low density of fish than in areas of

high density, and thus they would be likely to target the most productive areas. This fleet's fishing response to local fish density can be modelled by a functional response of type III with the following equation:

$$F_t = [F_Y]_t \; \frac{\left([B_{J,A}]_t\right)^{\kappa+1}}{\left(B_H\right)^{\kappa+1} + \left([B_{J,A}]_t\right)^{\kappa+1}} \tag{2.19}$$

F_Y is the annual fishing rate (same as the constant annual fishing rate used in the first model), B_H is the half-saturation stock biomass concentration, and the power κ determines how sensitive fishing is to changes in local density.

The stock biomass concentration $B_{J,A}$ considers both adults and juveniles:

$$[B_{J,A}]_t = \sum_l \left[W_l \left(J_{t,l} + A_{t,l} \right) \right] \tag{2.20}$$

with W_l the average individual weight in length class l, and $A_{t,l}$ and $J_{t,l}$ the numbers of adults and juveniles at time t in length class l.

The former fishing rate definitions were length independent. The final step in modelling the fishing rate is to make it length dependent to simulate length selectivity caused by fishing gears used in blue whiting fishery (chapter 6). We modify equation (2.19) so that the maximum fishing rate decreases with decreasing length following a sigmoidal function:

$$F_{t,l} = \frac{[F_Y]_t}{1 + f_a \; \exp(-f_b \; L_l)} \left(\frac{\left([B_{J,A}]_t\right)^{\kappa+1}}{\left(F_H\right)^{\kappa+1} + \left([B_{J,A}]_t\right)^{\kappa+1}} \right) \tag{2.21}$$

where f_a and f_b are constant parameters that will be estimated so that the first part of equation (2.21) fits ICES estimations of fishing mortalities at age (chapter 1).

2.4 Conclusions

For this first component of the blue whiting population model, a life-stage structure was combined with a length structure. This made possible the inclusion of survival functions specific to each blue whiting life stage, while describing individual growth with the von Bertalanffy equation. The advantage was a fishing mortality which could then also be a function of length.

Before implementing the spatial model (chap. 3), it is important to note the following features of the population growth model component:

(1) Larval mortality is density-dependent to simulate aggregation effects on either competition or predation.

(2) From larvae to adults, individual growth is food and temperature dependent.

(3) The fishing functional response equation is equivalent to a density-dependent fishing mortality.

Those features will all be depending on spatial variations of one or more variables.

Chapter 3

Spatial dynamics

Special care was taken into implementing spatial dynamics into the blue whiting model. The objective was to study the effect of bio-geophysical variables, such as food, temperature and currents, on population movements. Egg and larva drift was modelled using the Lagrangian particle tracking model `Ichthyop`, well adapted for passive transport with currents. Like larvae, juvenile movement is mostly dispersive and affected by currents. Adult movement however is more complex, including a migration cycle between spawning and feeding areas, and more advanced modelling methods were required.

Formerly, adult population movement was modelled using simple attractors located in spawning and feeding areas, which resulted in poor variability of migration pathways and population distributions. The following chapter describes how an existing particle tracking model (`Ichthyop`) was combined with an adapted version of Ritter's gradient computation method, to model adult migrations driven by environmental factors. Different environmental indices used to define gradients affecting juvenile and/or adult movement were also developed: for the feeding migration, the gradient should depend on both food and temperature variations, while spawning migration requires a gradient leading to areas with environmental conditions suitable for spawning.

3.1 Ichthyop model

3.1.1 Larval drift

The annual population recruitment of blue whiting juveniles might be strongly affected by larval drift, and connectivity between spawning grounds and potential nursery habitats for larvae needs to be assessed. Transport of blue whiting larvae was studied using Ichthyop, a particle tracking model initially designed to model passive transport of fish larvae affected by both currents and diffusion (Lett et al., 2008). Ichthyop is a free Java software, which was run here in batch mode using an editable XML template file with all available options and parameters. Instead of using outputs from the 'Regional Oceanic Modelling System' (ROMS) by Shchepetkin & McWilliams (2005), or outputs from 'Model for Applications at Regional Scale' (MARS) by Lazure & Dumas (2008) (Lett et al., 2008), velocity outputs from the NEMO-Medusa model (Madec & NEMO-team, 2008; Yool et al., 2013b) were used (chapter 4).

In Ichthyop, transport of particles is modelled using advection-diffusion equations with a Lagrangian approach (Lett et al., 2008). Advective movement is determined by the flow velocity fields, while diffusion is implemented following the model from Peliz et al. (2007). In this model, the horizontal diffusion coefficient is defined as:

$$K_h = \epsilon^{1/3} \cdot l^{4/3} \tag{3.1}$$

where ϵ is the turbulent dissipation rate [m^2.s^{-3}], and l is the length of the grid cell (value calculated by Ichthyop).

As advised by Monin & Ozmidov (1981) (Peliz et al., 2007), The value $\epsilon = 1.0 \cdot 10^{-9}$ m^2.s^{-3} was also used for blue whiting eggs and larvae. Ichthyop time step was set so as to not break the Courant–Friedrichs–Lewy (CFL) condition to ensure that the resulting particle movements reflect the data accuracy of flow variations in time and space. The distance travelled by a particle in one time step must be lower than the distance between two neighbouring grid cells' centres. For passive transport with NEMO velocity fields, the Ichthyop time step was fixed

to 1800 seconds. The tracking model interpolates flow velocity in time and space to allow for estimation of local velocity at the new particle position in each time step (Lett et al., 2008).

At the boundaries (coastlines), particle behaviour was set to bouncing. It means that if during one `Ichthyop` time step some particle movement forces them to cross a coastline, they would be repositioned in the ocean in a symmetrical location to the one they would have been inland had they not bounced on the coastline.

For the model's needs, particle release (also referred as spawning in Lett's paper) was designed so that 100 particles were initialised in the upper ocean layer (depth ≥ -50 m) at the centre of each ocean cell of the model grid and at the start of each model time step (5-day time steps). However, in an exploratory stage, other release options were also used, such as zone or patch release, and `Ichthyop` was run over longer time periods (up to 180 days of tracking). In particular, some tracking experiments were designed to study larval drift from hypothetical spawning areas. A sample of tracking results are available in appendix B. They show larva distributions very similar to the study from Bartsch & Coombs (1997).

3.1.2 Adult movement in `Ichthyop`: from passive to active advection

As `Ichthyop` was specifically designed to simulate passive transport and diffusion, the model in its original form is not suitable for adult migration modelling. There is however a very straightforward way of including active transport to `Ichthyop` by adding swimming velocities directly to the NEMO flow fields used in the particle tracking model. A similar method has been used before by Putman et al. (2012) where they added swimming velocity in defined areas to simulate migration of young loggerhead sea turtles. In the blue whiting case however, swimming velocity is added to the flow velocity for each cell of the NEMO grid before being used as input in `Ichthyop`. Thus, `Ichthyop` produces tracks that result from both currents and swimming combined.

Implementing swimming externally to `Ichthyop` has a few advantages. First, it gives the opportunity for easy implementation of swimming rules while focusing only on local swimming direction and speed at a time t. Swimming rules can include very basic boundary conditions, such as swimming parallel to the coastline or to a defined isobath. They also can include large scale behaviours, such as migrations where direction and speed can either be constant or dependent on environmental factors.

The second advantage of this method is the possibility of modifying the NEMO 3D flow field so that it always reflects currents experienced by fish at their average swimming depth. In fact, controlling swimming depth is very complicated within `Ichthyop`. For the blue whiting model, spatial movement shall be kept in 2D. In the particle tracking model, it is possible to turn off vertical advection and stay at the same depth layer for the whole run. While larval drift did not cause much problem because of their transport in the surface layer (≥ -50 m), the fact that adults are mesopelagic with an average swimming depth of -450 m but also can move in slightly shallower waters (< -200 m) made their swimming depth highly dependent on the release location in `Ichthyop`. Adult individuals released in much shallower waters than their average swimming depth will keep swimming at that depth for the whole tracking simulation which is very inconvenient as hydrodynamics experienced by those individuals would not be the same than those experienced at the average swimming depth. To force all individuals released in `Ichthyop` to move according to the same flow field independently from their initial swimming depth, all depth layers of the new velocity fields are identical. This results in blue whiting adults always swimming either at -450 m depth or at 90% of the water column depth if they end up in shallower waters.

New velocity fields U (longitudinal) and V (latitudinal) are produced by adding fish swimming velocity components to the corresponding NEMO flow field:

$$U = U_{\text{flow}} + U_{\text{swim}} \qquad\qquad V = V_{\text{flow}} + V_{\text{swim}} \qquad (3.2)$$

The first step in modelling adult movement was to define a default swimming

rule which would be used whenever no other swimming rules exist or can not be applied. Blue whiting's size range suggests they would not compensate currents to move in the direction they want but rather drift with them (Chapman et al., 2011) and avoid swimming against currents if the resulting movement is not beneficial. In the case fish have no other than currents as driver for orientation, the swimming direction was assumed to be determined by what Chapman et al. (2011) called active downstream orientation. Therefore, by default, blue whiting would swim at their average speed ($\bar{v}$), following the currents direction (θ_{flow}):

$$U_{\text{swim}} = \bar{v} \, \sin(\, \theta_{\text{flow}} \,) \tag{3.3}$$

$$V_{\text{swim}} = \bar{v} \, \cos(\, \theta_{\text{flow}} \,) \tag{3.4}$$

Fish's average swimming speed is assumed to be equal to body length per time unit (Varpe et al., 2005). For adults, an average speed ($\bar{v}$) of 0.25 m/s was considered for an average length of 25 cm. For some migration behaviours developed in next sections, the juvenile population was also included, and therefore we assumed an average speed of 0.20 m/s for an average length of 20 cm. This choice was made to reduce the number of transport matrices needed for the final model.

3.1.3 Connectivity matrices

Larva, juvenile and adult movement is modelled and calculated for each time step externally (5-day `Ichthyop` runs). Then it is stored in the form of connectivity or transport matrices which are used in the final spatial population dynamic model. For each cell in the model grid, the transport matrices give a list of estimated destination cells. For each destination cell, the estimated proportion of the starting cell population ending up in this final position are given. Each transport matrix is the result of a 5-day run in `Ichthyop` with the release of 100 individuals at the centre of each water cell of the model and at the correct depth.

In total, 72 transport matrices were produced per year from 1988 to 2050 for each type of population movement: larval drift (passive transport and diffusion in the sea surface layer), adult spawning migration (orientated movement with

drift by currents and dispersion, movement directed towards suitable spawning grounds), juvenile and adult feeding migration (orientated movement with drift by currents and dispersion, movement directed towards areas with higher food concentration), and juvenile/adult stochastic behaviour (non-orientated movement, only dispersion and drift with currents).

3.2 Migration driven by environmental factors

Blue whiting undertake migrations to switch between spawning and feeding areas in an annual cycle. Because fidelity to those spawning and feeding areas were observed, the simplest way to implement such migrations would be either to define the centre of gravity of those areas as simple attractor, so swimming directions would always point towards it, or to define some biological compass that would influence the general direction of movement and would lead individuals to those areas. However such methods considerably reduce variability in migration pathways and spatial distribution.

To study the effect of varying environment on population spatial dynamics, movement has to depend on environmental factors like temperature or food. We assume that individuals move towards areas with better environmental conditions. In this context, orientation would be determined by the local environmental gradient field.

This section describes the methods and algorithms used for computing the new velocity fields that combine both flow velocity components and directed swimming velocity components. The `R` code developed to produce the new fields to be used in `Ichthyop` is also available on the GitLab platform (links p. 3).

3.2.1 Gradient calculation method

A gradient field can be defined as a vector field in which each vector's direction and length at a location p represents the direction and rate of the fastest increase observed in a scalar field at that location. Direction and rate of fastest increase are respectively called aspect and slope. Algorithms to compute those values have been well developed for topography and are commonly used in geographic

information system (GIS). The data used to calculate aspect and slope is usually referred as elevations.

The common method to compute aspect and slope of a grid cell is to consider elevation values in its neighbouring cells and to derive two one-dimension gradient values in orthogonal directions (i.e. West-East and South-North). Differences between algorithms mostly reside in the number of neighbours considered (2 to 8) and whether or not their values are weighted by distance to the central cell. Based on algorithm comparison
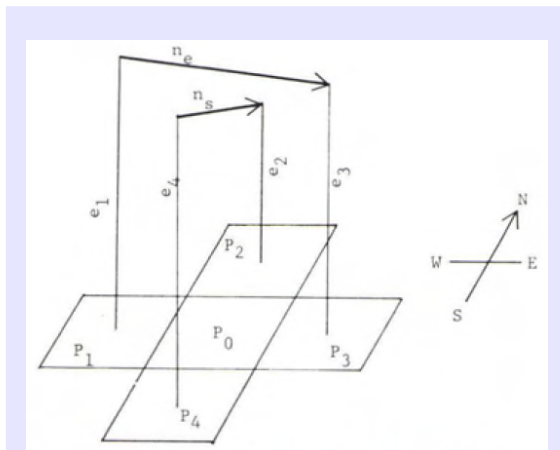
Figure 3.1: Schema from Ritter (1987) showing neighbouring cells involved in calculating aspect and slope for cell P_0, and the two orthogonal vectors $\mathbf{n}_E$ and $\mathbf{n}_S$. The lines e_1, e_2, e_3 and e_4 represent elevation values for each neighbouring cell.

studies of computation errors for both aspect and slope (Jones, 1998; Zhou & Liu, 2004), I first decided to use the method of Fleming & Hoffer (1979) but using the algorithm described by Ritter (1987). This algorithm considers four neighbouring cells and calculates the normal vector of a cell, which is the cross product between two orthogonal vectors, describing a gradient in the South-North and West-East directions (Fig. 3.1):

$$\mathbf{n} = \mathbf{n}_E \times \mathbf{n}_S \tag{3.5}$$

$$= (2d, 0, e_3 - e_1) \times (0, 2d, e_2 - e_4) \tag{3.6}$$

$$= (-2d(e_3 - e_1), -2d(e_2 - e_4), 4d^2) \tag{3.7}$$

where e_i is the elevation value in cell i and d is the distance between two adjacent cell centres either in the horizontal or vertical.

This algorithm is valid assuming the grid axes are aligned with W-E and S-N directions and assuming distance between adjacent cells in both directions are always equal. This is not the case of NEMO's grid whose axes might locally present deviations from the W-E and S-N directions (i.e. from -4° to 37° angle

deviation between longitudes 30°W-20°E and latitudes 40°N-80°N) and distance between adjacent cells decreases with increasing latitude. Thus I needed to adapt Ritter's algorithm to an 'irregular' grid like NEMO's.

In the model context, we need environmental gradient fields to orientate blue whiting movement and to simulate long distance population migrations that would target areas with best environmental conditions (food, temperature and/or salinity). Therefore, we need gradient fields that reflect larger scale gradients rather than being locally accurate.

Instead of adjacent cells, to calculate the gradient in a cell with centre p, we consider all cells inside a circle with centre p and radius Θ (Fig. 3.2). Thereafter, we refer to Θ as the gradient scale. Then, the circle area is split in four quarters, one for each cardinal direction, and the simple arithmetic means of elevation ($\bar{e}$) and distance from p ($\bar{d}$) are calculated. In the case that the circle includes land cells (Fig. 3.2b) or is overlapping the grid's boundaries, less cells are considered in some quarters to compute elevation and distance values. If one quarter does not have any cell, we use the elevation value in the central cell.

Once we calculated elevation and distance values, we define a normal vector whose coordinates (n_x,n_y,n_z) have the following values:

$$n_x = (\bar{e}_E - \bar{e}_W)(\bar{d}_E + \bar{d}_W) \tag{3.8}$$

$$n_y = (\bar{e}_N - \bar{e}_S)(\bar{d}_N + \bar{d}_S) \tag{3.9}$$

$$n_z = (\bar{d}_N + \bar{d}_S)(\bar{d}_E + \bar{d}_W) \tag{3.10}$$

where $\bar{e}_i$ and $\bar{d}_i$ are respectively average elevation and distance in quarter i.

In Ritter's algorithm, aspect is defined as the direction angle from the highest elevation value to the lowest, while we are interested in the opposite direction for the gradient. This is why n_x and n_y are of opposite sign than in the formulas described by Ritter (1987).

In the final step, the normal vector is used to calculate the gradient direction θ_g (similar to Ritter's aspect; in radian) and its value g (slope; in percent) as

(a) No land cells.

(b) Land cells present in quarters N and W.
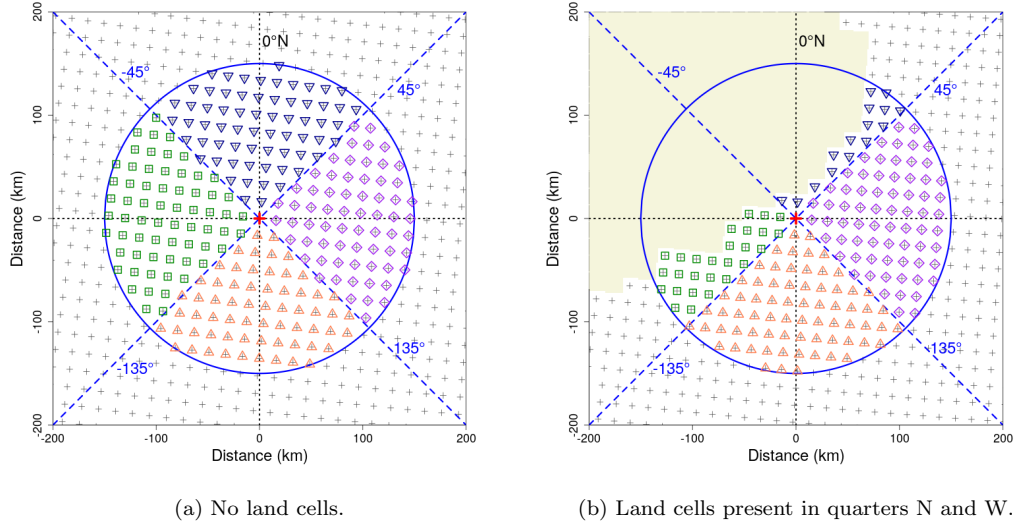
Figure 3.2: Examples of group of cells used in the new gradient algorithm for an irregular grid system like NEMO's. Every cells whose centre is inside the circle of radius Θ are used to calculate the local gradient (red cross). The gradient calculation area is split in four quarters and average elevation values and distance from central cell are calculated for N, E, S and W quarters. In these examples, the gradient scale is $\Theta = 150$km.

follows:

$$\theta_g = \begin{cases} \pi/2 - \beta & \text{if } n_x < 0 \\ -\pi/2 - \beta & \text{if } n_x > 0 \\ \pi & \text{if } n_x = 0 \text{ and } n_y > 0 \\ 0 & \text{if } n_x = 0 \text{ and } n_y < 0 \\ \varnothing & \text{if } n_x = n_y = 0 \end{cases} \quad \text{where} \quad \beta = \tan^{-1}\left(\frac{n_y}{n_x}\right)$$

(3.11)

$$g = 100\frac{\sqrt{n_x^2 + n_y^2}}{n_z}$$

(3.12)

The advantage of the new algorithm is its flexibility. It is well adapted to irregular grid systems since the local gradient of any cell is always calculated from cells within a same distance from its centre. Thus, at the lowest possible value for the gradient scale - minimum radius that ensures at least one cell in each quarter is selected for gradient computation - and in a grid defined by regular longitudinal and latitudinal intervals between cells, the gradient computed at low
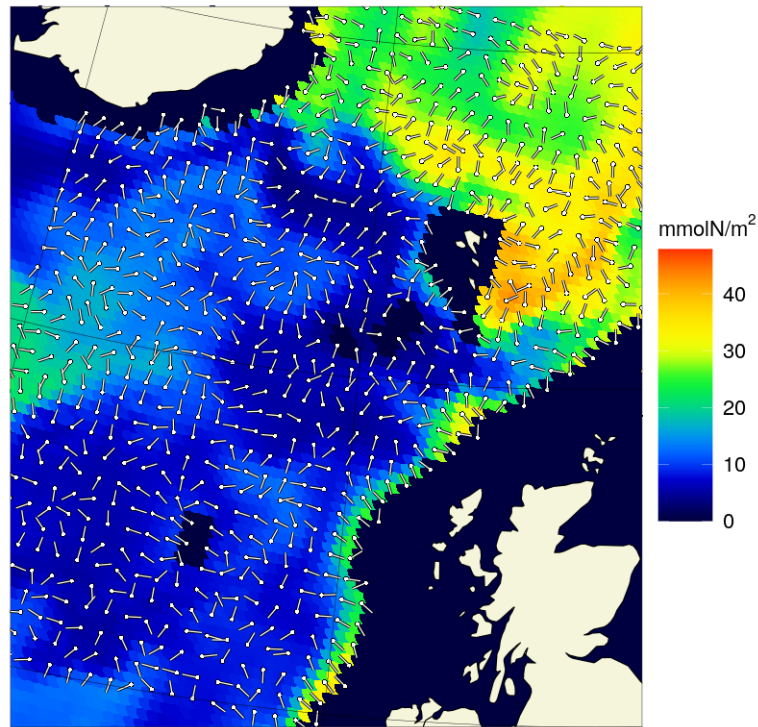
(a) $\Theta = 30$ km
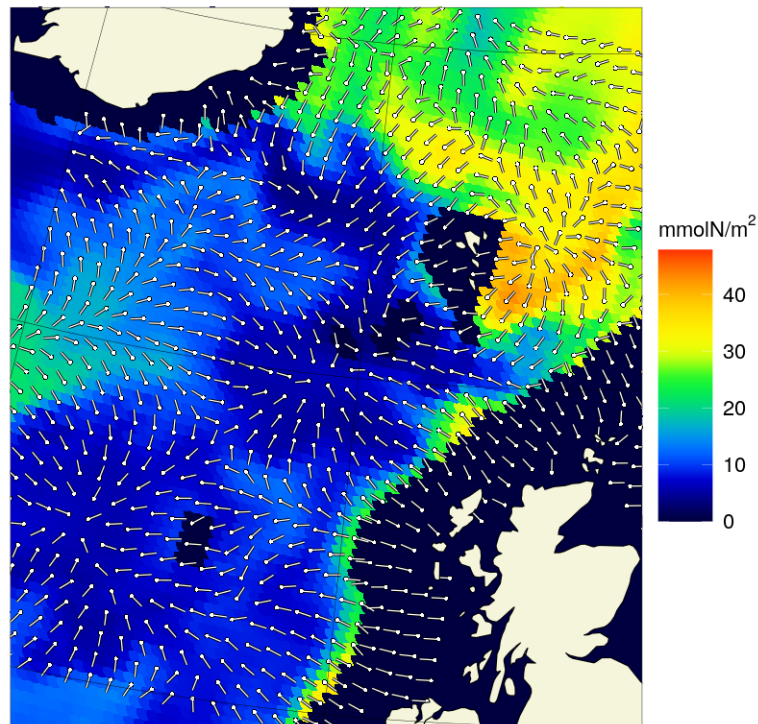
(b) $\Theta = 150$ km

Figure 3.3: Examples of gradient direction fields calculated on mesozooplankton concentration fields from NEMO-Medusa outputs (see chapter 4) and using two different gradient scales. Gradient directions are represented by white arrows with a plain point corresponding with the cell centre from which direction was calculated. The background colours give mesozooplankton concentration calculated by NEMO-Medusa for June 1994.

latitudes would be very similar to a gradient computed with Ritter's algorithm (four neighbouring cells) while the number of cells involved in the gradient computation would increase with latitude.

The gradient scale also determines the spatial scale for detecting elevation changes around a cell. Figure 3.3 shows examples of two gradient direction fields calculated with different gradient scales. In the first map, we see that gradient directions are more chaotic with a low Θ value, especially in areas with very low variations in zooplankton concentration, whereas higher Θ seem to stabilize the directions towards the closest and highest values of zooplankton concentration. In terms of fish migration, this is useful to simulate long distance migration pathways towards best suited areas.

Assuming $\bar{d}_N = \bar{d}_S = \bar{d}_E = \bar{d}_W = \bar{d}$ in equations (3.8)-(3.10), the ideal gradient scale for the model was defined so that an individual moving at its average speed and following a gradient direction calculated at time t would have travelled the mean distance $\bar{d}$ at time $t + \Delta t$. This means that an individual would be able to reach at $t + \Delta t$ any area 'detected' as more suitable by the local gradient at time t. In a continuous spatial system with no boundaries, $\bar{d}$ is the mean distance between the centre of a circle with radius Θ and any points within that circle, and can be calculated:

$$\bar{d} = \int_0^\Theta r\, C\, dr \Big/ A \qquad \text{where} \quad C = 2\,\Theta\,\pi \quad \text{and} \quad A = \pi\,\Theta^2 \qquad (3.13)$$

$$\Rightarrow \bar{d} = \frac{2}{3}\,\Theta \qquad (3.14)$$

With a model time step $\Delta t = 5$ days and a constant swimming speed $\bar{v} = 0.25$ m/s, the mean distance travelled would be around 100 km. Thus, the ideal gradient scale for the blue whiting model was estimated to be $\Theta = 3/2\,\bar{d} = 150$ km (i.e. figure 3.3b) and this value was kept for the whole study.

3.2.2 Defining the growth potential variable

The blue whiting population migrate into the Norwegian Sea, their main feeding area, and stay there over summer. Most of their annual body growth would then take place during that season. As seen in last chapter, blue whiting growth equations take into account both food and temperature. Assuming feeding migration would target areas that are most profitable to growth, the von Bertalanffy growth equation (2.11) was used to develop a variable describing the growth that an individual with average length (L) would get from experiencing local food (ρ) and temperature (T) over one time step. The variable was called growth potential (G_L) and is written as follows:

$$G_L = L_\infty - L - \left(L_\infty - L \right) \exp \left(- k \, \Delta t \right) \tag{3.15}$$

where k and L_∞ are:

$$k = \frac{\mu_0}{3} \, (Q_\mu)^{T/10} \tag{3.16}$$

$$L_\infty = \frac{(Q_\mu \, Q_\tau)^{-T/10}}{\mu_0 \, a^{1/3}} \left(\frac{\sigma_0 \, \rho}{1 + \tau_0 \, \sigma_0 \, \rho} \right) \tag{3.17}$$

The gradient computation method was then used to calculate the G_L gradient field at each time step. Those gradient fields will be used conjointly with NEMO flow fields to drive blue whiting adults from their spawning areas off British Isles to their feeding grounds. Most of the population was expected to get into the Norwegian Sea by following G_L gradients.

Juveniles would also be attracted by those feeding areas. For this reason, a series of transport matrices were computed to be suitable for both juveniles and adults combined, when they enter feeding phases. In equation (3.15), the average length L was fixed to 20 cm to include a younger population, based on average length distributions from ICES reports (ICES, 2004, 2005, 2016a).

3.2.3 Defining the spawning habitat suitability index

Defining a variable to drive spawning migrations was more challenging than for feeding migrations. Optimal conditions for spawning are defined by ranges of several variables: temperature (9-10°C), salinity (35.3-35.5) and depth (250-600 m) (Miesner & Payne, 2018). First, a function of temperature (T), salinity (S) and depth (Z) was developed, whose global maximum coincided with optimum ranges of all three variables.

For each variable, we write a Gaussian function:

$$f_T = \exp\left(-\frac{(T - \bar{T})^2}{2(\omega_T)^2}\right) \tag{3.18}$$

$$f_S = \exp\left(-\frac{(S - \bar{S})^2}{2(\omega_S)^2}\right) \tag{3.19}$$

$$f_Z = \exp\left(-\frac{(Z - \bar{Z})^2}{2(\omega_Z)^2}\right) \tag{3.20}$$

where $\bar{T}$, $\bar{S}$ and $\bar{Z}$ are average values of the variable's optimum range, and ω_T, ω_S and ω_Z the standard deviation which were estimated with the minimum and maximum values of the optimum ranges as follows:

$$\omega_T = (T_{\max} - T_{\min})/2$$

$$\omega_S = (S_{\max} - S_{\min})/4$$

$$\omega_Z = \begin{cases} (Z_{\max} - Z_{\min})/2 & \text{if } Z > \bar{Z} \\ Z_{\max} - Z_{\min} & \text{otherwise} \end{cases}$$

We then combine all three Gaussian functions to build the index Ω describing habitat suitability for spawning, taking values between 0 and 1:

$$\Omega = f_T \, f_S \, f_Z \tag{3.21}$$

This first version of Ω created many difficulties related to the importance of each environmental variable and their relationships with each other. According to Miesner & Payne (2018), salinity and temperature play an important role in the spreading of the population over spawning areas and so are likely to be essential for detecting suitable spawning habitats. Depth is also important for spawning, however in the first steps of developing Ω, it was found that using depth as a driver for the whole spawning migration caused individuals to get first very attracted to the continental slope but then to fail following temperature and salinity gradient towards suitable spawning grounds. Therefore, it was decided that depth would be involved in the migration only once temperature and salinity optimum ranges are reached.

Following these ideas, the spawning habitat suitability index is given by:

$$\Omega = \begin{cases} f_T \ f_S & \text{if } T \notin [T_{\min}, T_{\max}] \text{ and } S \notin [S_{\min}, S_{\max}] \\ f_T \ f_S \ f_Z & \text{if } T \in [T_{\min}, T_{\max}] \text{ and } S \in [S_{\min}, S_{\max}] \text{ but } Z \notin [Z_{\min}, Z_{\max}] \\ 1 & \text{otherwise} \end{cases}$$

$$(3.22)$$

This new version for Ω improved the success of spawning migration. Individuals would still get attracted by the continental slope area, but gradients along isobaths were more efficient to drive them towards the spawning areas. However, a problem was repeatedly encountered, where individuals coming from the Norwegian Sea stopped their migration just North of Shetland. It was likely caused by an increasing error in the gradient computation when approaching system boundaries such as land cells.

This limitation decided the use of a simple latitudinal and longitudinal gradient outside of a roughly defined area, including the known spawning grounds. This avoids that migration pathways stick too much to coastlines, and reduces gradient errors early in the migration. $f_{\text{lat,lon}}$ is a gradient increasing linearly to reach 1 at the boundaries of A_s, which is delimited by longitudes 20°W and 2°W and by latitudes 53°N and 60°N. This area is supposed to contain the main spawning grounds west of British Isles. Nevertheless suitable spawning habitats

outside this area can still be detected if individuals move through an area with suitable temperature and salinity.

So the final version for Ω is:

$$\Omega = \begin{cases} 1 & \text{if } T \in [T_{\min}, T_{\max}], \ S \in [S_{\min}, S_{\max}] \text{ and } Z \in [Z_{\min}, Z_{\max}] \\ (1 + f_T \ f_S \ f_Z)/2 & \text{if in } A_{\mathrm{s}} \text{ and } T \in [T_{\min}, T_{\max}] \text{ and } S \in [S_{\min}, S_{\max}] \\ (1 + f_T \ f_S)/2 & \text{if in } A_{\mathrm{s}} \text{ but } T \notin [T_{\min}, T_{\max}] \text{ and } S \notin [S_{\min}, S_{\max}] \\ (f_{\mathrm{lat,lon}} + f_T \ f_S \ f_Z)/2 & \text{if not in } A_{\mathrm{s}} \text{ but } T \in [T_{\min}, T_{\max}] \text{ and } S \in [S_{\min}, S_{\max}] \\ f_{\mathrm{lat,lon}}/2 & \text{otherwise} \end{cases}$$

$$(3.23)$$

The model grid resolution was not appropriate for defining suitable spawning areas with depth between 250 m and 600 m. So the optimum depth range was increased to 100-1000 m. This allowed for more cells located on the continental slope to be selected as potential spawning grounds.

3.2.4 Swimming direction and speed

Once the new movement fields were used in `Ichthyop` for spawning and feeding migrations and horizontal dispersion was added, we realised that individuals would all gather in the most suitable cells once they reach them with almost no dispersion around them. It meant that the directed movement with velocity components U and V (equation 3.2) is too strong for dispersion to take over. Biologically, this would mean that the whole population would only be interested in the most productive areas, disregarding altogether the negative effects of intra-species competition by feeding on the same resource of food. And if intra-species competition were considered in the model, by including a density-dependent mortality rate for both juveniles and adults, this problem would surely result in unrealistic high mortality rates recorded during the feeding season, likely causing the collapse of the population. To solve this, it was essential to force the swimming speed (v_{swim}) to decrease when approaching areas with high values of either G_L or Ω, making it thus possible for fish to switch from a migratory to a

more locally dispersive foraging behaviour.

First attempts were made by using the gradient value (slope) to determine swimming speed. In areas with few changes in environmental conditions, the swimming speed allocated to directed movement (active advection) would then decrease and reach zero in constant environments, thus allowing for dispersion. However gradients of G_L in the spawning areas and of Ω in the feeding areas tend to be weak and would allow too much dispersion at the start of the migrations, resulting in their failure at reaching suitable areas.

Assuming individuals switch from migrating to dispersing when approaching suitable environmental conditions, we define a swimming speed depending on local value of variable X (ρ, T, G_L or Ω):

$$v_{\text{swim}} = \bar{v} \, \exp\left(- \left[\frac{X}{X_c} \right]^p \right) \tag{3.24}$$

where X_c and p are constants that control the shape of the speed function. For migrations including both juvenile and adult populations, $\bar{v} = 0.20$ m/s, while for migrations only undertaken by mature adults, $\bar{v} = 0.25$ m/s.

To avoid swimming against currents with a resulting movement direction which stay the same as flow direction (fish goes backward), we define a condition to use the gradient direction only when swimming speed is greater than flow velocity:

$$\theta_{\text{swim}} = \begin{cases} \theta_{\text{flow}} & \text{if } \theta_g = \varnothing \text{ or if swimming against currents and } v_{\text{swim}} < v_{\text{flow}} \\ \theta_g & \text{otherwise} \end{cases} \tag{3.25}$$

This rule adds up to the rule for swimming behaviour in absence of environmental gradient ($\theta_g = \varnothing$) mentioned in section 3.1.2. We therefore rewrite equations 3.3 and 3.4 into the general form:

$$U_{\text{swim}} = \bar{v} \, \sin(\theta_{\text{swim}}) \tag{3.26}$$

$$V_{\text{swim}} = \bar{v} \, \cos(\theta_{\text{swim}}) \tag{3.27}$$

where θ_{swim} can switch between θ_{flow} and θ_g depending on local values of velocity and gradient.

3.3 Conclusions

Active swimming of juveniles and adults are modelled using a particle tracking model approach, similar to the larval drift model, which combines both passive and active movements. Directed movements specific to migratory behaviours are implemented externally, then directly added to flow fields used in the particle tracking model.

Speed and direction of migratory movements are determined by the local value and gradient of environmental factors. In the context of blue whiting feeding migrations, the growth potential variable was developed, which is both temperature and food dependent. Gradient fields of this variable will contribute to direct fish migrating from the spawning grounds to suitable feeding areas. Similarly, the final version of the spawning habitat suitability index allows for a gradient that direct adults from any initial location towards suitable spawning areas.

A new gradient algorithm, which is adapted for using in any grid definition and resolution, was here proposed. Its main advantage is the possibility to adapt the scale of the gradient computation. Here it was used to direct migratory movements towards suitable habitats.

Part III

Environmental data and model drivers

Chapter 4

NEMO-Medusa

After describing the spatial population model for blue whiting in the previous chapters, we know that currents, temperature, salinity and plankton (food) concentration will be needed as inputs for modelling migrations and individual growth. Outputs from the coupled physical-biogeochemical model NEMO-Medusa were chosen to fulfil this function. Chapter 3 already showed examples of gradient fields computed from the gradient algorithm described there and using the mesozooplankton variable from NEMO-Medusa (figure 3.3).

The following chapter aims at providing a literature background to both physical and biogeochemical model components, NEMO and Medusa, as well as a study of space and time variations of the different variables relevant to the blue whiting model. A particular emphasis on climate variations and projections is made, considering that the North Atlantic subpolar gyre seems to affect blue whiting spatial dynamics, especially spawning distribution and migration (chapter 1). This brings us to the final part of this chapter which covers predictions of spawning areas using NEMO, and how suitable spawning habitat may vary in time, depending on climate changes. While the blue whiting model runs only considered NEMO-Medusa outputs from 1988 to 2050 (chapter 9), longer term forecasts to the end of the century (2099) are also given here for the IPCC's climate scenario RCP 8.5.

4.1 NEMO

NEMO (Nucleus for European Modelling of the Ocean) is an ocean circulation modelling framework, which consists of three engines (Madec & NEMO-team,

2008). The first one, OPA (Océan PArallélisé), is used to model the ocean dynamics and thermodynamics. The second is the Louvain-la-neuve Ice Model (LIM) and focuses on sea-ice dynamics and thermodynamics. The third deals with biogeochemical processes and is referred to as TOP (Tracer in the Ocean Paradigm). Depending on the application, all model engines might not necessary be used. Thus, for the Medusa model coupled with NEMO version 3.4, only OPA version 9 (OPA9) (Madec et al., 1998; Madec & NEMO-team, 2008) and LIM version 2 (LIM2) (Timmermann et al., 2005) are used (Yool et al., 2011, 2013b), while biogeochemistry is handled by Medusa (described in more details in section 4.2).

The OPA9 model was configured at global scale for the purpose of research projects on regional ocean modelling (ROAM) led by the National Oceanography Centre of University of Southampton (UK) and supported by the Natural Environmental Research Council (NERC) (Yool et al., 2011, 2013b, 2015). Following a request issued in 2015, outputs from NEMO-Medusa were made available to us for the period 1988-2099. This included NEMO temperature, salinity and flow velocity fields with an approximate horizontal resolution of $0.25°$, in a tripolar grid configuration (considers two pole position in the Northern Hermisphere, one in Canada and one in Siberia).

Outputs were obtained from two different runs, one called 'historical' and the second 'projection'. NEMO can take into account external forcing at the surface boundary (e.g. atmospheric pressure affecting the ocean surface pressure gradient) (Madec & NEMO-team, 2008). In the case of NEMO-Medusa, external climate forcing variables for NEMO were either historical values of atmospheric CO_2 concentrations (historical run) or surface temperature and salinity fields extracted from outputs of the HadGEM2-ES Earth System model (UK Met Office Hadley Centre) configured under the RCP 8.5 climate scenario (projection run) (Yool et al., 2015). The historical run was initialised in 1860 and ended in 2006, while the projection run started in 1975 using a re-gridded version of an other projection run with a lesser resolution ($1°$) which was initialised in 1860 (Yool et al., 2015).

For the blue whiting population modelling project, access to historical outputs was possible from start 1988 to end 2006, while projection outputs were available

from start 2006 to end 2099, both with a five-day time step. The 2006 historical outputs were only used in the particle tracking model `Ichthyop` (chapter 3) to produce the five-day time step track outputs to end 2005 (start of year 2006 needed for last 2005 time steps). Vertical resolution differed slightly between both NEMO outputs, with historical being vertically split into 64 depth levels and projection into 75 depth levels. However, this only affected the depth level selected in each cell for representing average depth of either larvae (referred thereafter as surface layer) or juveniles/adults (deep layer) (see chapter 3).

4.1.1 Climate change scenario

Since 1988, the International Panel on Climate Change (IPCC) has worked on providing stakeholders, the scientific community and the general public with a common and full knowledge basis on most recent climate change research. To understand past, present and future climate changes, researchers combined their efforts in developing climate models, in which they tested a range of climate scenarios. Among recognised climate scenarios, four RCP scenarios (Representative Concentration Pathways), namely RCP2.6, RCP4.5, RCP6.0 and RCP8.5, were introduced and tested during IPCC's fifth assessment cycle, also called the fifth Coupled Model Intercomparison Project (CMIP5) (IPCC, 2013). Those scenarios take into account different intensities of anthropogenic forcing and are named after the resulting total radiative forcing predicted in 2100 relative to year 1750 (Stocker et al., 2013). Thus, RCP8.5 corresponds to a total radiative forcing of 8.5 W/m^2 by the end of 2100. It is the most extreme RCP scenario tested for AR5, and is supposed to describe a scenario of high greenhouse gas emissions as a consequence of the absence of climate change mitigation measures (Riahi et al., 2007, 2011). Time series of greenhouse gas emissions (e.g. CO_2) produced by RCPs (Stocker et al., 2013) are then used as input to Earth System Models (ESM), such as HadGEM2-ES (Collins et al., 2011; Jones et al., 2011). Here, NEMO-Medusa climate variations are determined by outputs from the HadGEM2-ES model run under the RCP8.5 scenario.

The HadGEM2-ES model was developed after the HadGEM1 model, which is a climate model with less complexity than the ESM (Johns et al., 2006). As an

Earth system model, HadGEM2-ES includes new model components that simulate both terrestrial and ocean carbon cycles, atmospheric chemistry and aerosols which would interact with each other and climate (Collins et al., 2011). The final model was considered stable to provide realistic predictions of global climate variations without artificial corrections (Collins et al., 2011). However, a comparative study of the performance of the CMIP5 climate models in the North-Atlantic region suggested that the HadGEM2-ES model might not reproduce a realistic stratification of the SPG area, which led to the model inability at simulating an SPG convection collapse observed around mid-21st century with some other models (Sgubin et al., 2017).

IPCC's climate scenarios are designed to describe and model climate changes at the global scale. When used for studying the effects of climate change on the bio-geophysical dynamics of particular regions (e.g. Arctic and North-Atlantic regions), model predictions may show local trends very different from those observed at the global scale. For example, a few studies showed forecasts of slow or abrupt freshening and/or cooling in the subpolar gyre region (Irminger Sea) over the 21st century (Hermanson et al., 2014; Gierz et al., 2015; Sgubin et al., 2017; van den Berk et al., 2021). Since we are only interested in the geophysical changes in the North-East Atlantic, in particular those related to the subpolar gyre dynamics, similar observations might be made for the NEMO outputs used in this modelling project.

Many studies can be found on the variations of SPG strength, most describing different methods to measure it (Häkkinen & Rhines, 2004; Hátún, 2005; Böning et al., 2006; Bersch et al., 2007; Born & Mignot, 2012; Wouters et al., 2013; Marzocchi et al., 2015; Berx & Payne, 2017; Foukal & Lozier, 2017; Biri & Klein, 2019). The most common SPG index (SPG-I) has been first computed by Häkkinen & Rhines (2004) and corresponds to the first principal component of an empirical orthogonal function (EOF1) for the sea surface elevation anomaly (Häkkinen & Rhines, 2004; Wouters et al., 2013; Berx & Payne, 2017). Among other indices, the barotropic stream function seems a good alternative, as it also allows for the study of SPG size (Marzocchi et al., 2015; Biri & Klein, 2019). In some cases, sea surface temperature (SST) was also considered a valid proxy

for SPG-I (Hátún, 2005). The following sections attempt to find a suitable proxy of the SPG index for studying variations of the SPG dynamics in NEMO outputs.

4.1.2 Predictions of North Atlantic geophysical dynamics

Currents

According to Marzocchi et al. (2015), NEMO at the 1/4° resolution can simulate efficiently ocean circulation, as well as eddy dynamics at a smaller scale. As NEMO flow fields will affect population movements in the blue whiting model, we wanted to know if flow variations could be observed at the studied depths and if they could be related to climate variations. Changes in the subpolar gyre strength are expected to affect dynamics in the North-East Atlantic region, so flow velocities in years with different SPG indices were compared. According to SPG index values (Hátún, 2005; Hátún et al., 2007; Berx & Payne, 2017), the years 1992 and 1994 were marked by a much stronger subpolar gyre than in years 2002 and 2004. Those years are chosen as examples of both climate regimes throughout the thesis.

As expected, currents in the deep layer (at average swimming depth of blue whiting adults) tended to reflect main currents of the surface layer (around 50 m deep) only weaker (fig. 4.1 and 4.2). The strong currents visible around latitude 52°N and longitude 30°W belong to the end of the Gulf Stream just before its separation. Marzocchi et al. (2015) actually showed that NEMO tended to exaggerate the Gulf Stream North-East separation position, placing it too far North. It could potentially result in an overestimation of its influence on the North-East Atlantic region.

The main difference in the NEMO flow fields between strong (1992, 1994) and weak (2002, 2004) SPG regimes was observed along the North-West edge of the Rockall Plateau (lon. 14-22°W, lat. 57-62°N). Stronger currents seem to be present in that area in years of strong subpolar gyre. Currents located South of the Rockall Plateau also tended to be stronger under strong SPG regime. However those changes seem to have little effect on the position of main currents or on the more eastern flow field.

In both figures 4.1 and 4.2, we can see the North-Atlantic shelf current (NASC)

(a) 1992

(b) 1994

(c) 2002

(d) 2004
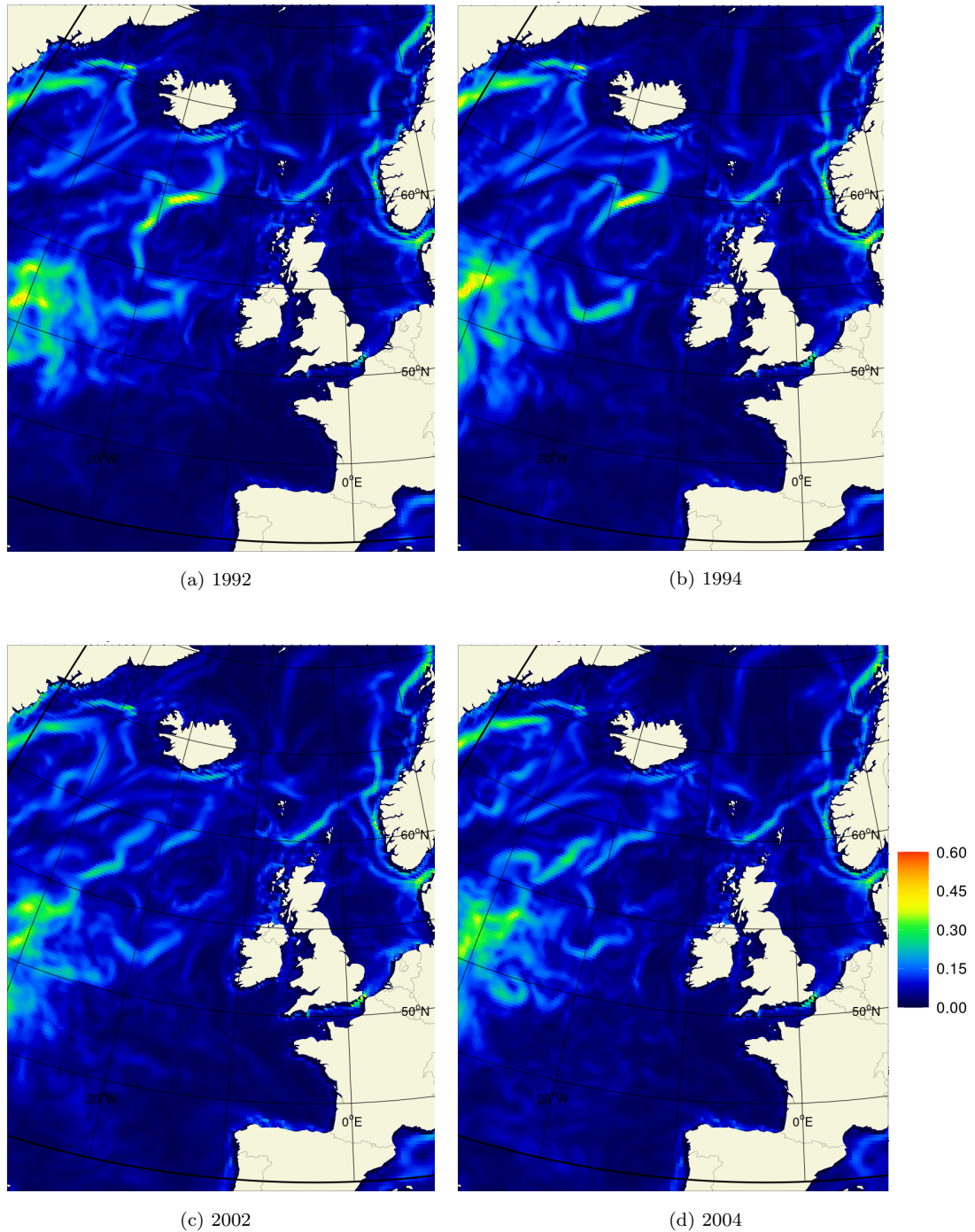
Figure 4.1: Intensity (m/s) of currents in the surface layer (at -50 m or at 50% of water column depth, calculated from the the surface) for years which are supposed to be under different climate regimes: strong supolar gyre in 1992 and 1994 ; weak subpolar gyre in 2002 and 2004.

(directed northward), which is particularly strong off North Scotland and in the Faroe-Shetland Channel in both SPG regimes.

(a) 1992   (b) 1994

(c) 2002   (d) 2004
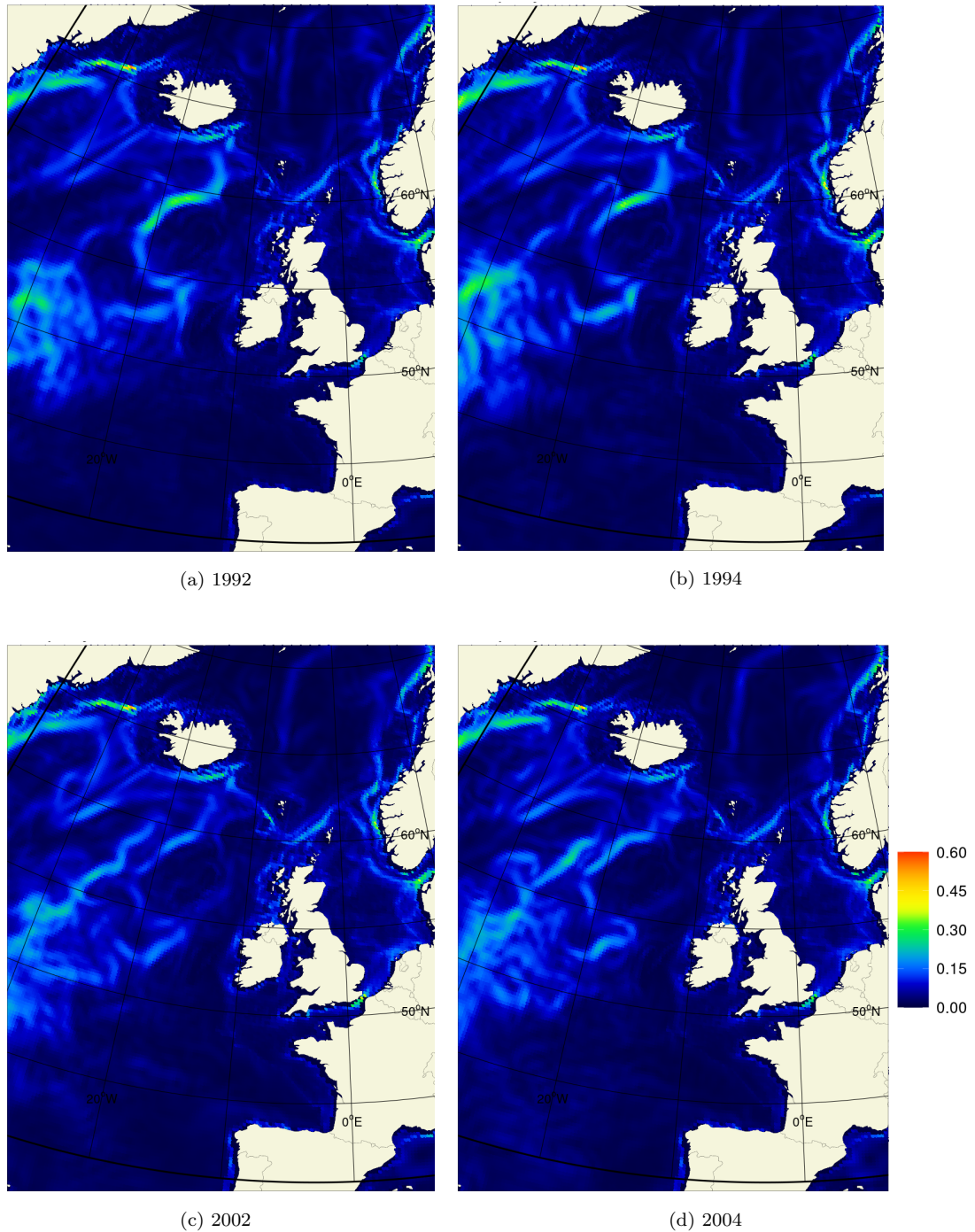
Figure 4.2: Intensity (m/s) of currents in the deep layer (at -450 m or at 70% of water column depth, calculated from the the surface) for years which are supposed to be under different climate regimes: strong supolar gyre in 1992 and 1994 ; weak subpolar gyre in 2002 and 2004.

Temperature and salinity

Temperature and salinity are both important physical variables in the blue whiting model. Spawning migration and location are both driven by those variables, while feeding migration and growth is affected by temperature (chap. 2 and 3).

Variation of average temperature and salinity was studied in four different areas and in both depth layers, over the model run period from 1988 to 2050 (fig. 4.3 and 4.4), as well as to the end of the century (fig. 4.5 and 4.6). This allowed us to notice some local disruption in time series between 2005 and 2006, which corresponds to the transition between outputs from the NEMO-Medusa historical run and outputs from the projection run. This disruption and its possible consequences for the blue whiting model are further discussed in section 4.1.3.
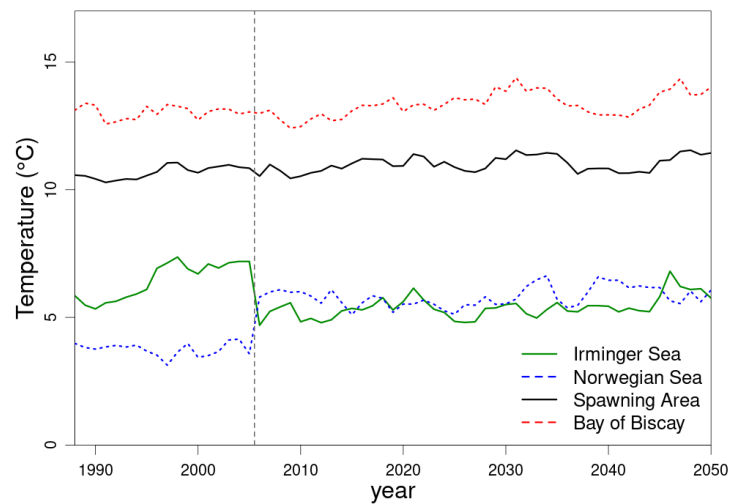
(a) Surface layer temperature
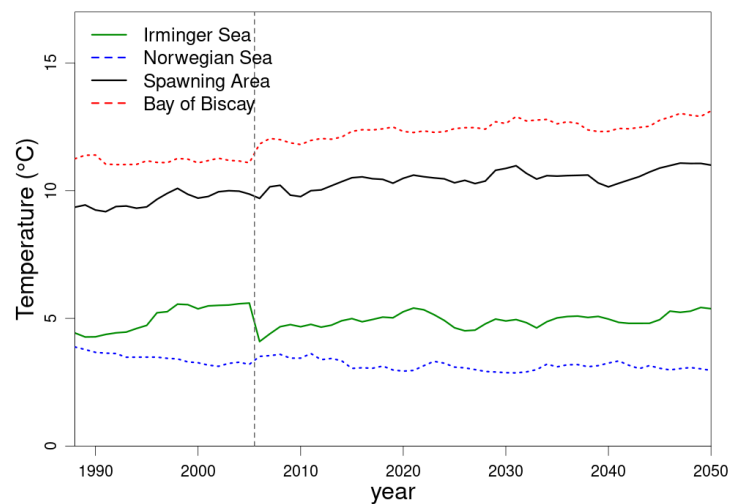
(b) Deep layer temperature

Figure 4.3: Annual mean temperature from 1988 to 2050, calculated for both surface and deep layers in defined areas: the Irminger Sea (plain green line; lon 50°W-30°W lat 55-65°N), the Norwegian Sea (dotted blue line; lon 14°W-6°E lat 62-72°N), area off the British Isles enclosing both Rockall and North of Porcupine Bank known to be blue whiting's main spawning area (black plain line; lon 20°W-5°W lat 52-62°N), and southern area enclosing Bay of Biscay (red dotted line; lon 15°W-0°E lat 42-52°N).
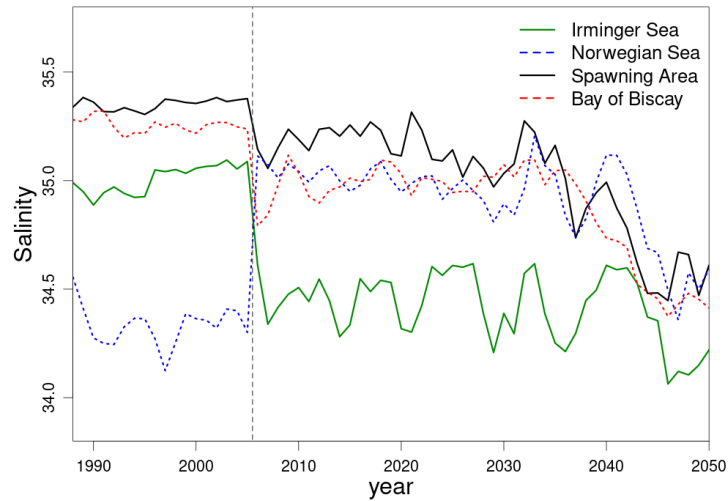
(a) Surface layer salinity
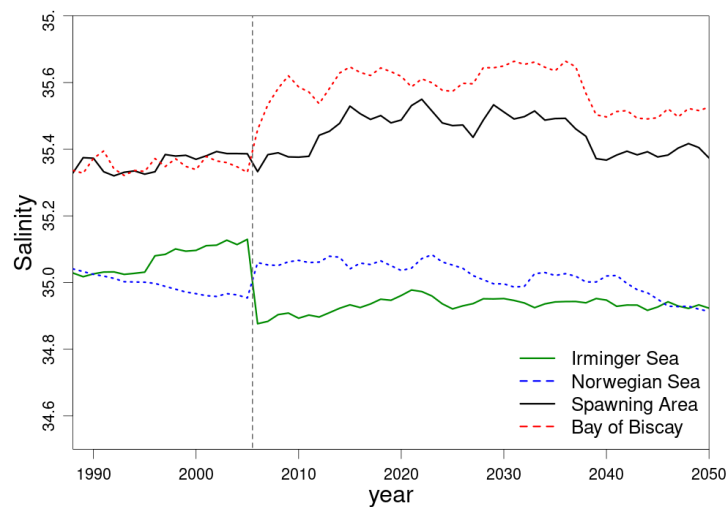
(b) Deep layer salinity

Figure 4.4: Annual mean salinity from 1988 to 2050, calculated for both surface and deep layers in defined areas (same as fig. 4.3).

In general, average deep and surface temperature seem to show only small variations from 1988 to 2050 (except for the disruption in 2005-2006), with mean surface values mostly between 10.4 and 11.4°C for the spawning area, between 12.7 and 14°C for the Bay of Biscay, between 4.8 and 7.1°C for the Irminger Sea, and between 3.5 and 6.5°C for the Norwegian Sea (fig. 4.3.a). In this time frame, the expected temperature increase trend seems to be only visible in the deep layer of the Bay of Biscay and the spawning area, with waters becoming around 1.7°C warmer in 2050 compared to 1988 (fig. 4.3.b). The Norwegian Sea however

seems to display a temperature decrease of 0.9°C in 63 years. Most trends are confirmed over the long-term, after 2050 (fig. 4.5), with a gain from 1.9 to 3.0°C in the surface layer between 2006 and 2099 in all areas, and from 2.3 to 3.3°C in the deep layer. The faster increase in temperature of the deep layer suggests a weakening of the thermocline. After temperature decreasing slowly from 1988 to 2055 in the Norwegian Sea deep layer, warming take place in this area at a similar rate than in other areas from 2055 onwards (+1.5°C between 2056 and 2099).

Annual average of surface salinity seems to start decreasing from 2030 onwards
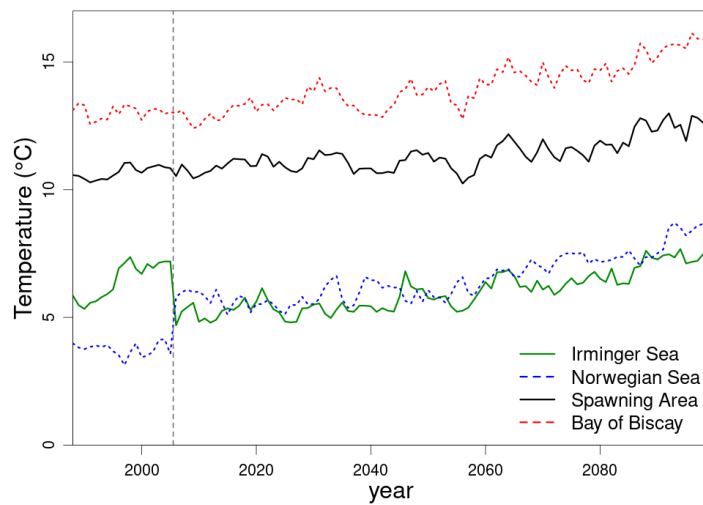
(a) Surface layer temperature
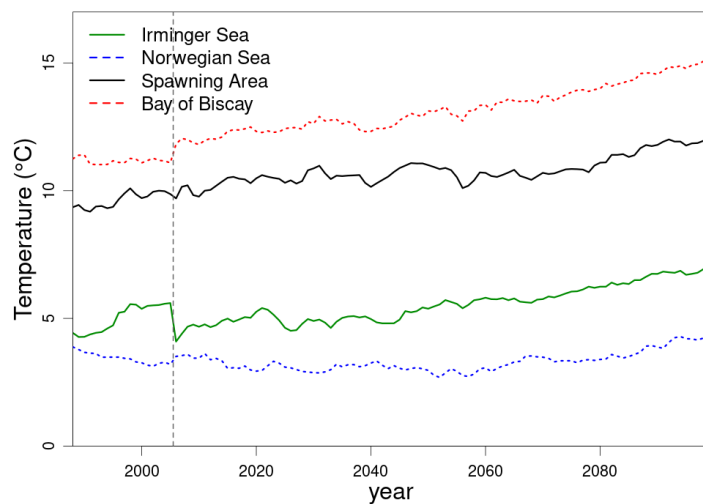
(b) Deep layer temperature

Figure 4.5: Same as figure 4.3 but from 1988 to 2099.
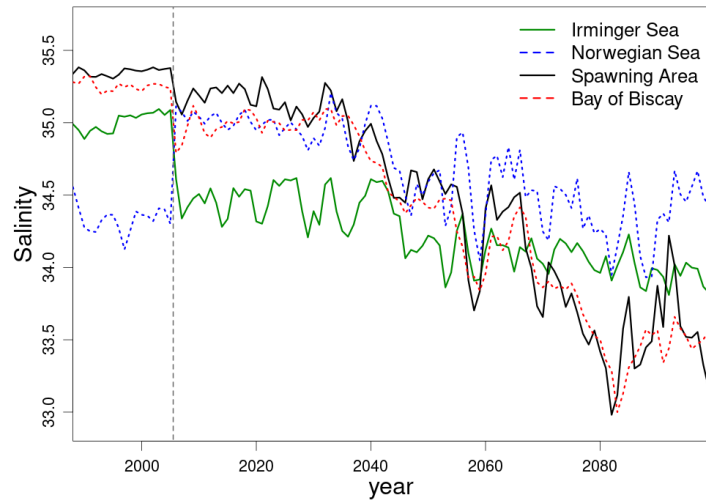
(a) Surface layer salinity
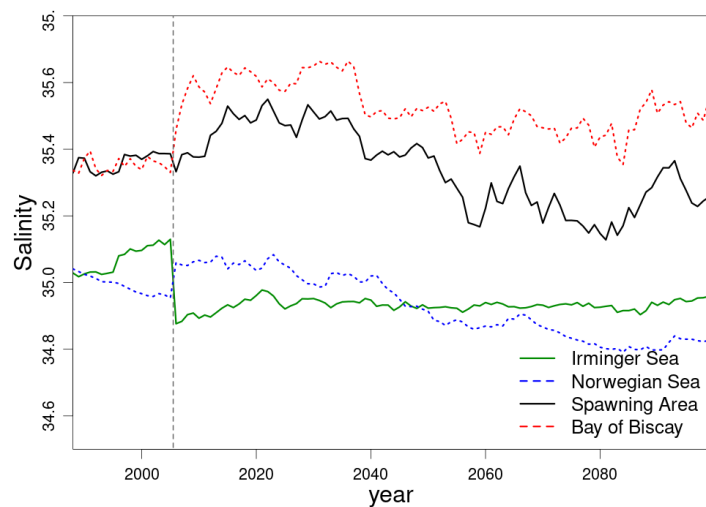
(b) Deep layer salinity

Figure 4.6: Same as figure 4.4 but from 1988 to 2099.

in all areas except for the Irminger Sea (fig. 4.4.a). In fact, surface salinity in the Irminger Sea seems to fluctuate a lot between 2006 and 2050, with freshening events that are most likely caused by the incursion of fresh water from ice melting, mostly from Greenland and the Arctic.

Over the century, the highest salinity decline in this NEMO-Medusa run takes place in the southern areas (e.g. blue whiting spawning area and Bay of Biscay, fig. 4.6.a), while in the Irminger Sea, the surface salinity average drops from 34.5 between 2006 and 2045, to 34.0 between 2046 and 2099 (fig. 4.6.c). In the deep layer, salinity changes are around 10 times smaller than in the surface layer (fig. 4.6.b).

A relationship between SPG index and annual average temperature or salinity in the Irminger Sea seems to exist, with temperature and salinity increasing when the subpolar gyre weakens. From 1993 to 2005, a strong negative correlation exists between SPG-I values and deep salinity ($r = -0.97$), surface salinity ($r = -0.94$), deep temperature ($r = -0.93$) or surface temperature ($r = -0.90$). Although much weaker in amplitude, the relationship seems also to exist in the blue whiting spawning area, with negative correlations between -0.85 and -0.92. This shows that NEMO is able to simulate SPG strength variations which are in accordance with observations, and suggests that the SPG dynamics have at least a partial effect on the spawning area's environmental conditions, supporting past studies (Hátún, 2005; Hátún et al., 2007).

Subpolar gyre dynamics

Based on the paper from Hátún (2005), water mass distribution was studied at the blue whiting swimming depth (-450 m), defined by their salinity ranges: $S \leq 35.10$ characteristic of the fresh SPG waters, $S > 35.35$ for the saline subtropical gyre (STG) waters, and mixed waters with $35.10 < S \leq 35.35$ (Hátún, 2005). First, the same years as in Hátún's paper (1993 and 1998) were compared and showed very similar spatial distribution of the water masses, as well as a similar westward shift of the STG waters over Rockall in the year of weak SPG. Those variations between weak and strong SPG were supported by further comparisons between years 1992, 1994 and 2002, 2004 (fig. 4.7). In years with a strong SPG, we see a very distinct narrower distribution of STG waters off Ireland ($\approx$ 53-54°N), while in years with a weak SPG, STG waters would reach areas south of Iceland (especially visible here in 2002).

Comparing water masses distribution from 2000 to 2050, it seems that STG waters which already covered all spawning area in 2000, with a very wide distribution at 53-54°N, are spreading North-West between 2000 and 2020 (fig. 4.8). Distribution of STG water in southern Icelandic waters seems to become permanent after 2020. We note that waters that were defined as SPG waters by Hátún (2005) seem to have receded throughout the century (fig. 4.8, water mass distribution in year 2099).
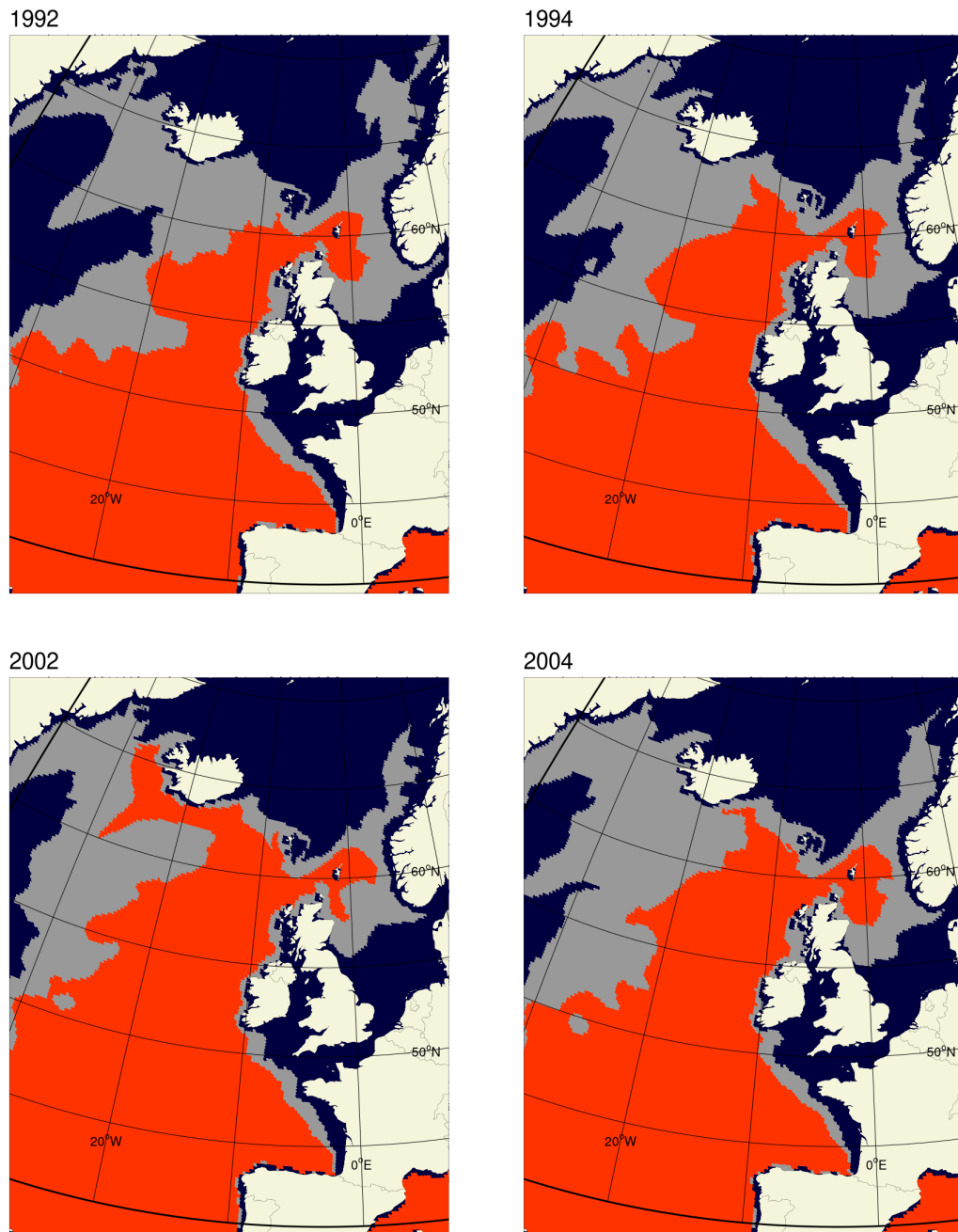
Figure 4.7: Spatial distribution of water masses in the deep layer, as defined by their annual average of salinity: saline STG water if $S > 35.35$ (red), fresher SPG water if $S \leq 35.10$ (dark blue), and mixed water if $35.10 < S \leq 35.35$ (grey) (Hátún, 2005). Years 1992 and 1994 are supposed to be characterized by a stronger subpolar gyre than years 2002 and 2004.

According to Miesner & Payne (2018), blue whiting spawning distribution is closely related to salinity, with an optimum range between 35.3 and 35.5. This mostly corresponds to STG waters defined by Hátún (2005). Therefore, calculating an index that would describe changes in STG water mass distribution might help understand outputs of the blue whiting model. By calculating the total sur-

face covered by STG waters in latitudes $\geq 53°$N and in longitudes $\geq 5°$W, it is possible to describe variations in STG water distribution over the blue whiting spawning area (fig. 4.9 and 4.10).

Time series of the size of the area covered by STG waters were marked by a sharp increase between 1991 and 1996, directly followed by a small drop, just before increasing again between 2006 and 2020 (fig. 4.9). Apart from the drop in size around 2005, the variable seemed to follow the general increase of the SPG
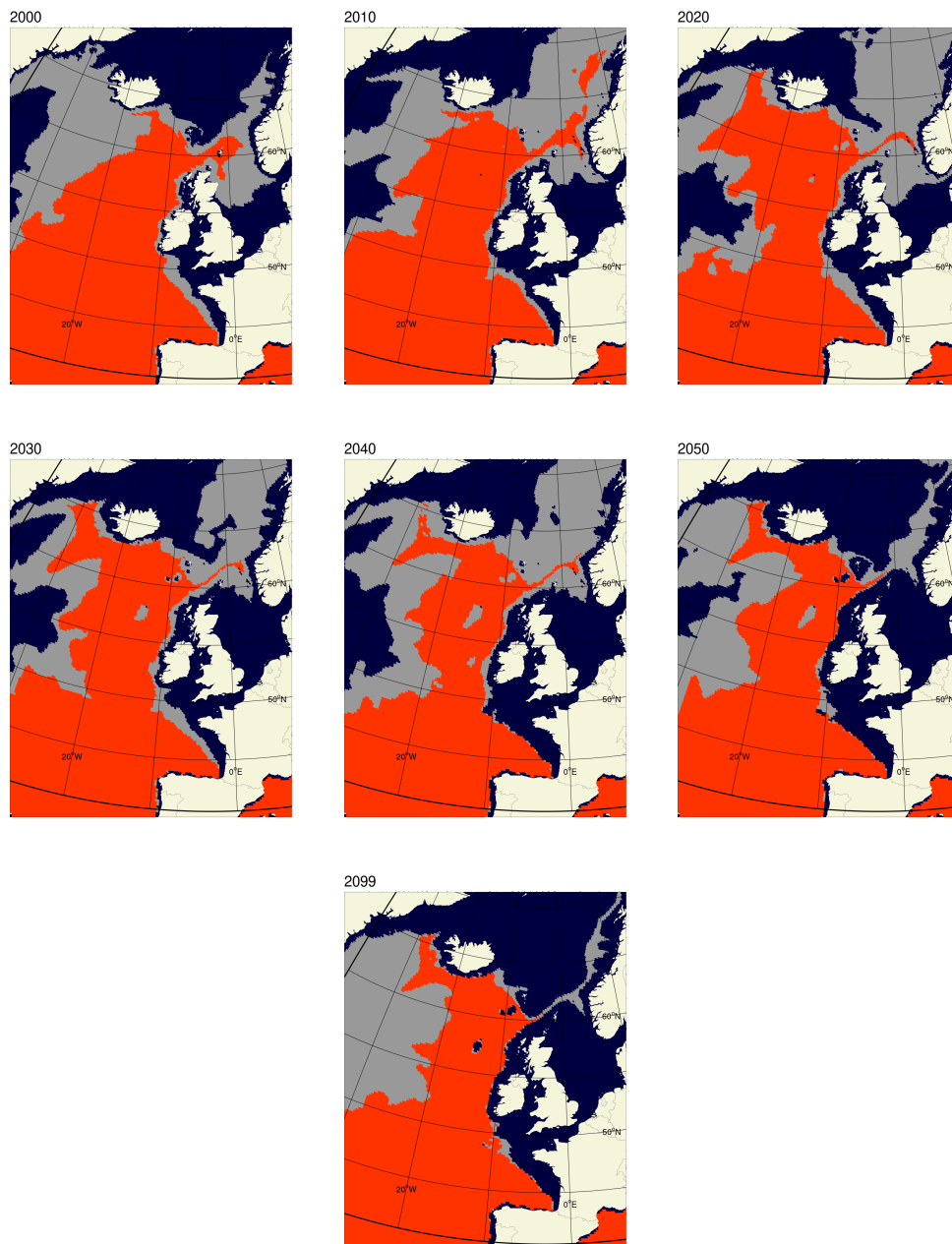
Figure 4.8: Variation of spatial distribution of water masses in the deep layer (see fig. 4.7) as predicted by the NEMO model between 2000 and 2099.
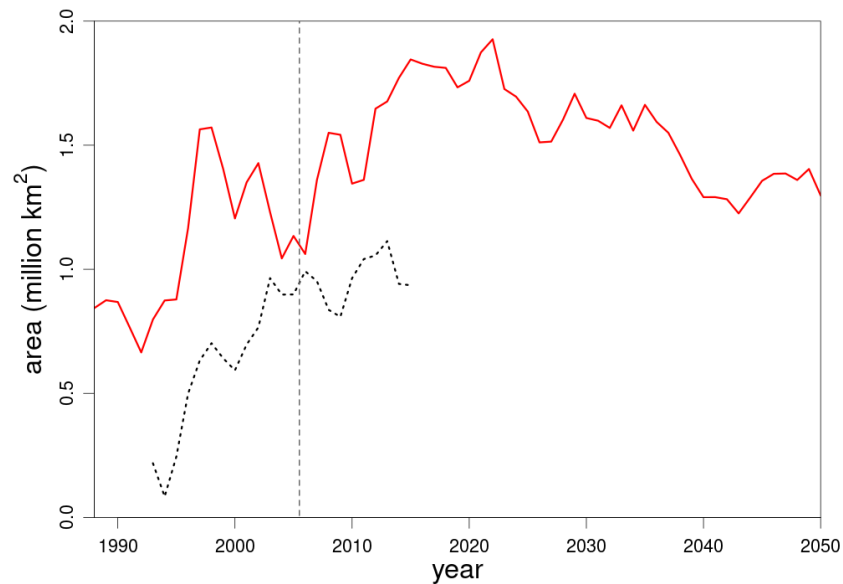
Figure 4.9: Area covered by the STG water distributed in latitudes $\geq 53°$N and longitudes $\geq 5°$W from 1988 to 2050 (red line), and comparison with annual SPG index values from 1993 to 2015 (black dotted line).
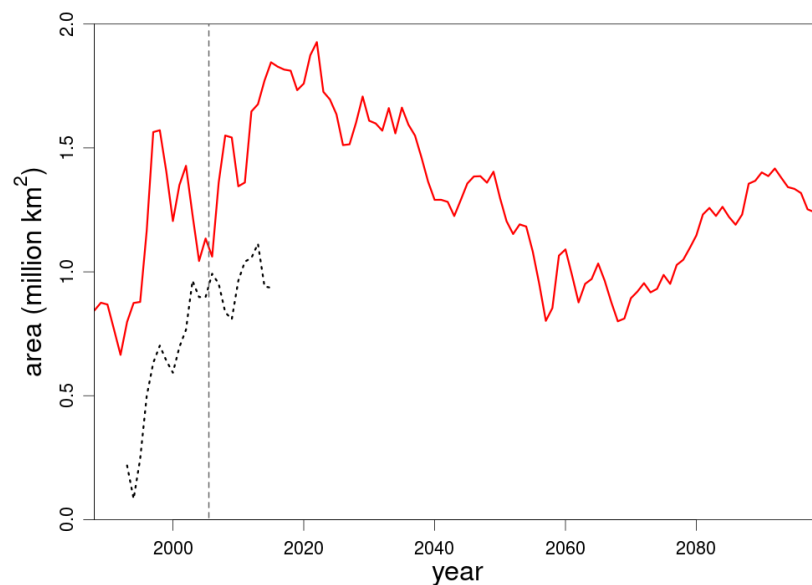
Figure 4.10: Area covered by the STG water distributed in latitudes $\geq 53°$N and longitudes $\geq 5°$W from 1988 to 2099 (red line), and comparison with annual SPG index values from 1993 to 2015 (black dotted line).

index, suggesting that it might be a good proxy index to describe SPG strength variation, with high value corresponding to the weak SPG regime, when STG waters spread farther north and west over the Rockall Plateau. After 2020, this new SPG index started a slow decrease until 2070 (fig. 4.10). However, maps of water mass distribution in 2030, 2040 and 2050 (fig. 4.8) gave no indication

of a strengthening of the subpolar gyre. This could be the result of the North Atlantic freshening over this period, which might have resulted in a shift of the temperature and salinity properties of both SPG and STG waters. Nevertheless, while this variable might be unsuitable to describe SPG strength variations after 2020, it is still relevant for studying the effect of varying salinity distributions on blue whiting population dynamics, especially those related to spawning in this area.

4.1.3 Disruption in the model outputs

As mentioned previously, a disruption in the NEMO outputs was detected between years 2005 and 2006 when studying temperature and salinity time series, and needed further investigation. These years correspond to the transition between the historical outputs and the projection outputs. In the time series, we already noted that some areas seemed to be more affected than others by this transition between model outputs, in particular northern areas (Irminger Sea and Norwegian Sea). The disruption in salinity also tended to be more pronounced than in temperature (fig. 4.3 and 4.4). Therefore, the estimated spatial distribu-
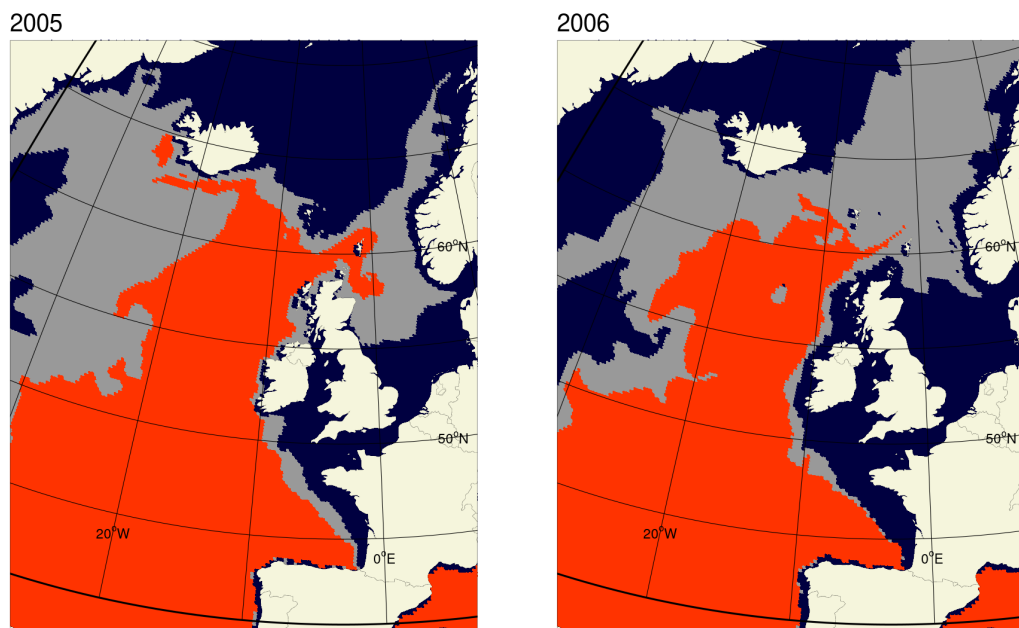
Figure 4.11: Comparison of water mass spatial distribution between the last year of the historical run (2005) and the first considered year of the projection run (2006). Water masses are defined by the same salinity thresholds than in fig. 4.7.
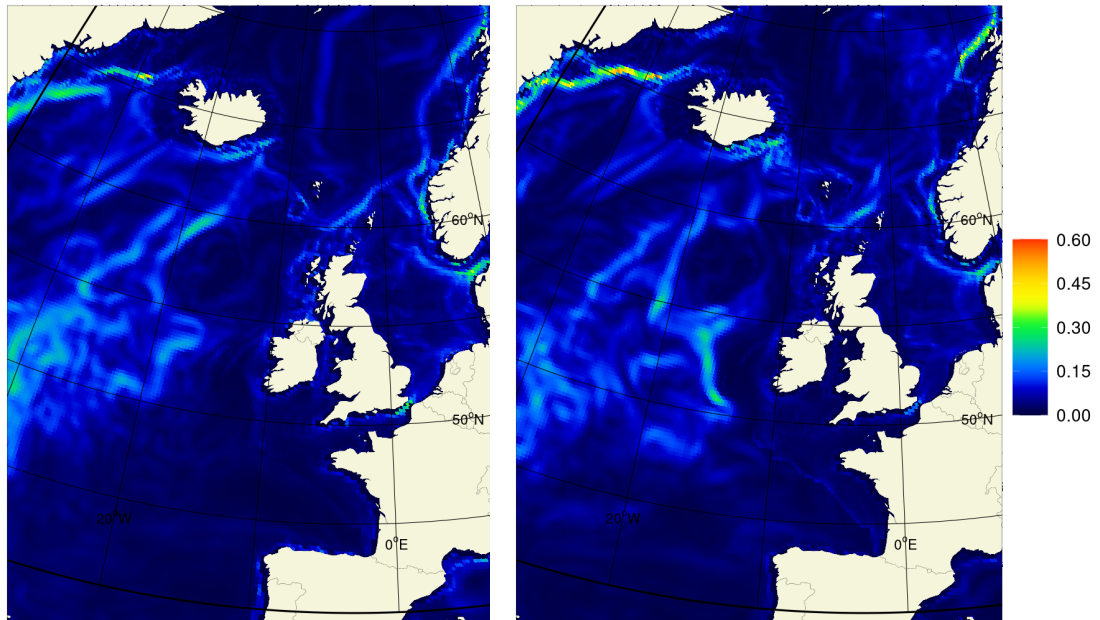
Figure 4.12: Comparison between maps of annual mean flow intensity (m/s) calculated in the last year of the historical run (2005) and in the first considered year of the projection run (2006).

tions of SPG and STG waters were also investigated in 2005 and in 2006.

Changes in the coverage of STG waters between both years were relatively light and appeared relatively realistic (fig. 4.11). In contrast, the limit between North Atlantic waters and Arctic waters seemed to become unclear in the NEMO projection run, while SPG waters seemed to suddenly spread east- and northward. Moreover, the projection run showed fresher water all over the French and British continental shelf in 2006, which suggested that inflow of freshwater from rivers was more important in the projection run than in the historical run.

Waters with salinity between 35.10 and 35.35, which was previously assumed to represent mixed SPG and STG waters, were distributed all over the Norwegian Sea in 2006. This clearly showed the lack of a strong horizontal salinity gradient over the Iceland-Faroe ridge in the projection outputs, while present in the historical ones. In contrast, the longitudinal salinity gradient between SPG and STG waters in the North Atlantic increased between historical and projection NEMO outputs.

A brief study of the currents in 2005 and 2006 provided further evidence of the spatial differences between historical and projection outputs (fig. 4.12). First,

we note that strong currents between latitudes 50 and 55°N shifted to a more eastward position in 2006, and followed exactly the shelf edge of the Porcupine Bank. Currents marking the end of the Gulf Stream seemed to be however much weaker than in 2005. Currents between Iceland and Greenland seemed to be much stronger in 2006 than in 2005. The Norwegian Sea seemed to be covered by more eddies in 2006 than in 2005. This latest observation might explain the very homogeneous salinity field observed over the whole Norwegian Sea in 2006.

In the context of the blue whiting model, temperature, salinity and currents are expected to have the strongest effect on population distribution and growth in the spawning area according to previous studies (Hátún et al., 2007; Hansen & Jákupsstovu, 1992; Skogen et al., 1999; Bartsch & Coombs, 1997; Svendsen et al., 1996). Since the data disruption in this area was almost non-existent compared to other areas, the effect of this disruption on the blue whiting population dynamics might be limited. Therefore, it was considered acceptable to continue using NEMO as input data in the model.

Finally, the fact that the 2005-2006 disruption in the NEMO outputs is not only present in temperature and salinity fields but also in flow fields made simple adjustive correction methods impossible to use. Moreover, correcting salinity and temperature fields to smooth the transition between both years while keeping the same uncorrected flow fields might lead to further model issues.

4.2 Medusa 2.0

Medusa, which stands for Model of Ecosystem Dynamics, nutrient Utilisation, Sequestration and Acidification, is the biogeochemical model component of NEMO-Medusa, whose outputs were used here, and was developed by Yool et al. (2011, 2013b). Medusa 2.0 is a nutrient-phytoplankton-zooplankton-detritus (NPZD) model, which has the particularity to use more than one currency, namely nitrogen (N), silicon (Si) and iron (Fe) (Yool et al., 2013b). Some of the model state variables are also expressed in organic carbon (C), using fixed C:N ratios. The model produces outputs for a total of 15 3-D water column state variables, including phytoplankton, chlorophyll, and micro- and mesozooplankton.

Simulations of NEMO-Medusa at a global scale have proven to perform well at reproducing general spatial and seasonal patterns present in observations (Yool et al., 2013a,b). And compared to similar models from CMIP5 (including HadGEM2-ES), its performance at predicting chlorophyll, primary production, dissolved inorganic carbon and alkalinity seemed to be among the best (Yool et al., 2013b). However, discrepancies between observed and simulated distributions were present in some regions. For example, Yool et al. (2013b) mentioned that primary production in the subtropical gyres tended to be lower in the model simulations than in the observations.

In terms of the model capability at providing meaningful climate projections, Yool et al. (2013a) showed that NEMO-Medusa forecasts of primary production were in agreement with other model studies. Moreover, the model was able to simulate variability between regions in the response to different climate scenarios (here RCP 2.6 and 8.5). Over the 21st century, a decline in primary production (-21%) was predicted in the North Atlantic, while the Arctic experienced a strong increase ($+59\%$). However, Yool et al. cautioned about deficiencies of the NEMO-Medusa model at predicting accurately biogeochemical processes, especially at smaller spatial scales. Hence the importance of studying any Medusa variable relevant to the blue whiting model.

4.2.1 Mesozooplankton

Initially, the NEMO-Medusa outputs of mesozooplankton concentration were supposed to be used in the blue whiting model as the food input data. However, for several reasons presented thereafter, this idea was abandoned.

Quarterly maps of spatial distribution from the historical run revealed that the mesozooplankton concentration was at the highest in coastal areas throughout the year (fig. 4.13). The planktonic bloom seemed to first appear in subtropical waters, likely around the end of the first quarter and the start of the second, before spreading northward, covering the North-East Atlantic area and the Norwegian Sea by the third quarter.

The same type of maps were produced from the projection run. They showed plankton distribution patterns that were very different from the historical run results, in both time and space (fig. 4.14). This time, the highest densities of

(a) 2005 - Quarter 1

(b) 2005 - Quarter 2

(c) 2005 - Quarter 3

(d) 2005 - Quarter 4
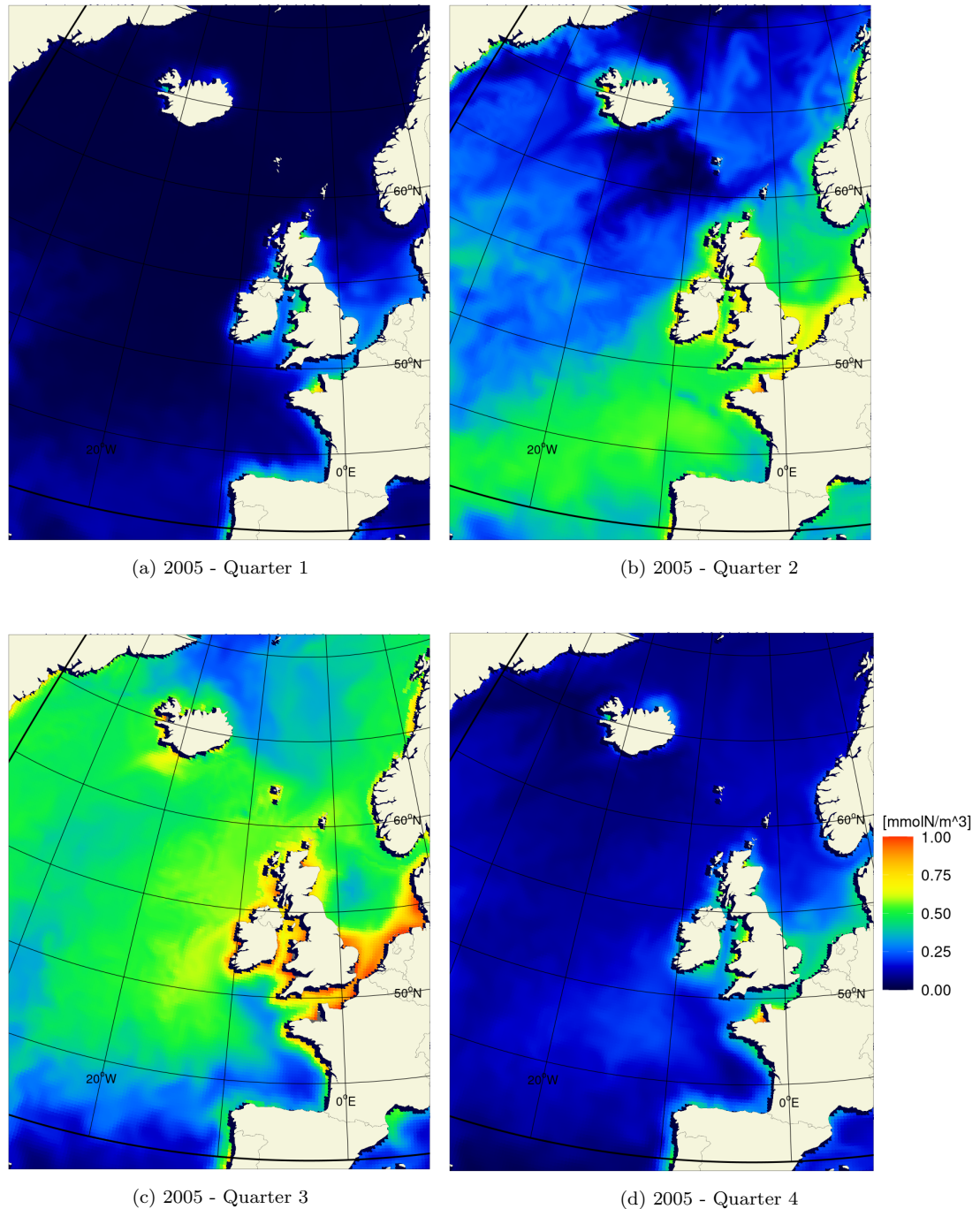
Figure 4.13: Quarterly mean concentration of mesozooplankton (mmolN/m^3) from the last year of NEMO-Medusa's historical run (2005).

mesozooplankton throughout the year were observed in the North Sea. It was also the main starting location of the planktonic bloom appearing in quarter 1. In quarter 2, an increase in plankton concentration similar to the one observed in the historical run was observed in subtropical waters, although it seemed to spread northward at a faster speed. Finally, a hotspot area for zooplankton seemed to

(a) 2006 - Quarter 1

(b) 2006 - Quarter 2

(c) 2006 - Quarter 3

(d) 2006 - Quarter 4
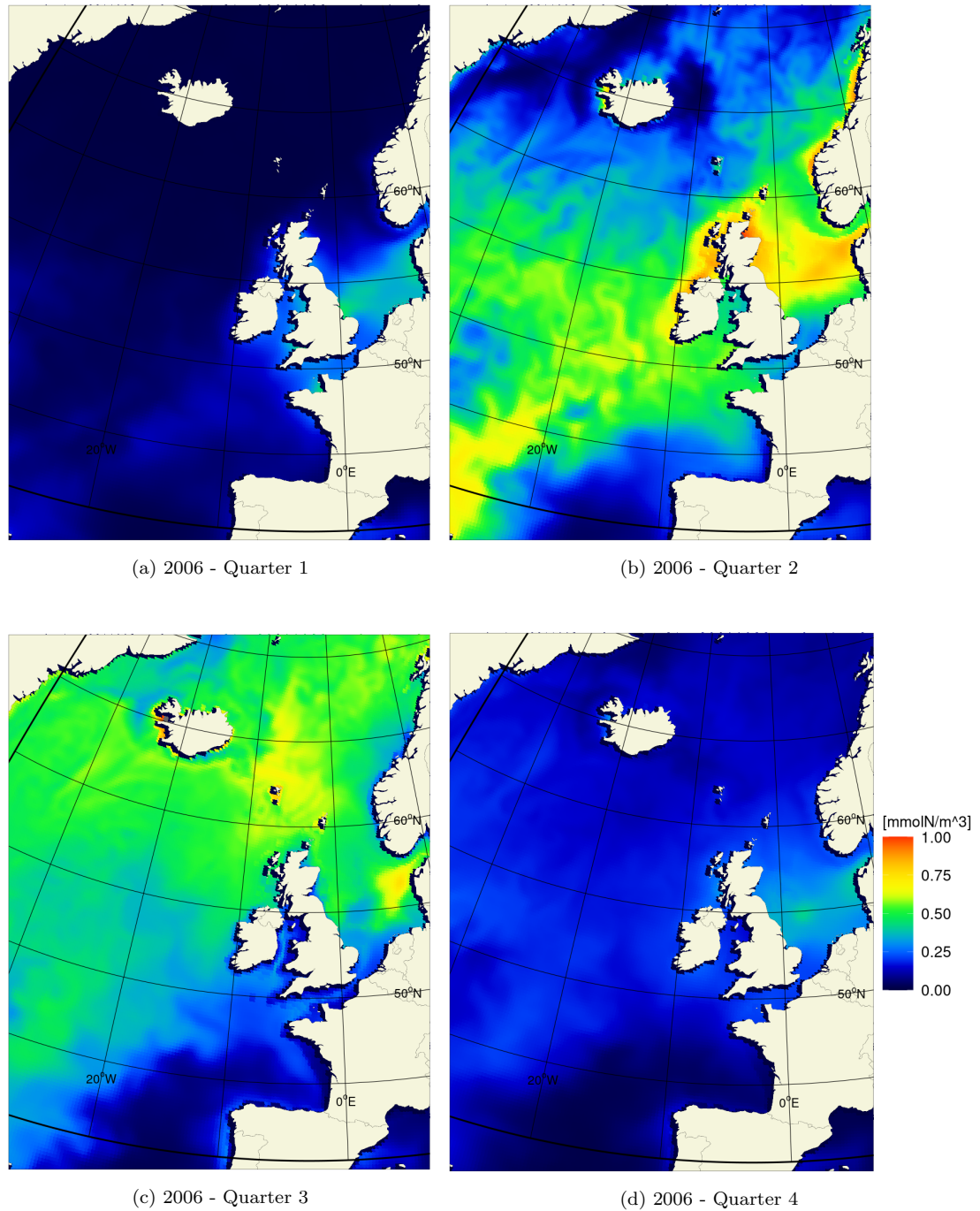
Figure 4.14: Quarterly mean concentration of mesozooplankton (mmolN/m^3) from the the first considered year of NEMO-Medusa's projection run (2006).

appear north of the Faroe Islands during the third quarter. This hotspot area was mostly non-existent in the historical run.

The first reason for not choosing the NEMO-Medusa mesozooplankton variable as blue whiting food for the model was the lack of a clear mesozooplankton

hotspot area in the Norwegian Sea between April and September in the historical outputs. While blue whiting migrate to the Norwegian Sea for the feeding season, the historical zooplankton distributions suggested that staying in the spawning area would be more advantageous for them, if they were indeed feeding on this mesozooplankton population. Thus, this incoherence suggested that the mesozooplankton modelled by NEMO-Medusa was not sufficiently representative of the blue whiting diet. And although distributions observed from the projection outputs might be closer to the expected food distributions for blue whiting (especially in quarter 3), the early bloom of mesozooplankton in the Porcupine Bank area would be attracting the migrating population to that area instead of the Norwegian Sea, which bring us to the second reason.

The blue whiting migration model was designed so that the population would follow food gradients to reach their feeding area. In this context, the NEMO-Medusa variable was unsuitable in simulating realistic blue whiting migration into the Norwegian Sea, whether it was from the historical or projection run. Strong attraction to coastal areas, especially in the historical run period, presented a major problem for modelling migration of a mesopelagic fish. Restricting the mesozooplankton fields to areas deeper than 200 m solved the problem only partially, as gradients expanded most of the time farther offshore and would still make the coast act as an attractor.

Finally, mesozooplankton outputs were very different between the historical and projection run, suggesting different population dynamics. It made the direct use of both outputs in the blue whiting model questionable. It was supposed that the 2005-2006 transition could result in major changes in the blue whiting population dynamics, starting with different feeding migration pathways leading to very different population distributions between both years.

4.3 Theoretical spawning areas of blue whiting

4.3.1 Definition

Theoretical spawning areas suitable for blue whiting were defined by the spatial distribution of optimum spawning conditions. These optimum conditions include temperatures between 9 and 10°C, salinities between 35.3 and 35.5, and a water

column depth between 250 and 600 m (Miesner & Payne, 2018). Since the NEMO outputs will be used in the blue whiting model, it became important to study NEMO predictions of suitable spawning areas.

NEMO fields of temperature, salinity and depth were used to compute theoretical distributions of suitable spawning areas for each time step of the spawning season, from the start of February to the end of April. These distributions were then used to estimate the probability of each cell in the NEMO-Medusa spatial domain to be suitable for spawning over the whole duration of the spawning season.

4.3.2 NEMO predictions

Overall, the highest probability of suitable spawning conditions over the whole season were often predicted along the French and British continental shelf and over the Rockall Plateau between 1988 and 2020 (fig. 4.15 and 4.16). In years of weak SPG (2002/2004), the quasi entirety of the Rockall Plateau was covered by suitable spawning areas for the whole season, while suitable spawning grounds seemed to be more limited to the southern part of the Rockall Plateau in years of strong SPG (1992/1994). In years of weak SPG, suitable spawning areas also seemed to appear in more northern areas between Iceland and Scotland.

NEMO predictions of blue whiting spawning grounds from 2000 to 2099 suggested a northward shift of the distribution (fig. 4.16). Over the century, it seems that the blue whiting population will loose progressively all the usual spawning locations off British Isles and will be forced to spawn in new suitable locations, mostly over the ridge between Iceland and Scotland and off the northern coast of Iceland.

Time series of mean latitude and longitude of the predicted suitable spawning areas showed both a northward and westward shift by the end of the century (fig. 4.17). From 1988 to 2015, the centre of gravity moved from the Porcupine Bank area to areas around the latitude of the Rockall Plateau. Between 2015 and 2040, the average location of the spawning grounds seemed to show no significant trend. We noted that during this period, the surface covered by suitable habitat decreased and/or became more occasional over the season (fig. 4.16). The westward shift of the distribution seemed to mostly take place between 2040 and

2065: finding suitable spawning conditions in Icelandic waters in February-April became progressively more likely. The 2065-2099 period was marked by the progressive and definitive loss of spawning areas along the British continental shelf and over most of the Rockall area, which resulted in the final increase in mean latitude observed in the 1988-2099 time series.

(a) 1992   (b) 1994

(c) 2002   (d) 2004
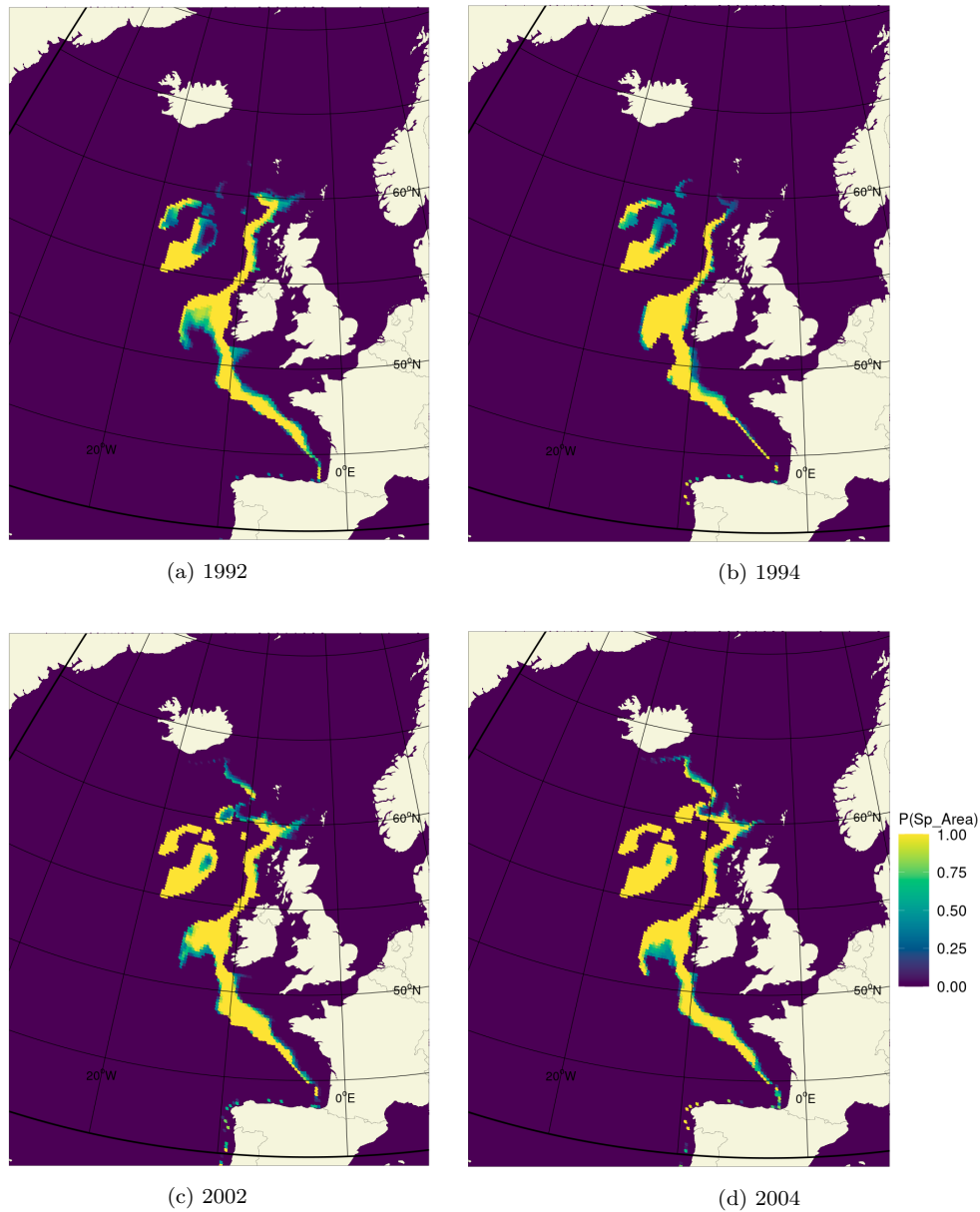
Figure 4.15: Spatial distribution of suitable spawning grounds according to the defined environmental conditions, estimated for different years and during the theoretical spawning period (from start of February to end of April). Years 1992 and 1994 were marked by a stronger subpolar gyre than years 2002 and 2004. For each cell of NEMO's spatial domain, the proportion of the spawning period's time steps in which that cell was a suitable spawning habitat is calculated. Areas in yellow are suitable for the whole duration of the spawning period.

(a) 2000　　　　　(b) 2010　　　　　(c) 2020

(d) 2030　　　　　(e) 2040　　　　　(f) 2050

(g) 2099
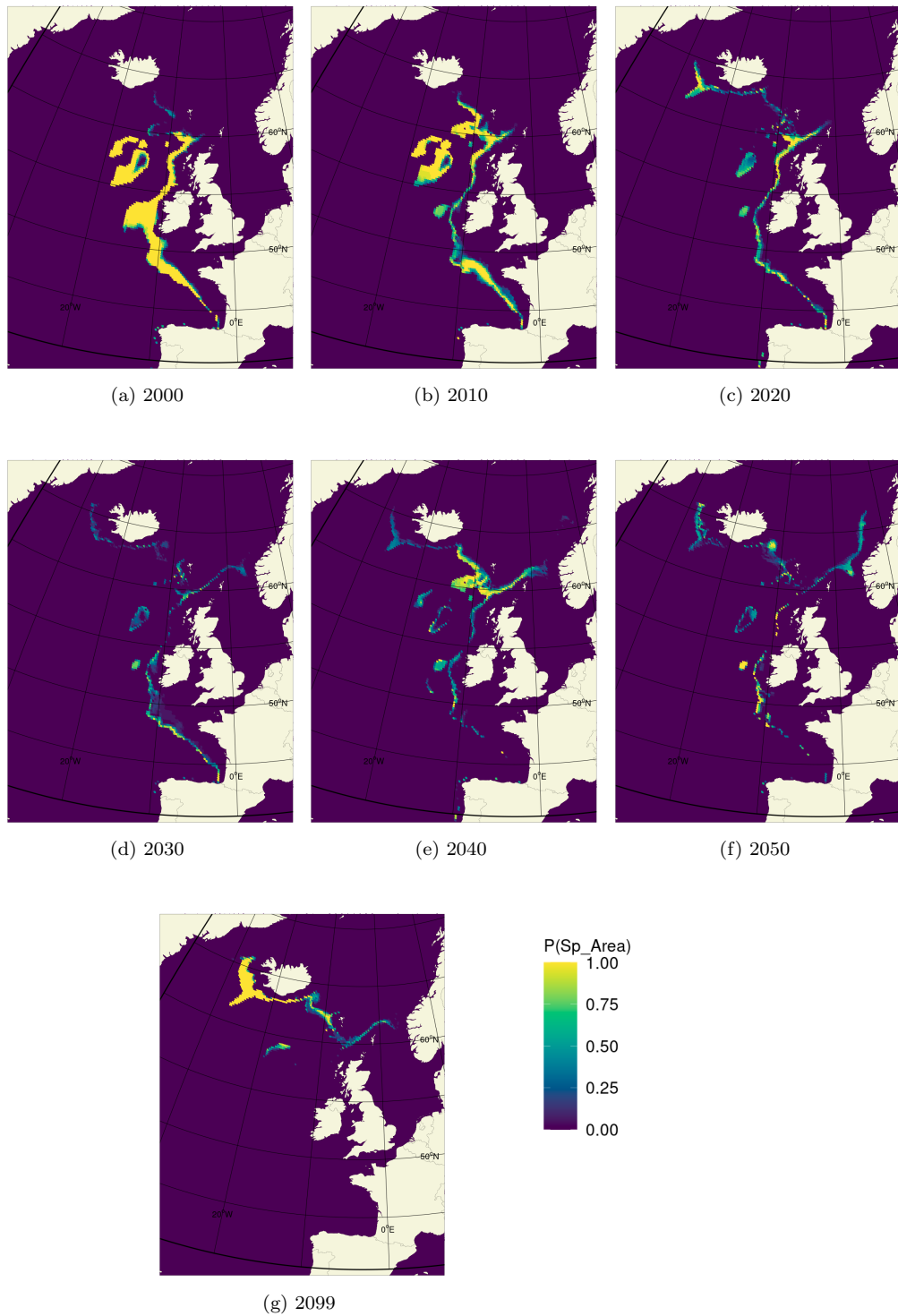
Figure 4.16: Variation in spatial distribution of suitable spawning grounds from 2000 to 2099 (see fig. 4.15). Apart from year 2000, every other distribution was computed from projection outputs of NEMO-Medusa.

(a) Mean latitude (1988-2099)

(b) Mean latitude (1988-2050)

(c) Mean longitude (1988-2099)

(d) Mean longitude (1988-2050)
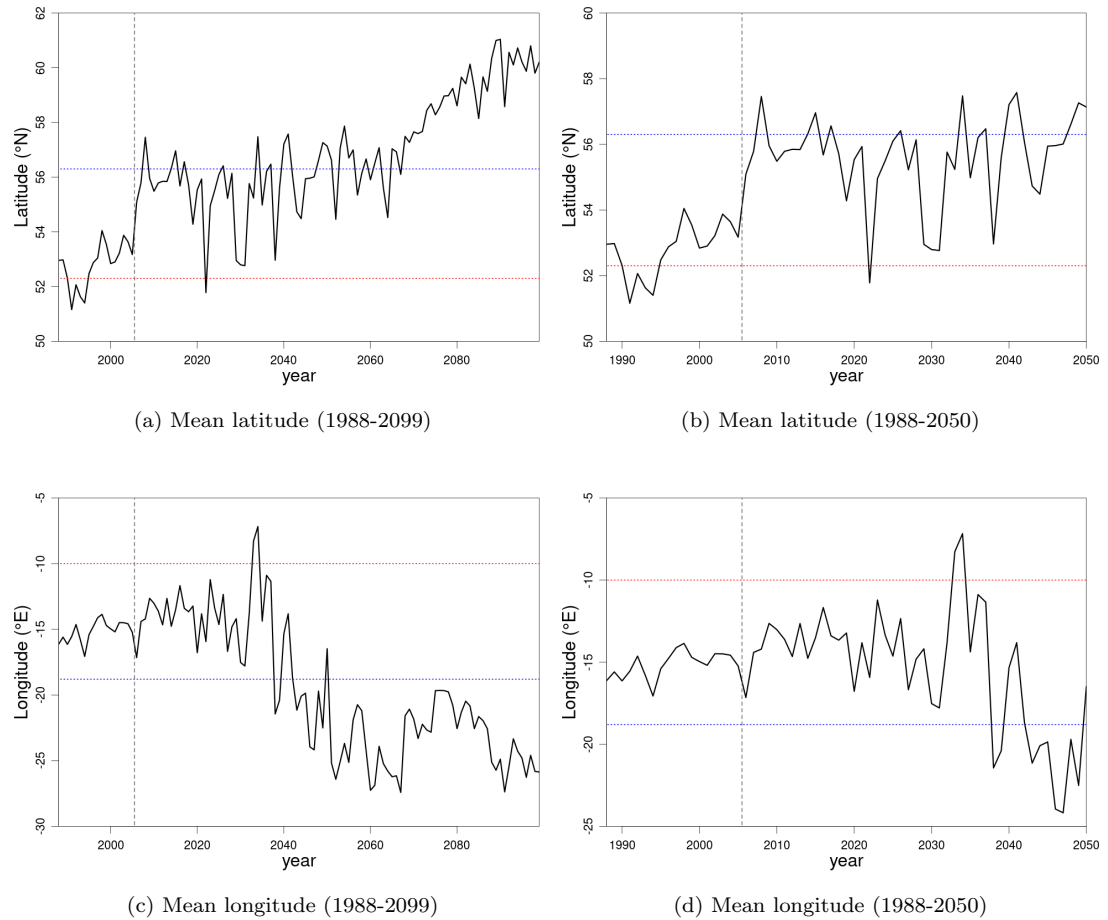
Figure 4.17: Time series of mean latitude and longitude of predicted suitable spawning areas for the whole NEMO-Medusa run period from 1988 to 2099 (a and c) and just for blue whiting model's run period, from 1988 to 2099 (b and d). For mean latitude time series (a, b), the blue and red dotted lines represent respectively the location of the Rockall Plateau and the location of Porcupine Bank. In mean longitude time series (c, d), the Rockall Plateau's location is still represented with the blue dotted line, while the red dotted line represents the longitude of the continental shelf at a latitude similar to the one of the Rockall Plateau.

4.4 Discussion

At the end, only output variables from the NEMO model component of NEMO-Medusa were considered satisfactory enough to be used directly into the blue whiting model. Although a disruption in the outputs was present when changing from the historical to the projection NEMO simulation, it seemed to have a greater impact in northern and western regions. The effect on the physical conditions of the main spawning area was more limited, and so it was assumed that the data disruption would not cause any brutal changes in spawning distributions and larval transport. Historical and projection outputs of NEMO-Medusa have been usually used jointly in the past (Yool et al., 2013a, 2015, 2017; Magozzi

et al., 2017), but no disruption in the dataset was mentioned. However, most model studies were realised over longer term runs and/or at the global scale, which would make this disruption insignificant when studying overall variations and trends. While the disruption might not affect significantly blue whiting population dynamics, it will be important to keep it in mind when analysing any outputs from the population model.

Compared to the physical variables, the disruption observed in the mesozooplankton outputs was harder to dismiss as negligible. The annual cycle of spatial distribution seemed to suggest very different dynamics of mesozooplankton between the historical and projection outputs. Since the Medusa outputs of mesozooplankton were first considered to be used in the model as the blue whiting food variable, it will most likely result in a similar disruption in the blue whiting model outputs. Moreover, most spatial distributions showed the variable was unsuitable for using it in the model as the variable leading the blue whiting population into the Norwegian Sea during their feeding migration. According to the Medusa outputs, coastal areas would represent a very strong attractor for the post-spawning population in the second quarter, whereas the main feeding grounds of blue whiting are supposed to be located in the Norwegian Sea (Bailey, 1982; Trenkel et al., 2014). This suggested that the mesozooplanktonic population described by Medusa was no match to the blue whiting diet. In fact, past studies of stomach contents showed that blue whiting seem to mostly prey on euphausiids, hyperiids and copepods (Bachiller et al., 2016; Prokopchuk & Sentyabov, 2006; Dolgov et al., 2010; Lopez-Lopez et al., 2017; Cabral & Murta, 2002). These taxa combined together might show very different spatial distributions than the Medusa mesozooplankton variable, since the later described dynamics of the whole planktonic group, including all taxa belonging to this group. Thus, computing a food variable more representative to the blue whiting diet is necessary for the model (chapter 5). Machine-learning methods could be used to model this new variable, while the Medusa variable might still be considered as one of the predictors. This way, it might offer significant insight for predicting spatial distribution changes in response to environmental changes, especially those caused by the chosen climate change scenario.

Climate variations in the NEMO-Medusa simulations seemed to be best repre-

sented by variations in the STG water mass distribution off the British Isles. Like in the observations made by Hátún (2005), the coverage of STG water in this area tended to extend when the subpolar gyre was weakening. Considering the short time period available for the comparison between the SPG index and the STG water cover area west of the British Isles, it was difficult to assess if the latest was a good proxy for describing SPG strength variations simulated by NEMO over the whole model period (1988-2050). However, the variable was judged to be well adapted to describe climate changes affecting directly the conditions of the main blue whiting spawning grounds. For example, while years were sampled to represent both weak and strong SPG regimes according to the SPG index, this NEMO climate index seemed to suggest that conditions over the spawning grounds between 1994 and 2004 could be more similar than the SPG index values implied.

NEMO predictions of blue whiting spawning areas helped formulate a few early assumptions about the effect of climate on blue whiting spatial dynamics. Thus, assuming that the blue whiting population successfully reach and cover all the suitable spawning areas by the end of their pre-spawning migration, it was hypothesised that a SPG weakening would result in a north- and westward expansion of the adult spawning distribution. Finally, the clear reduction and light northward shift of suitable spawning area between 2010 and 2050 are expected to affect adult migration success as well as larval drift over this period. These changes in spawning area distribution seem to be the result of the decreasing coverage of warm and saline waters in the area off British Isles, caused this time by a freshening of the subpolar gyre region (van den Berk et al., 2021).

Chapter 5

Predicting Distributions of Food Available to Blue Whiting in the Environment

The blue whiting population model needs input of various physical and biological variables. In the previous chapter, the NEMO-Medusa outputs of currents, temperature and salinity were considered satisfactory enough to fulfil this role. However, doubts were cast on the choice of the mesozooplankton variable as input for the blue whiting food (adults and juveniles). Here, the blue whiting diet was further and thoroughly investigated, and a more appropriate food variable was defined. New predictions of food fields were computed using random forest models trained on relevant CPR datasets. Blue whiting prey selectivity was also determined and used in the computation of the new food input variable.

5.1 Introduction

The ultimate objective of this study was to develop a food variable specific to blue whiting, whose predictions could then be used as input in a spatial population model. Either from a lack of observation data or from an attempt at simplifying feeding dynamics, some spatial models of fish population dynamics might be bypassing the use of a food variable whose variations in time and space would correspond to prey dynamics of the studied species. For example, Boyd et al. (2018) used phytoplankton biomass as a proxy for the food variable of mackerel, with the risk that variations in time and space might not be representative of the real food variations. In the case of blue whiting, this would be inappropriate for

studying the effect of climate variations on both population growth and distribution. Therefore, a thorough study of the diet of blue whiting and the spatial dynamics of its main preys is necessary for the process of developing a better food variable for this species.

In past studies, euphausiids, amphipods (mostly hyperiids) and copepods were repeatedly present in the diet of blue whiting, with a few recurring species and some variation which could be related to the different sampling locations (Cabral & Murta, 2002; Prokopchuk & Sentyabov, 2006; Dolgov et al., 2010; Bachiller et al., 2016; Lopez-Lopez et al., 2017). This suggested that blue whiting might have a selective diet, and that the availability of the different preferred preys might vary between locations. Prey selectivity is usually determined by comparing the proportion of each prey in the diet with their relative proportion in the environment (Manly et al., 1972). As growth depends on the food uptake which would then take implicitly into account any diet preferences, we define the food variable as the concentration of food in the environment which is directly of interest to the blue whiting population.

Since the food variable is needed as input to a spatial population model where long-term predictions are needed, it is essential for this study to find a method that will enable to make food predictions over the whole time and spatial domain of the model, based on observations. In this context, machine-learning methods seem well adapted, as they allow for the training of a statistical model over observations of the variable of interest (here food), looking for potential relationships with other known variables called predictors (Hastie et al., 2009). Some of these methods have already proved satisfactory in the study of variations of population distribution and their potential environmental drivers (Zarauz et al., 2008; Miller et al., 2014; Brun et al., 2016). In theory, such a model could also be used to make predictions of plankton at any time and space, as long as values of predictors are known, although it is mandatory in that case to assess the model's ability at forecasting and extrapolating before its validation (Guisan et al., 2002; Brun et al., 2016). The model performance at predicting blue whiting food was therefore taken into account in selecting the most suitable machine-learning method for the following study.

5.2 Material and methods

5.2.1 Stomach contents

To identify main preys of blue whiting, the stomach records from Cefas's integrated database and portal for fish stomach records (DAPSTOM) were used. DAPSTOM gathers stomach records of 188 species which were sampled over the past 100 years (Pinnegar et al., 2015). In the case of blue whiting, stomach records were available between 1961 and 2011 (Fig. 5.1) and came from samples around Iceland and the Norwegian Sea and from samples above the continental plateau from the Bay of Biscay to the Irish and Celtic Seas (Fig. 5.2). Southern records accounted for 59% of sampled stomachs over the whole period and for 62% of stomachs sampled after 1988.

DAPSTOM offers a simple online visualisation tool of their dataset, which was used to roughly identify main preys. However, online estimates of prey proportions in the diet were subject to errors due to overlapping group names of prey in the raw dataset and sometimes repetition of a sample's data entry, which is the reason why further analyses were done using the processed version of the dataset. Nevertheless, the online tool was also used to identify the main competitors of blue whiting.

The raw dataset gives prey items identified and their minimum number ob-
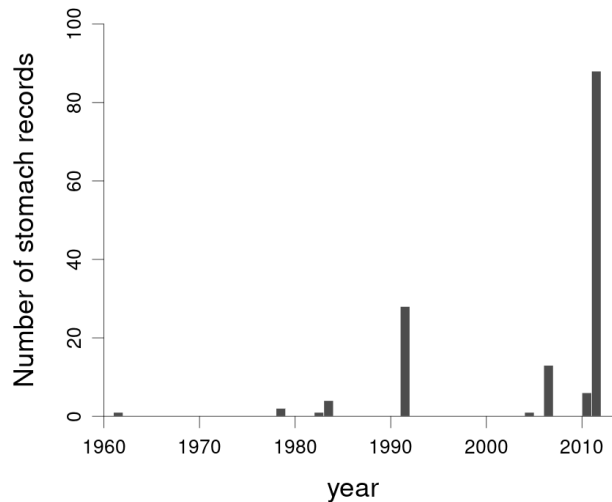
Figure 5.1: Number of stomach records available by year for blue whiting, over the period 1960-2011 (DAPSTOM).
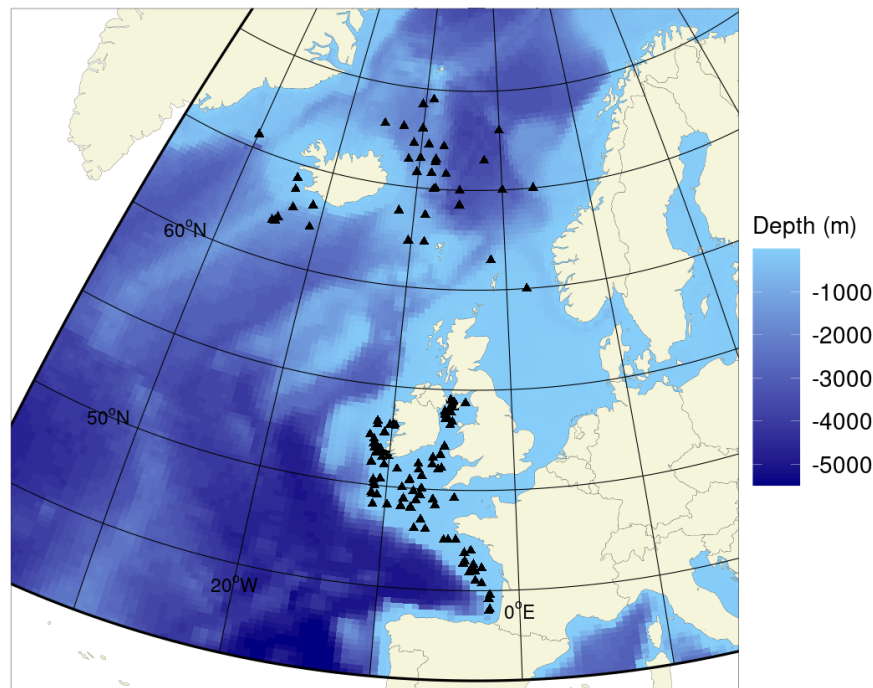
Figure 5.2: Location of blue whiting stomach records available on DAPSTOM, from 1978 to 2011. Water column depth is represented with a blue gradient and was taken from depth average estimated for each cell of the blue whiting model domain.

served for each sampled stomach and sample location. It also includes average fish length from samples. Figure 5.3 shows the fish length distribution of the sampled stomachs. After some data corrections and standardisation of spatial information, the dataset was simplified to better suit study purposes. In the original dataset, taxonomic identification accuracy varies between preys. For example, not all hyperiids were identified at the species level, and apart from *Parathemisto abyssorum*, *Themisto libellula* and *Parathemisto oblivia*, any other hyperiids were only acknowledged under the family name Hyperiidae. Therefore, to avoid overlapping prey groups, the data was simplified by defining the dominant taxa groups, taking into account the main preys identified previously on the online portal. Any prey items which did not belong to the defined taxa groups were only acknowledged as 'other' and empty stomachs as 'empty'.

Each prey group's proportion in the diet was calculated. Variation in diet between areas and length classes was also compared. To do that, two length classes were defined, one for fish smaller than the maturation length $L_m = 21$ cm, and one for fish longer than L_m, which would be respectively representative of juve-
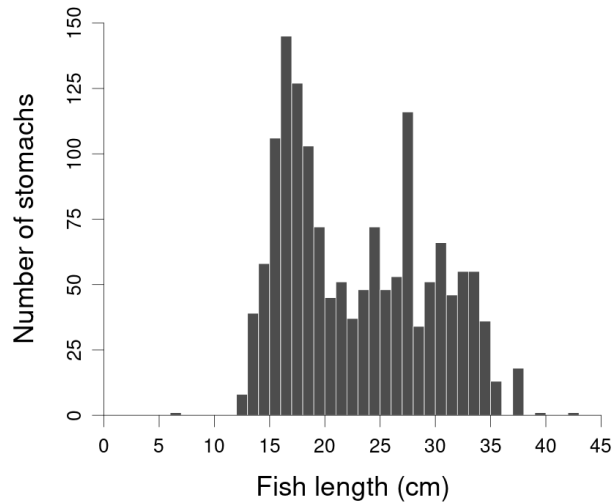
Figure 5.3: Length distribution (cm) of fish sampled for stomach records (DAPSTOM).

nile and adult life stages, matching blue whiting model's life stage definitions. Spatially, the dataset was also split in two, and comparison was made between diets of fish sampled north and south of the latitude 55°N.

5.2.2 CPR data

Once main preys were identified, the next step was to study their environmental spatial distribution. The Continuous Plankton Recorder (CPR) has been sampling plankton in the ocean surface layer continuously along ship paths (mainly merchant) in the last century. The resulting dataset gives information on encountered species or taxa groups and their observed and estimated numbers in samples, as well as sample location coordinates. CPR data for available and relevant taxa was used to estimate spatial distribution of blue whiting food in the North-East Atlantic.

Only data from 1988 to 2014 was conserved for the project (Fig. 5.4), to match the time of NEMO-Medusa outputs. The CPR device filters plankton continuously at a depth around 7 m (Richardson et al., 2006). Plankton is filtered and recorded between two silk bands of 270 µm mesh. To facilitate data analyses, the plankton collected along one route is then split. As a result, each sample point on the map in figure 5.5 corresponds to 10 nautical miles of tow and an average volume of water filtered around 3 m^3.
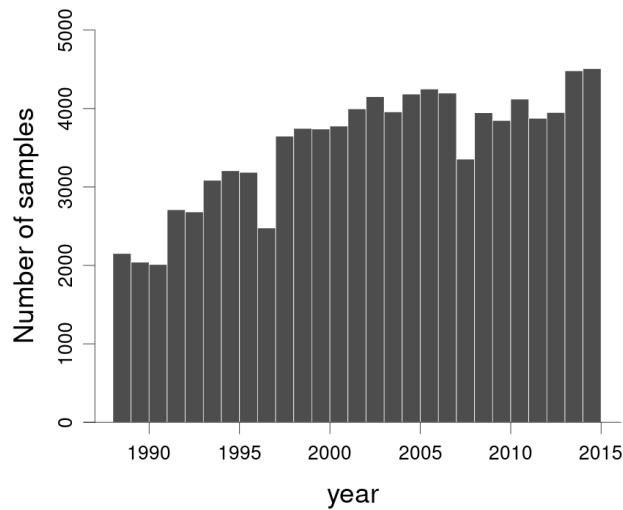
Figure 5.4: Number of CPR samples available for blue whiting food study, over the period 1988-2014.

After the CPR sampling, zooplankton is processed in two different ways depending on their size. For studies of zooplankton with size >2 mm, the eye-count method is used, counting the total number of individuals observed for each sample and identifying taxa. For zooplankton <2 mm, zooplankton traverses are defined and examined, counting and identifying taxa only in those traverses, which would account for 1/50 of the total silk sample. Both zooplankton count values are only

Table 5.1: Categories used during CPR sample processing for the two zooplankton counting stages (zooplankton traverse and eyecount). The number counted in a sample is recorded in the dataset following its category. For each category, an accepted count value is given for the sample. In the case of eyecount method, the accepted value corresponds to the abundance per sample, and in the case of zooplankton traverse, it needs to be multiplied by 50 to get the abundance per sample (Richardson et al., 2006).

Number counted	Category	Accepted value	Abundance per sample for zooplankton traverse
1	1	1	50
2	2	2	100
3	3	3	150
4-11	4	6	300
12-25	5	17	850
26-50	6	35	1750
51-125	7	75	3750
126-250	8	160	8000
251-500	9	310	15500
501-1000	10	640	32000
1001-2000	11	1300	65000
2001-4000	12	2690	134500

stored semi-quantitatively in the final dataset, according to logarithmic categories (table 5.1). The accepted count value for each category corresponds to the estimated abundance per sample for zooplankton > 2 mm, but needs to be multiplied by 50 to get the abundance per sample for zooplankton identified with the traverse method (Richardson et al., 2006). For this study, abundance values were divided by the standard value of water volume filtered by sample (~ 3 m^3) to obtain biomass concentrations (in mg/m^3).

To test the hypothesis that the mesozooplankton variable from NEMO-Medusa is not suitable to use as food variable in the blue whiting model, quarterly averages of spatial distribution of the CPR taxa were studied and compared with NEMO-Medusa mesozooplankton. For the purpose of this comparison, a coarser spatial grid of 1° in longitude and 1° in latitude was used. CPR abundance values were averaged in each cell and over the considered time period.

To identify environmental factors potentially affecting time and spatial variation in zooplankton abundance, NEMO-Medusa outputs were used. For each sample's average location, environmental variables from NEMO-Medusa were
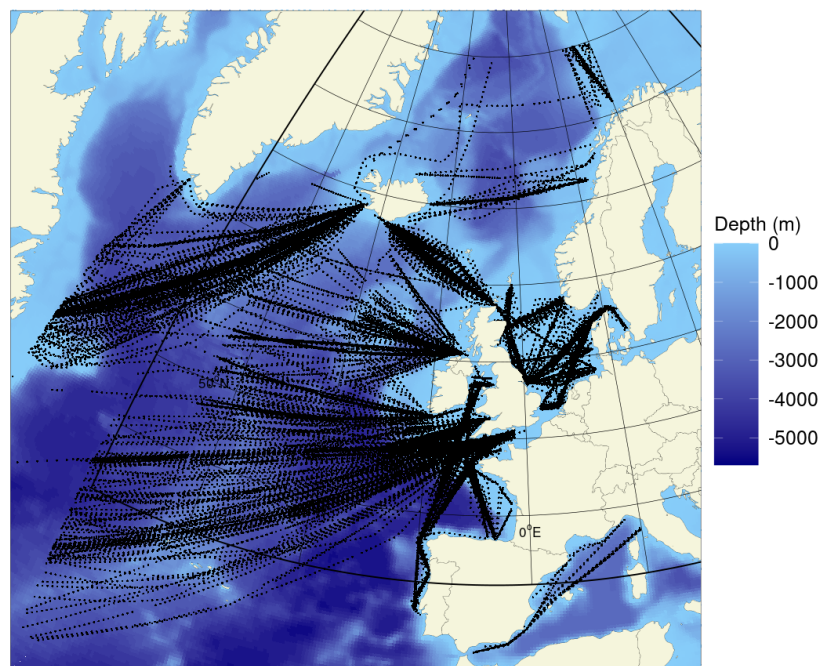
Figure 5.5: Location of CPR samples used for blue whiting food study, from 1988 to 2014. Water column depth is represented with a blue gradient and was taken from depth average estimated for each cell of the NEMO-Medusa model domain.

extracted from the nearest NEMO-grid cell centre. This included sea surface temperature (SST), surface salinity (SSS) and average mesozooplankton concentration in the surface layer (mezo). Day time of CPR samples were also taken into account and processed against sunset and sunrise hours to split the CPR dataset into night and day samples and to test if CPR could detect increased zooplankton abundance at night caused by their diel vertical migration (Beare & McKenzie, 1999).

CPR coverage was very poor in the Norwegian Sea over the studied period (Fig. 5.5) and therefore special care was taken, when assessing machine-learning models for predicting zooplankton distribution in this area.

5.2.3 Machine-learning models

Many different machine-learning methods exist, whether supervised or unsupervised (Hastie et al., 2009; Valletta et al., 2017). In the early attempts to predict plankton abundance in the whole model's spatial domain and time period, general additive models (GAM), which are supervised methods, were used (Annex A). Their main advantage are the possibility to select and add predictors step by step, and to be able to measure each predictor's effect on the studied variable, as well as look for effect of interactions between predictors. GAM predictions of abundance distribution were encouraging for some of the CPR taxa studied. However, GAMs seemed inappropriate for one taxa, as the model seemed to overly smooth spatial variations (see annex A). Moreover the predictor selection process was very time-consuming and prone to many mistakes because of the high number of environmental drivers tested. For those reasons, other machine-learning models were considered.

Random forests

Random forests belong to the unsupervised machine-learning methods and produce models that are built from multiple decision trees. While a single decision tree would lead to large over-fitting issues, the use of many decision trees which are then averaged to give the final random forest model will considerably reduce this effect (Breiman, 1996, 2001; Cutler et al., 2007; Hastie et al., 2009; Rodriguez-Galiano et al., 2012).

The random part of this method comes from the fact that each tree is trained on a subset of the studied data which has been randomly sampled with replacement. Moreover, each tree considers only a limited and fixed number of predictors at each node. Those predictor candidates are also randomly picked from the defined list of predictors considered for the model (Breiman, 2001). Liaw & Wiener (2002) advised to set this predictor subset number (n_p) to no more than the squared root of the total number of predictors ($n_p \leq \sqrt{N_p}$).

Cross-validation is directly incorporated in the random forest method. Because each decision tree is grown on a random subset of the data, which is often referred to as bagging or bootstrap aggregating (Breiman, 1996), an out-of-bag error (OOB) is computed for each of them. The OOB is the error produced by one single-tree model when this model is used on the rest of the dataset (the part that has not been used for training the tree). When the final model is obtained by averaging predictions from all trees, all OOB values are used to compute a measure of importance for each predictor (Breiman, 2001; Cutler et al., 2007).

For this study, the R package and its function `randomForest` (version 4.6-14) were used (Liaw & Wiener, 2002). The function allows for direct computation of predictor importance, which is measured either as the increase in mean squared error in percent (%IncMSE) which uses OOB values or as the increase in node purity (IncNodePurity). The %IncMSE gives the error increase that would result from removing one predictor. Important predictors have high values of %IncMSE, since it means that the model performance is highly affected by their presence. For one predictor, increase in node purity indicates the total number of decrease in the residual error caused by splitting with that predictor. While %IncMSE is a measure of predictor importance when testing the performance of single-tree models (using OOB), IncNodePurity is a measure of predictor importance during the training process of single-tree models. Because of this, we expect that predictors which have a strong relationship with the studied taxa abundance will have high values for both importance indices.

For each CPR taxa, the random forest model was averaged from 500 trees. This was to make sure that the model's residual error had been reduced to its minimum (Breiman, 2001; Liaw & Wiener, 2002).

Collinearity between variables

When using machine-learning models to study and predict the response of a variable to different environmental predictors, it is important to consider collinearity between those predictors (Dormann et al., 2013). For the purpose of this study, the Pearson's correlation coefficient (r) was used to detect collinearity in a set of predictor candidates for plankton population distribution. Dormann et al. (2013) recommends to consider only variables with correlation coefficients $|r| < 0.7$.

Correlation coefficients were computed for each pair of the following predictors: sea surface temperature (SST) and sea surface salinity (SSS) at time t or averaged over the year, water column depth, NEMO-Medusa mesozooplankton, a binary night/day time factor, latitude and day of the year (table 5.2). The correlation threshold used here was $|r| < 0.35$. For SST and SSS, the choice between considering the variable value at time t or averaged over the year was mainly made by looking at correlations with the other predictors. SST_t was the only variable to be highly correlated (above the threshold) with the day of the year. SST_t also had the highest correlation coefficient (albeit under the threshold) with the mesozooplankton variable. Thus, SST_y was selected over SST_t as predictor for the random forests. For the salinity variables, the highest correlations were found with SST_y. Since both SSS_t and SSS_y showed very similar correlations with the other predictors, the variable SSS_t was finally chosen for the random forests, as it had a slightly lower correlation with SST_y than SSS_y. Latitude being highly

Table 5.2: Pairwise correlations (r) between potential predictors to use in machine-learning models. According to the predictor selection criteria ($|r| < 0.35$), values in bold are considered to be too highly correlated, with high risk of collinearity.

Predictors	Day of year	Day-Night	SST_t	SST_y	SSS_t	SSS_y	Depth	mezo
day-night	-0.04	-	-	-	-	-	-	-
SST_t	**0.37**	0.08	-	-	-	-	-	-
SST_y	-0.01	0.01	**0.72**	-	-	-	-	-
SSS_t	0.00	-0.05	0.19	0.31	-	-	-	-
SSS_y	0.00	-0.04	0.23	0.32	**0.98**	-	-	-
depth	0.01	-0.01	0.13	0.19	0.29	0.29	-	-
mezo	0.15	0.20	0.28	-0.03	-0.16	-0.13	-0.19	-
lat	0.02	-0.03	**0.53**	**-0.76**	-0.14	-0.14	-0.34	0.01

SST_t and SSS_t are respectively sea surface temperature and salinity at time t, while SST_y and SSS_y are the annual average of SST and SSS. Depth is the water column depth, mezo is the NEMO-Medusa mesozooplankton variable and lat stands for latitude.

correlated with SST_y (here $|r| > 0.7$), the variable was dismissed from the models.

In the early stages of testing the random-forest method, the Chlorophyll-a concentration variable from the NEMO-Medusa historical outputs was also used as predictor and was found to improve considerably the quality of the models. However, the variable was missing from the available NEMO-Medusa projection outputs, and so it was dismissed afterwards. This problem also concerned the phytoplankton variable from NEMO-Medusa. Therefore, although the mesozooplankton variable was poorly adapted to blue whiting feeding dynamics, it was kept as predictor as the only available biological variable in both NEMO-Medusa outputs at our disposal. This ensured that at least one biological variable was present for producing food concentration forecasts with the random forests.

Spatial and time assessment of model performance

For the purpose of training machine-learning models, it is common and good practice to use a subset of the whole dataset, and to keep the rest for testing the resulting trained models. Using data subsets and testing are already inherent to random forests (Breiman, 2001; Cutler et al., 2007) and could in theory be dismissed altogether. However, random forests were used here to make predictions of plankton distribution for each time step and for the whole spatial domain of the blue whiting model. Since the CPR dataset is limited by its coverage in time and space, a satisfactory level of model performance was needed and expected from the random forests after 2014 (last year available in the CPR dataset) and in areas where CPR sampling was quite low or non-existent, especially the Norwegian sea which was of high interest for this study. Therefore, subsets of the CPR dataset were defined successively in time and space to assess the model performance at extrapolating or forecasting (Elith & Leathwick, 2009; Brun et al., 2016).

For the two experiments, the random forest model was trained on 80% of the CPR dataset and the last 20% were used for model testing. Time subsets were defined to ensure that the model testing would assess forecast accuracy of the trained model. Thus the training data included all data from January 1988 to June 2010, while the testing data included data from June 2010 to December

2014.

For the spatial split of the dataset, the total number of CPR samples available for this study in each areas of the North-East Atlantic (as defined by ICES) was considered. The objective was to get a few large and continuous areas out of the training phase of the model, to be then able to test the model performance at predicting abundance values in those test areas by comparing the random forest predicted values with the CPR observations. The test areas were chosen so that the sum of all their CPR samples would be equal to 20%, while keeping as few separate areas as possible to increase the quality of model testing. In total, six (almost) continuous areas could be identified (5.6): three large areas including (1) around the Azores in the South, with 3686 records (ICES area 10.a), (2) off the British Isles with 4103 records (6.b, 7.c, 7.k), and (3) around Iceland and North-East Greenland with 2563 records (5.a, 14.a); three smaller areas and very
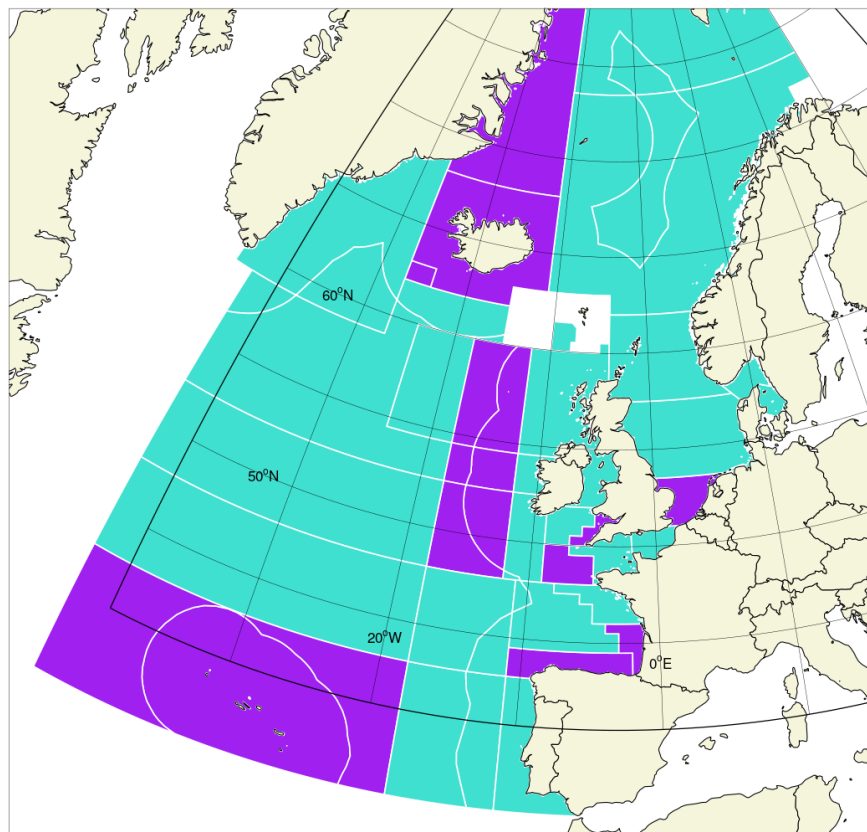
Figure 5.6: Spatial split of the CPR dataset for random forests, using ICES areas. First, random forest model is trained on 80% of the CPR dataset which corresponds to all data sampled in areas in blue. Then, the resulting model is tested with the environmental conditions from areas in purple and predictions are compared to the CPR abundance values in those areas.

close to coasts including (4) the Bay of Biscay with 1143 records (8.b, 8.c), (5) part of the Celtic Sea with 4202 records (7.f, 7.h), and (6) the southern North Sea area with 3365 records (4.c).

Model accuracy was assessed using two different indicators as suggested by Dormann et al. (2013) (1) Pearson's coefficient of determination (r^2) to test the model performance at predicting the real value; (2) the root mean squared error (RMSE) which is equivalent to the standard deviation of residuals and thus gives a measure of distance between the real and predicted values.

5.2.4 Selectivity Index

Predicted biomass concentrations of the studied zooplankton taxa were used to define prey selectivity of blue whiting. To find the right formula for calculating selectivity indices that will serve in the blue whiting model, the energy balance equation for blue whiting defined in chapter 2 was used. We recall that the model assumes the Holling type II functional response for food (eq. 2.6). To describe the energy income generated by the uptake of a unique prey kind and its contribution to body maintenance, the differential equation can be rewritten specifically for each prey item i as follows:

$$\frac{dW_i}{dt} \;=\; \frac{I_{\max}\alpha_i\rho_i}{\rho_H + \sum_{j=1}^{n}\alpha_j\rho_j} \;-\; \lambda W_i \tag{5.1}$$

For n the number of prey kinds or taxa, W_i is the body mass specifically explained by the uptake of prey kind i, whose biomass concentration in the environment is equal to ρ_i and whose selectivity index is α_i ($I_{\max}$ is maximum uptake rate, ρ_H is half-saturation food biomass concentration and λ is cost rate). If we consider the proportion of prey i in the environment $p_i = \rho_i / \sum_{j=1}^{n} \rho_j$, by using the equilibrium solution of equation 5.1 we find that the proportion of prey i in the diet is equal to:

$$\pi_i \;=\; \frac{\alpha_i p_i}{\sum_{j=1}^{n}\alpha_j p_j} \tag{5.2}$$

The proportion in the environment of each prey (p_i) could be calculated from

the outputs of the random forest model, and proportions in the diet (π_i) were estimated previously from DAPSTOM. Therefore, these values could be used to approximate the selectivity index α for each prey. Considering $\sum_{i=1}^{n} \alpha_i = 1$ and after solving equations 5.2 for α_i, the selectivity index α_i for prey i is equal to:

$$\alpha_i \;=\; \frac{\pi_i/p_i}{\sum_{j=1}^{n} \pi_j/p_j} \tag{5.3}$$

This selectivity index is known as Manly's or Chesson's alpha (Manly et al., 1972; Chesson, 1983) and is frequently used to measure diet breadth of fish (Saikia, 2016). In this study, the average alphas for each prey item were calculated and used on the predicted zooplankton distribution fields to derive one unique blue whiting food field per time step. For each cell of the model grid at coordinates (x, y) and at time t, the new food variable (ρ) is then equal to:

$$\rho_{x,y,t} \;=\; \sum_{i=1}^{n} \alpha_i \left[\left(\rho_i \right)_{x,y,t} \right] \tag{5.4}$$

5.3 Results

5.3.1 Blue whiting diet

According to the stomach records, it seemed that blue whiting preyed mainly on four species: *Parathemisto abyssorum* (Hyperiidae) (42.3%), *Nyctiphanes couchi* (Euphausiidae) (14.5%), *Calanus finmarchicus* (copepod) (6.7%) and *Themisto libellula* (Hyperiidae) (5.6%). Together, those four species accounted for 69.1% of items found in sampled stomachs. In the Norwegian Sea, the main feeding grounds for blue whiting population, *P. abyssorum* seems to be the dominant prey item (26.5%) followed by *C. finmarchicus* (22.3%), Euphausiids (20.4%) and *T. libellula* (18.5%) (tables 5.3 and 5.4). *C. finmarchicus* was only identified in the Norwegian Sea and the euphausiid *N. couchi* was essentially present in stomachs sampled in southern and coastal areas, especially in the Bay of Biscay where it could reach up to 90% of items found in stomachs. Empty stomachs were encountered mostly in the Irish Sea (42.8% of stomachs), Celtic Sea (32.0%),

Table 5.3: Total number of stomachs (N_{st}) of blue whiting recorded per ICES area between 1960 and 2011, along with proportions of the four main species in the diet (*Parathemisto abyssorum*, *Nyctiphanes couchi*, *Calanus finmarchicus* and *Themisto libellula*) in percentage of total prey items recorded in stomachs. The last column of the table gives the total proportion of the four species together.

Code	Area name	N_{st}	P. abyss.	N. couchi	C. fin.	T. lib.	Total prop.
2.a	Norwegian Sea	187	26.5	0	22.3	18.5	67.3
4.a	Northern North Sea	49	0	0	0	0	0
5.a	Iceland Grounds	72	0	0	0	0	0
7.a	Irish Sea	166	0	0	0	0	0
7.b	West of Ireland	40	0	6.3	0	0	6.3
7.e	Western English Channel	24	14.2	0	0	0	14.2
7.g	Celtic Sea North	159	88.6	0	0	0	88.6
7.h	Celtic Sea South	98	87.3	0	0	0	87.3
7.j	South-West of Ireland - East	154	0	51.6	0	0	51.6
8.a	Bay of Biscay - North	31	0	21.4	0	0	21.4
8.d	Bay of Biscay - Offshore	108	0	91.7	0	0	91.7
12	North of Azores	9	0	0	0	0	0
14.a	North-East Greenland	29	25.7	0	0	0	25.7
14.b	South-East Greenland	3	0	0	0	0	0
	All areas	1129	42.3	14.5	6.7	5.6	69.1

West of Ireland (35.1%) and in the Bay of Biscay (34.5%) (table 5.4). Lowest proportion of empty stomachs was found in the Norwegian Sea area with 8.6% (when considering areas with number of sampled stomach > 60).

Dominant euphausiid prey items were recorded either as Euphausiidae (15.1% of recorded items) or one of the following taxa: *N. couchi* (14.5%), *Meganyctiphanes norvegica* (1.4%), and *Thysanoessa* spp. (< 1%). Hyperiids were also sometimes recorded just as Hyperiidae (7.1% of prey items). While *C. finmarchicus* seemed to be the only dominant copepod prey in the blue whiting diet, some stomach records only referred to the taxa name *Calanus* spp. (1.0%). In the last case, it was assumed that items recorded as *Calanus* spp. predominantly comprised *C. finmarchicus*, and any other species of *Calanus* was neglected. While the problem with euphausiids and hyperiids might appear similar at first, blue whiting tend to prey on a larger range of euphausiid and hyperiid species, whose presence in stomachs varied with the sampling location. In the case of euphausiids, this observation was in agreement with their known spatial distribution, with *N. couchi* in southern areas such as the Bay of Biscay and *M. norvegica* in the Norwegian Sea (Lindley, 1982).

Table 5.4: Total number of stomachs of blue whiting (N_{st}) and number of empty stomachs ($N_\emptyset$) recorded per ICES area between 1960 and 2011, along with proportions in the diet of the three defined prey groups (Hyperiidae, Euphausiidae and *Calanus* spp.) in percentage of total prey items recorded in stomachs. The last two columns give the total proportion of other prey items found in stomachs and specify those preys (and their proportion in the diet) when the total proportion is higher than 10% and those secondary preys have proportions higher than 5%. Stomachs sometimes contained non-identifiable digested remains and/or gut everted/regurgitated items, which are not given here.

Area	N_{st}	$N_\emptyset$	Hyperiid	Euphausiid	*Calanus*	Other	Taxa names and proportions
2.a	187	16	52.5	20.4	23.8	3.3	
4.a	49	0	0	16.7	0	83.3	*M. poutassou* (62.5%), *Melanogrammus aeglefinus* (8.3%), *Trisopterus esmarki* (8.3%)
5.a	72	25	16.2	71.7	8.2	3.9	
7.a	166	71	0	75.9	0	24.1	*Pasiphaea sivado* (9.0%)
7.b	40	12	2.5	30.0	0	67.5	Teleostei (32.5%), eggs (10%), *Pasiphaea sivado* (6.3%)
7.e	24	5	14.2	0	0	85.8	*Limacina retroversa* (51.9%), crustacean larvae (12.3%), crustacea (6.6%)
7.g	159	35	91.5	5.3	0	3.2	
7.h	98	47	87.3	1.4	0	11.3	Crustacean larvae (5.5%)
7.j	154	56	22.7	72.7	0	4.6	
8.a	31	17	25.0	42.9	0	32.1	*Gobius* spp. (14.3%), *Argentina sphyraena* (7.1%)
8.d	108	31	3.5	95.2	0	1.3	
12	9	0	13.3	84.6	0.6	1.5	
14.a	29	6	71.8	18.9	2.1	7.2	
14.b	3	0	0	100	0	0	
All	1129	321	55.3	31.8	7.6	5.3	

Because of the irregularities in taxa names mentioned above, any species names of euphausiids or hyperiids were disregarded thereafter and included in their respective taxa group, Euphausiidae or Hyperiidae. It is also very rare that species are identified among hyperiids and euphausiids during the CPR data collection process, and abundance data is available only at this taxa level. Thus, the decision to keep only Euphausiidae and Hyperiidae as taxa groups was compatible with the use of CPR data in this study. At the end, three main prey types were kept: Euphausiid, Hyperiid and *C. finmarchicus*.

In some sampled areas, the previously defined taxa groups were not enough to explain the diet composition (table 5.4). For those areas, the presence of other taxa found in stomachs was briefly investigated. Those mainly included fish (sometimes blue whiting itself), crustaceans (including larvae) and gastropods (here *L. retroversa*). Crustaceans, and mainly the decapod *P. sivado*, were found

Table 5.5: Proportions in the diet (in percentage of total number of prey items recorded in stomachs) of the three main taxa groups (Hyperiidae, Euphausiidae, *C. finmarchicus*) when the dataset is first split between juveniles ($L < 21$ cm) and adults ($L \geq 21$ cm), and then between South (lat $< 55°$N and North (lat $\geq 55°$N). Total number of stomachs and number of empty stomachs are also given for each data split.

	Juveniles	Adults	South	North
N stomachs	590	539	780	349
N empty	183	138	274	47
Hyperiidae	58.0	52.0	61.7	46.5
Euphausiidae	36.4	26.3	32.1	31.4
C. finmarchicus	0.2	16.7	0	18.3
Other	5.4	5.0	6.2	3.8

in stomachs sampled West of Ireland (7.b), in the Irish Sea (7.a), in the Celtic Sea (7.h) or the English Channel (7.e). Except for the stomachs sampled in the North Sea, intake of other species seemed to occur in majority in areas where high proportions of empty stomachs were recorded. In the northern region of the North Sea (4.a), stomach records suggested that blue whiting also ate their own juveniles as well as other small gadoids (*M. aeglefinus* and *T. esmarki*).

After splitting the data between juveniles and adults, we observed that most items of *C. finmarchicus* were found in adults (table 5.5). And the split between the North and South sampled areas showed that *C. finmarchicus* was exclusively found in the North. This suggested that in the northern areas (mainly in the Norwegian Sea and around Iceland) blue whiting undergoes a light ontogenetic shift in its diet. Proportions of euphausiids seemed to decrease from juvenile to adult stage, while they were fairly constant in the diet between southern and northern areas. In contrast, intake of hyperiids was much higher in the South but showed little difference between juveniles and adults.

Stomach records only gave the number of prey items, while we need dry weights to calculate proportions in the diet in weight units (here expressed in mg) that will be used later to calculate selectivity indices. The literature was searched for averaged values of dry weight and/or size for each prey. For *C. finmarchicus*, the average dry weight estimate of 0.32 mg was used, assuming an average individual length of 2.5 mm, which were values suggested by Pitois & Fox (2006). It was harder to find studies on euphausiids and hyperiids, but considering a few species

like *N. couchi* or *T. libellula*, dry weights were roughly estimated for both prey groups. Based on study from Lindley et al. (1999), dry weight (in mg) could be estimated for *N. couchi* using the formula:

$$DW = 10^{(2.556 \ \log(L) \ + \ 0.665)}/1000 \qquad (5.5)$$

Assuming an average length $L = 12$ mm, *N. couchi*'s dry weight was estimated to a value around 2.65 mg.

In the same way, based on a study from Dale et al. (2006), dry weight was estimated for *T. libellula* with:

$$DW = 10^{(2.689 \ \log(L) \ - \ 2.326)}/1000 \qquad (5.6)$$

With an average length around 11 mm, dry weight of *T. libellula* was around 2.98 mg.

Because of uncertainties surrounding the dry weight estimates for both hyperiids and euphausiids, and considering the previous values, an average dry weight of 3.0 mg was finally assumed for both taxa in the rest of the study.

For all the main species identified at the start of this section, blue whiting seemed to be competing mainly with herring and European mackerel. DAP-STOM records showed that predators of *T. libellula* were either blue whiting (53.3%), Norwegian herring (39.4%) or cod (7.2%). *P. abyssorum* was found in herring's (42.1%), blue whiting's (36.2%) and mackerel's (21.6%) stomachs. In the South, blue whiting and herring were both important predators of *N. couchi*, constituting respectively 45.9% and 47.9% of recorded stomachs with this prey. Haddock would also prey sometimes on *N. couchi* or other Euphausiidae, representing less than 10% of predator stomach records. While *C. finmarchicus* figured among blue whiting preys, its main predators were essentially mackerel (87.7%) and herring (11.7%), blue whiting accounting for only 0.4% of predator stomach records with this prey item.

5.3.2   Observed prey distributions

CPR versus mesozooplankton from NEMO-Medusa

Using CPR data for Euphausiid, Hyperiid and *C. finmarchicus* available, and the dry weight values for each taxa group estimated previously, average prey concentration was calculated in each 1° spatial cell and for each quarter (fig. 5.7). Prey concentration values seemed to be higher from April to September (quarters 2 and 3), especially in the area South of Greenland and between Greenland and Iceland.

The CPR coverage was low in the Norwegian Sea and almost non-existent for
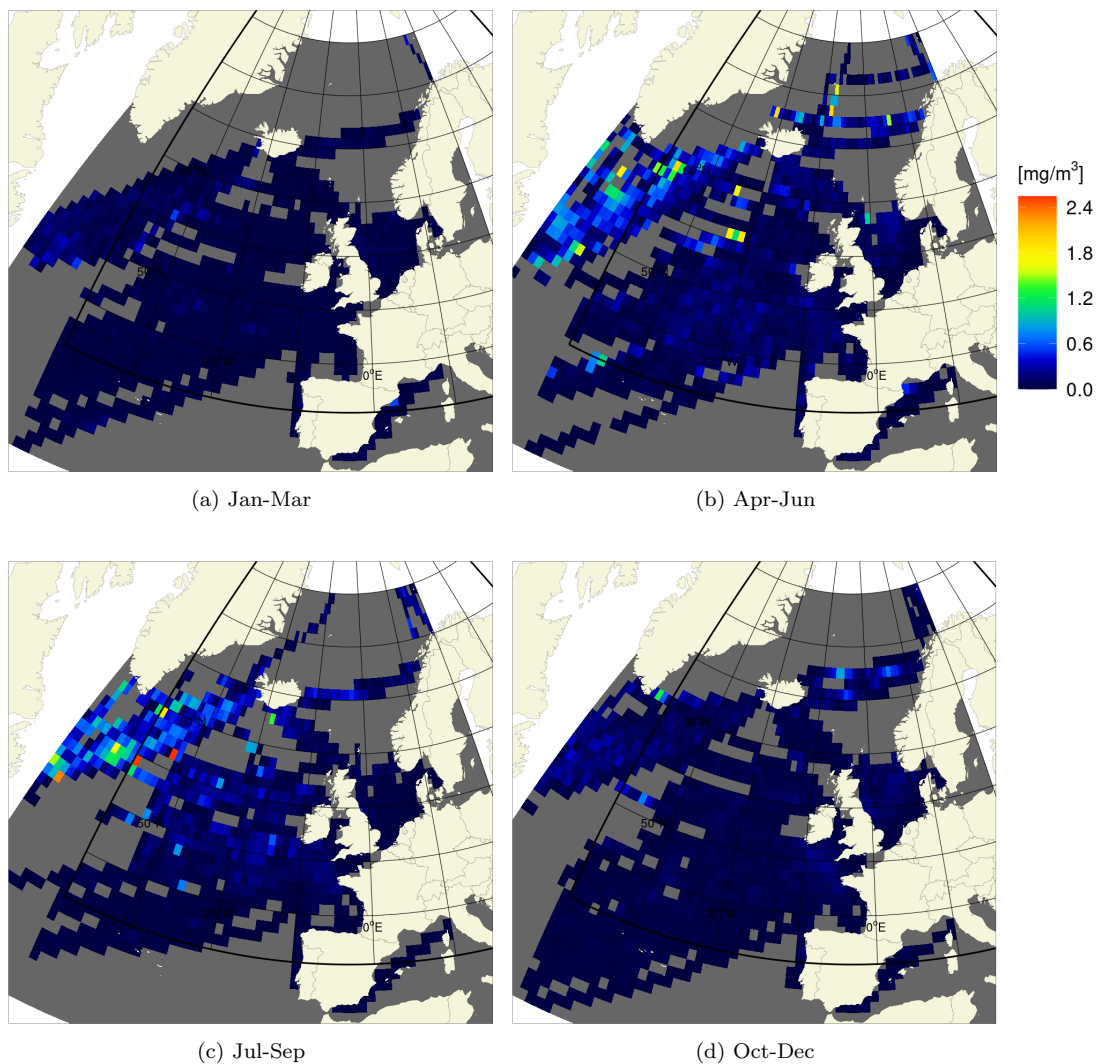
Figure 5.7: Average quarterly concentration (mg/m³) of plankton belonging to any of the three studied taxa (Euphausiids, Hyperiids and *C. finmarchicus*), computed from CPR data between 1988 and 2014. The map's resolution is 1° in both longitude and latitude. Cells with no CPR data available in the time period considered are represented in gray.

(a) Apr-Jun

(b) Apr-Jun
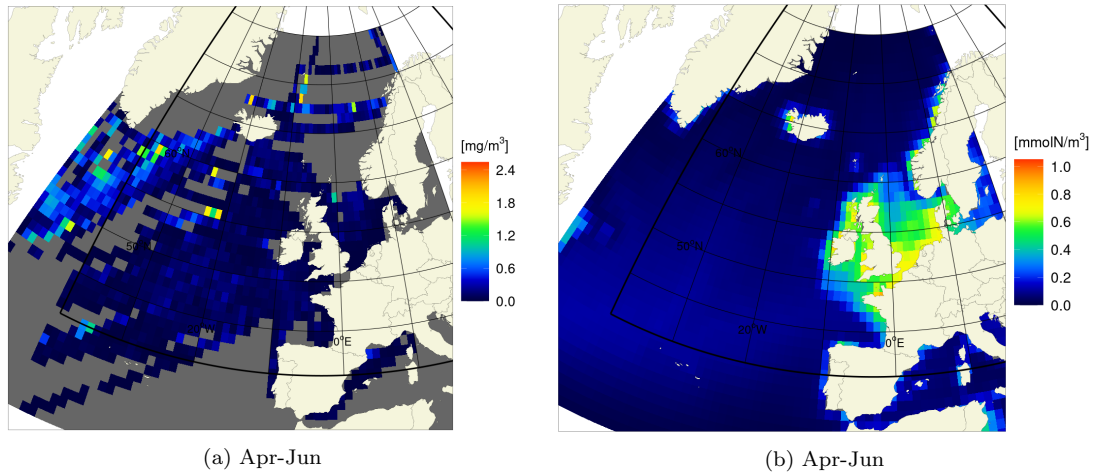
Figure 5.8: Comparaison between the CPR plankton distribution and the NEMO-Medusa meso-zooplankton distribution in April-June (quarter 2): (a) the map of average concentration (mg/m^3) of the three CPR taxa and (b) the map of average concentration (mmolN/m^3) of meso-zooplankton from NEMO-Medusa.

first and third quarters. Nonetheless, high plankton concentration values were observed North of Iceland in the second quarter (fig. 5.7.b) and suggested that peaks of concentration also occurred in the Norwegian Sea during the warmer season. In fact, monthly maps of CPR's plankton concentration were also studied over the year and showed that concentration seemed to start increasing at the end of the second quarter (from June). Unlike other surveys (Prokopchuk & Sentyabov, 2006; Bachiller et al., 2016), the lack of CPR data from July to September in this area prevented the observation of high concentration values during summer. Nevertheless, the slightly higher concentration values still observed in the region after September (fig. 5.7d) supported the assumption that zooplankton biomass increased during summer.

The CPR plankton concentration variable was compared with the mesozooplankton concentration computed by the NEMO-Medusa model. It confirmed the fact that the NEMO-Medusa variable would have been unfit to be used as food variable in the blue whiting model. The high plankton concentrations in coastal areas predicted by NEMO-Medusa were non-existent for the three main taxa groups combined which constitute blue whiting's diet (fig. 5.8). Coastal areas, especially around the British Isles, tended to show high density of CPR sampling (fig. 5.5), and thus observing quasi-absence of suitable preys in those
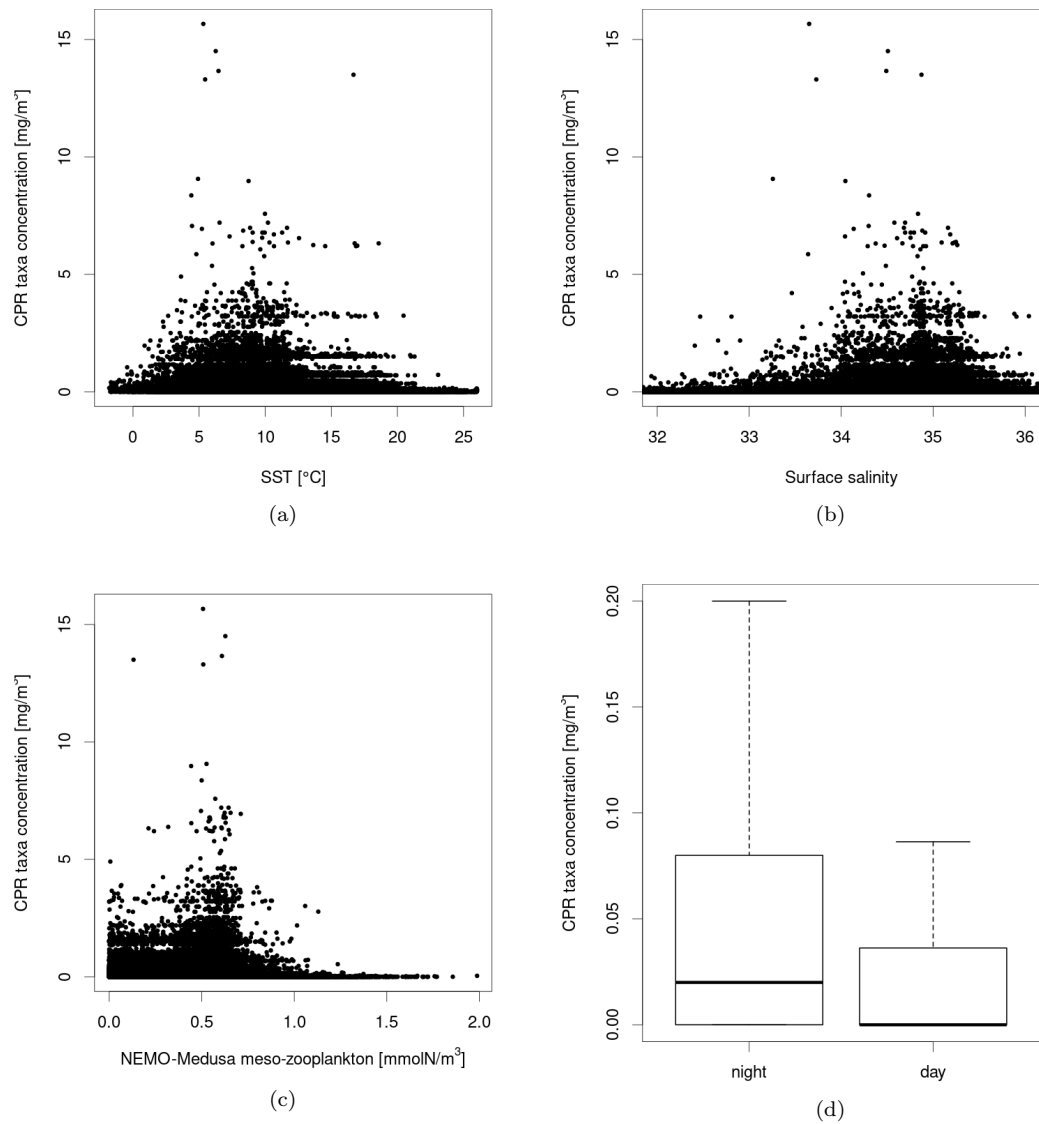
Figure 5.9: Detecting potential response from CPR taxa concentration (mg/m^3) to varying environmental conditions. Scatter-plots show CPR plankton concentration distributions when plotted against (a) local sea surface temperature (SST), (b) surface salinity or (c) the meso-zooplankton concentration value computed by the NEMO-Medusa model. (d) Boxplots of taxa concentration from CPR sampled during day time or night time to investigate the effect of vertical diel migration on CPR plankton concentration estimates (semi-quantitative estimates).

areas showed that those areas were most likely unsuitable for the main blue whiting preys.

Environmental drivers

Local environmental drivers that could explain the spatial distribution of the main blue whiting preys described previously were investigated. Temperature and

salinity were considered, as well as the mesozooplankton variable from NEMO-Medusa since the model predicted values in offshore areas might still partly explain the varying concentration of the studied taxa from the CPR data.

Scatter-plots of both surface temperature (fig. 5.9a) and surface salinity (fig. 5.9b) suggested optimum conditions for the studied taxa (all three groups combined) to be between 5 and 14°C with salinities between 34 and 35.5. Plotting the CPR plankton concentration against local mesozooplankton values from NEMO-Medusa (fig. 5.9c) supported the previous statement that both variables were very different. As we saw on the distribution maps, high values of NEMO mesozooplankton were not met with high values of CPR concentration, and CPR samples where NEMO predicted values were over 1 mmolN/m^3 showed quasi-null concentration. For low values of the NEMO variable ($<$ 0.4 mmolN/m^3), the CPR concentration values seemed to be uniformly distributed, suggesting independence between both variables. However, peaks of CPR concentration values seemed to coincide with NEMO values between 0.5 and 0.7 mmolN/m^3. For this reason, the NEMO-Medusa mesozooplankton variable was not ruled out as potential predictor for the studied taxa.

Plankton concentration values tended to be higher during night time than day time (fig. 5.9d) and suggested that CPR was indeed able to detect diel vertical migrations of plankton. This observation made it essential to include a night-day binary predictor in the following random forests, as to avoid underestimating plankton concentration values that were sampled during day time.

5.3.3 Predicted prey distributions

The same predictors were used in the random forest models for each taxa group. Those predictors were SST_y, SSS_t, NEMO-Medusa mesozooplankton (mezo), water column depth, the day/night factor (daytime) and the day of the year (yearday). Accidentally, all random forests were performed on CPR abundance values multiplied by 50 as if all the studied taxa had been counted with the zooplankton traverse method in CPR samples (table 5.1), instead of the eye-count method used for taxa with average size over 2 mm. These abundance values were corrected after being predicted by the random forests.

All random forests trained on a subset of the data (either in time or in space)

showed a r^2 value around 0.9 for that same subset (table 5.6). However, the models were far less effective in predicting taxa abundance from the test data subsets, with r^2 ranging from 0.03 (euphausiid's model tested in time) to 0.08 for both euphausiids and hyperiids. Random forests were doing slightly better at predicting *C. finmarchicus* abundance values in time and space, with $r^2 \approx 0.2$. RMSE values were lower for random forests predicting abundances of either euphausiids or hyperiids in time or space, compared to *C. finmarchicus*, but this was caused by the lower values and much smaller range of values of observed CPR abundances for those taxa compared to *C. finmarchicus*. Thus, the fact that the random forests of *C. finmarchicus* were performing better on the test subsets suggested that random forest's performance at forecasting in both space and time increased

Table 5.6: Random forest model performances for each taxa in space and time. In both cases, prediction accuracy was studied first on the train data and then on the test data. For each model assessment, the Root Mean Squared Error (RMSE) is first given, followed by Pearson's coefficient of determination (r^2) in brackets. The random forest models are written with their predictors ordered from the most to the least important according to the %IncMSE.

Random-forest model	space train	space test	time train	time test
Euph ~ daytime + depth + yearday + mezo + SST_y + SSS	4.97 (0.90)	9.10 (0.08)	4.41 (0.89)	14.38 (0.03)
Hype ~ daytime + SST_y + depth + SSS + mezo + yearday	2.05 (0.90)	4.76 (0.06)	1.98 (0.90)	5.61 (0.08)
Cfin ~ SST_y + yearday + mezo + SSS + depth + daytime	27.64 (0.90)	32.36 (0.19)	26.01 (0.90)	54.35 (0.18)

Table 5.7: Performance assessment of random forest models in each area that was not included in the training dataset. Here each area was defined by its ICES code. For each area, N is the total number of CPR samples collected in this area in 1988-2014. For each taxa model and area, the Root Mean Squared Error (RMSE) is first given, followed by Pearson's coefficient of determination (r^2) in brackets. Values in bold indicate either lower RMSE or higher r^2 than the corresponding value computed for all areas together (in column space test from table 5.6).

ICES code	Area name	N	Euph	Hype	Cfin
4.c	Southern North Sea	3365	**2.24** (<1e-3)	**0.50** (<1e-3)	**4.73** (<1e-3)
5.a	Iceland Grounds	2544	11.46 **(0.124)**	**3.93 (0.086)**	86.84 (0.157)
6.b	Rockall	1603	**3.71 (0.094)**	10.69 (0.041)	**14.90** (0.014)
7.c	Porcupine Bank	286	**3.40 (0.139)**	4.85 **(0.063)**	**7.26** (0.017)
7.f	Bristol Channel	787	**6.82 (0.126)**	**1.72 (0.175)**	**6.66** (0.022)
7.h	Celtic Sea South	3415	16.91 (0.050)	**2.65 (0.204)**	**7.73** (0.018)
7.k	South-West of Ireland - West	2214	**4.72** (0.062)	8.73 (0.045)	**2.76** (0.011)
8.b, 8.c	Bay of Biscay Central and South	1143	**3.92** (0.058)	**1.01** (0.003)	**2.66** (0.019)
10.a	Azores Grounds	3686	**5.71** (0.012)	**1.25** (0.045)	**0.83** (0.003)
14.a	North-East Greenland	19	**7.21** (0.008)	**4.44** (0.006)	57.00 (0.002)

with the variable's range of values used to train the model. This seemed to be confirmed after discovering the error made with the abundance values (wrongly multiplied by 50) when attempting to train the models with the right values: the `randomForest` R function was much slower to compute and often crashed before the end.

Ranfom forest performance was also studied for each area that constituted the spatial test data subset (map in fig. 5.6). In general, random forests were performing better at predicting taxa abundance in test areas surrounded by areas that were used to train the models (table 5.7). For euphausiids, the best model performances were observed around Iceland (5.a), in the Rockall (6.b) and Porcupine Bank (7.c) areas and in the Bristol Channel (7.f). For hyperiids, r^2 was higher in the southern area of the Celtic Sea (7.h) and in the Bristol Channel (7.f), as well as around Iceland (5.a) and over Porcupine Bank (7.c). Random forest of *C. finmarchicus* abundance seemed to only perform well in the icelandic coastal area (5.a) with $r^2 \approx 0.16$, and with $r^2 < 0.03$ in any other area tested.

Euphausiids

According to the %IncMSE importance index, the diel binary predictor (day versus night) seemed to be the most important predictor in estimating euphausiid CPR abundance, with values of %IncMSE above 30% for both subset experiments (fig. 5.10). The other predictors had %IncMSE values between 22 and 30% and their order of importance varied between random forests trained with a spatial subset and with a time subset of the data.

On the contrary, increase in node purity (IncNodePurity) seemed to be much lower for the Day/Night predictor and water column depth (fig. 5.10). This was also the case in random forests built for the other two taxa (fig. 5.14 and 5.18. For Day/Night, this was caused by the fact that it was a binary predictor, which means there was only one split possible (night or day) to try and predict abundance values. Thus, the total number of decrease in the residual error caused by splitting with this predictor in a decision tree only relied on that one single split. In comparison, splitting with a predictor like temperature would result in a series of splits at different values of the variable's range, each contributing in reducing

the residual error and increasing the IncNodePurity value. Continuous predictors (SST, SSS, mezo, day of year) with large range of values tended to have higher IncNodePurity. In the case of the depth predictor, its lower IncNodePurity value (around a factor two compared to the other four predictors mentioned previously) was most likely due to its range definition. Since the water column depth values were approximations extracted from the NEMO model mesh definition, which gives only depth class values with exponentially increasing intervals from the surface to abyssal depths, the depth predictor was only taking a limited number of values and resulted in a limited number of potential splits in a decision tree.

The order of predictor importance was exactly the same between both random forests when considering IncNodePurity. However, most values were higher in the spatial subset experiment. The day of year, followed closely by SST_y, mezo and SSS_t were the predictors that caused the highest decrease of residual error in
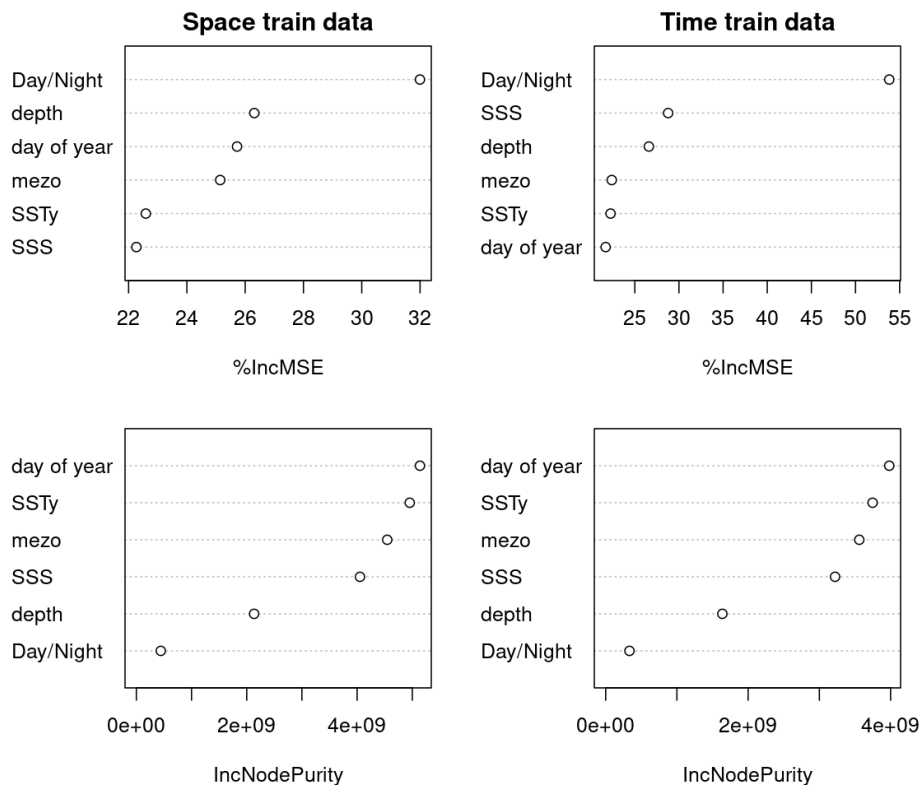
Figure 5.10: Importance of predictors in random forest models for predicting abundance of Euphausiids. Importance is given by the increase in MSE (%IncMSE) and by the increase in node purity (IncNodePurity). Predictors are written in order of decreasing importance when read from top to bottom. Predictor importance was studied for both random forests, either trained on a spatial subset (left) or time subset (right) of the CPR dataset.
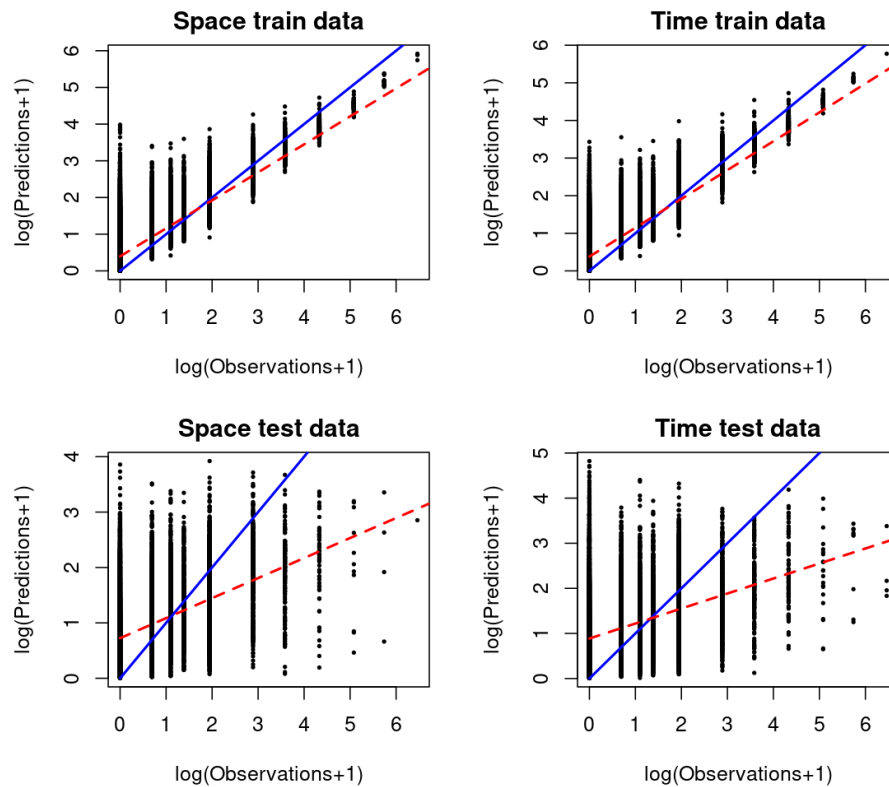
Figure 5.11: Predicted against observed abundance values (in logarithmic scale) for Euphausiids for both spatial subsets (train/test) and both time subsets of the CPR dataset. The continuous blue line represents predicted values equal to observed values. The dashed red line is the regression curve between predicted and observed values. Because CPR plankton abundance observations are given by categories with boundaries defined in log scale, both predictions and observations are log-transformed to improve visualisation of the distribution of predicted values at low CPR abundance value.

training of single-tree models.

Figure 5.11 shows prediction performances of random forest models for euphausiid abundance. Overall, models tended to overestimate low abundance values and to underestimate high abundance values. This effect seemed to be amplified when the models were tested on new data (test data subset in space or time). Random forest models seemed to be less effective at predicting high abundance values from areas or time periods that were excluded from the model training process.

Predicted values for Euphausiid abundance in the selected test areas were compared with the CPR observations (fig. 5.12). In general, the random forest tended to overestimate euphausiid abundance: observed median value was al-
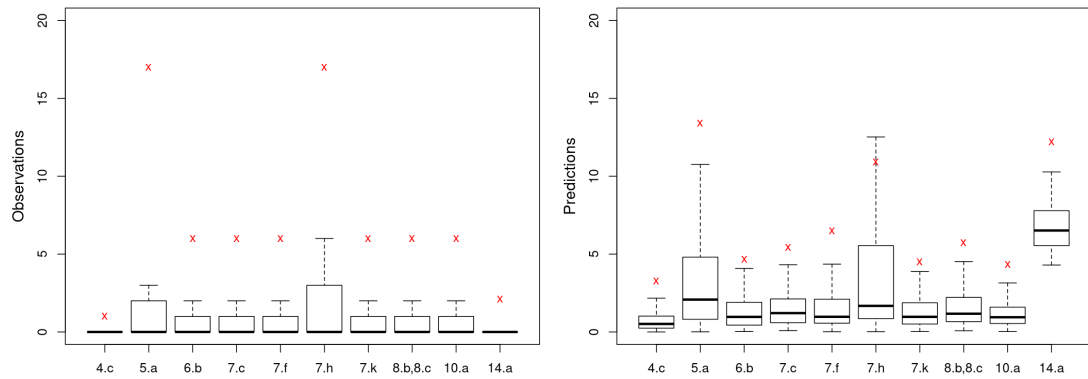
Figure 5.12: Euphausiid abundance observations from CPR (left) and predictions in each area used to test the random forest model's performance in space. Lower and upper edges of the box represent first and third quartiles, the bold line in the box is the median and lower and upper hinges are placed at 1.5*IQR (interquartile range) from the box edges (default setting for `boxplot` function in R). Red Xs give the 0.95 quantile.

ways 0, while predicted median values varied around 1-2 individuals per sample. Predicted abundance for the North-East Greenland area (area 14.a) were the farthest from predicted values, however this area only counted 19 CPR samples which were most likely not enough to be representative of euphausiid population in this area. Quantile 0.95 was used to study trends in abundance variations between areas. Without area 14.a, random forest predictions showed similar abundance variations between areas. Among them, Iceland grounds (5.a) and the Celtic Sea South area (7.h) were the two tested areas where euphausiids were most likely to be found.

An example of predictions of euphausiid concentration in the year 2000 is given in figure 5.13 and was computed by the final random forest model trained on the entire dataset (no time or spatial subset). Predictions for other years were also studied and all featured a similar annual variation. According to the model predictions, most of the euphausiid population was located in the Norwegian Sea throughout the year. A peak in productivity seemed to occur during the second quarter, around May-June, resulting in high concentrations of euphausiid in the Norwegian Sea and the Irminger Sea, South-East of Greenland. As shown in fig. 5.13, a late bloom might also take place over the French continental slope, in the Bay of Biscay, where concentration values predicted for the third annual quarter were almost as high as in the Norwegian Sea for the same period.

(a) Jan-Mar 2000

(b) Apr-Jun 2000

(c) Jul-Sep 2000

(d) Oct-Dec 2000
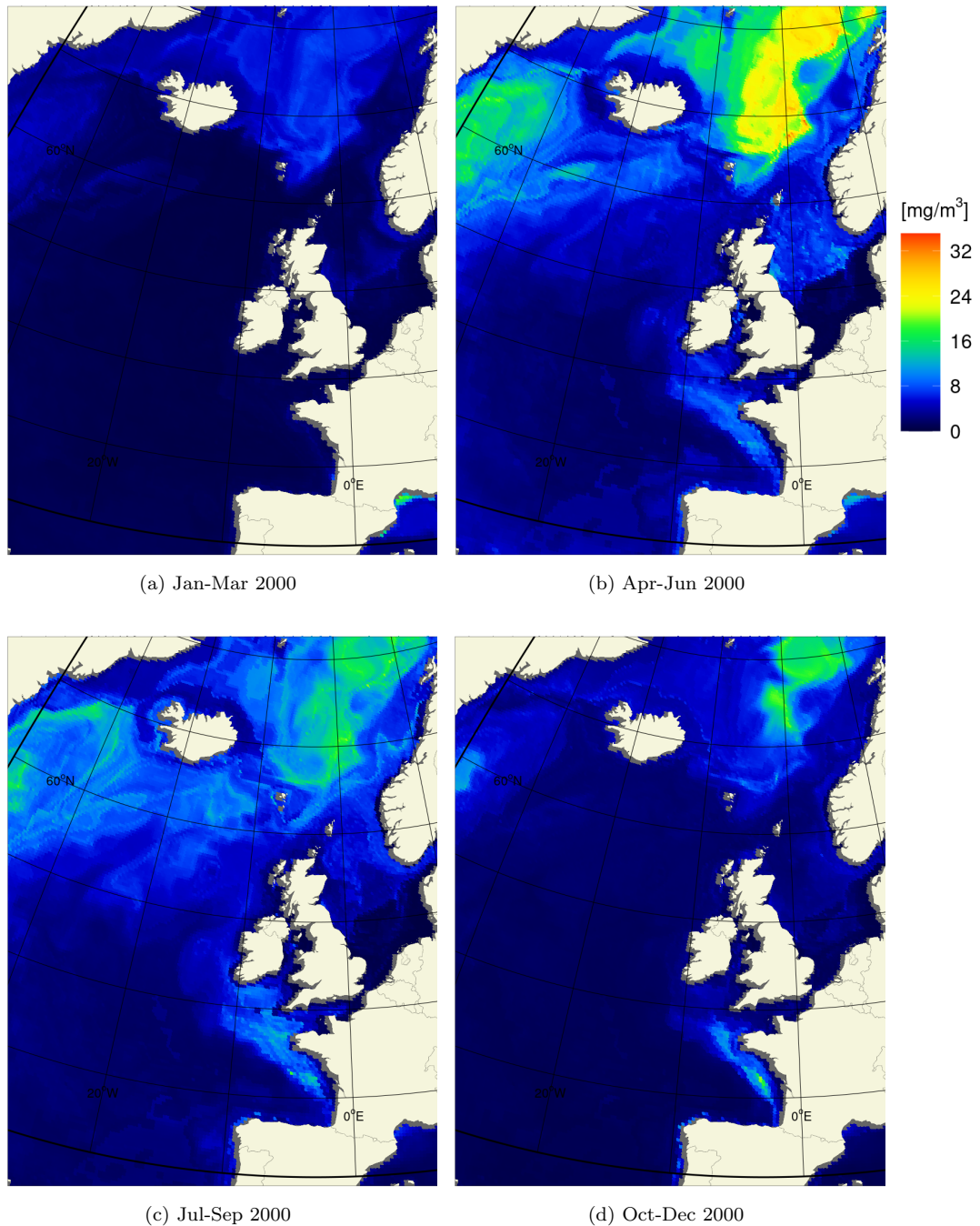
Figure 5.13: Quarterly averaged predictions of Euphausiid concentration (mg/m^3) in year 2000. Prediction maps are obtained from running the general random forest model (which was trained over the entire CPR dataset) over the whole spatial domain of NEMO-Medusa at each timestep.

Hyperiids

As for euphausiids, the Day/Night predictor seemed to be the most important predictor in estimating hyperiid abundance with random forests. For both random forest experiments, %IncMSE values for this predictor varied between 44

and 61%, and the difference with the %IncMSE value of SST_y, their second most important predictor, was always greater than 10 (fig. 5.14). Water column depth effect seemed to be higher when the random forest was trained on a subset of the spatial domain than when trained on the time subset. Mezo and day of year were both the least important predictors, with %IncMSE values still above 20%.

Hyperiid's random forest models also tended to overestimate abundance in locations where low abundance values had been observed from CPR (fig. 5.15). Model performance decreased drastically when used on the test data subsets. Like for euphausiid, figure 5.15 shows that random forests encountered similar difficulties at predicting high abundance values in areas or over time periods which were not included in the training process of the models.

Predicted values of abundance for each test area (fig. 5.6) were compared with the observed CPR values in the same areas (fig. 5.16). First, by looking at the
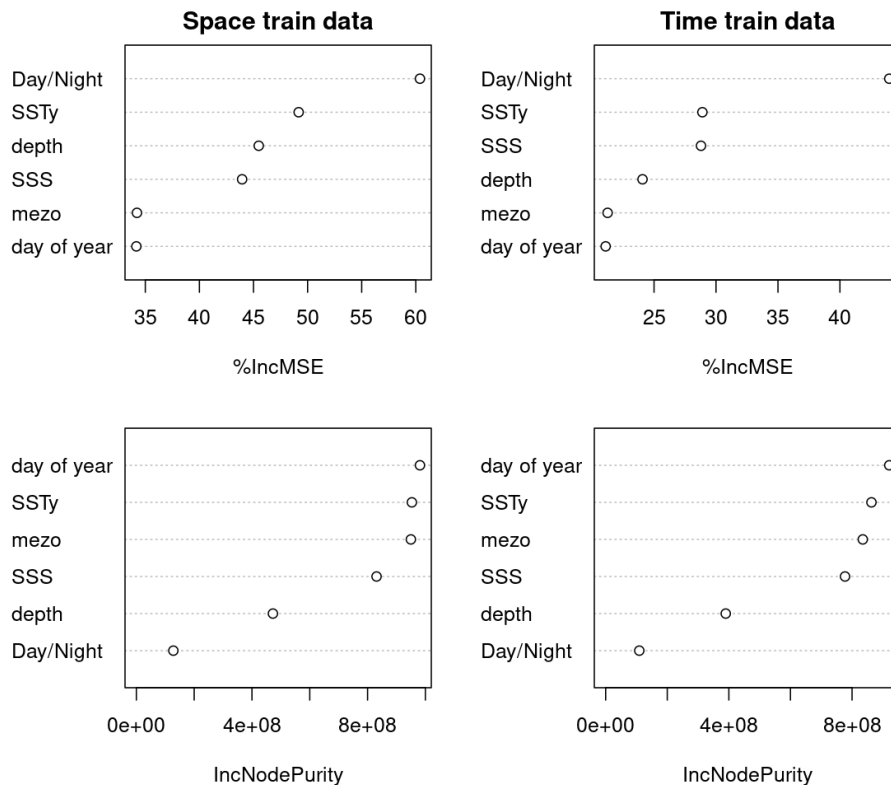
Figure 5.14: Importance of predictors in random forest models for predicting abundance of Hyperiids. Importance is given by the increase in MSE (%IncMSE) and by the increase in node purity (IncNodePurity). Predictors are written in order of decreasing importance when read from top to bottom. Predictor importance was studied for both random forests, either trained on a spatial subset (left) or time subset (right) of the CPR dataset.

boxplots only, we noticed that the model seemed to fail in reproducing abundance variation patterns observed by CPR. CPR observations suggested higher
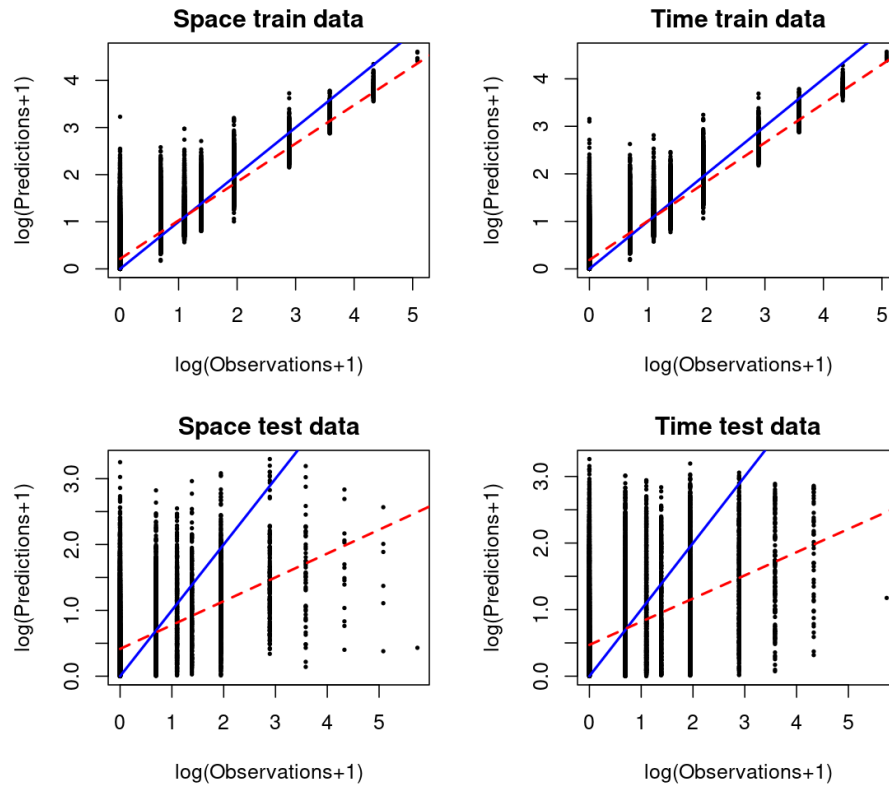
Figure 5.15: Predicted against observed abundance values (in log scale) for Hyperiids for both spatial subsets (train/test) and both time subsets of the CPR dataset. The continuous blue line represents predicted values equal to observed values. The dashed red line is the regression curve between predicted and observed values.
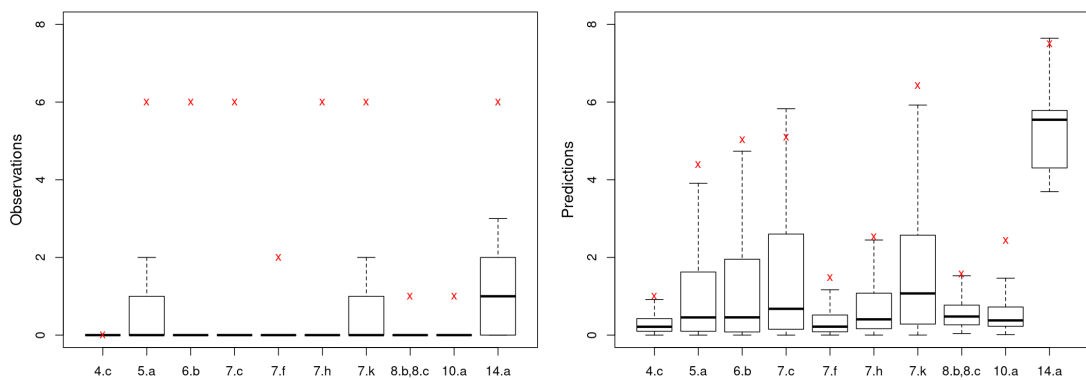
Figure 5.16: Hyperiid abundance observations from CPR (left) and predictions in each area used to test the random forest model's performance in space (see fig. 5.12 for details).

(a) Jan-Mar 2000

(b) Apr-Jun 2000

(c) Jul-Sep 2000

(d) Oct-Dec 2000
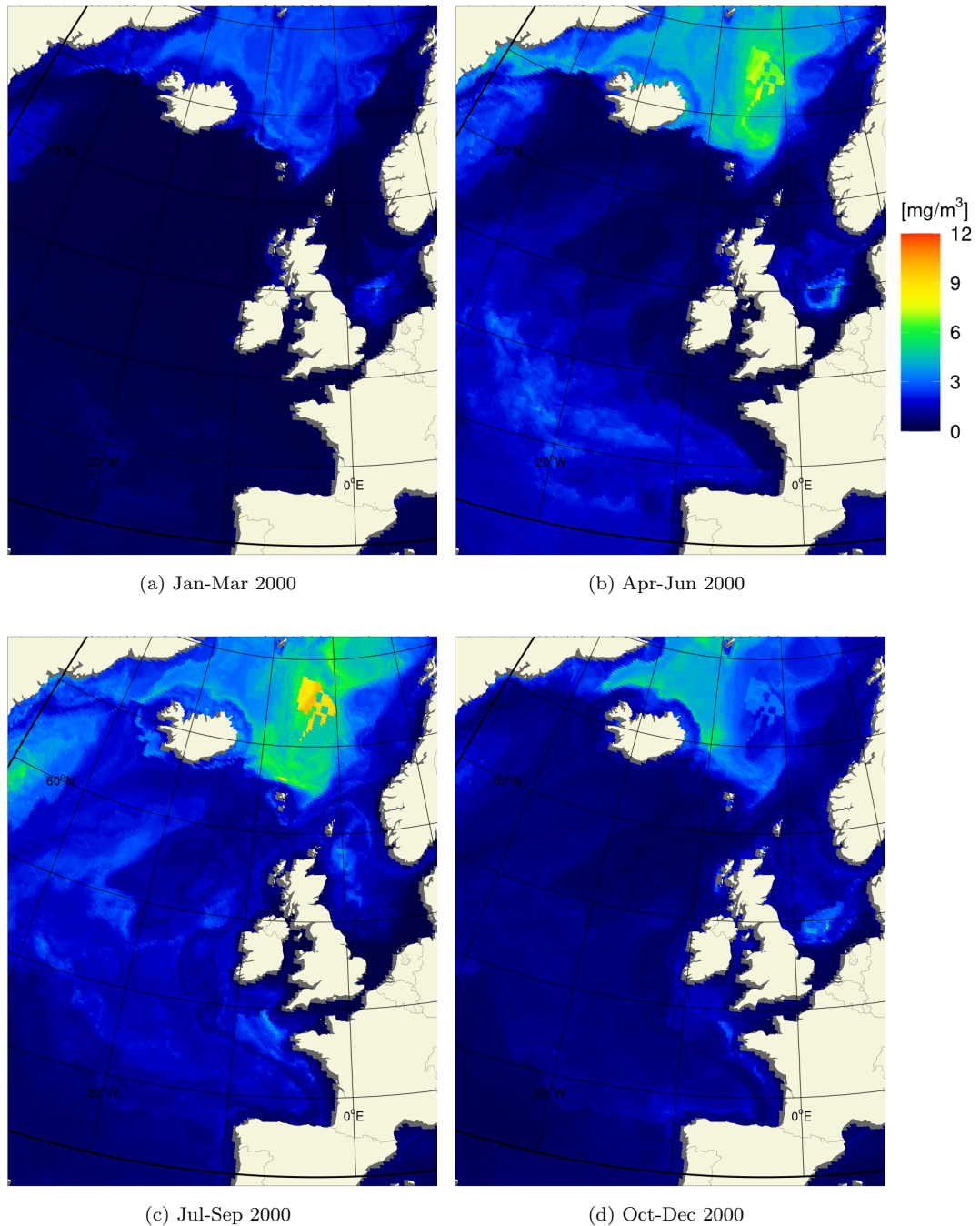
Figure 5.17: Quarterly averaged predictions of Hyperiid concentration (mg/m^3) in year 2000. Prediction maps are obtained from running the general random forest model (which was trained over the entire CPR dataset) over the whole spatial domain of NEMO-Medusa at each timestep.

abundance on Iceland grounds (5.a), in the region South-West of Ireland (7.k) and North-East Greenland (14.a). The model predicted higher abundance values not only in those areas but also in the Rockall and Porcupine Bank areas (6.b and 7.c), while hyperiids were mostly found to be absent in those areas (in at

least 75% of CPR samples). However, those areas had a high 0.95 quantile value ($Q_{0.95} = 6$) for the CPR observations, which suggested that the random forest training was sensitive to high abundance values. In fact, predicted distributions seemed to reflect the variation pattern of $Q_{0.95}$ of CPR observations (fig. 5.16).

Predictions from the final random forest model for hyperiids suggested that the highest concentration values were found in the Norwegian Sea, with an annual bloom happening in the second quarter. For example, the quarterly averaged predictions of year 2000 (fig. 5.17) showed hyperiid concentration increasing from April to September (quarters 2 and 3). Smaller blooms seemed to take place South-East of Greenland and the North Sea. Between April and June, hyperiids also started appearing in the North Atlantic offshore (mostly below 55°N in 2000) and then the population seemed to shift to northern as well as shallower areas (e.g. July-September 2000 in fig. 5.17). The Norwegian Sea distribution also seemed to move to western areas in the last quarter.

In the Norwegian Sea, we noticed the presence of a patch of higher abundance values whose strange shape looked constant from April to December (fig. 5.17). The same patch could be found in predictions of other years. This disruption in the predicted field suggested a lower performance of the random forest model for hyperiids in this area.

C. finmarchicus

Random forest models for *C. finmarchicus* were probably the most stable models of the three taxa studied here. Training random forests on different data subsets (always 80% of the dataset) in either time or space did not cause any noticeable changes in model properties. Importance of predictors were almost the same between time and space subset experiments (fig. 5.18). The annual averaged temperature (SST_y) was the most important predictor in terms of both %IncMSE ($\approx 32\%$) and IncNodePurity indices. In terms of %IncMSE, it was followed by surface salinity (SSS) ($\approx 29\%$), the Day/Night factor ($\approx 22\%$) and water column depth ($\approx 19\%$). Mezo and day of year were the least important predictors, their %IncMSE varying between 12 and 16%.

We saw previously that model performances were higher for *C. finmarchicus* than the other two taxa, with RMSE values approaching 0.2 (table 5.6). This was

Space train data

SSTy
SSS
Day/Night
depth
mezo
day of year

15   20   25   30

%IncMSE

Time train data

SSTy
SSS
Day/Night
depth
mezo
day of year

15   20   25   30

%IncMSE

SSTy
day of year
mezo
SSS
depth
Day/Night

0.0e+00   1.0e+11

IncNodePurity

SSTy
day of year
mezo
SSS
depth
Day/Night

0.0e+00   1.0e+11
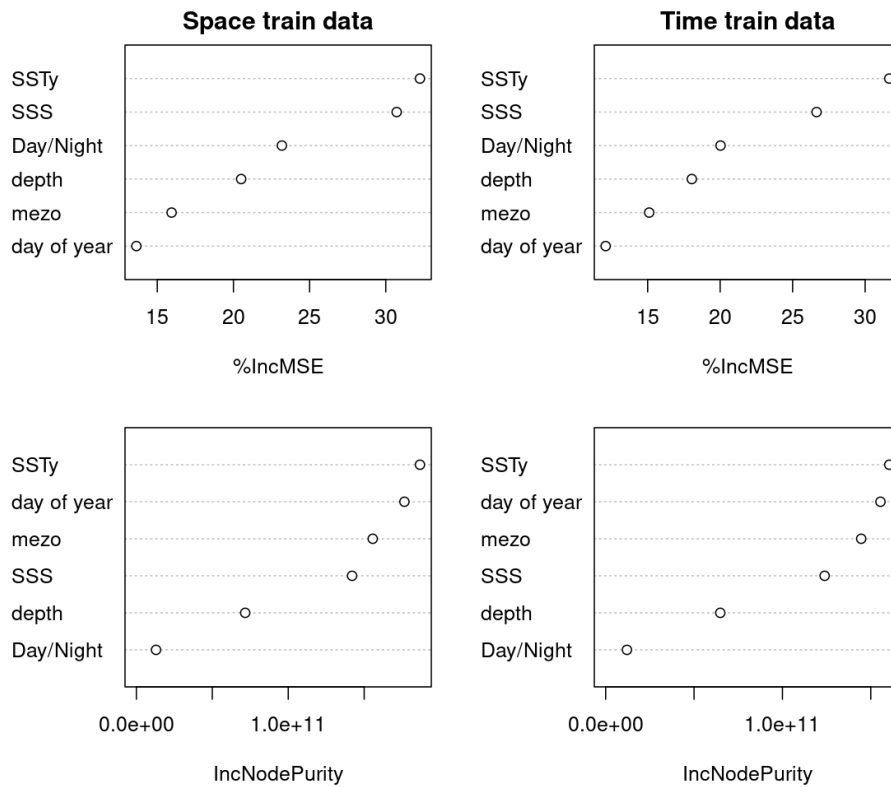
IncNodePurity

Figure 5.18: Importance of predictors in random forest models for predicting abundance of *C. finmarchicus*. Importance is given by the increase in MSE (%IncMSE) and by the increase in node purity (IncNodePurity). Predictors are written in order of decreasing importance when read from top to bottom. Predictor importance was studied for both random forests, either trained on a spatial subset (left) or time subset (right) of the CPR dataset.

confirmed with the regression performed between predicted and observed values, especially for random forests used on the test data subsets (fig. 5.19). Compared to the results for euphausiids and hyperiids, we noticed that the models for *C. finmarchicus* seemed to be more effective at predicting high values ($\geq$ 17 individuals per sample).

Among the test areas, only the areas around Iceland (5.a) and North-East Greenland (14.a) seemed to repeatedly harbour *C. finmarchicus*, whose presence was found in at least 50% of CPR samples taken in those areas (fig. 5.20). The highest abundance values were also predicted in those areas by the random forest model. In areas where *C. finmarchicus* was absent from CPR samples, predicted values tended to approach zero (areas 4.c, 8.b,8.c and 10.a). In the tested areas west and south-west of the British Isles (6.b and 7.c,f,h,k) where the taxa was

scarcely identified in CPR, the model seemed to keep predictions at low values. Thus, most predictions seemed to be very close to their observed values. The
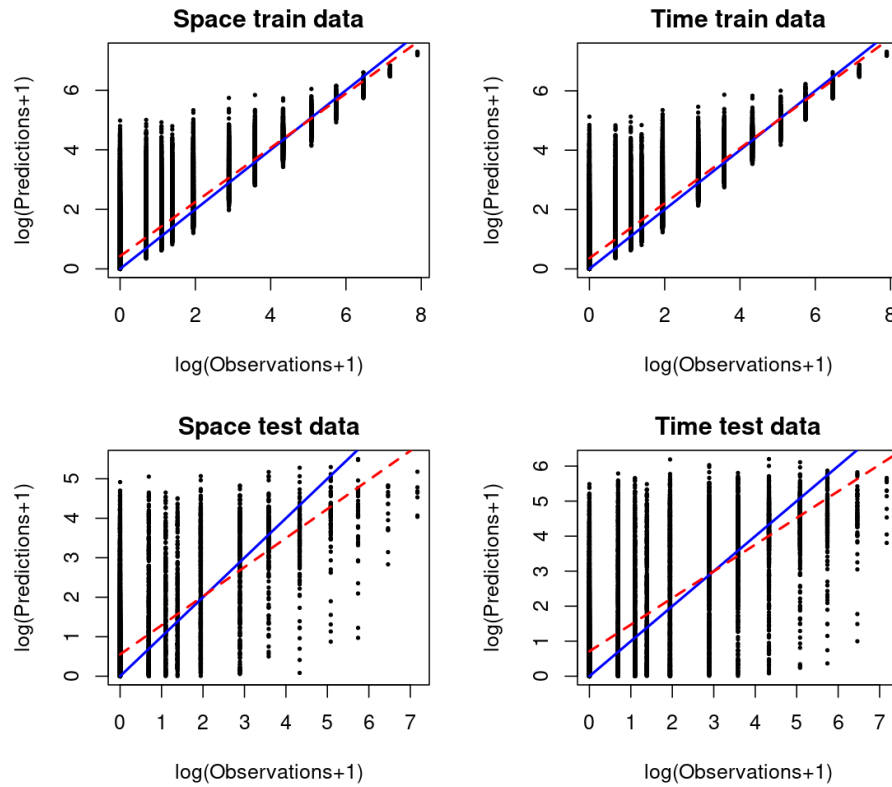
Figure 5.19: Predicted against observed abundance values (in log scale) for *C. finmarchicus* for both spatial subsets (train/test) and both time subsets of the CPR dataset. The continuous blue line represents predicted values equal to observed values. The dashed red line is the regression curve between predicted and observed values.
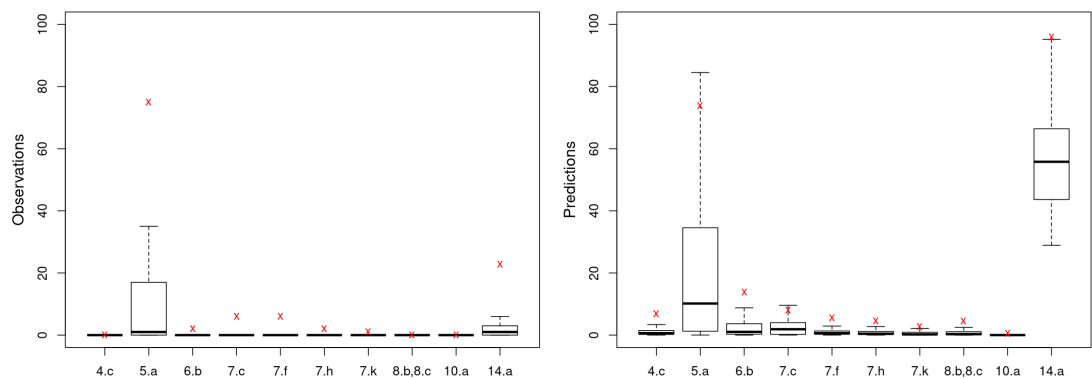
Figure 5.20: *C. finmarchicus* abundance observations from CPR (left) and predictions in each area used to test the random forest model's performance in space (see fig. 5.12 for details).

(a) Jan-Mar 2000

(b) Apr-Jun 2000

(c) Jul-Sep 2000

(d) Oct-Dec 2000
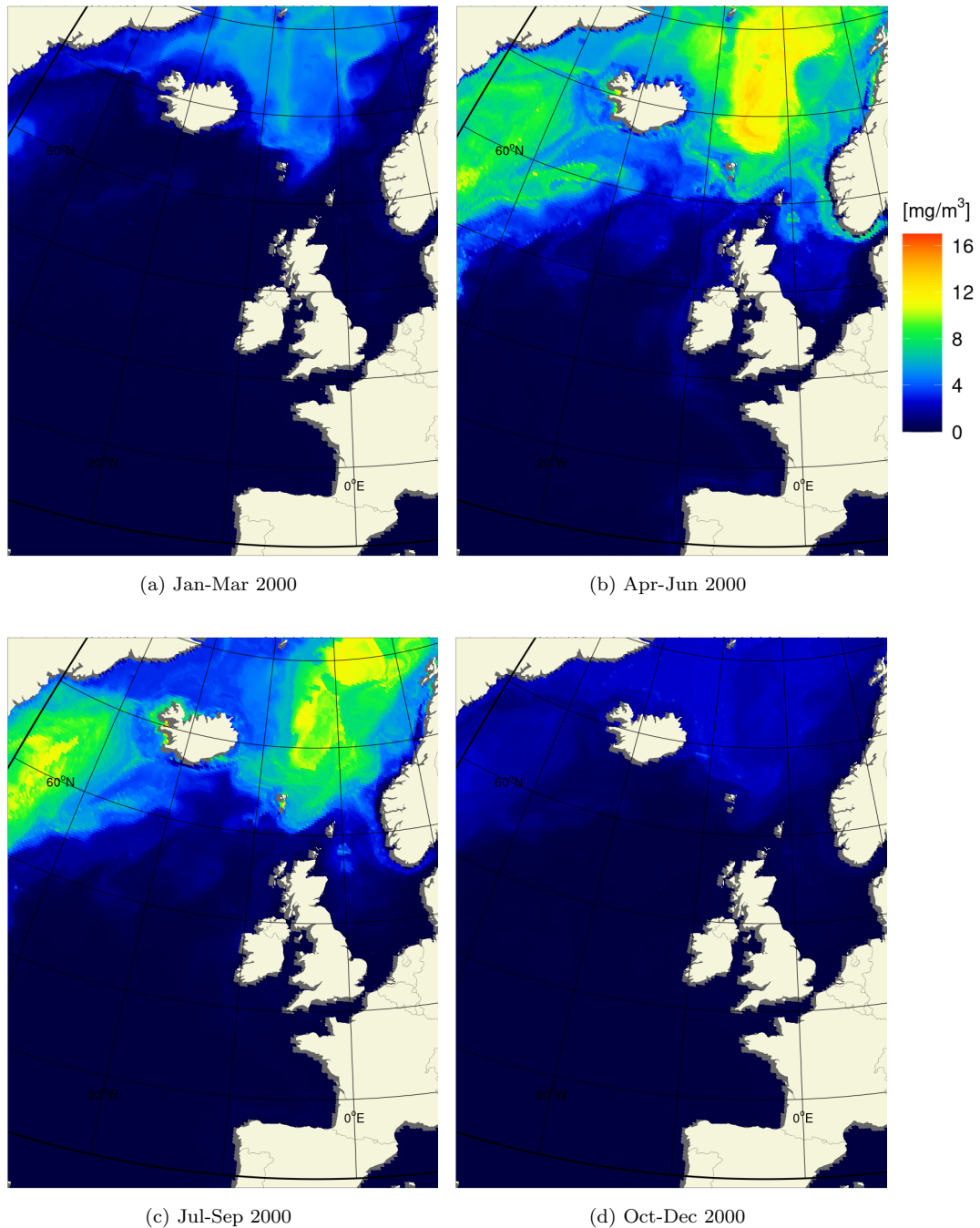
Figure 5.21: Quarterly averaged predictions of *C. finmarchicus* concentration (mg/m^3) in year 2000. Prediction maps are obtained from running the general random forest model (which was trained over the entire CPR dataset) over the whole spatial domain of NEMO-Medusa at each timestep.

North-East Greenland area (14.a) was the exception, with a distribution of very high abundances compared to the CPR observations. This difference was most likely caused by the extremely low number of samples in that area (table 5.7).

Population of *C. finmarchicus* seemed to be mostly confined to the northern latitudes, especially the Norwegian Sea. In figure 5.21, we can see that population concentration reached the highest values in the Norwegian Sea (10°W-10°E, 62-75°N) during the second quarter of the year 2000. A slower and weaker bloom seemed also to take place in the Irminger Sea between April and September. Quarterly averaged values tended to be higher in the first quarter than the last, which suggested that the model might be simulating an annual *C. finmarchicus* bloom starting in March.

5.3.4 Blue whiting food

According to the prey biomass concentration values predicted by the random forest models, *C. finmarchicus* was the dominant taxa present in the environment when blue whiting stomachs were sampled. In the northern areas (lat$\geq$ 55°N), the prey population was composed of 81% of *C. finmarchicus*, 14% of euphausiids and 5% of hyperiids. While in southern areas (lat< 55°N), the prey population was constituted of 59% of euphausiids, 16% of hyperiids and 25% of *C.finmarchicus*. For the whole diet dataset, the average proportion in the environment was estimated to be 0.21 for euphausiid, 0.07 for hyperiids and 0.72 for *C. finmarchicus*.

Proportions of prey in the environment along with prey proportions in the diet (section 5.3.1) were used in equation 5.3 to produce a selectivity index (α) for each prey and each stomach record from DAPSTOM. Table 5.8 gives average alphas for different data subsets. High selectivity indices were found for euphausiid (0.41-0.72) and hyperiid (0.28-0.55), while selectivity for *C. finmarchicus* was hardly more than 0.01. A shift in the blue whiting diet might occur from juvenile life stage to adult, with increasing prey selectivity for hyperiid. This shift was

Table 5.8: Average selectivity indices (α) calculated for Euphausiid (E), Hyperiid (H) and *C. finmarchicus* (C). Diet proportions and corresponding predicted proportions in the environment were used to calculate alpha indices for each diet record.

Data	α_E	α_H	α_C
Juveniles	0.68	0.32	< 0.01
Adults	0.54	0.44	0.02
South	0.72	0.28	0.00
North	0.41	0.55	0.04
All	0.62	0.37	0.01

also present and actually more important when moving from southern to northern areas.

Overall, euphausiid seemed to be the most preferred prey with $\alpha_E = 0.62$, followed by hyperiid with $\alpha_H = 0.37$. Blue whiting did not seem to like to prey on

(a) Jan-Mar 2000   (b) Apr-Jun 2000

(c) Jul-Sep 2000   (d) Oct-Dec 2000
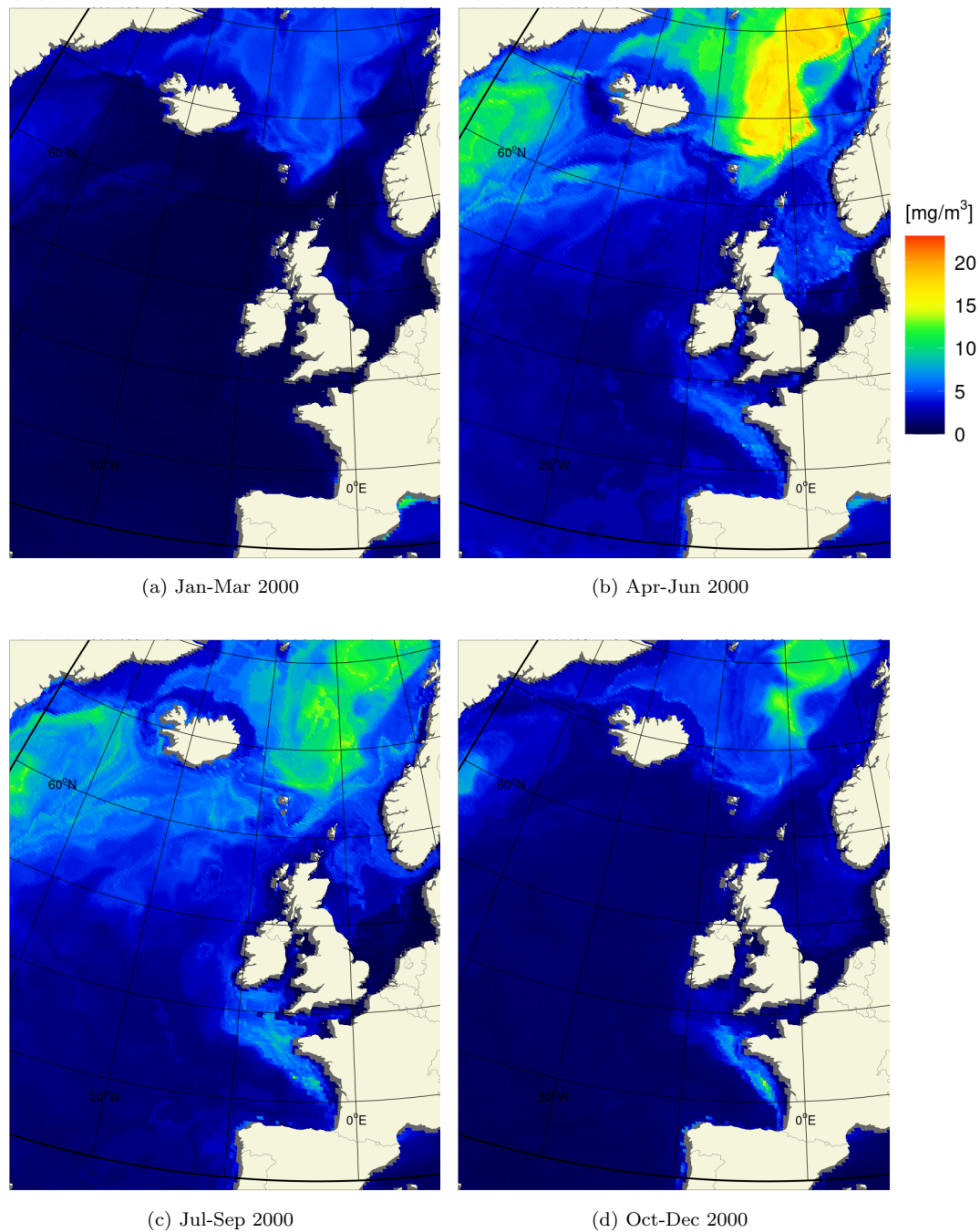
Figure 5.22: Quarterly averaged predictions of blue whiting food concentration $(\mathrm{mg/m^3})$ in year 2000. The final food variable is computed using predictions of Euphausiids, Hyperiids and *C. finmarchicus* population and the corresponding selectivity (alpha) indices (eq. 5.2).

C. finmarchicus with $\alpha_C = 0.01$, and the high proportions found in the diet were probably due to the very high concentrations present in the environment. These selectivity index values were the ones chosen to compute the new food fields that were used in the blue whiting model and for the rest of the study.

We looked previously at predictions of population distribution for each taxa separately. Figure 5.22 shows an example of the new food field resulting from combining predicted distributions of all three taxa and applying selectivity according to equation 5.4. This highlighted the fact that euphausiid population distribution highly influenced the food distribution available to blue whiting, as the food and euphausiid fields looked very alike (fig. 5.13 and 5.22). Nevertheless, hyperiid population seemed to become more important to blue whiting during the third quarter, when the particular spatial feature of high hyperiid concentrations noticed in the Norwegian Sea (fig. 5.17) became visible in the food fields (fig. 5.22c). In general, combining all three prey distributions in one food field resulted in blue whiting food distributions supporting the assumption of the Norwegian Sea as being the most suitable feeding area.

5.3.5 Climate effect

The random forest models used to predict blue whiting food were all using environmental drivers from NEMO-Medusa outputs as predictors. In chapter 4, we saw that the NEMO model was capable of representing climate driven processes, such as the subpolar gyre strength variation, through currents velocity, temperature and salinity. Since temperature and salinity were predictors, as well as the NEMO-Medusa mesozooplankton variable which is also sensitive to environmental changes (Yool et al., 2013b), the new food distribution was expected to be also affected by climate variations. Thus, years supposed to be in different climate regimes were compared to each other.

In 1992 and 1994, the subpolar gyre was strong. Like the food predictions seen previously, the Norwegian Sea was a hot spot for blue whiting feeding in those years. This time however, similar high levels of food concentration were also predicted South-East of Greenland (fig. 5.23a and 5.23b). Moreover some medium levels of food concentration seemed to extend from that region to areas South of

Iceland. This feature seemed to be strongly diminished in years of weak subpolar gyre, like in 2002 and 2004 (fig. 5.23c and 5.23d). This suggested that the strong subpolar gyre regime benefited the plankton population in the Irminger Sea and would also potentially benefit blue whiting if used as feeding habitat.

In the Norwegian Sea, distribution changes were less impressive. Nevertheless,

(a) Apr-Jun 1992

(b) Apr-Jun 1994

(c) Apr-Jun 2002

(d) Apr-Jun 2004
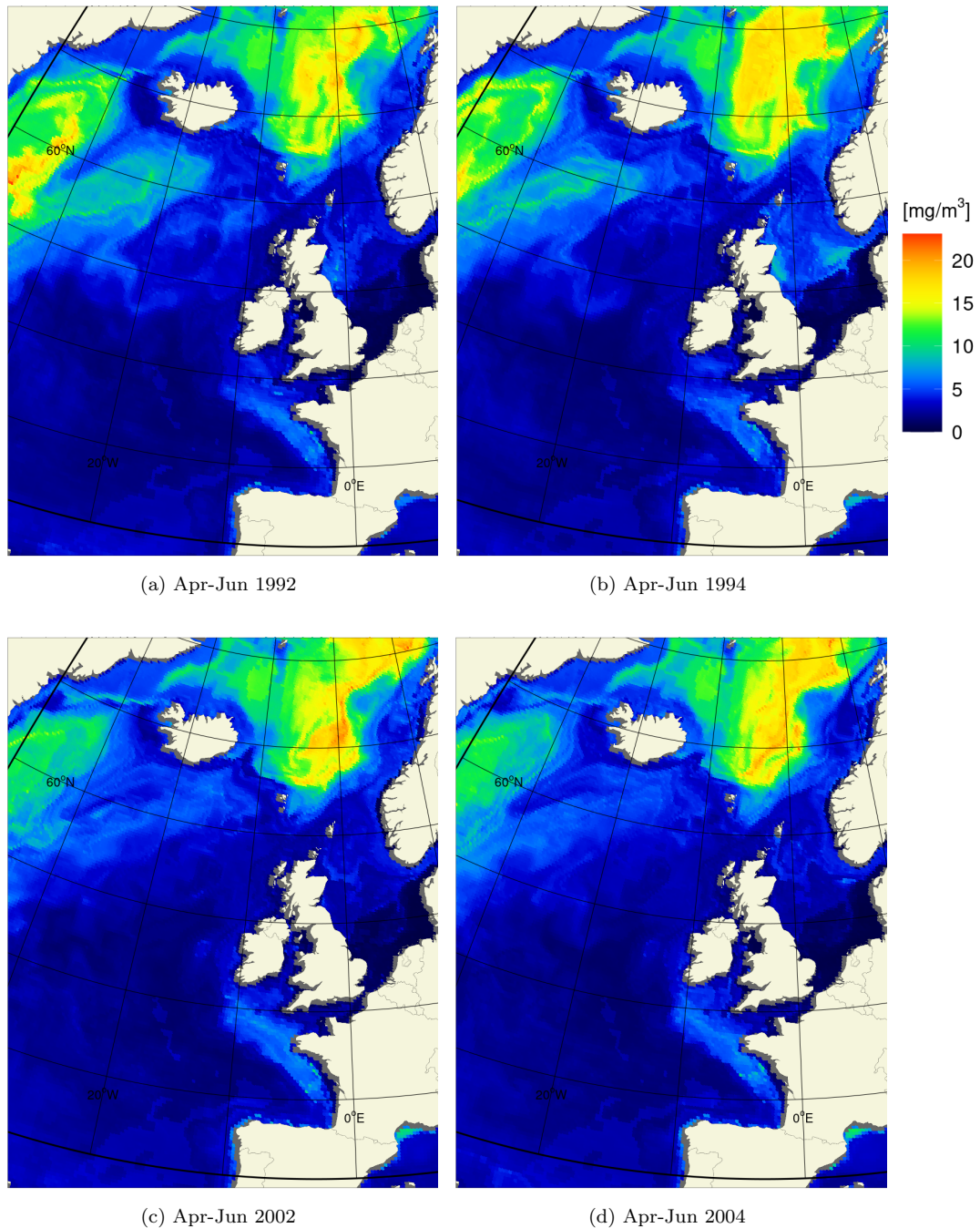
Figure 5.23: Variation in food average spatial distribution between four different years (1992, 1994, 2002, 2004) in quarter 2. Years 1992 and 1994 were both marked with relatively stronger subpolar gyres than years 2002 and 2004.

the centre of distribution might be shifting slightly southward in years of weak subpolar gyre. While food seemed to be more concentrated in latitudes higher than 65°N in 1992 and 1994, some high concentration spots (> 20 mg/m^3) were found below that same latitude in 2002 and 2004 (fig. 5.23). Thus, the subpolar gyre might also affect environmental conditions in the Norwegian Sea, which in turn might induce changes in the blue whiting prey distribution. In this case, a weak subpolar gyre might be more beneficial for blue whiting as it seemed to allow for a more southern distribution of food, which would reduce the distance travelled from spawning grounds to suitable feeding areas.

5.3.6   Forecasts

With a ten-year interval from year 2000 to year 2050, figure 5.24 gives the predicted mean spatial distribution of food concentration between April and June. In 2000, most food was concentrated in the Norwegian Sea and was spread quite homogeneously over the whole area between latitudes 63-72°N and longitudes 6°W-10°E. In the same year, concentrations in the Irminger Sea were low (< 14 mg/m^3). From 2000 to 2010, the Norwegian Sea distribution appeared to have shifted drastically, as the usual food hotspot in the Norwegian Sea was restrained to the North-East region in 2010, while food concentrations almost doubled in the Irminger Sea.

After 2010, the prey population was mostly distributed over western areas of the Norwegian Sea (65-70°N, 10°W-0°E). The Irminger Sea seemed to become a more reliable and productive feeding area than the Norwegian Sea over this period, most of the time with food concentrations higher than in the Norwegian Sea (e.g. fig. 5.24e).

Over the southern continental slope, off France and British Isles, a small population of prey (5-10 mg/m^3) seemed to be undertaking a slow northward shift of distribution from 2000 to 2050. In 2000, most of those food concentrations were found under latitude 50°N. In years 2010, 2020, 2030 and 2040, preys were mostly predicted around latitudes 47-53°N. In 2050, concentrations of food had dropped considerably in the area off France. Higher concentrations (around 10 mg/m^3) were only found and distributed sparsely over the continental slope off Ireland (e.g. food spot around latitude 55°N in light green in figure 5.24f).

(a) Apr-Jun 2000   (b) Apr-Jun 2010   (c) Apr-Jun 2020

(d) Apr-Jun 2030   (e) Apr-Jun 2040   (f) Apr-Jun 2050
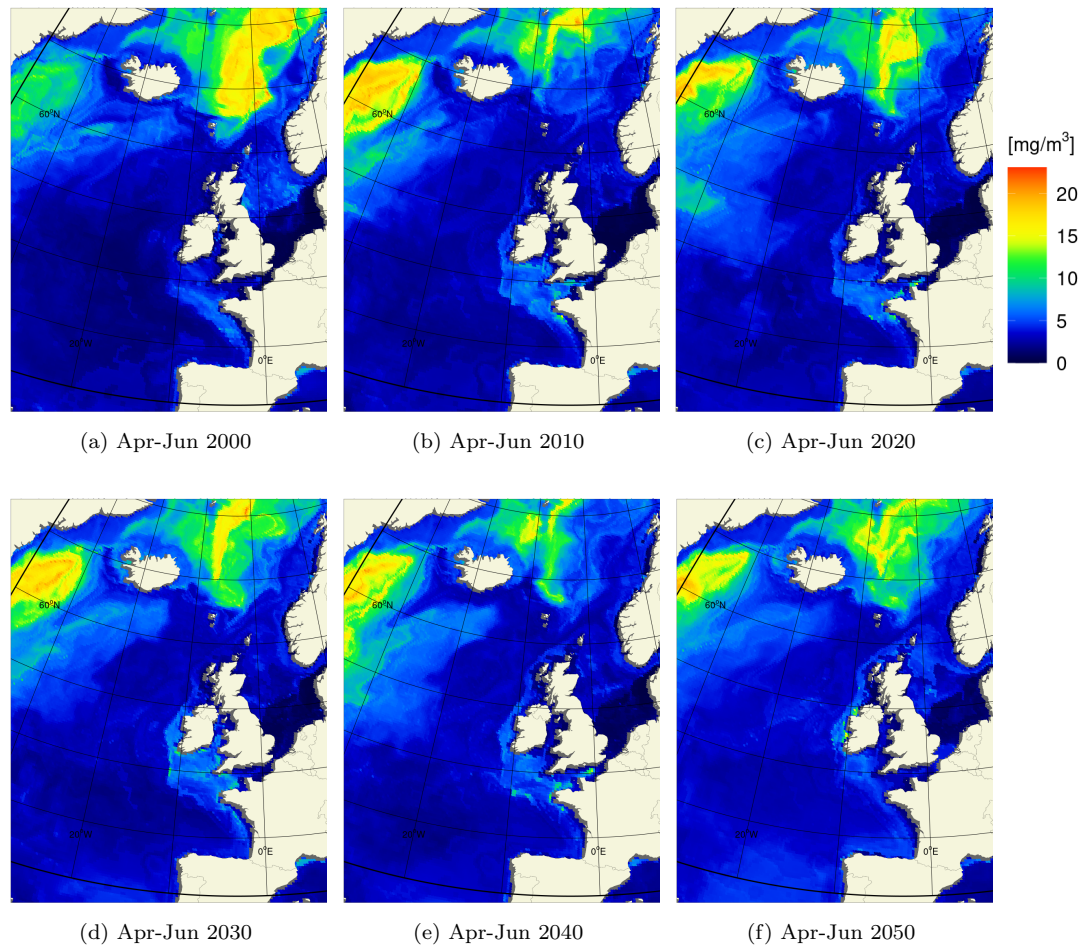
Figure 5.24: Predictions (a-c) and forecasts (d-f) of blue whiting food concentration averaged over the period April-June (quarter 2) for years between 2000 and 2050.

In time series of environmental variables (including the new food variable) in different areas (fig. 5.25), it was first noticed that the 2006 disruption of NEMO modelled values (chap. 4, sec. 4.1.3) was also visible in the food time series. Apart from this disruption in the variable's variation, blue whiting food appeared to be mostly negatively correlated with surface temperature in both the Norwegian Sea (cor= -0.84) and the Irminger Sea (cor= -0.74). In the Bay of Biscay, variation of the food's median value was very weak, but the $Q_{0.95}$ value suggested a small positive correlation with SST between 1988 and 2030 (cor= 0.26).

The effect of salinity variation on food seemed to be stronger in the Irminger Sea (fig. 5.25b), especially after 2020. From 1988 to around 2015, while the relationship between both variables was weaker than between food and SST, food seemed to be also negatively correlated with salinity (cor= -0.77). Between 2010

and 2030, the relationship between food and salinity became positive (cor= 0.53). After 2030, food tended to be progressively more positively correlated with salinity variation.

Time series of the NEMO mesozooplankton (mezo) variable were very different to the new modelled blue whiting food variable. The only exception might be for food and mezo variation in the Irminger Sea between 1996 and 2012 which tended to follow similar trends (fig. 5.25b). However the mezo variable tended to stay negatively correlated with salinity over the whole period, from 1988 to 2050.
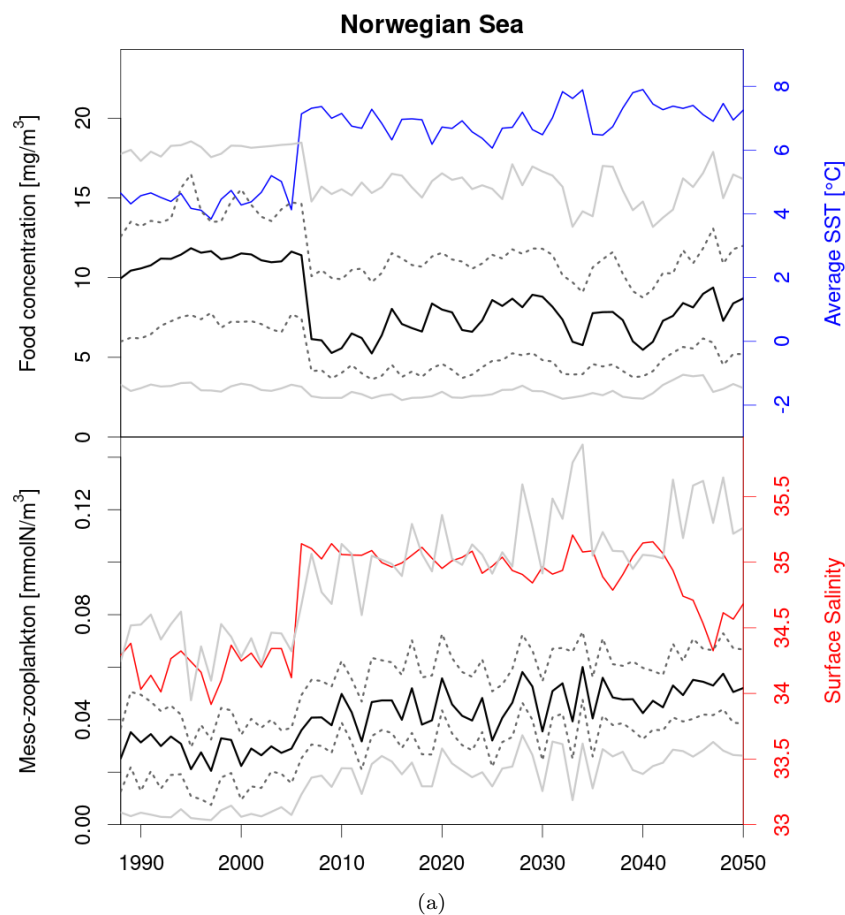
Figure 5.25: Time series of average concentration of food (top graphs) available in April-June (quarter 2) from 1988 to 2050 in the Norwegian Sea (a), in the Irminger Sea (b) and in the Bay of Biscay (c). Comparison with time series of NEMO-Medusa variables which were used as predictors in the random forests: annual average of SST (blue in top graphs), surface salinity (red in bottom graphs), and mesozooplankton (in bottom graphs). Medians (plain black), first and third quartiles (dotted gray) and quantiles 0.05 and 0.95 (plain gray) were plotted for both the food variable and the mesozooplankton variable.

(b)

(c)
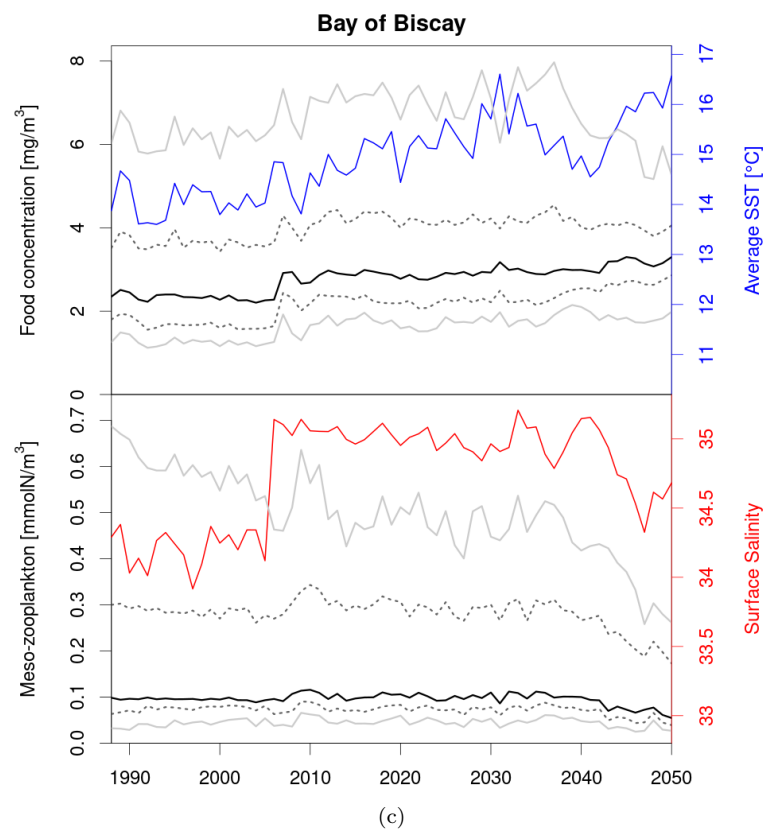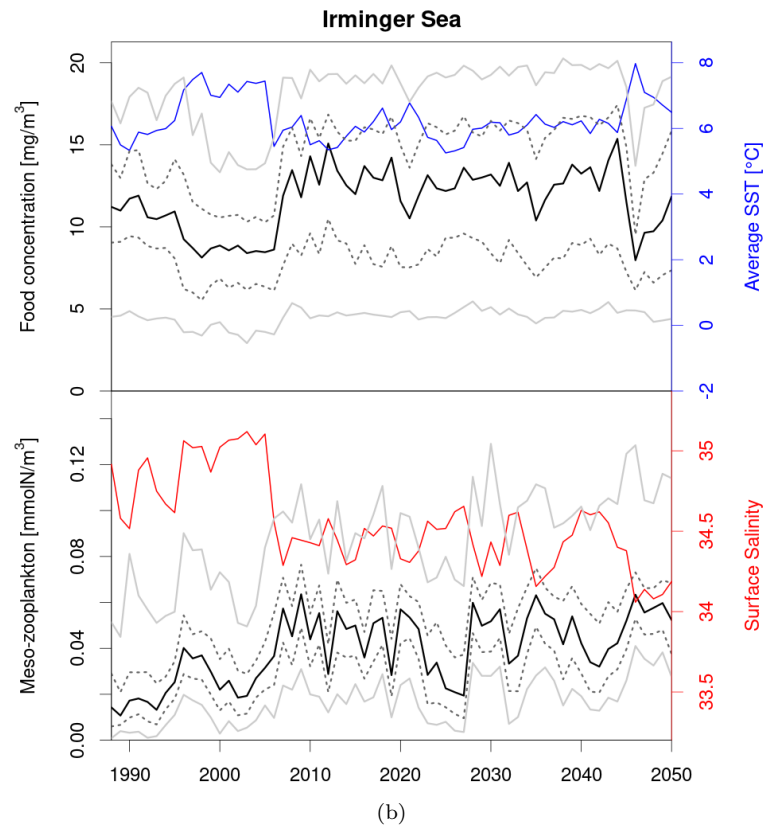
Figure 5.25: *continued.*

5.4 Discussion

Analyses of DAPSTOM dataset of blue whiting stomach records confirmed that euphausiids, hyperiids and copepods (*C. finmarchicus*) are the main preys of the North-Atlantic blue whiting population. They also showed that the Norwegian Sea provided with the most suitable food for blue whiting, while southern areas along the continental shelf caused lower feeding incidence. Those observations were in agreement with several past studies (Geistdoerfer, 1983; Prokopchuk & Sentyabov, 2006; Utne et al., 2012a; Bachiller et al., 2016) and already showed that the NEMO-Medusa mesozooplankton variable was inappropriate to describe feeding behaviours of blue whiting.

The random-forest predictions of spatial distribution of euphausiids, hyperiids and *C. finmarchicus* all presented the Norwegian Sea as the most productive area between April and September. This further disqualified the NEMO-Medusa mesozooplankton variable as an appropriate food variable for the blue whiting model. The predictions were supported by available studies on these taxa distribution in the North-East Atlantic. Thus, zooplankton sampling realised by Bachiller et al. (2016) for their study suggested high abundances of *Calanus* spp., euphausiids and hyperiids in the Norwegian Sea in May-June. A spatial model for the population of *C. finmarchicus* in the Norwegian Sea showed also very similar distributions in the area (Hjøllo et al., 2012).

Variations in the selectivity index values for euphausiids and hyperiids suggested that prey preferences of blue whiting might vary between the southern and northern areas, as well as between juveniles and adults. In parallel, the very low α values of *C. finmarchicus* indicated that their high presence in the diet was only due to extremely high abundance in the environment. This was further confirmed by the null α value in the South data subset, as *C. finmarchicus* are absent from that area (Planque & Fromentin, 1996).

As we know, the southern areas are likely nursery areas for southward drifting larvae (Bailey, 1982), and adults spotted in those areas are often young mature adults about to spawn for the first time (Brophy & King, 2007). Thus, the similar α values observed between the South data subset and the juvenile subset could be explained by the fact that the southern subset was in majority composed by juveniles. Like in previous studies (Cabral & Murta, 2002; Dolgov et al., 2010;

Bachiller et al., 2016), an ontogenetic shift was observed in the diet: while juveniles have a strong preference for euphausiids, they seem to become less selective between euphausiids and hyperiids when growing up. Nevertheless, the stronger shift in prey selectivity observed between the southern and the northern individuals also points towards a strong effect of an individual's location on its prey preferences. Such variations in prey selectivity caused by changes in food conditions have been observed in the past for the larval cod population (Munk, 1995). Therefore, prey selectivity of blue whiting is also likely affected by local environmental conditions.

Including ontogenetic shifts and area-dependent variations of prey selectivity in the blue whiting model would have added unnecessary complexity, as well as uncertainties, to the model. Therefore, only the average α indices calculated from the whole dataset were retained for the computation of the final food variable for both juveniles and adults. According to these values, blue whiting's most preferred preys are euphausiids ($\alpha = 0.62$), followed by hyperiids ($\alpha = 0.37$), while the *C. finmarchicus* population is mostly dismissed as a food source ($\alpha = 0.01$).

A mild climate effect seemed to be visible in the variations of food distribution. A strong SPG might increase productivity in areas south of Greenland and Iceland, making them highly suitable for blue whiting feeding. In a recent study, observations of juveniles in the Irminger Sea suggested that a third larval drift pattern exists and takes larvae and juveniles from the Rockall Plateau area to Greenland waters (Post et al., 2019). During strong SPG years, stronger westward currents would be favourable to this westward larval transport, and the high food concentration of food observed in the Irminger Sea would also favour high recruitment success of juveniles in that area. Thus, these blue whiting food distributions supports Post et al.'s claim of a suitable feeding habitat west of Greenland, whose quality might be varying with climate changes according to these predictions.

Long-term predictions suggested a negative relationship between food concentration and SST in both the Norwegian Sea and the Irminger Sea. In terms of spatial distribution of food, a local sea warming seemed to result in major surface reduction of the local suitable feeding area. Comparing salinity and food variations in the Irminger Sea suggested the presence of a slow shift of the food

response to salinity changes. This could be the result of the SPG freshening and/or the collapse of the deep-ocean convection, which has also been predicted by many other climate models (van den Berk et al., 2021; Sgubin et al., 2017).

Random forest performance was quite high in the training data subsets in either time or space. Since the random forest method includes cross-validation, this should guaranty that the model performance at interpolating stay relatively high (Brun et al., 2016). Here, the focus was on testing the model performance at extrapolating in areas that have been entirely excluded from the training process, and forward in time. Results showed seemingly poor performances of the models at extrapolating in time and space. According to Elith & Leathwick (2009), this was to be expected. The prediction error seemed to increase when attempting to use the model in areas surrounding the spatial domain of the training data.

Since the final random forest models used for predicting the blue whiting food variable were trained again on the entirety of the CPR dataset, the error caused by the poor extrapolating performance in space should be minimised in most areas relevant to the blue whiting spatial dynamics, except for the Norwegian Sea. However, while CPR samples were scarce in the Norwegian Sea over the studied period, other studies validated the random-forest predicted presence of high concentrations of these species in the area during summer (Bachiller et al., 2016; Hjøllo et al., 2012).

While we hoped for a better forecasting performance of the random forests, some predicted future trends of the food variable were encouraging and convinced us to accept these models as the best available method for producing long-term predictions of blue whiting food to use as input in the population model. For example, the random-forest models seemed to be able to detect the shift in the SPG ocean circulation predicted between 2010 and 2050 (van den Berk et al., 2021; Sgubin et al., 2017), which translated into a shift of the relationship between salinity and food in the Irminger Sea.

To conclude, random-forest models trained on CPR data produced satisfactory predictions of blue whiting food, which can now be used directly in the spatial model of blue whiting population dynamics. A thorough study of the species diet and prey selectivity helped the development of a well-tailored food variable,

improving our understanding of the species feeding behaviours in both time and space.

Chapter 6

Spatial properties of blue whiting fishing

Fishing is an important component of the blue whiting model (chap. 2) and it is essential to comprehend the time and spatial dynamics of the blue whiting fishery which need to be represented in the final model. Therefore, the objective here was to derive general properties of the fishery over time and space from the available ICES fishing data and reports. The following observations helped to choose the fishing equations implemented and tested in the final population model (chapter 2).

6.1   Fishing history and data

For the purpose of studying the time and spatial dynamics of blue whiting fishery in the model context, catch data which included spatial information was needed. The Eurostat/ICES database provide historical and official annual catch of blue whiting in tonnes from 1960 to 2010 (ICES 2011, Copenhagen). Catch statistics are given per FAO/ICES fishing areas (see map in fig. 6.1) and per country. First, the dataset was used to determine main fishing areas, by looking at the cumulated total catch over the whole time period available. Industrial exploitation of the North-East Atlantic blue whiting stock started in the 1970s. Bailey (1982) mentioned that blue whiting fishing was already practised before that time, however they were usually taken as by-catch and poorly documented. This was reflected in the catch-per-ICES-area dataset, which presented very low total catch values from 1960 to 1974. A small peak was observed in the early 1970s,

which corresponds to the time when the first experimental fishing of the stock was conducted by Norway, using pelagic trawls (Bailey, 1982; Monstad, 1990). As a result, average catch densities in the different ICES areas were calculated over the period 1975-2010.

After 1975, the fishery rapidly developed, with an annual total catch increase of more than 1 million tonnes reached in 1980, and with most catches coming from the Norwegian Sea and from Russia (USSR at the time) (Monstad, 1990). After 1982, however, most blue whiting landings happened in the spawning area
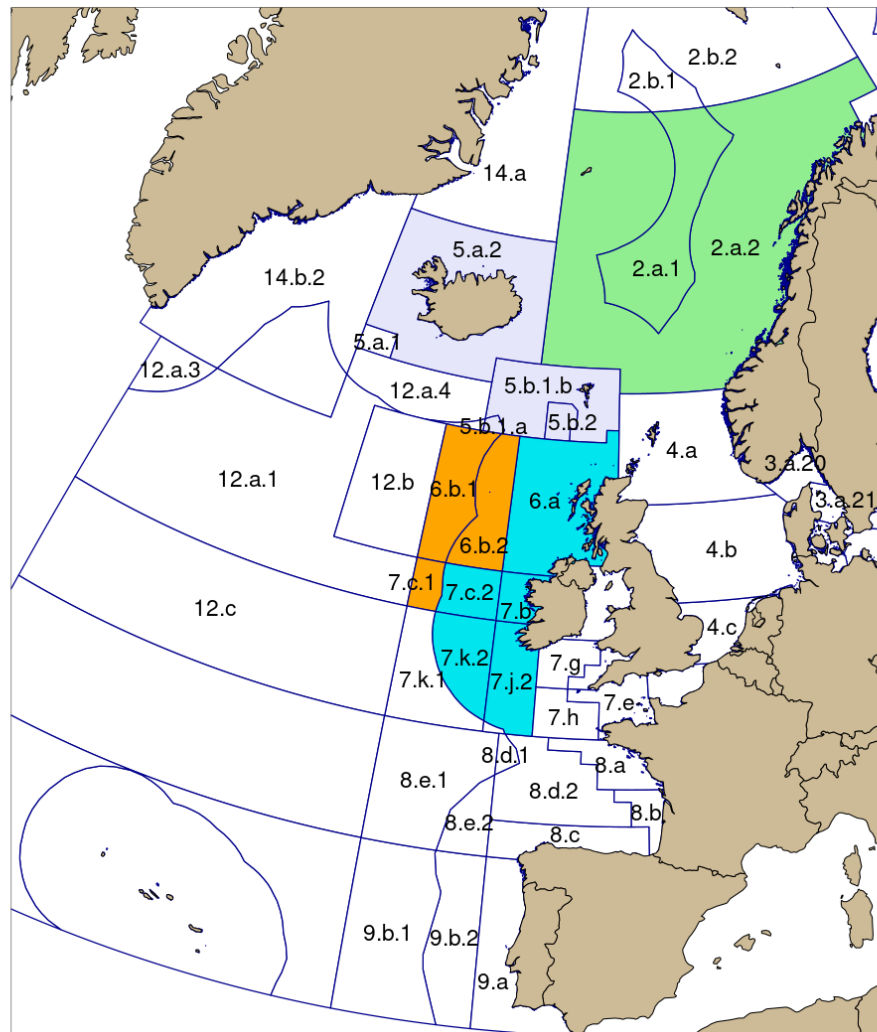
Figure 6.1: Map of ICES statistical fishing areas. Coloured areas represent potential areas of high stock abundance and so areas of interest to fishing fleet: (1) the Norwegian Sea area (2.a in green) as main feeding ground for blue whiting, (2) Iceland and Faroese waters (5.a.2, 5.b.1 and 5.b.2 in purple), (3) the continental shelf off British Isles (6.a, 7.b, 7.c.2, 7.k.2 and 7.j.2 in blue), and finally (4) Rockall Plateau area (6.b and 7.c.1 in orange).

west of the British Isles (Monstad, 1990; ICES, 2019b). While some nations like Norway and Russia were present from the very beginning of the stock industrial exploitation, other countries joined the fishery more recently. For example, Iceland's contribution to the annual total catch values only started to increase considerably after the mid-1990s (Pálsson, 2005; Bjørndal, 2009; Bjørndal & Ekerhovd, 2014). To understand how the different countries are involved in the blue whiting fishery and to determine any preferred fishing location for the main participants, the total catch contribution of each country was calculated for different areas. For that, four areas were defined according to their importance in the annual migration cycle of blue whiting (fig. 6.1): (1) the Norwegian Sea area (ICES area 2.a) as main feeding grounds ; (2) the Scottish and Irish continental shelf area (areas 6.a, 7.b, 7.c.2, 7.j.2 and 7.k.2) as main spawning area ; (3) the Rockall Plateau area (areas 6.b and 7.c.1) as extended spawning area ; (4) Faroese and Icelandic waters (5.a.2 and 5.b) as migration routes between spawning and feeding grounds. Results will help identify possible bias caused by changes in the fishing activities, and help with the interpretation of fishing records.

Seasonal shifts in fishing fleet activity distribution seemed to be concurrent with annual adult migrations (Monstad, 1990; ICES, 2016a, 2019a,b). Since catches seemed to vary both in time and space, within and between years, relationships between catch distribution, population distribution and/or climate variation were investigated. The catch-per-area dataset was used to try and detect any changes in catch distribution that would suggest an effect of the subpolar gyre. While this dataset had the advantage to provide with long-term records of spatial distribution of fishing activity, its time and spatial resolutions were insufficient either for evaluating the spatial distribution of fishing pressure on the blue whiting stock or for studying seasonal variations in catch distribution. In fact, fishing effort is most likely to be concentrated in the exclusive economic zones (EEZ) crossed by the stock (Ekerhovd, 2010) and along the Scottish and Irish continental shelf where most spawning take place according to the 2016-2019 spawning stock acoustic surveys (ICES, 2019b). In a few ICES reports on the blue whiting stock (ICES, 2004, 2005, 2007, 2011b, 2012b, 2013, 2014, 2016a), qualitative maps of catch distribution were available with a spatial resolution of 1° in longitude and 0.5° in latitude, and some of these maps were also declined into quarterly

catch distributions (ICES, 2004, 2005, 2007, 2016a). The qualitative dataset was extracted from these maps, where catch is given by four classes of minimum value (10, 100, 1000 and 10000 tonnes). This catch distribution data was available for years 2003, 2004, 2006, 2010-2013 and 2015, but only years 2003, 2004, 2006 and 2015 had quarterly data. Average annual and seasonal spatial distribution were calculated from this dataset. Considering the quantity and quality of this data, spatial representation of annual fishing activity will only help with formulating general assumptions on spatial distribution of fishing pressure.

6.2 Observations

6.2.1 Spatial distribution of fishing pressure

Records of total blue whiting catch by ICES area between 1960 and 2010 showed that most fishing during this period took place West of Ireland and Scotland, in the Faroese waters and in the Norwegian Sea (Fig. 6.2). In the same areas,
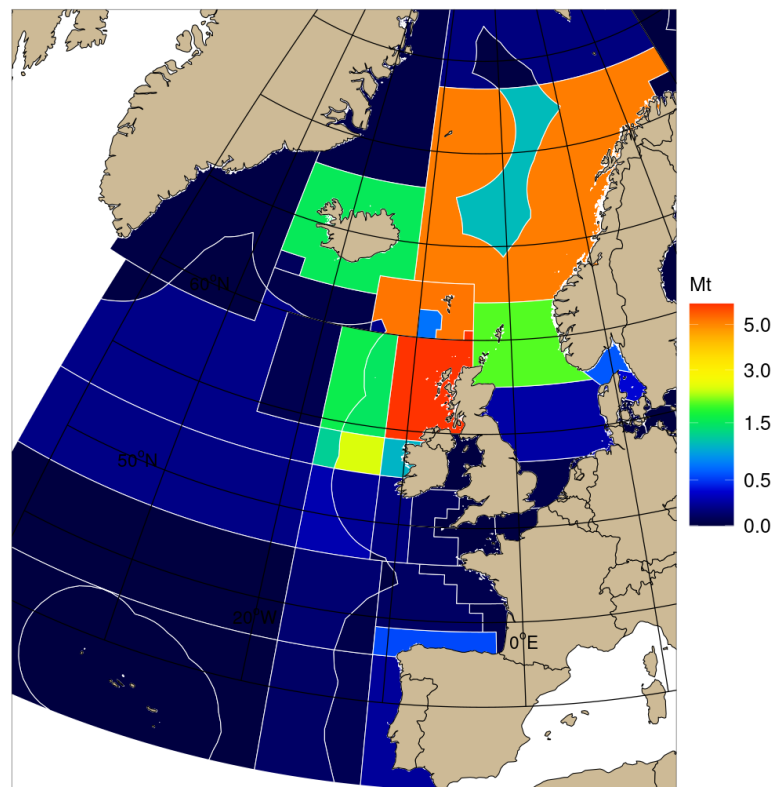
Figure 6.2: Total blue whiting catch (million tonnes) by ICES area between 1960 and 2010 (ICES data). Total catch values are represented with a logarithmic scale.

the highest average catch densities were observed (fig. 6.3). Those areas are known to be important for blue whiting population either as seasonal habitat (spawning/feeding) or as migration corridors (Faroe-Shetland and Faroe Bank Channels). The large amount of catch recorded there suggests that these areas are regularly targeted by blue whiting fishing fleets because of the higher probability of fishing success.

Some ICES areas, where the total catch recorded in the period 1960-2010 was very low (< 0.5 Mt), presented a similar or higher average catch density than areas with relatively high total catch. For example, the area 9.b.2 off Portugal seemed to have an average catch density value of more than 0.5 tonnes/km², while the total catch in the area was among the lowest (< 0.1 Mt). This could be the result of a low but regular by-catch of blue whiting in that area. In contrast, an area with a relatively high 1960-2010 total catch but a very low average catch density (examples with the North Sea area 4.a and with Icelandic waters in 5.a.2) might be explained by a few sporadic high catch events over the whole period, most likely taking place in a small portion of the area.
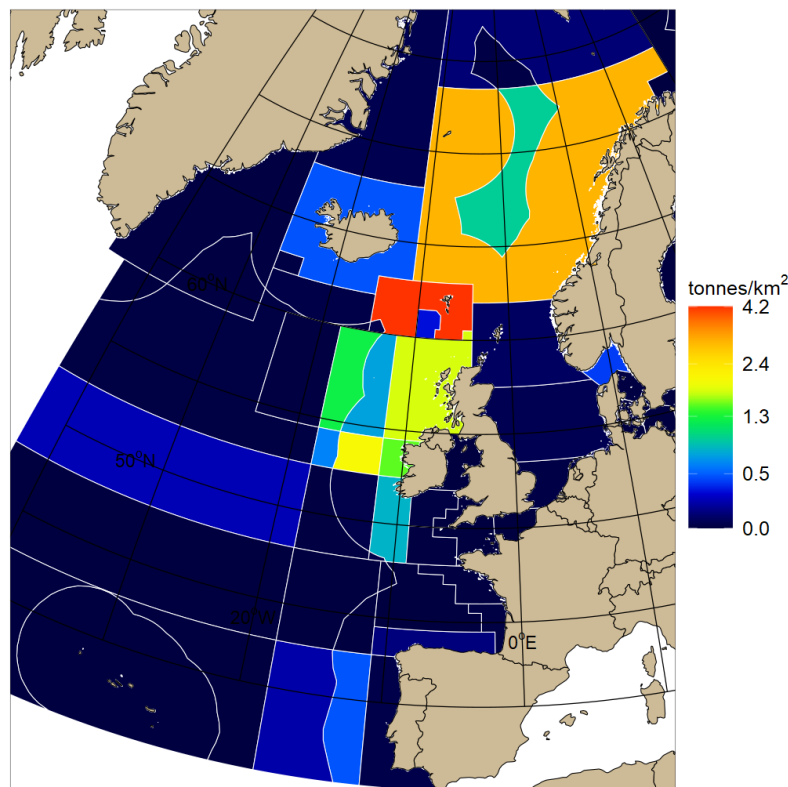
Figure 6.3: Average catch density (tonnes/km²) of blue whiting in ICES areas for the period 1975-2010 (ICES data). Values represented with a logarithmic scale.

Over the period 1978-2010, 13 nations contributed with more than 100 thousand tonnes of the total blue whiting catch (table 6.1). Since all members of the EU were given equal access to the different EEZ of other EU members under the Common Fishery Policy (CFP), the EU was treated as one single country thereafter. Overall, Norway and Russia were the main contributors to the total catch reported each year (35% in average for Norway and 24% for Russia), followed by the EU (20%), the Faroe Islands (10%) and Iceland (10%). Except for Russia, all other main participants were considered coastal states to this fishery, which means that their EEZ was included in the blue whiting distribution area (Ekerhovd, 2010). For this reason, Russian blue whiting fishery took place in the international waters of North-East Atlantic and the Norwegian Sea, unless bilateral agreements existed between Russia and other countries to be able to fish in their EEZ (Ekerhovd, 2010). In figure 6.4, we see that Russia was a major participant of the blue whiting fishery in the Norwegian Sea (68% of catches)

Table 6.1: Total catch and annual mean catch (tonnes) of the countries that participated in the blue whiting fishery between 1978 and 2010. For each country, their contribution to the total reported catch over this period (ICES historical catch data) is given in percent. Catch and contributions are also given for the fishing fleets of EU countries.

Country	Total catch 1978-2010 (tonnes)	Mean Catch (tonnes)	Contribution (%)
Norway	$11,705,692$	$354,718$	35.4
Russia	$8,049,333$	$243,919$	24.3
EU	$6,516,762$	$197,478$	19.7
Denmark	$2,010,031$	$60,910$	6.1
Netherlands	$987,388$	$29,921$	3.0
Spain	$924,304$	$28,009$	2.8
UK	$879,220$	$26,643$	2.7
Ireland	$493,114$	$14,943$	1.5
Germany	$456,308$	$13,828$	1.4
Sweden	$263,277$	$7,978$	0.8
France	$213,675$	$6,475$	0.7
Portugal	$125,440$	$3,801$	0.4
Estonia	$55,900$	$1,694$	0.2
Poland	$46,594$	$1,412$	0.1
Latvia	$37,969$	$1,151$	0.1
Lithuania	$23,462$	711	< 0.1
Finland	81	3	< 0.01
Faroe Islands	$3,450,787$	$104,569$	10.4
Iceland	$3,344,023$	$101,334$	10.1
Greenland	$19,629$	595	< 0.1
All	$33,086,226$	$1,002,613$	100.0

and in the Icelandic and Faroese waters (33% of catches), with most of the catch taken in EEZ areas (2.a.2 and 5.b.1.b), suggesting that most Russian blue whiting fishery (here 83% of their total catch) was dependent on bilateral fishing quota agreements set with the other countries. Surprisingly, Norway did not make most of the catch in the Norwegian Sea, instead the Norwegian fleet seemed to be very active over the spawning grounds (including Rockall area). While most of the spawning area is covered by EEZ of EU countries, the EU only came second in that area. The high contribution of the EU to the total catch taken outside of the four defined areas ('Other') can be explained by the regular catch by the EU fishing fleet in three distinct areas: the Galician Sea (mostly 8.c and 9.a), the North Sea (4.a), and the Skagerrak and Kattegat seas (3.a.20 and 3.a.21).

Iceland contribution to the total catch was very low in almost all defined
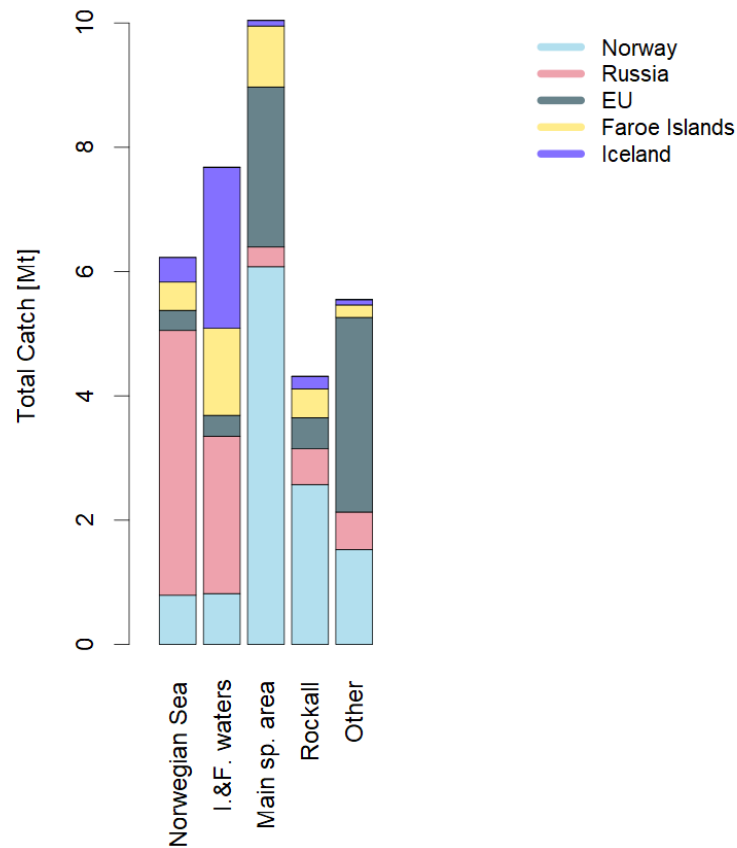
Figure 6.4: Total catch contribution of nations in areas of ecological importance to blue whiting: the Norwegian Sea, Icelandic and Faroese waters, the main spawning area along the continental shelf, and the Rockall Plateau area. Greenland also contributed to total catch but with values less than 10000 tonnes and is therefore not represented here. Catch contributions to the 'Other' area represent fish caught in any ICES areas not included in the defined areas of figure 6.1.
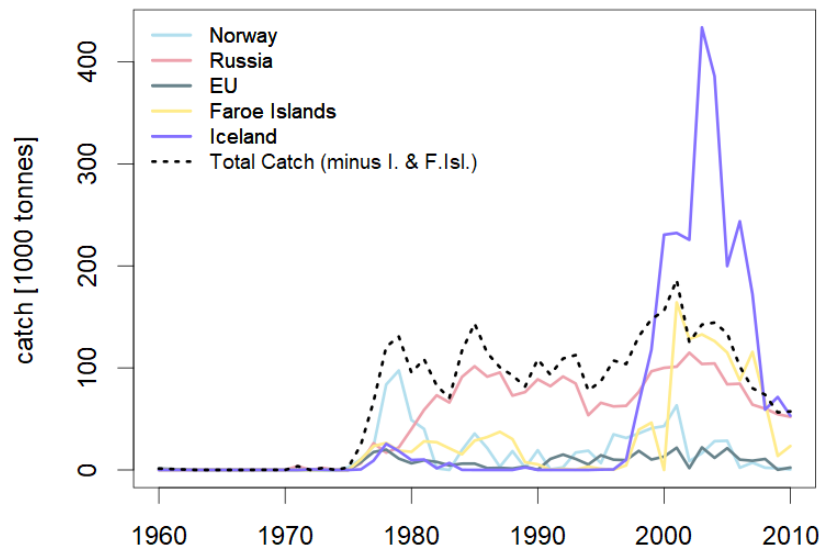
Figure 6.5: Annual catch of nations in Icelandic and Faroese waters (ICES historical catch data). This area is defined by ICES areas 5.a.2, 5.b.1 and 5.b.2 (fig. 6.1). The black dotted line gives the annual total catch when removing catch contributions of both Iceland and Faroe Islands.

areas, except in the Icelandic and Faroese waters (fig. 6.4). Considering that Iceland really started a proper exploitation of the blue whiting stock in the late 1990s (Bjørndal & Ekerhovd, 2014; Bjørndal, 2009; Pálsson, 2005), the fact that Icelandic total catch in the Icelandic and Faroese waters was almost as important as Russia, a major, regular and more experienced player in this fishery, suggests that Iceland both favoured its own EEZ as well as Faroese EEZ (ICES, 2007) and fished blue whiting with far more intensity than other nations in this area. Time series of catch in this area for each nation confirmed that Icelandic catch of blue whiting increased exponentially between 1995 and 2003, reaching values from twice to thrice the catch taken by Russia in the same area (fig. 6.5). While the catch increase was less spectacular, a similar observation could be made for Faroe Islands fishing activity in this area. Russia however kept a very constant range of catch in that area between 1985 and 2005, which was most likely due to its fishing activity limited by quotas agreed with Iceland. Nevertheless, this suggested that the catch increase observed from 1995 to 2003 might be less related to stock biomass increase than it was to fishing activity increase. Removing both catch of Iceland and Faroe Islands would then smooth catch fluctuations in the Icelandic and Faroese waters over the period 1980-2010 (fig. 6.5). Without taking into account both Iceland and Faroe Islands fishing activities, catch still

increased between 1995 and 2003, which was most likely caused by the strong
year-classes observed in that period. In the same way, the strong catch decrease
observed after 2003 was likely the result of successive years of poor stock recruit-
ment (ICES, 2007).

The qualitative average distribution of blue whiting catch (fig. 6.6) gives us
more insight on the true spatial distribution of catch and fishing high spots inside
the ICES areas. From east of Iceland to the Porcupine area west of Ireland, blue
whiting fishing seemed to be mainly concentrated along the continental shelf and
over the Rockall Plateau. In the Norwegian Sea, catch distribution was spread
over the whole area, with a slightly higher catch concentration in the southern
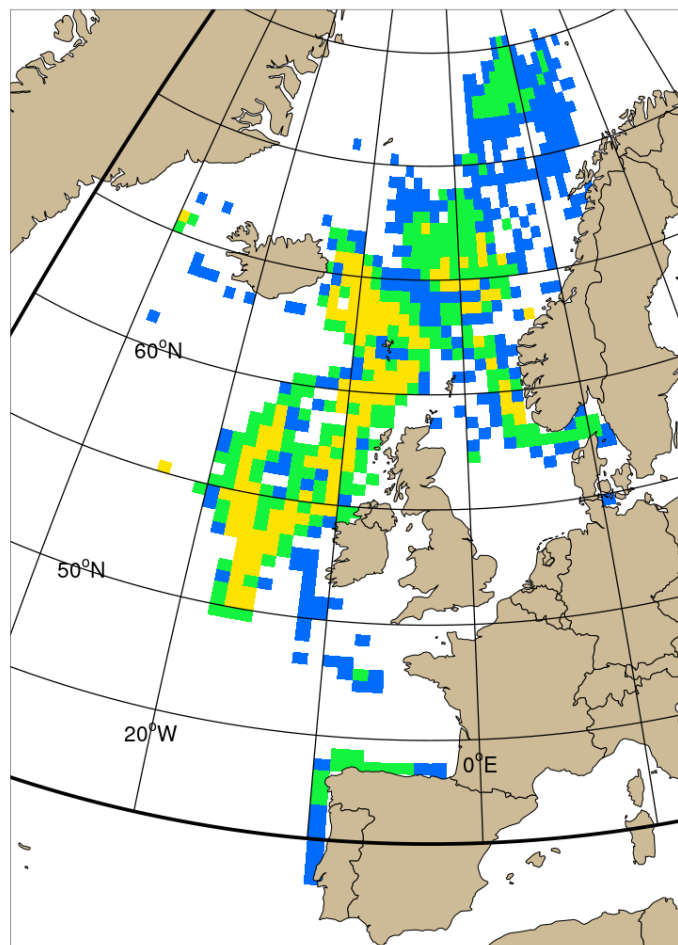
Figure 6.6: Qualitative average distribution of blue whiting catch, derived from annual catch
maps of years 2003, 2004, 2006, 2010, 2011, 2012, 2013 and 2015 from ICES reports (ICES,
2004, 2005, 2007, 2011b, 2012b, 2013, 2014, 2016a). Catch values between 10 and 100 tonnes
are represented in blue, between 100 and 1000 tonnes in green, and between 1000 and 10000
tonnes in yellow.

area which stretches towards the South continental shelf of Norway and into Sk-agerrak strait. In the South, blue whiting catch of the Galician fishery took place mostly off the North and West Spanish coast.

6.2.2 Relationship between fishing and migration cycle

We previously saw average spatial distributions of annual catch, which seemed to cover most of the theoretical stock distribution range. Next, the quarterly average distributions of catch (ICES qualitative data) were studied to verify the fishing response to population annual migrations (fig. 6.7).

During the third and fourth quarters, fishing seemed to be almost non-existent in the main blue whiting spawning area - which was also identified as the main fishing area in the previous section. As blue whiting spawning took place mostly between February and May, this means that fishing fleets only targeted areas which had high catch probability, in relation to their knowledge of the popula-tion migration cycle. This was supported by the catch distribution of the first quarter which showed scarcely any catch in the Norwegian Sea compared to other quarters.

The April-June (quarter 2) catch distributions were of great interest, as the time period covered both the end of the blue whiting spawning season and the post-spawning feeding migration season. During this quarter, highest catch numbers were encountered in the northern part of the main spawning grounds, off northern Scotland (fig. 6.7.b), which was representative of the spawner distribution in the late spawning season (Bailey, 1982; Monstad, 1990; ICES, 2005, 2019b). Catch were also important in the area between Iceland and Faroe Islands and in the southern area of the Norwegian Sea. Since the area west of Faroe Islands is one of the main migration corridors for blue whiting, this catch distribution seemed to indicate that the fishing fleet followed the feeding migration. In fact, the ob-served changes of catch distribution throughout the year suggested that fishing distribution moved together with the population movements over the spawning or feeding grounds and in-between.

(a) Quarter 1

(b) Quarter 2

(c) Quarter 3
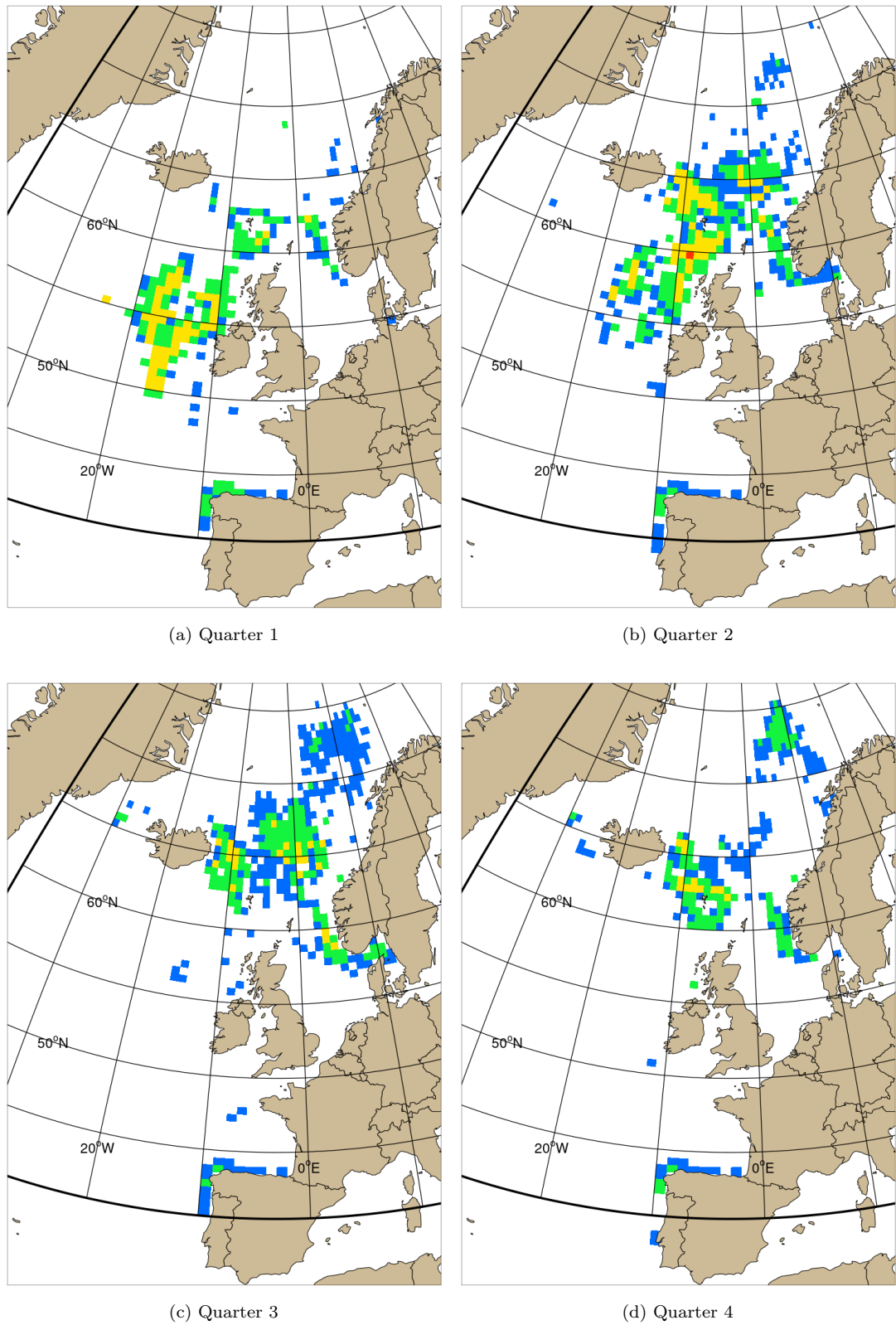
(d) Quarter 4

Figure 6.7: Qualitative average distributions of blue whiting catch, derived from quarterly catch maps of years 2003, 2004, 2006 and 2015 from ICES reports (ICES, 2004, 2005, 2007, 2016a). Catch values between 10 and 100 tonnes are represented in blue, between 100 and 1000 tonnes in green, between 1000 and 10000 tonnes in yellow, and greater than 10000 tonnes in red.

6.2.3 Recruitment and/or climate effect

The same years chosen in chapter 4 for comparing variable states under different climate regime were used. According to Hátún et al. (2009a), years 1992 and 1994 were under a strong SPG regime, while years 2002 and 2004 were marked by a much weaker SPG. The distributions of catch density per ICES area of the four selected years showed very distinct patterns between 1992/1994 and 2002/2004 (fig. 6.8). When the SPG was strong, fishing seemed to be confined to the continental shelf areas of the spawning grounds (1992/1994), while fishing distribution seemed to expand into the Rockall Plateau areas in years of weak SPG (2002/2004). This observation was in agreement with the assumption that SPG affects population distribution over the spawning grounds, causing a more western distribution in years of weak SPG (Hátún et al., 2009a,b). This also supported the idea of a blue whiting fishing activity following stock distribution.

Catch densities in 1992 and 1994 were very low compared to those in 2002 and 2004. If catch variation was a good proxy of stock biomass variation, this would suggest that stock recruitment was higher around the weak SPG period than during strong SPG. According to Payne et al. (2012) who based their observations on the 2010 ICES stock assessment, recruitment seemed indeed affected by the SPG dynamics, although no direct correlation between the two variables was found. Considering the history of the blue whiting fishery discussed previously, we could wonder if observed stock fluctuations might be partially explained by the fast development of the blue whiting fishery between 1991 and 2004 and the resulting overexploitation of the stock around the year 2003. Recruitment would then be also affected by the changes in intensity of fishing activities, and the proposed relationship with the SPG strength could simply be a coincidence.

Time series of annual total catch and average catch density in the same four areas of interest, as defined at the start of this chapter (fig. 6.1), were used to help identify any possible misinterpretation of catch data and avoid misled relationships between climate/recruitment and fishing (fig. 6.9). The ICES estimated values of SSB (ICES, 2019b) were highly correlated to the annual total catch over the period 1981-2010 ($r = 0.961$), even when Iceland contribution was excluded ($r = 0.945$). They seemed to tell a story of a blue whiting stock whose abundance

increased considerably from 1991 to 2003, consequently increasing landings, and whose recruitment variations, compared to climate indices, seemed to be affected by SPG dynamics. However, fluctuations in catch over high fishing grounds such as the main spawning area seemed to tell a different story.
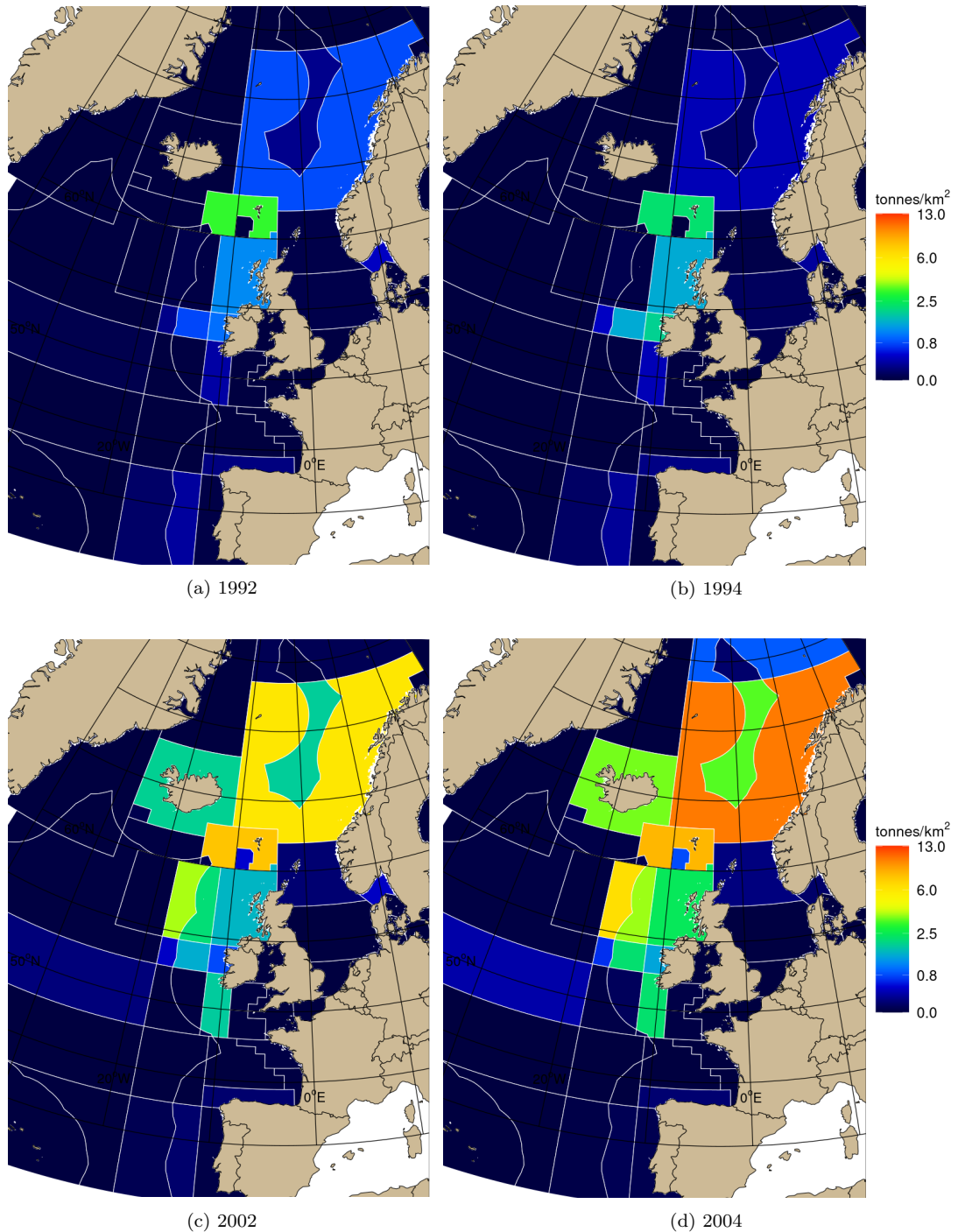
Figure 6.8: Estimated mean catch density (tonnes/km^2) in ICES areas (ICES data), in two years with a strong subpolar gyre regime (1992, 1994) and in two year with a weak subpolar gyre regime (2002, 2004) (chapter 4).

At first, all areas except the main spawning area (when considered alone) appeared to display similar rise and fall of catch values between 1995 and 2010. However, we already know that most of the catch variation observed in Icelandic and Faroese waters was caused by Iceland entering the blue whiting fishery and by the attempt of both Iceland and Faroe Islands to strengthen their claim of fishing right over the stock. Norway, Russia and the EU all acted the same way in their EEZ or in the international waters (Ekerhovd, 2007) and this increase in fishing activity between 1991 and 2003 was clearly reflected in the annual catch time series of the Norwegian Sea and the spawning areas after combining Rockall area to the main spawning area (fig. 6.9.a).

It is quite difficult to separate catch variations due to changes in stock abundance and those due to changes in fishery dynamics. Albeit less clear than in catch data or in ICES stock assessment model results, some increase between 1992 and 2004 seemed to be visible in the stock indices estimated from the Norwegian and Russian spawning stock surveys (ICES, 2004, 2005). Age distribution data from both catch and surveys also pointed towards an increase in first-year recruitment over the period 1991-2004 (ICES, 2005). Both observations seemed to indicate that the catch increase observed in 1991-2004 can at least be partly explained by an increase in stock recruitment caused by an other driver than fishing. It is however harder to determine if the low recruitment years that followed 2004 was mainly the result of the intense fishing or other environmental changes.

Since 1980, the main spawning area has been the most important fishing grounds, and as such, it was considered to be the less affected by the increase in fishing exploitation after 1990. Thus, we note that the drop in the catch density of the main spawning area observed between 1998 and 2004 was concomitant with increasing catch density in the Rockall area (fig. 6.9.b). Assuming that fishing fleets followed stock movements, this suggested that the spawning stock distribution might have either expanded or shifted westward, covering more of the Rockall Plateau. Moreover, this event coincided with a weak SPG regime (e.g. 2002-2004 marked by the dotted lines in fig. 6.9.b), supporting the claim that SPG affects blue whiting spawning distribution (Hátún et al., 2009a,b). This, however, was not enough to support any close relationship between recruitment variation and SPG dynamics. While catch variations in the spawning areas between 1990 and
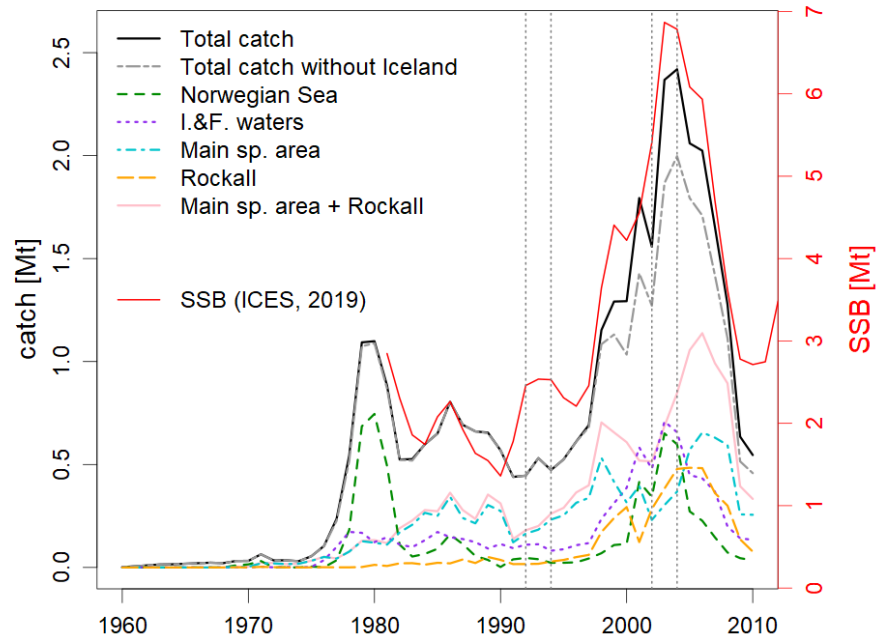
(a) Estimated catch (total and in defined areas).
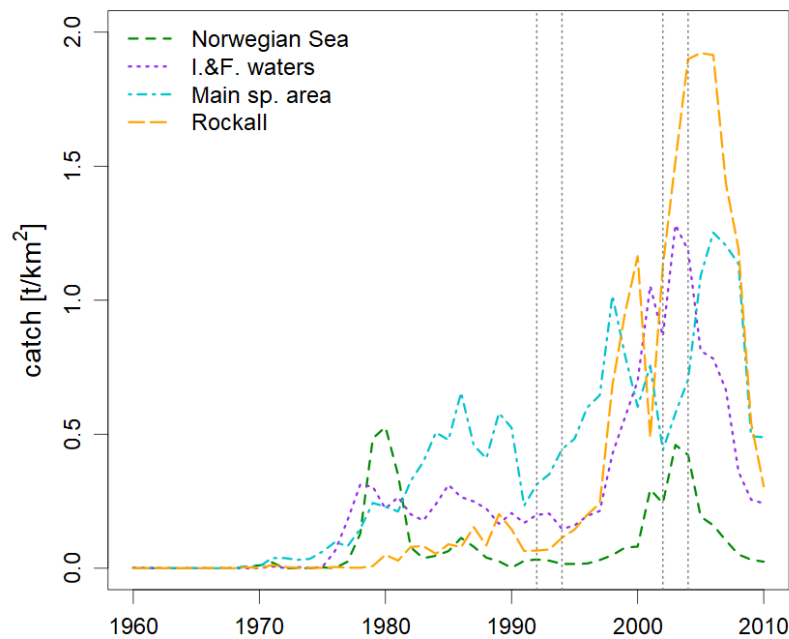
(b) Estimated catch density in defined areas.

Figure 6.9: Time series of blue whiting catch (million tonnes) and catch density (tonnes/km^2) in defined areas (fig. 6.1) from 1960 to 2010 (ICES data). (a) The solid pink line gives the annual catch (million tonnes) of both the main spawning area and Rockall area combined, and time series of SSB values (million tonnes) (red line and right scale) estimated by ICES (2019b) is also represented here for comparing with total catch. The four vertical grey dotted lines mark the years given as examples in other figures for years with strong (1992, 1994) or weak (2002, 2004) subpolar gyre.

2004 were most likely caused by a combination of fishery development, recruitment variations and climate change, the relationship between the three was here unclear.

6.3 Conclusions

The blue whiting fishery became considerably more important from 1970 to 2005, attracting progressively more nations in the activity. The high fluctuations of catch observed between 1990 and 2010 were likely the result of both the rapid expansion of the fishery over this period and variations in first-year recruitment. Whether or not climate variations directly affected those fluctuations in catch and population biomass was still unclear with these observations.

Most fishing effort was concentrated in the Norwegian Sea, in areas off the British Isles, over the Rockall Plateau, and in Icelandic and Faroese waters. Seasonal variations in the catch distribution suggested that the fishing fleet followed the seasonal migrations of the blue whiting population. This last observation was what led to consider at first a spatially uniform fishing activity in the blue whiting population model.

Part IV

Model results

Chapter 7

Feeding migrations

After spawning in the area off the British Isles, most blue whiting adults undertake a migration towards their main feeding grounds in the Norwegian Sea (Bailey, 1982). While it has not been clearly determined how adults find their way back to suitable feeding areas, some assumptions have been made on the role of physical drivers (temperature and currents) at influencing the choice of migration pathways on both sides of Faroe Islands (Hansen & Jákupsstovu, 1992; Hátún et al., 2007, 2009a).

In the following chapter, with the help of the particle tracking model `Ichthyop`, different implementations of the adult movement were tested. The effect of currents on the blue whiting migration was investigated, and the importance of using other environmental variables as cues to direct successfully the adult migration towards suitable feeding areas was studied. Finally, variability in the modelled migrations was studied against migration timing and climate variations. This was necessary to assess the model performance at predicting successful feeding migrations into the Norwegian Sea.

7.1 Importance of environmental factors

7.1.1 Effect of currents

In chapter 4, we observed the presence of strong northward currents along the continental shelf and hypothesized that currents would explain most of the blue whiting migration from the spawning grounds west of British Isles to the Norwegian Sea. This hypothesis was tested with Ichthyop, by adding to the NEMO
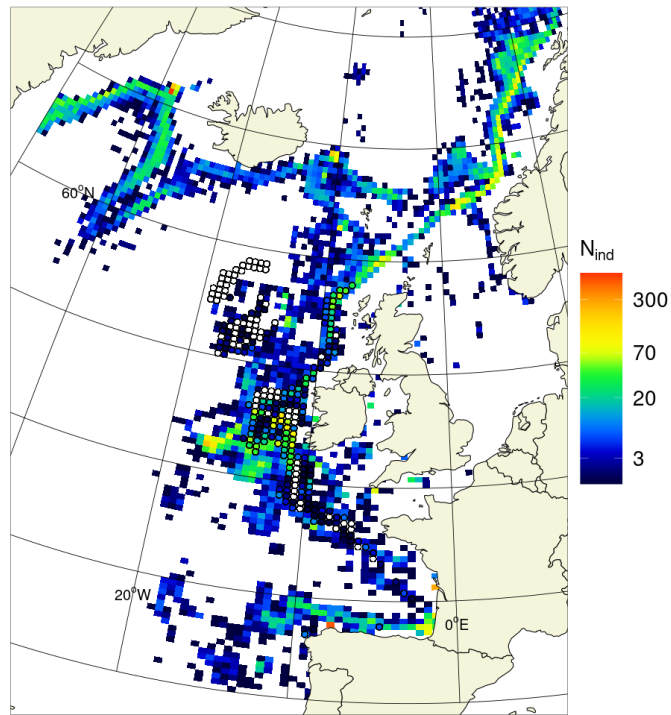
(a) Positions after 120 days (16/03/1994 - 14/07/1994).
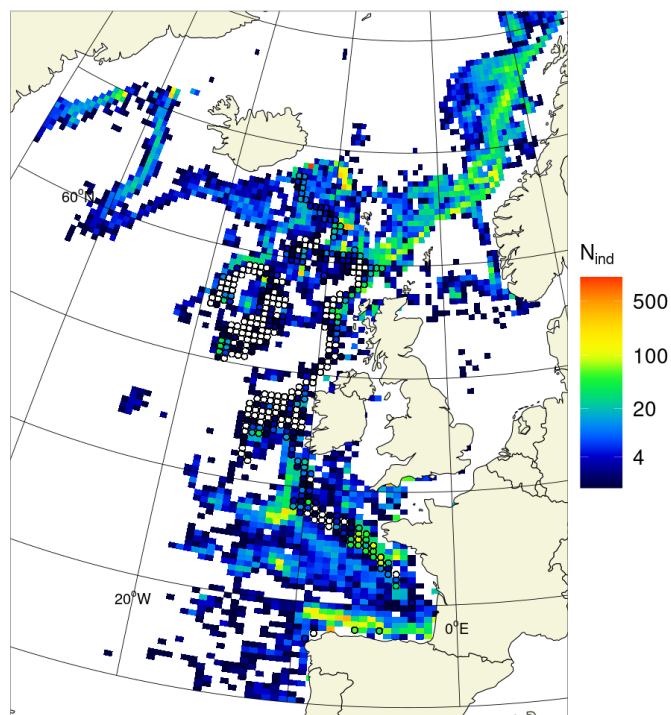
(b) Positions after 120 days (16/03/2004 - 14/07/2004).

Figure 7.1: Maps of adult distribution after 120 days of migration following currents (a) in 1994 (strong SPG), and (b) in 2004 (weak SPG). Migration was initialised in March the 16th, with 100 individuals released in each cell of the theoretical spawning habitat (black circles). Individuals are always swimming in the same direction of the currents with a constant speed of 0.2 m/s.
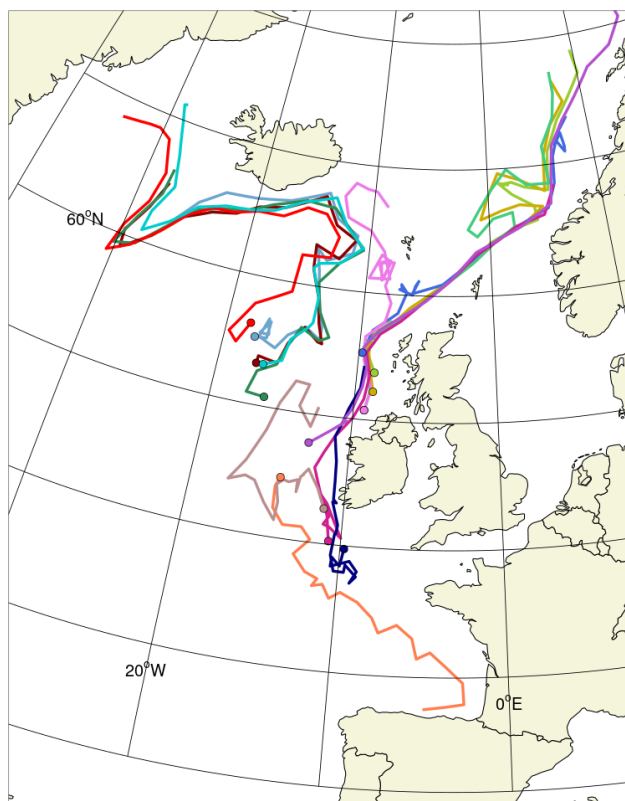
Figure 7.2: Examples of 120-days migration pathways in the 1994 `Ichthyop` tracking run, simulating adults swimming in flow direction and including horizontal dispersion (fig 7.1.a). Starting positions are represented by circles filled with corresponding trajectory's colour.

flow field a swimming component, which has always constant speed and the same direction than flow.

Figure 7.1 gives two examples of population distribution after 120 days of migration. Swimming in flow direction for 120 days with dispersive behaviours resulted in an almost continuous population distribution along the whole European continental shelf, with about 31% reaching the Norwegian Sea area (mostly along the continental shelf) and a high retention of the population above the spawning grounds ($\approx$ 33%). In the first example, a large proportion (22.5%) of the population was strongly affected by the subpolar gyre currents and migrated westwards, past Iceland. Examples of pathways from the 1994 run are shown in figure 7.2. In contrast, in the second example, a large proportion ended in the South, either in the Bay of Biscay or off Portugal (25%). In 2004, some individuals still followed the subpolar gyre currents towards Greenland but compared to 1994, the greater number of individuals found south-east of Iceland in 2004

suggested that westward currents were weaker that year.

Swimming in flow direction seemed to be an effective strategy for migrating towards the main feeding grounds. In average, 41% of the initial population reached the Norwegian Sea after migrating for 180 days. In 1994, 31% of these successful northward migrating individuals were travelling from southern spawning area (latitude below 52°N), while they represented only 5% of the individuals reaching the Norwegian Sea in 2004. Since 1994 and 2004 were assumed to be under different SPG climate regimes, this suggested that southern spawning individuals might be more sensitive to changes in currents induced by climate change.

However, the ability to swim in the exact direction of currents is supposed to be very rare among pelagic species (Chapman et al., 2011). While these results showed that northward migrating fish highly benefit from shelf currents to reach their destination faster, it was essential to consider other drivers to explain this northward migration. Furthermore, the resulting migration speed of individuals migrating either westward or northward tended to stay high (> 0.2 m/s) for the whole simulation period. As a consequence, around 10% of these individuals had already left the spatial domain after 120 days, and more than 20% after 180 days.

7.1.2 Food gradient

In a new version of the feeding migration model, food was considered the main driver for the blue whiting feeding migration, and individuals would swim in the direction of a positive food gradient as long as the later existed. According to food fields (chap. 5), we expected to see a majority of migration pathways leading to the Norwegian Sea area, but also South and West of Iceland in some years, depending on strength of the subpolar gyre (fig 7.3).

Early attempts at simulating migration motivated by food gradients showed that all individuals would end in very specific cells, where food is locally the highest, with almost non-existent dispersing behaviours. The strong directed movement would ultimately bring any individual back to the same cell even after dispersion. To correct this issue, the swimming speed was changed from a constant to a food dependent function (chap. 3), so that individuals would reduce their directed swimming speed when approaching areas with high concentrations

(a) 1994

(b) 2004
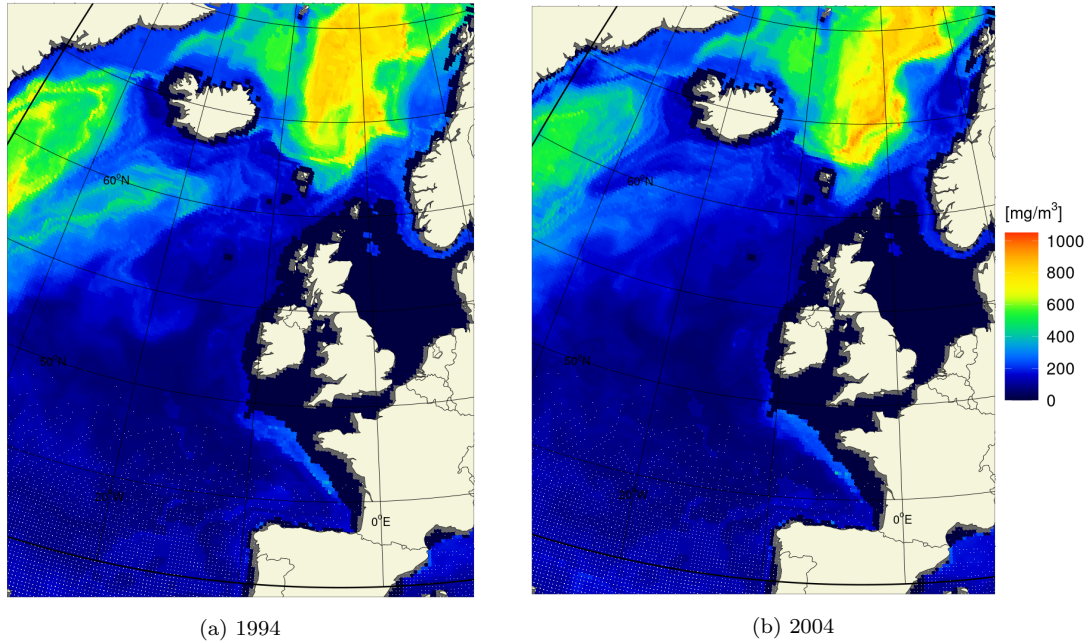
Figure 7.3: Maps of food (mg/m³) available to blue whiting, averaged over the migration season (16/03 - 14/07) in 1994, year with a strong SPG (a) and 2004, year with a weak SPG (b).

(a) Positions after 120 days

(b) 120-days trajectories
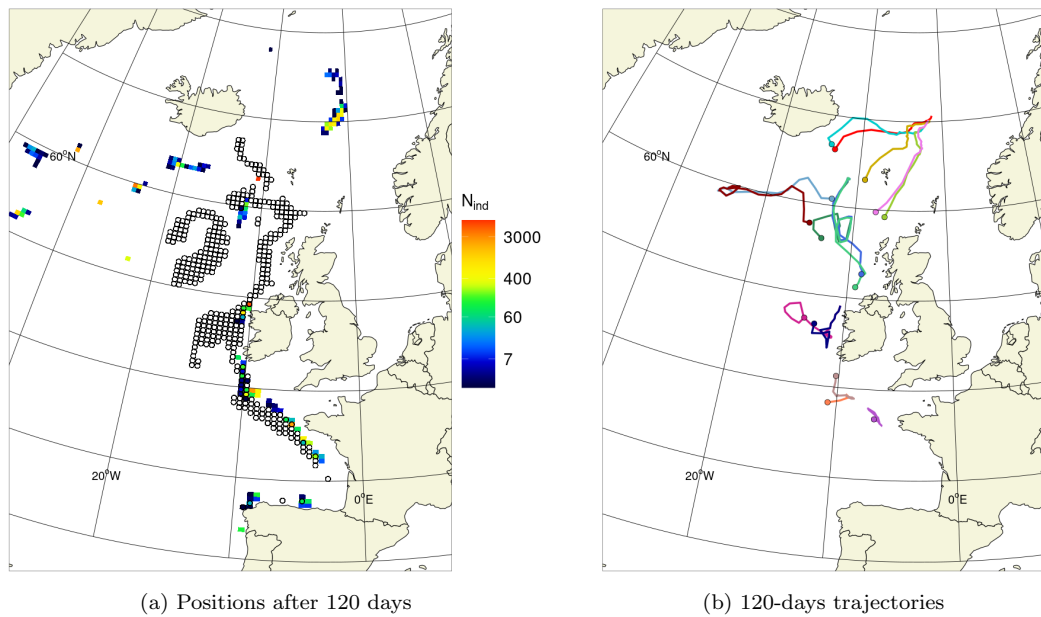
Figure 7.4: Tracking results for adult migration following food gradients in 2004: (a) distribution of individuals after 120 days of tracking, (b) examples of migration pathways from the same `Ichthyop` run (starting locations are represented by color filled circles). For the simulation, 100 individuals were released the 16th of March in each cell of the theoretical spawning habitat for the studied year (black circles in map (a)). Swimming was described by the equation 3.24 (chapter 3), with maximum swimming speed $v_{max} = 0.2$ m/s and speed parameters $F_c = 600$ mg/m³ and $p = 4$.

of food, thus allowing dispersive movement to take over. Currents still affected movement speed and direction in this new implementation.

Changing the value of speed parameter F_c affected both migration success and dispersion. While it increased the total area occupied by adults at the end of the migration period, decreasing F_c resulted in individuals settling for areas with lower food concentration very early in the migration process. Therefore, the speed parameter had to be a compromise between successfully reaching highly beneficial feeding areas and successfully dispersing around those areas. After a short sensitivity analysis, F_c value was fixed at 600 mg/m^3.

With the set of swimming speed parameters defined in figure 7.4, successful migrations into the feeding areas of the Norwegian Sea, in average, only accounted for 15% of the individuals released. As illustrated by the example of tracking results in figure 7.4.a, a large proportion of individuals would usually get attracted by western areas South of Iceland and in the Irminger Sea, while individuals released in southern areas of the spawning grounds tended to stay along the continental shelf, with only a few migrating to the Spanish coasts. It seemed that successful northward migration into the Norwegian Sea came mostly from individuals already located in the most northern parts of the spawning grounds (fig. 7.4.b), suggesting that food might not be enough as a driver to explain the observed main migration into the Norwegian Sea undertaken by adults from spawning areas North of latitude 54°N. Other physical drivers need to be considered in the feeding migration model, such as temperature, which brings us to the next section.

7.1.3 Migration motivated by fitness

In ecology, fitness is defined as a set of conditions that optimises an individual or population's success, either by increasing its survival, by improving its reproduction success or by accelerating its growth. In the following case, blue whiting adults are seeking areas that will maximise their individual growth during the feeding season. While growth definitely depends on food availability, for a lot of marine species it also depends on the temperature of the water they move in.

(a) 1994   (b) 2004
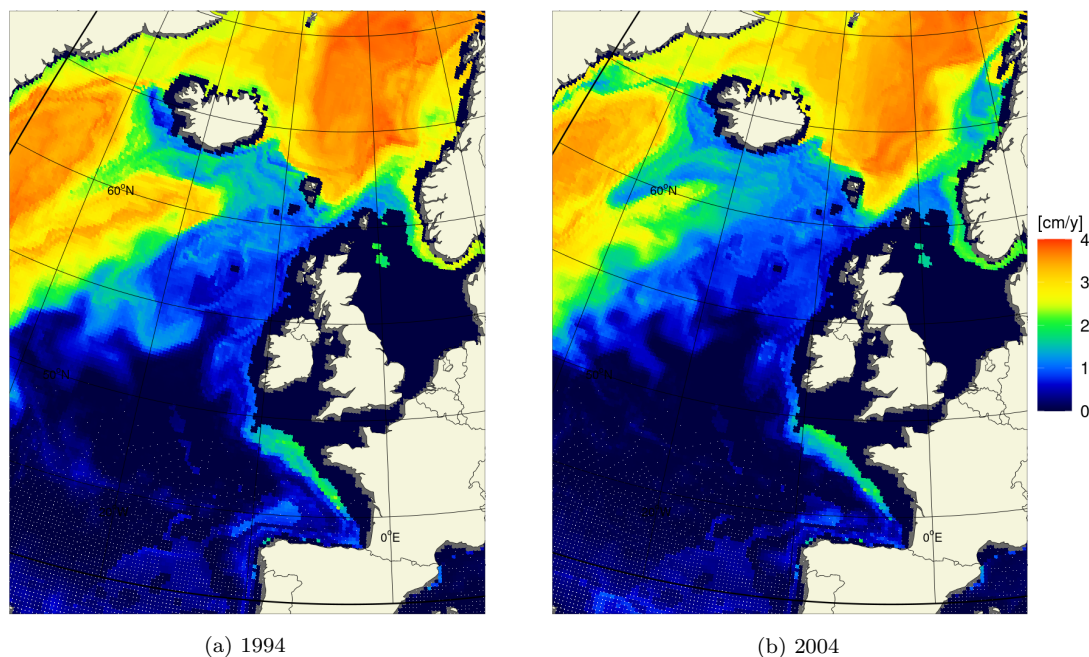
Figure 7.5: Maps of theoretical growth (cm/year) gained by a 20 cm long adult fish after a year, if local environmental conditions were constant throughout the year. Values were averaged over the migration season (16/03 - 14/07) in 1994 (a) and 2004 (b).

Thus, it was assumed that blue whiting migrated towards feeding habitats with optimum temperature range, and a growth index G_L was developed, which was both food and temperature dependent (eq. 3.15 in chap. 3). This growth index thus described the potential growth which an individual with an initial length of 20 cm could reach in one year if it stayed in the exact same environmental conditions.

Compared to the food fields, the growth fields presented a very marked gradient at the limit between the Norwegian Sea and the North Atlantic, defined by the Iceland-Shetland section (fig. 7.5). This should improve migration success from continental shelf areas North of latitude 54°N. The new variable seemed to also make the Irminger Sea very attractive for adults who might consider it as a possible feeding habitat. Therefore, westward migrations into the Irminger Sea were still expected in this model setting.

As for the food gradient migration, swimming speed was defined by equation 3.24 (chapter 3) and different parameter values were tested to determine the best set of parameters that would offer a compromise between migration success and

dispersion around the feeding hot spot areas. For the following results, only the final speed parameter values were used, which are $G_c = 3.5$ cm and $p = 20$ (eq. 3.24).

Tracking results were very similar to those obtained previously with the food gradient. The northward migrating individuals ended in a very similar location in the Norwegian Sea (fig. 7.6). A few cells still appeared to act as strong sinks (> 3000 individuals in one cell at the end of the run). After many attempts at correcting this sink effect, it was concluded that this might be caused by numerical error at solving movement at the system's boundaries, either defined by `Ichthyop` or by the gradient field definition. For example, the sink cell observed at (11°W, 60.5°N) seemed to be located just next to a cell shallower than 200 m, which was not included in the growth gradient field computation ($G_L = 0$ at this location in fig. 7.5). The 200 m depth limit was originally defined to avoid individuals swimming too close to coast lines. In this case, however, it might cause
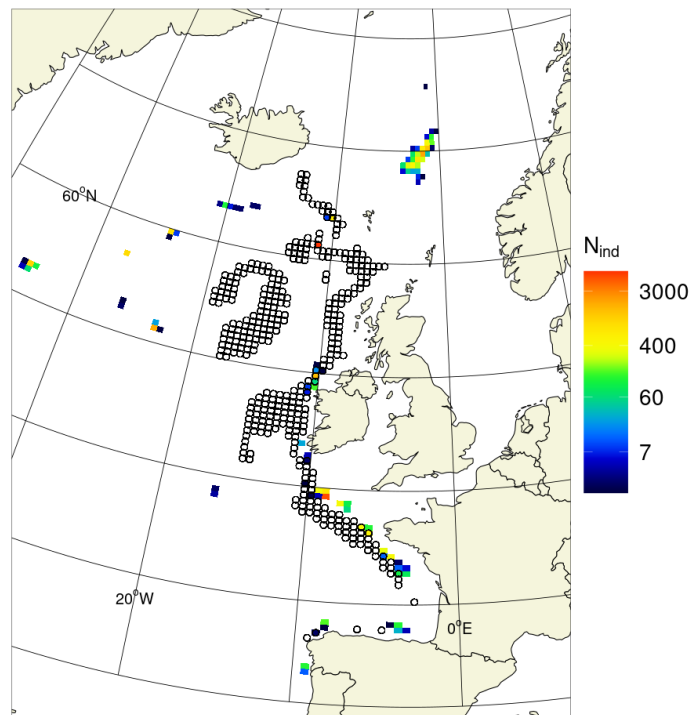
Figure 7.6: Maps of adult distribution after 120 days of migration following growth gradients in 2004. Migration was initialised the 16th of March, with 100 individuals released in each cell of the theoretical spawning habitat (black circles). Swimming is described by the equation 3.24 (chapter 3), with maximum swimming speed $v_{\max} = 0.2$ m/s and speed parameters $G_c = 3.5$ cm and $p = 20$.

(a) $t = 30$ days

(b) $t = 60$ days

(c) $t = 90$ days

(d) $t = 120$ days
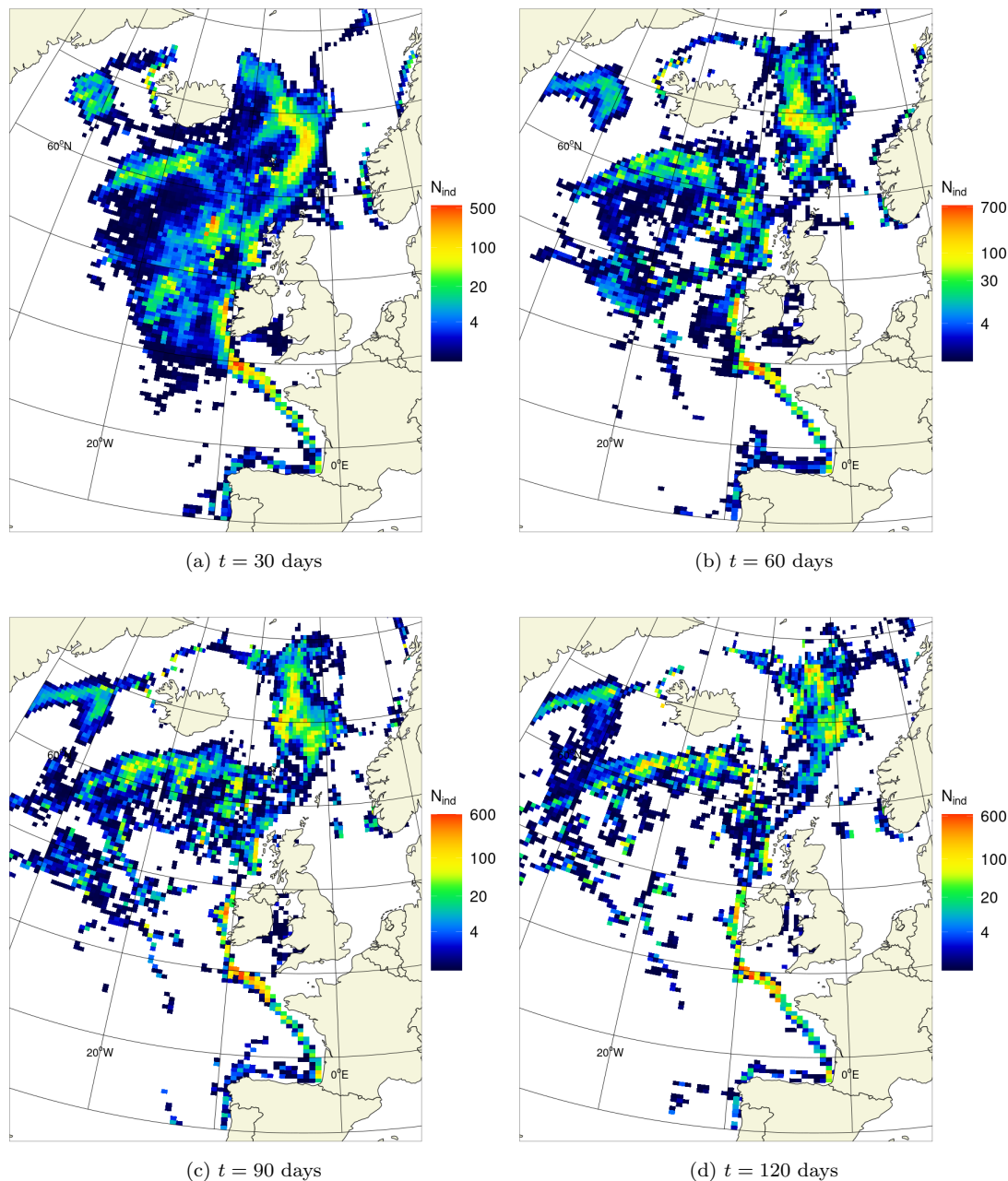
Figure 7.7: Average distribution of adults migrating from the spawning grounds to suitable feeding areas, at different time t after the defined starting date (16/03), calculated from `Ichthyop` runs of each year in the period 1988-2050. Individuals were still initialised in the theoretical spawning habitat (100 ind/cell), and swimming speed was still defined according to function 3.24 (chapter 3), with maximum swimming speed $v_{max} = 0.2$ m/s and speed parameters $G_c = 3.5$ cm and $p = 20$. Starting positions are not represented here, as they varied between years with the spawning area.

a few isolated shallow cells to become obstacles to migration, probably in close relation to gradient values, G_L values and flow surrounding those cells. Although it would be in the model's best interest to try and correct this effect in the future, it was considered as an acceptable error for this first issue of the blue whiting

model. In fact, the average end distribution showed that this error was not always present and not significantly enough to overall affect migration patterns (fig. 7.7).

Feeding migrations of adults departing from the theoretical spawning grounds were simulated for every year in the studied period 1988-2050 and for different starting dates between start of February and start of May. Average spatial distribution of individuals at different time t after migration started were calculated to study the model ability at reproducing the known migration routes. In the following example, migration started the 16th of March and average distribution was studied at time $t = 30, 60, 90$ and 120 days of migration (fig. 7.7).

With this feeding migration model, we observed a large proportion of individuals entering the Norwegian Sea after only one month, with the average position of their distribution in the area moving slowly northward over time. An other large amount of individuals seemed to undertake a westward migration into the Irminger Sea, although it looked like the model allowed for some of these individuals to come back towards the Norwegian Sea by using a route North of Iceland. Among the westward migrating individuals, most individuals that reached the Irminger Sea early in the season tended to leave the spatial domain for continuing their migration along Greenland shores. In contrast, late westward migrating adults would still occupy in majority the area South of Iceland after 120 days, showing a much slower westward migration into the Irminger Sea. A last group of individuals, mostly from the southern regions of the spawning grounds seemed to stay in the same location for the whole migration season. All of these results were overall in agreement with past studies of adult post-spawning migration behaviours (chap. 1).

7.1.4 Note on the use of biological compass in movement modelling

The fact that individuals of a same population tend to repeat the same migration cycle every year might indicate that they possess some kind of biological compass, which gives them the ability to follow environmental cues to always successfully reach the same location (Lohmann et al., 2008). For some species (e.g. some migratory birds and sea turtles), the geomagnetic field can be for example used

for orientation and navigation (Lohmann, 1991; Wiltschko, 1995). Others will use hydrography or chemical, olfactory, and/or visual cues to navigate (Wallraff, 2004; Lohmann et al., 2008). But most species probably combine and use information coming from different sources at different time of their life cycle (Bingman & Cheng, 2005; Lohmann et al., 2008). However, such behaviours are harder to observe and study for migratory pelagic fish and it is scarcely known what they would mainly use to guide themselves between breeding and feeding areas.

In the first exploration stages for building the migration model, the low success of individuals reaching the Norwegian Sea led us to force the general direction of movement, assuming blue whiting might have a biological compass similar to birds or turtles, which allows them to travel to the same feeding grounds every year. Following this idea, it was assumed that a proportion P_C of the swimming direction was determined by the biological compass direction θ_C which is constant:

$$\theta_{\text{swim}} = \tan^{-1} \frac{(1 - P_C) \sin(\theta_g) + P_C \sin(\theta_C)}{(1 - P_C) \cos(\theta_g) + P_C \cos(\theta_C)} \tag{7.1}$$
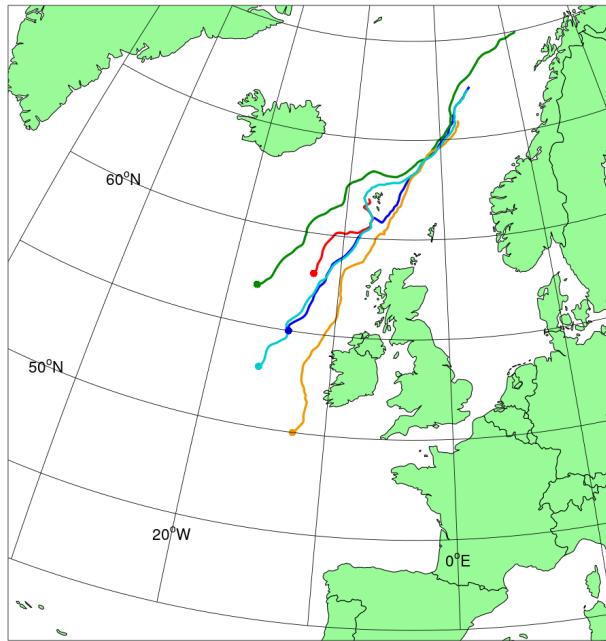
Figure 7.8: Example of tracking results for adult migration motivated by a biological compass of 30°N: (a) distribution of individuals after 120 days of tracking: examples of migration pathways from the same `Ichthyop` run (starting locations are represented by color filled circles). For the simulation, individuals were released the 16th of March in 1989. Swimming was constant ($v = 0.2$ m/s). Flow drift was included, but not dispersion.

The advantage of implementing this biological compass was that any individual would reach the Norwegian Sea by Summer, ensuring feeding migration success from any starting position in the spawning areas (fig. 7.8). However, the forcing compass direction tended to suppress variability in pathways taken to reach the destination. Moreover, this implementation of the biological compass was not capable of recognising suitable feeding areas, which might slightly change between years, and thus individuals would fail to adapt their swimming behaviour when approaching such areas.

7.2 Model variability

7.2.1 Relationship between migration timing and success

According to Pointin & Payne (2014), spawning tend to take place earlier in the southern areas of the spawning grounds than in the northern areas. Possible explanations proposed for this varying spawning timing along the latitudinal gradient were that (1) spawning conditions are either met earlier or last less long in the South than in the North, causing adults to move northward over the spawning season, or that (2) southern spawning individuals reach their spawning areas earlier than northern spawning individuals. A third reason was suggested here, which is that early spawning might also be motivated by the time, the currents and the environmental gradients (food and temperature) needed to reach successfully the main feeding grounds in the Norwegian Sea.

For different migration starting dates, adult migration were tracked until the start of August, from the 100 individuals initialised in every ocean cells in the region between longitudes 0-25°W and latitudes 45-65°N. One individual's feeding migration was considered successful, when they crossed the Iceland-Shetland section and ended in the Norwegian Sea by the start of August. In figure 7.9, the proportion of migration success of each starting cell is given for three different starting dates (04/02, 06/03 and 05/04) and in two different years (1994 and 2004).

Highest migration success rates were observed along the continental shelf from the Porcupine area to the Shetland-Iceland section. The areas defined by the

(a) Start: 04/02/1994   (b) Start: 06/03/1994   (c) Start: 05/04/1994

(d) Start: 04/02/2004   (e) Start: 06/03/2004   (f) Start: 05/04/2004

Figure 7.9: Maps of feeding migration success (proportion of individuals successfully reaching areas North of Faeroe Islands by the start of August (03/08), in %) for different starting dates (in February (a and d), in March (b and e), and in April (c and f)) and in years with different SPG strength: strong SPG in 1994 (a-c), weak SPG in 2004 (d-f). 100 individuals were released from each cell between latitudes 45 and 65°N and longitudes 0 and 25°W. Red areas correspond to 100% failure and dark green areas to 100% success.

highest probabilities of reaching the Norwegian Sea matched surprisingly well the observed spawning distributions from past studies and surveys (Hátún et al., 2009a; Payne et al., 2012; Gastauer et al., 2016; Marine Institute et al., 2013, 2014, 2018, 2019), which suggested either that blue whiting post-spawning migration into the Norwegian Sea was strongly conditioned by their spawning location, or that spawning location might be chosen to ensure return to their preferred feeding grounds. The area defined by the highest migration success tended to withdraw northward over time between February and April, meaning that adults migrating from southern areas (e.g. Porcupine Bank) needed to leave early and before the end of the spawning season to successfully reach the feeding area in the Norwegian Sea.

Finally, feeding migration seemed to be successful in more western areas in 2004 than in 1994. As the subpolar gyre was weaker in 2004 than 1994, this suggested that migration success was affected by variation in SPG strength. In other words, adults departing from the Rockall Plateau area seemed to be more likely to reach the Norwegian Sea when the subpolar gyre was weak. However, this high success probability seemed to disappear with time, suggesting that, like for adults from southern spawning areas, adults from the Rockall Plateau also need to start their migration early to be able to reach the Norwegian Sea.

7.2.2 The subpolar gyre effect on migration pathways

Since the migration model already seemed to respond to climate variations such as changes in the SPG strength, the next thing to investigate was how modelled migration pathways might be affected by different SPG regimes, and if those agreed with Hátún et al.'s claim that weak SPG leads to more individuals travelling west of Faroe Islands to enter the Norwegian Sea (Hansen & Jákupsstovu, 1992; Hátún et al., 2007). Using the same `Ichthyop` run design that produced the overall average spatial distributions of figure 7.7, the average spatial distribution of adults were studied in the early stages of their migration ($t = 30$ days after migration started) during the strong SPG regime of 1992-1994, and during the weak SPG regime of 2002-2004. And to check the migration timing effect on the migration pathways, two different starting dates (24/02 and 16/03) were also considered.

Whatever the SPG regime, the Faroe-Shetland channel always seemed to be an important migratory route for blue whiting. At $t = 30$ days after the migration started, all averaged distributions revealed an important flow of individuals east of Faroe Islands (fig. 7.10). However, in 2002-2004, a second important migratory route west of Faroe Islands was also present. This seemed to support the theory that the SPG dynamics affect migration patterns around Faroe Islands (Hátún et al., 2007). These results also confirmed the migration timing effect, since individuals starting migrating mid-March seemed to be more stationary than those starting earlier, especially when starting in southern areas.

(a) 1992-1994
start: 24/02

(b) 2002-2004
start: 24/02

(c) 1992-1994
start: 16/03

(d) 2002-2004
start: 16/03
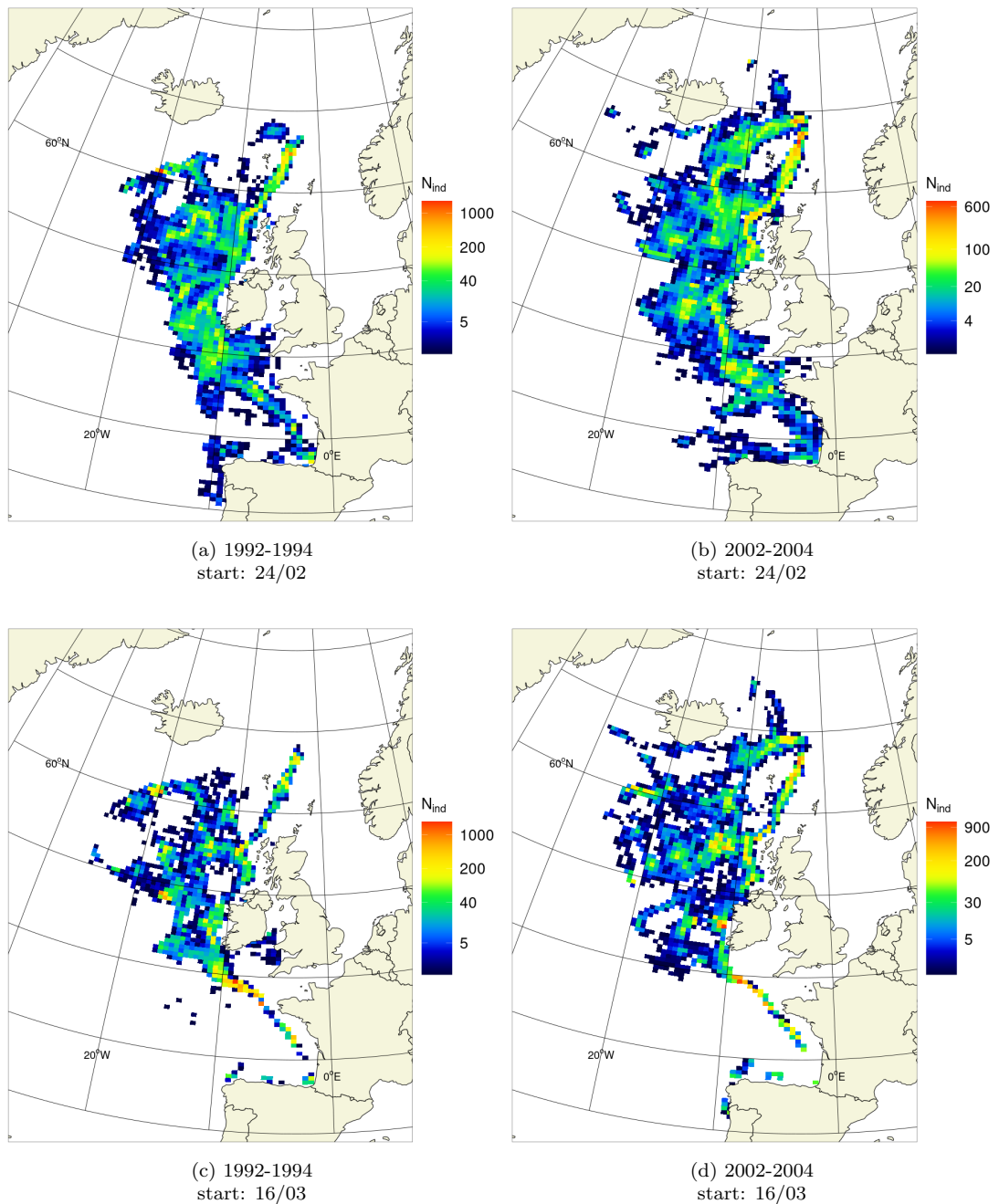
Figure 7.10: Maps of average distribution after 30 days of migration for two different starting dates and two different climate regimes. Average distributions were calculated from `Ichthyop` outputs of (a,c) 1992-1994 (strong SPG) and (b,d) 2002-2004 (weak SPG).

In these experiments, adults always started their migration from theoretical spawning areas defined by the optimum environmental conditions for spawning, and so starting locations varied between years (fig. 7.12.b). Therefore, to determine the influence of the starting location on the migration pathway around Faroe Islands (either East or West) and to further understand the effect of varying SPG

strength on those pathways, we focused on the individuals crossing the Iceland-Shetland section and studied their starting position depending on whether they went west or east of Faroe Islands in each year between 1988 and 2050. First, this revealed that the West pathway was undertaken by individuals starting in significantly more western positions than the East pathway (fig. 7.11 and 7.12.a). However, we noted here that average final positions (after 180 days of migration) showed no clear difference between individuals that travelled either west or east of Faroe Islands (fig. 7.11).

Time series of the proportion of individuals that undertook either the East and West pathway showed no clear relationship with any time series of average starting longitudes (fig. 7.12). While the West pathway was mostly exclusively followed by individuals starting in the western areas of the spawning grounds, the proportion of individuals migrating along this route was not conditioned by the overall initial spawning distribution. However, knowing that SPG strength
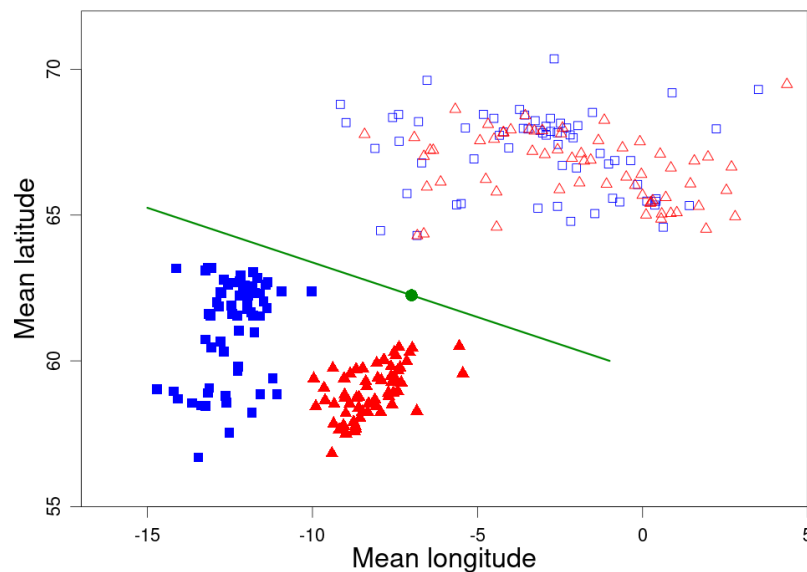
Figure 7.11: Average starting positions (filled symbols) and average positions after 180 days (empty symbols) in each year between 1988 and 2050 for individuals whose migration pathway went east of Faroe Islands (red triangles) and for individuals whose migration pathway went west of Faroe Islands (blue squares). Average positions were calculated from all 180-days tracking outputs of a same year, where starting dates were either 04/02, 24/02, 16/03 or 05/04. The green line represents the Iceland-Shetland section and the green dot marks the location of Faeroe Islands.
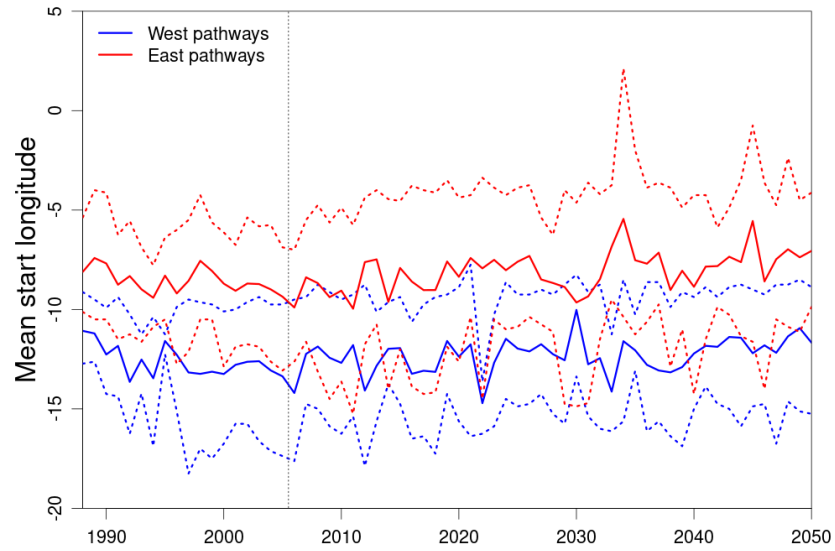
(a) West-East
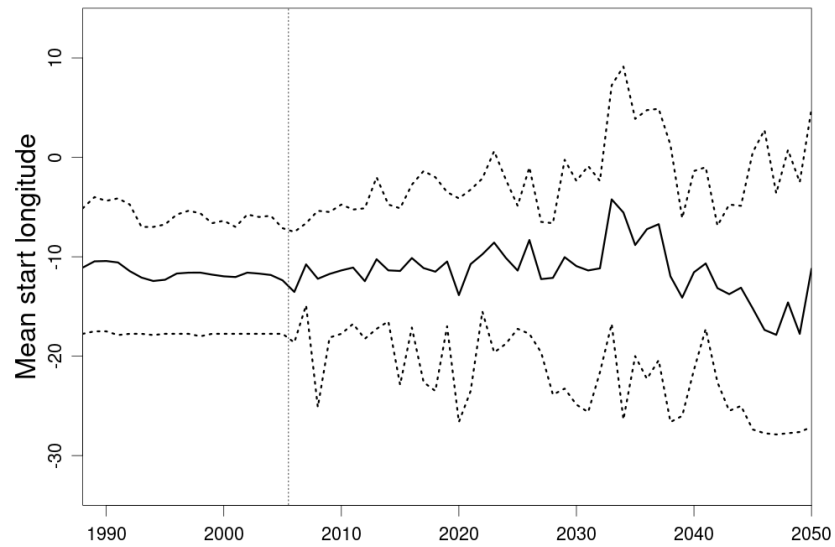
(b) All

Figure 7.12: Time series of feeding migration properties: (a) average longitude of starting positions (plain line) for pathways west of Faroe Islands (blue) and east of Faroe Islands (red), (b) average longitude of all starting positions (plain black line) which is also the average longitude of the theoretical spawning area, (c) average proportion of individuals that undertook a migration west of Faeroe Islands (plain blue line), and (d) average proportion of individuals that undertook a migration east of Faeroe Islands (plain red line). Dotted lines of time series (a) and (b) represents the 0.05 and 0.95 quantiles. Pale blue lines in (c) and pale red lines in (d) represent both minimum and maximum values of pathway proportions, resulting from runs with different starting dates. The vertical grey dotted line marks the disruption in the NEMO-Medusa dataset, between historical and projection model outputs (see chap. 4).
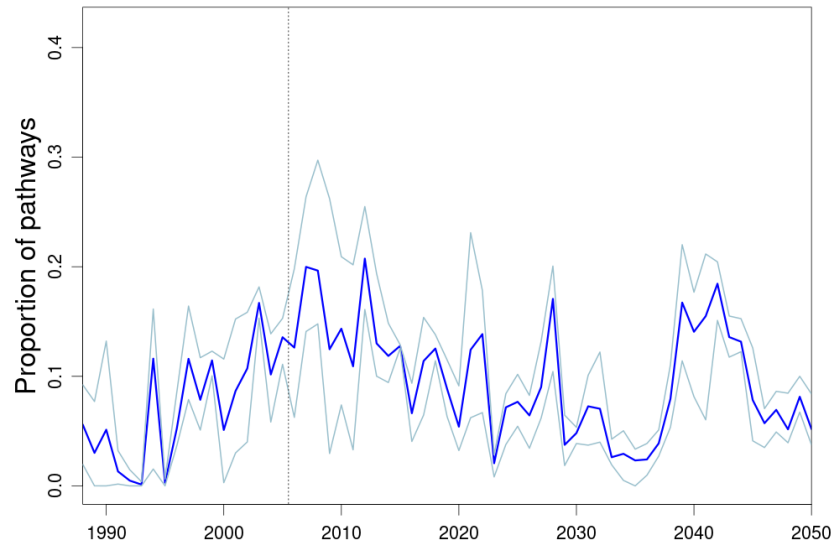
(c) West
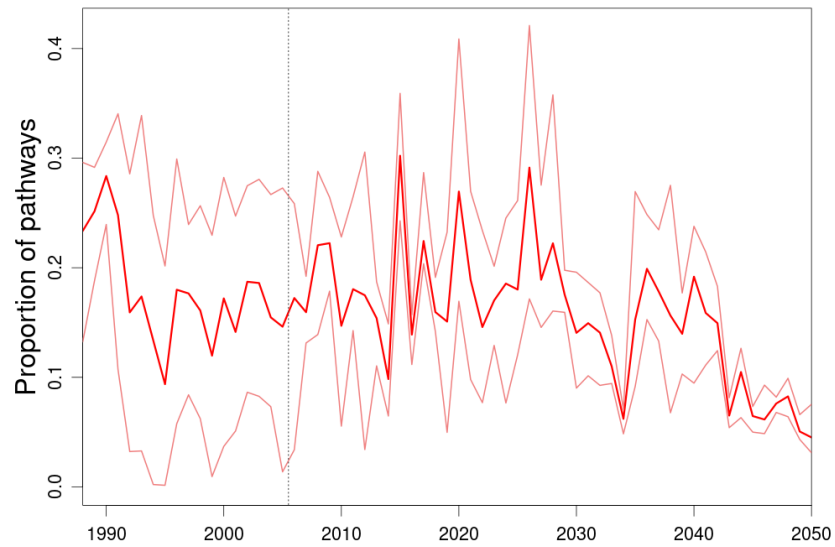
(d) East

Figure 7.12: *continued.*

decreased between 1990 and 2015 (Chapter 4), it appeared again that the proportion of individuals migrating west of Faroe Islands increased with the weakening of the subpolar gyre (fig. 7.12.c). In contrast, no clear relationship between the proportion of East pathways and SPG strength could be observed over 1990-2015, but the decrease observed after 2030 suggested that the changes observed in the theoretical spawning distribution after that year (Chapter 4) could diminish the

importance of this migratory route.

7.3 Conclusions

For the first time, migrations of adult fish were modelled so that they would follow environmental gradients. In the context of blue whiting, the final results were very encouraging since the model managed to reproduce successful feeding migrations into the Norwegian Sea, even though the deterministic component of individual movement was only influenced by local currents and gradients of food and temperature. The model also allowed for westward migrations which have been suspected to exist by Post et al. (2019).

The model performance at simulating variability was also very satisfactory. Similar northward migration patterns to those derived from catch data were observed (Hansen & Jákupsstovu, 1992; Hátún et al., 2007, 2009a), while northward migration success seemed to be very sensitive to both the starting location and timing of the migration. The model was thus able to respond to both spatial, annual and long-term variations of environmental conditions.

According to the model, successful migrations into the Norwegian Sea seemed to be driven by both currents and fitness. As long as individuals were travelling through the spawning areas, which had very low food concentrations, migrations were mostly affected by currents. The gradient of the growth index, which depends on both food and temperature, only became important for the migration direction once individuals reached the northern areas between north of Scotland and Iceland.

Starting positions in the spawning area seemed to strongly influence migration pathways taken by individuals. Thus, among northward migrating individuals, those initially located in a more western position over the Rockall Plateau tended to migrate west of Faroe Islands, while those located over the continental shelf migrated through the Faroe-Shetland Channel. Variations in SPG strength were shown to have also a significant effect on the migration pathway taken by individuals from the Rockall area. These results supported some of the assumptions made by Hátún et al. (2007) to explain the observed migration pathway variability.

Chapter 8

Spawning migrations

Currently, no study on the blue whiting pre-spawning migration exists. Therefore, most assumptions made in the following chapter were solely based on our knowledge of the suitable spawning conditions, and on spawning distributions estimated using NEMO-Medusa values for temperature and salinity (chapter 4).

With the same methods used previously for the feeding migration (chapter 7), spawning migrations were modelled. The first objective was to find the right model implementation to produce migrations that would successfully reach suitable spawning areas between February and April.

Several experiments were also performed to study the effect of migration timing, starting location, as well as climate variations on the migration success. The predicted and expected spawning distributions were compared to assess the model performance.

8.1 Variables and parameters of the spawning migration model

As for the feeding migration, the spawning migration was mostly determined by gradient fields. The spawning habitat suitability index variable (Ω) whose value would increase when approaching suitable spawning conditions was developed (chap. 3). The advantage of this variable was its semi-flexibility: individuals are attracted by default to the known spawning area off the British Isles, but would change their destination at any time if a suitable spawning habitat was detected before they reached the usual spawning region. Average Ω fields and predictions

are presented in the next section for comparing with `Ichthyop` tracking results and for evaluating the success of the modelled spawning migrations.

While the optimum depth range used to calculate the Ω index was assumed to be 100-1000 m, only Ω values present in waters deeper than 120 m were considered in the gradient calculation to avoid adults swimming too close to coastlines and thus resulting in them getting stuck at the system's spatial boundaries. The 120 m depth limit was found to be the best isobath to limit the occurrence of this error.

The swimming speed function for the spawning migration was the same than the one used for the feeding migration. By dropping the directed swimming speed value to 0 m/s when approaching areas of high spawning suitability ($\Omega \rightarrow 1$), dispersive behaviour became dominant and adults could spread over the whole spawning area defined by any neighbouring cells with high Ω values. In equation 3.24 (chap. 3), the Ω_c parameter, controlling where the speed inflection occurs, was set to 0.98, and the power p to 100 for the following spawning migration model. As a result, when $\Omega_{(x,y,t)} = \Omega_c = 0.98$, swimming directed speed dropped to 0.074 m/s. Besides dispersion, individual movement was still affected by currents.

8.2 Spawning habitat suitability (Ω) index

8.2.1 Gradient variability during the migration season

In the following model definition, migrating adults followed a gradient to reach optimum spawning habitats. Since the spawning habitat suitability index Ω was dependent on local temperature and, in some cases, on local salinity (see eq. 3.23 in chap. 3), the gradient fields used at the beginning of the migration might look very different to gradient fields during the spawning season, thus possibly leading adults temporary towards areas judged 'suitable' at the time of the migration which were unsuitable during the spawning season. To study this effect, the Ω fields in December, around the start of the spawning migration, were compared with the Ω fields of the spawning season between the 30th of January and the 16th of March.

(a) December average   (b) Spawning season average
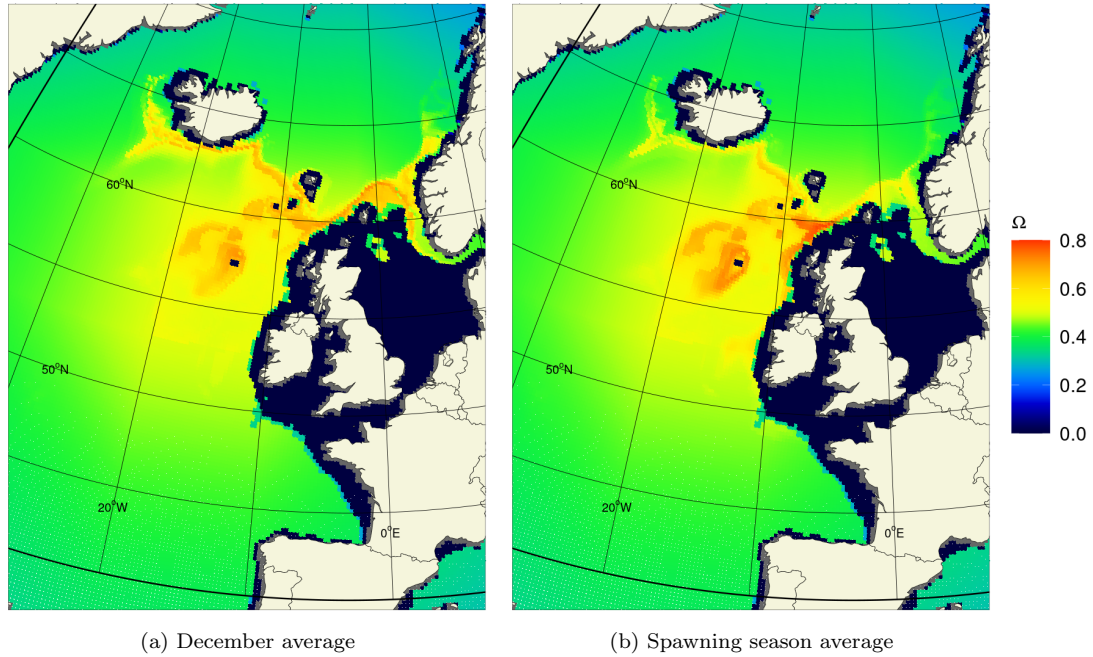
Figure 8.1: Maps of spawning habitat suitability index (Ω) averaged over December (a) and over spawning season (b) from all years between 1988 and 2050. Here, the defined spawning season runs from the 30th of January to the 16th of March.

Spawning migration from areas south of the main spawning grounds was expected to not be affected by changes in local temperature or salinity over the migration season, as the Ω field seemed to stay constant south of the Porcupine area (fig. 8.1). This suggested that temperature and salinity optimum conditions for spawning were almost never met in regions south of Porcupine from December to March. In the North, however, suitable spawning areas were spotted in more northern locations in December than in the spawning season. For example, we could expect that some adults departing from the Norwegian Sea and travelling sufficiently close to the continental slope would be first attracted by areas north of Shetland. As a consequence of reaching a suitable habitat, their directed swimming speed would drop and they would stay in the area until the local Ω value decreased enough to make their speed increase again and to make them follow new Ω gradients. We could then expect some individuals undertaking a much slower spawning migration towards the areas off Scotland, following the southward shift of the suitable conditions for spawning.

According to figure 8.1.b, the most attractive spawning grounds seemed to include the continental shelf area off Scotland and south of Faroe Islands, as well

as the Rockall Plateau. Because the plateau area between Iceland and the Faroe Islands seemed to become suitable for spawning very early in the season (high Ω values in December), we also expected a lot of individuals to be retained in the area for the spawning season, even though the area covered much less grounds than the Rockall Plateau.

8.2.2 Expected spawning distributions

With adult migration following Ω gradients, modelled spawning distributions in `Ichthyop` simulations were expected to correspond to the maps of suitable spawning habitats defined by Ω. Part of the study was focused on assessing how efficient the particle tracking model was at simulating spawning migration which would successfully result in expected spawning distributions. Furthermore, we wanted to assess both the role of climate in spawning migrations and distributions, and how the predicted changes in theoretical spawning areas between 2000 and 2050 (see chap. 4) might affect modelled migration results. To do that, simulations of spawning migrations were performed for years 1992, 1994, 2002 and 2004 as examples of migrations under different SPG regimes, and for the period 2000-2050 sampled with a 10-year interval. To help with this study, Ω fields were here described for the same sampled years.

Compared to the estimated spawning areas presented in chapter 4, maps of spawning habitat suitability had the advantage of giving a more nuanced picture of the expected spawning habitats, where Ω values between 0.5 and 1 indicated that temperature and salinity optimum conditions were met. Thus, the weakening of the subpolar gyre between 1992-1994 and 2002-2004 mainly resulted in a northward shift of the distribution of the optimum temperature and salinity range (fig. 8.2). This caused previously non-existent spawning habitats to appear in 2002 and 2004 in the 100-1000 m deep areas between Iceland, the Faroe Islands and Rockall, while southern spawning habitats formerly spotted in 1992 and/or 1994 (e.g. north of Porcupine Bank) disappeared in 2002/2004. According to these Ω fields, we expected adults from southern areas, like the Bay of Biscay, to reach the most southern suitable spawning areas during years of strong SPG (1992/1994), mostly located on the continental shelf around the northern

Porcupine Bank area. However, in years of weak SPG (2002/2004), those fish might be equally attracted by the Rockall Plateau area and the Scottish shelf. For individuals coming from the Norwegian Sea, we expected migration to lead to different spawning areas depending on whether their migration path took them east or west of the Faroe Islands. Because of this, and assuming that the popu-

(a) 1992 (b) 1994

(c) 2002 (d) 2004
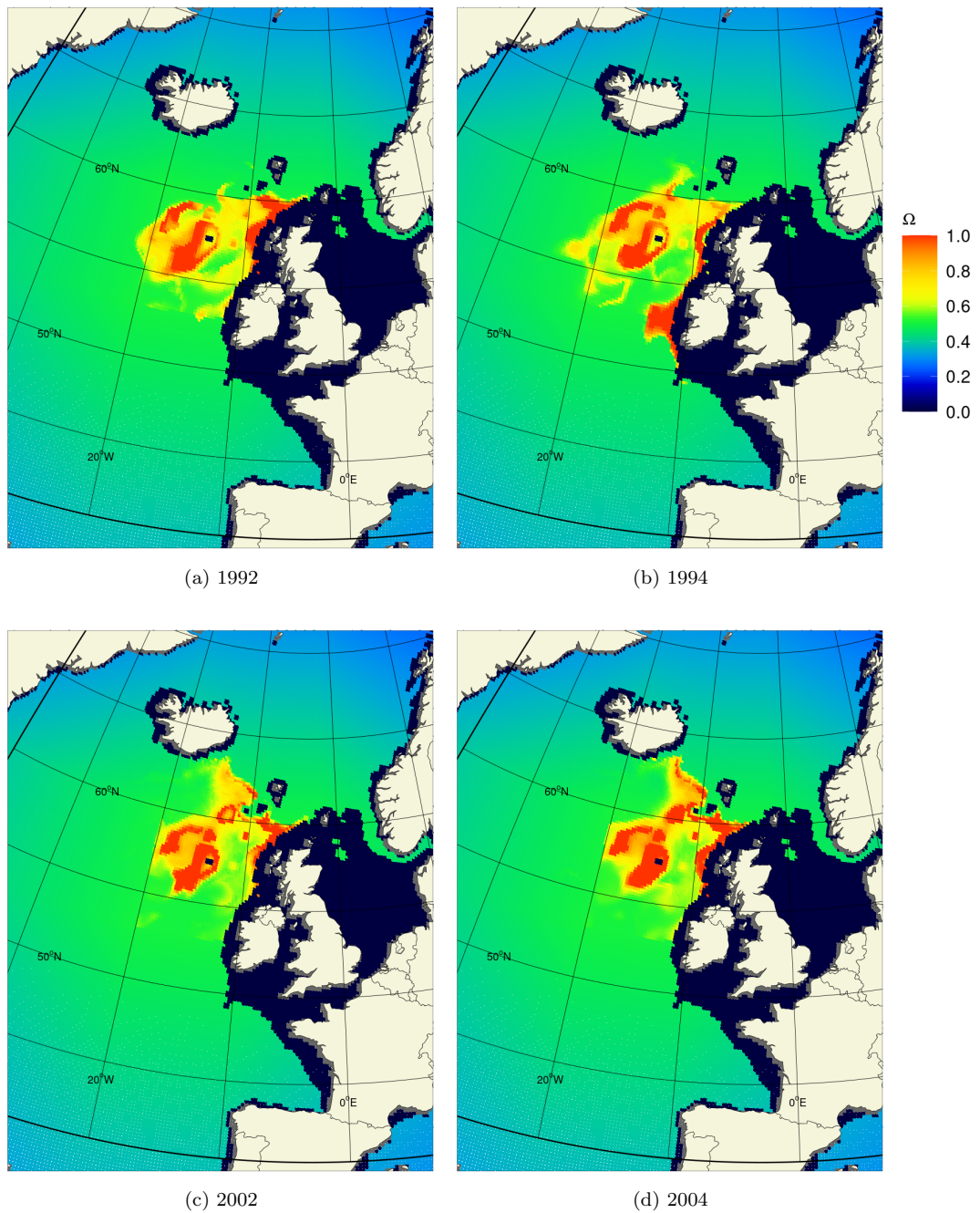
Figure 8.2: Average spawning habitat suitability index (Ω) in spawning season (30/01 - 16/03) in years 1992 (a) and 1994 (b), where SPG was strong (chapter 4), and in years 2002 (c) and 2004 (d), where SPG was weak.

(a) 2000   (b) 2010   (c) 2020

(d) 2030   (e) 2040   (f) 2050
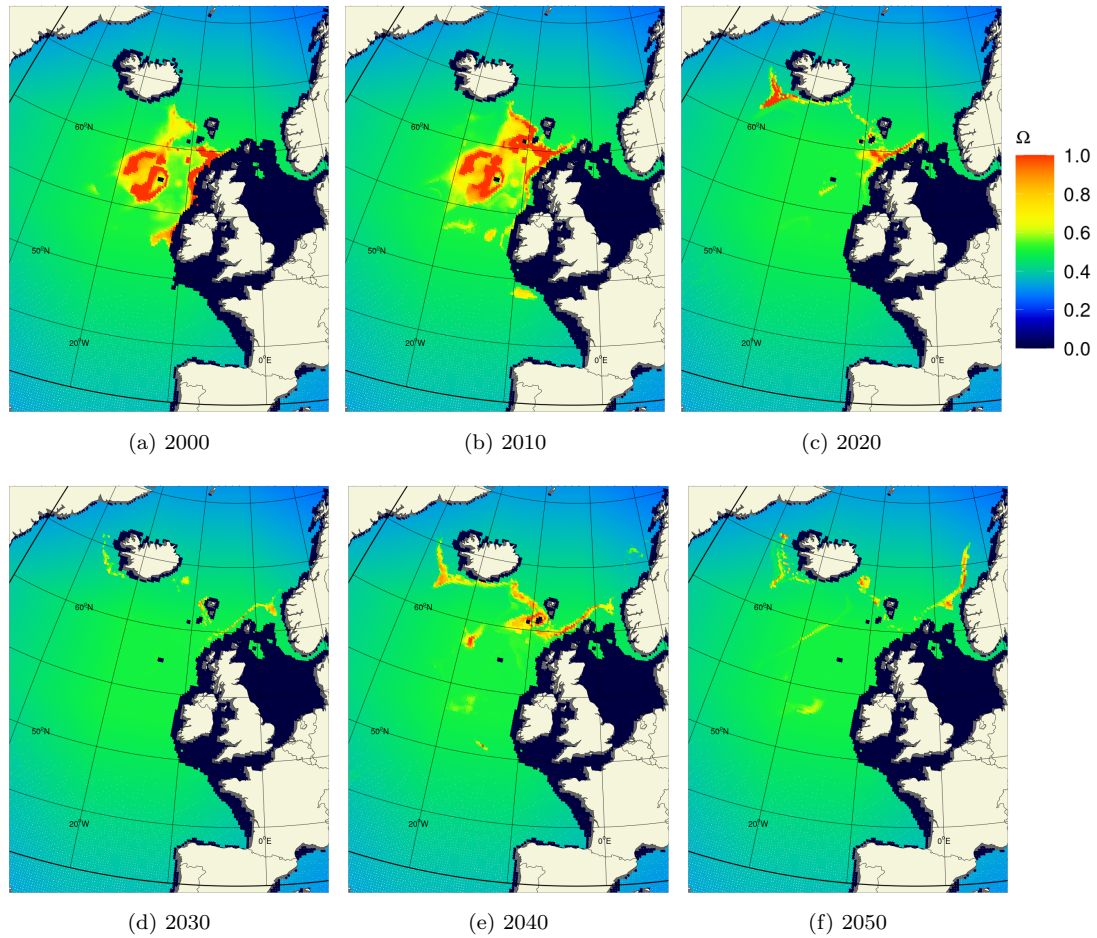
Figure 8.3: Predictions of average spawning habitat suitability index (Ω) in spawning season (30/01 - 16/03) in years 2000 (a), 2010 (b), 2020 (c), 2030 (d), 2040 (e) and 2050 (f).

lation distribution in the Norwegian Sea was similar between both SPG regimes, we expected the Rockall Plateau area only to be reached by southward migrating fish during years of strong SPG, when the areas between Iceland and Faroe Island were not suitable for spawning.

Distribution of suitable spawning habitats were predicted to change drastically between 2010 and 2050 (chap. 4). Yet the definition of the spawning habitat suitability index assumed that, in the absence of clear environmental cues to direct adults to suitable spawning locations, the later would first show fidelity to their old spawning region by migrating in the general direction of the area west of British Isles. In the long-term, we could see that this presented a problem for hypothetical adults migrating from the Bay of Biscay. In figure 8.3, we see that most suitable spawning areas, from 2020 onwards, were located in latitudes greater than 57°N, while gradients in the area between latitudes 53°N and 57°N

were almost non-existent ($\Omega \approx 0.5$ and $\Delta\Omega \approx 0$). It would be then difficult, perhaps impossible, for southern adults to reach the suitable spawning habitats in the North. Adults from the Norwegian Sea would not be faced with this problem and were expected to reach predominantly the new spawning areas predicted off Norway and/or in eastern and southern Icelandic waters. This would most likely depend on their initial position in the Norwegian Sea.

8.3 Migration variability

8.3.1 Relationship between migration timing and success

First, the effect of the migration starting date on the spawning distribution and on the probability of reaching a suitable spawning habitat before the end of the spawning season (here defined as the 16th of March) was investigated. 30 thousand individuals were initialised with uniform distribution in four different zones, with one located in the Bay of Biscay and three in the Norwegian Sea (see zone boundary definitions in fig. 8.5). The simulations were repeated for four different starting dates (21/11, 06/12, 21/12 and 05/01) in years 1992-1994, 2002-2004 and 2000-2050, and adult migration lasted until the end of the spawning season. Average spawning distribution were calculated from track positions recorded over the spawning period defined from the 30th of January to the 16th of March.

Starting the spawning migration early seemed to present a clear advantage for reaching the spawning areas in time (fig. 8.4). Adults were then distributed all over the continental shelf off Ireland and Scotland, and over the Rockall Plateau

Table 8.1: Average migration success ratio for different starting dates in selected years between 2000 and 2050. Migration success is defined as the success probability for an individual to reach and stay in a suitable spawning habitat during the spawning season. It is obtained by calculating the average Ω from the average spawning distribution of adults. For each year, the best migration success value is highlighted in bold.

Dates	2000	2010	2020	2030	2040	2050
21/11	0.670	0.492	0.379	**0.530**	0.574	0.482
06/12	**0.713**	0.462	0.373	0.483	**0.582**	0.479
21/12	0.709	0.474	0.380	0.465	0.573	0.423
05/01	0.575	**0.526**	**0.486**	0.456	0.532	**0.491**
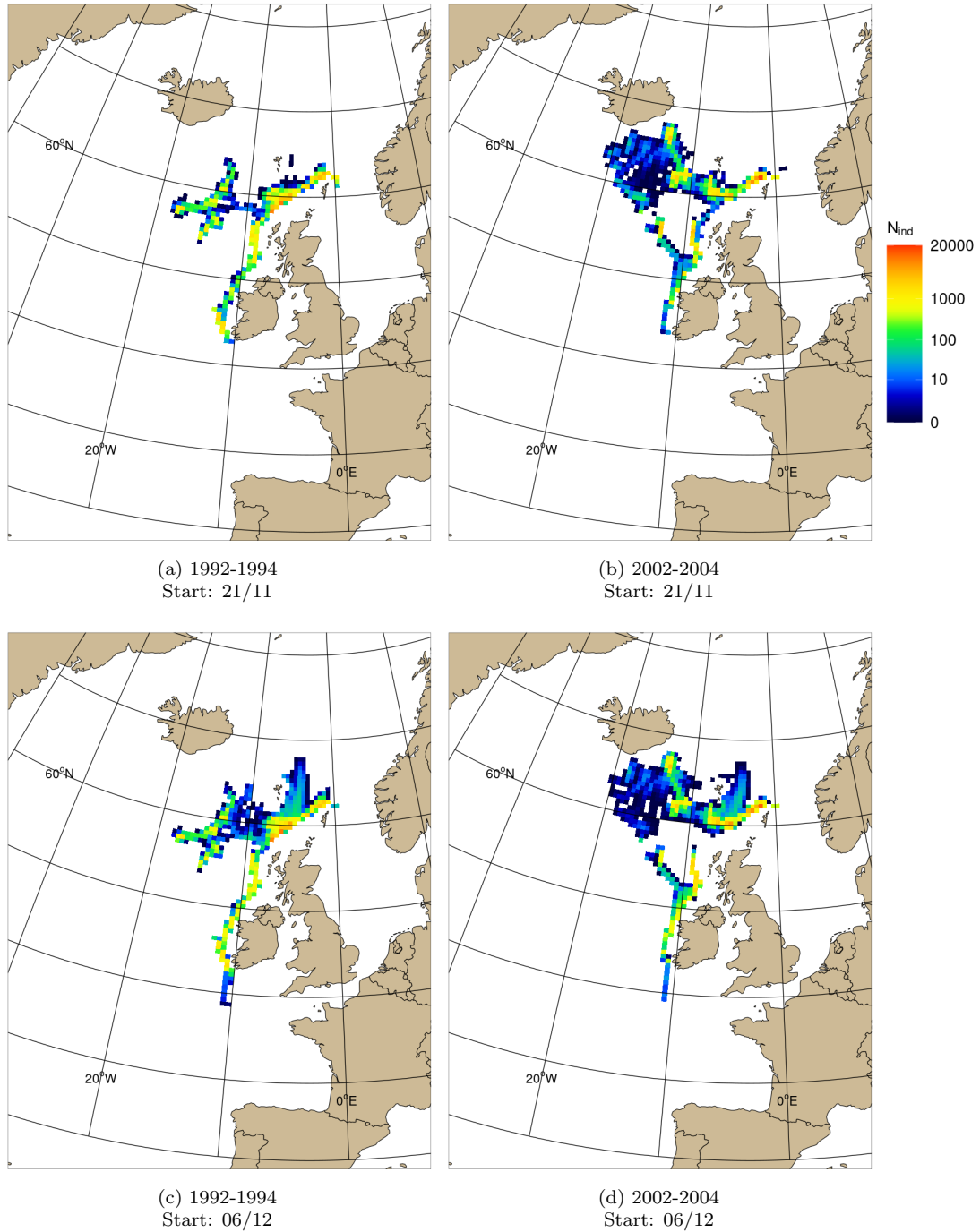
Figure 8.4: Average adult distribution during the spawning season (30/01-16/03) in years 1992-1994 (a,c,e,g) and years 2002-2004 (b,d,f,h) after migration from areas in the Norwegian Sea (90000 individuals) and the Bay of Biscay (30000 individuals), with varying starting dates: the 21st of November (a,b), the 6th of December (c,d), the 21st of December (e,f), and the 5th of January (g,h).

in 1992-1994. With later starting dates, the final average distributions revealed individuals still on their way to the spawning areas. The most extreme results from the 05/01 starting dates showed large amount of adults still present in the

(e) 1992-1994
Start: 21/12

(f) 2002-2004
Start: 21/12

(g) 1992-1994
Start: 05/01

(h) 2002-2004
Start: 05/01
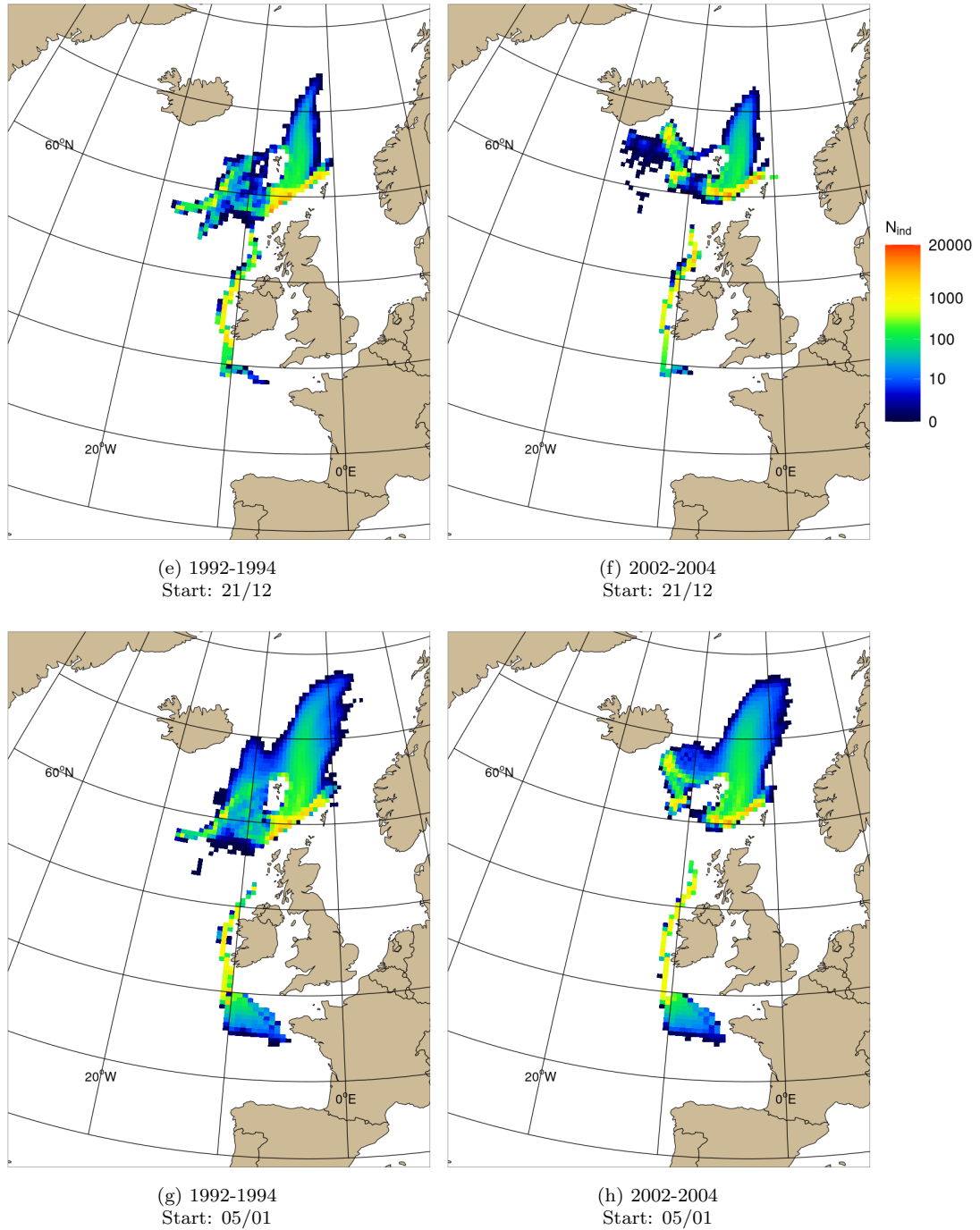
Figure 8.4: *continued.*

middle of the Norwegian Sea and south of the Porcupine Bank area during the spawning period. We could already note here that, as expected, southward migrations from the Norwegian Sea in 2002-2004 seemed to stop in the areas over the Iceland-Shetland section, almost never reaching the Rockall Plateau area, while a portion of northward migrating adults from the Bay of Biscay changed their path along the continental shelf to cross Rockall trough and reach the western

side of the plateau.

In the simulations performed for sampled years between 2000 and 2050, the starting date with the highest migration success varied between years (table 8.1). Overall, the early starting dates 21/11 and 06/12 allowed for the best migration success ratios. But for three years of relatively low migrations success ratios (2010, 2020 and 2050), the best starting date for spawning migration appeared to be the 5th of January. Considering that the migration success ratio gave a mean score of Ω experienced by all tracked individuals during the spawning period, success ratio values less than or close to 0.5 implied that most individuals never reached suitable spawning locations. Together with the prediction maps of Ω, this suggested that variations in distribution of suitable spawning habitat might jeopardize both the success of the modelled spawning migration and the benefits of an early start. However, migration timing might affect migration success from each of the different starting zones very differently, which is why migration results from each starting zone were next studied separately.

8.3.2 Relationship between final distribution and starting position

This time, spawning migrations from different starting zones were studied separately. In the North, adults departed either from the South-West, South-East or the North regions of the Norwegian Sea, while in the South they departed from the Bay of Biscay (fig. 8.5). First, the starting date was fixed to the 21st of November, since most individuals seemed to be able to reach their spawning destination when starting this early (fig. 8.4). For each starting zone, its resulting average spawning distribution was computed under different climate regimes (strong SPG of 1992-1994 versus weak SPG of 2002-2004) to both determine the range of possible spawning areas which can be reached from these locations and to investigate a potential climate effect. Then, the study was expanded to test the effect of migration timing for the different starting zones, either under strong SPG conditions, weak SPG or for forecast years.

Adults migrating from the South-West Norwegian Sea area tended to cover all the available northern spawning areas during the spawning season (fig. 8.5.a and
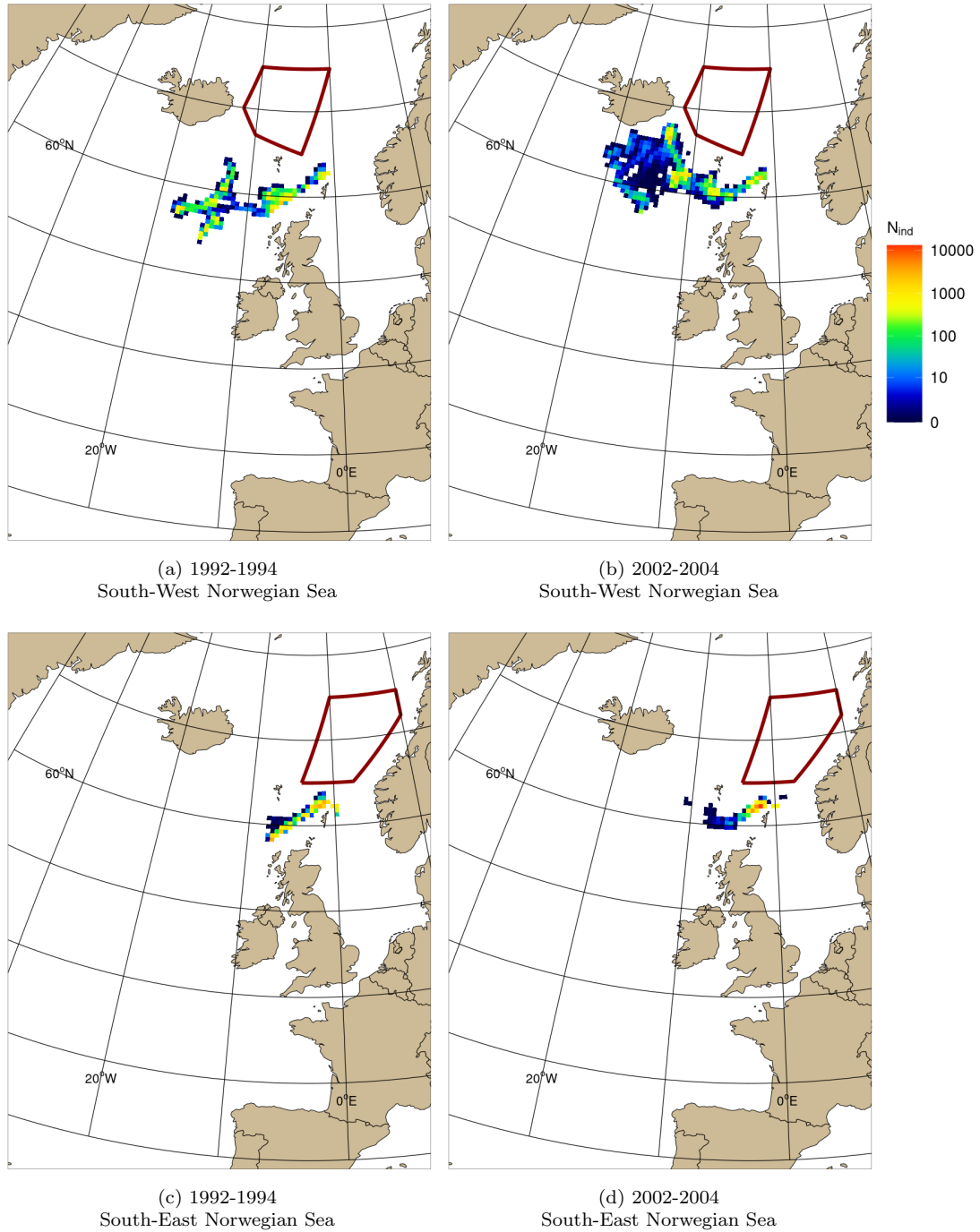
Figure 8.5: Average adult distribution during the spawning season (30/01-16/03) in years 1992-1994 (a,c,e,g) and years 2002-2004 (b,d,f,h) after migration started the 21st of November from different zones: South-West Norwegian Sea (a,b), South-East Norwegian Sea (c,d), North Norwegian Sea (e,f), and Bay of Biscay (g,h). Each zone is represented on the maps by dark red polygons. Each `Ichthyop` run was initialised with 30000 individuals released homogeneously in a zone.

b). In contrast, migrations that started in the South-East area seemed to always end over the continental shelf off Shetland and North Scotland (fig. 8.5.c and d). The North area seemed to produce very similar results to the South-West area,

(e) 1992-1994
North Norwegian Sea

(f) 2002-2004
North Norwegian Sea

(g) 1992-1994
Bay of Biscay

(h) 2002-2004
Bay of Biscay
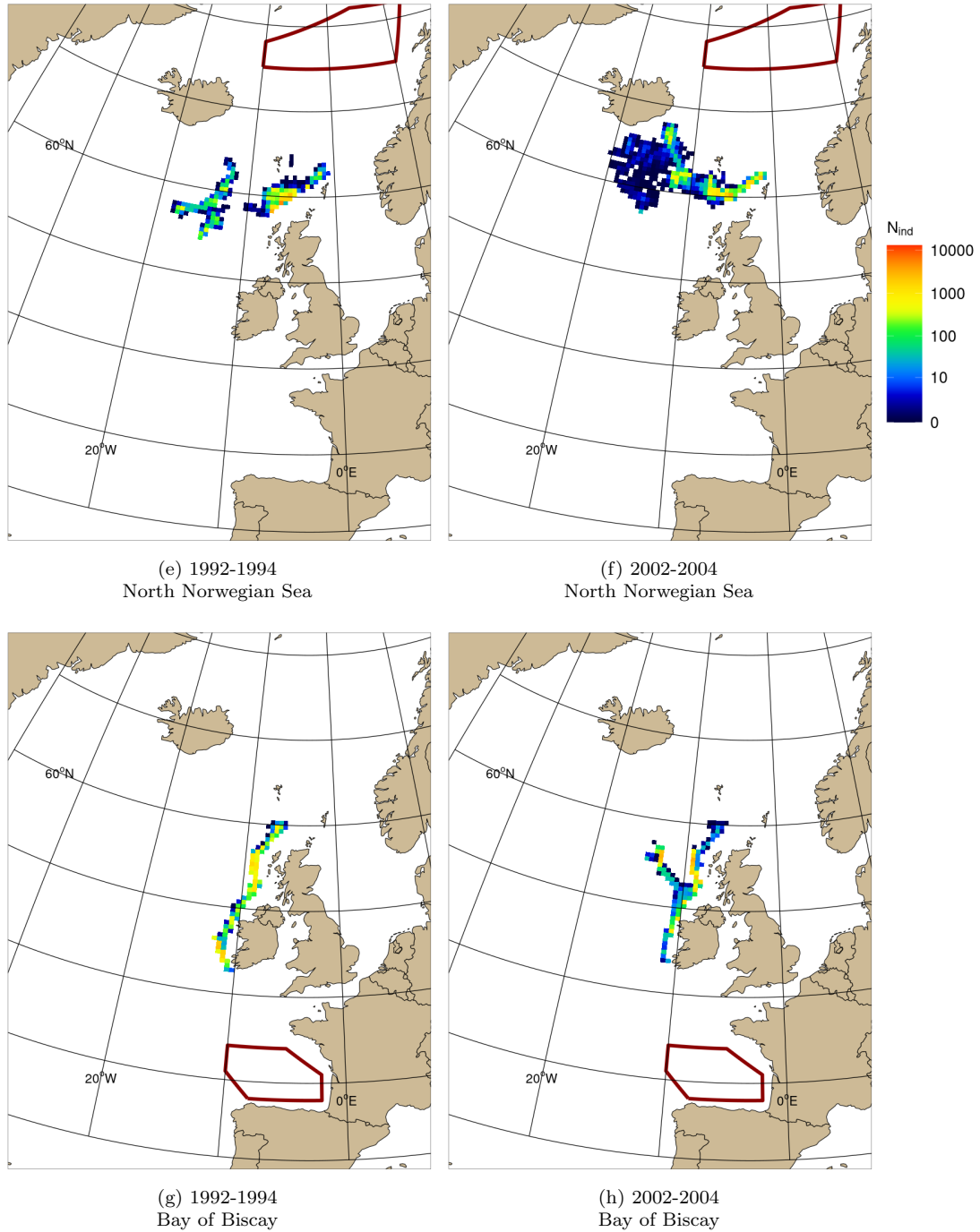
Figure 8.5: *continued.*

but with slightly more individuals over the continental shelf and less in the most western spawning areas, suggesting that more individuals undertook the route east of Faroe Islands (fig. 8.5.e and f). Finally, adults from the Bay of Biscay mostly migrated along the continental shelf to end off the coasts of Ireland and Scotland during the spawning season (fig. 8.5.g and h).

In years of strong SPG (1992-1994), part of the average spawning distributions

of the North and South-West Norwegian Sea migration groups covered the northern side of the Rockall Plateau, but they were almost absent from this area in years of weak SPG (2002-2004). In figures 8.5.b and f, adults were mostly distributed over the section between Iceland and North Scotland. A very dispersed patch of adults was also present between Iceland and the Rockall Plateau. Looking at Ω fields in December 2002 and 2004 revealed that areas off the South-West coast of Iceland had suitable spawning conditions at the start of the migration season. However, those areas disappeared before the spawning season started (fig. 8.2.c and d). Thus, individuals found between Iceland and Rockall in 2002-2004 were most likely individuals who first migrated into the South-West Icelandic waters, and who were then travelling back towards east of Iceland and the Rockall Plateau, after their former locations became unsuitable for spawning.

Some of the Bay of Biscay adults migrated towards the Rockall Plateau in 2002-2004 but not in 1992-1994 (fig. 8.5.g and h). Since the Rockall Plateau area was a suitable spawning habitat in both periods (fig. 8.2), this might indicate a change in the hydrodynamics of the region between both periods. The stronger currents present along the continental shelf during years of strong SPG might hinder individuals to break out from the shelf to target the Rockall Plateau. Moreover, considering the suitable spawning area of the Porcupine Bank in 1994 (fig. 8.2.b), we should have expected more individuals dispersed in that area. The fact that the whole spawning distribution was very limited to the shelf and expanded far north to the Scottish shelf, might be an other evidence of the effect of very strong currents on the modelled migration of southern adults.

Spawning migration success were in general higher for adults travelling from the South-West and North Norwegian Sea areas, but surprisingly low for individ-

Table 8.2: Average migration success ratios in 1992 and 1994 (combined) for each starting zone and for different starting dates. 1992 and 1994 were years with a strong SPG. For each zone, the best migration success value is highlighted in bold. Stars indicate when the average Ω experienced by individuals is superior or equal to 0.75.

Dates	S-W Norw. Sea	S-E Norw. Sea	N Norw. Sea	Bay of Biscay
21/11	0.796 ⋆	0.566	**0.790 ⋆**	**0.805 ⋆**
06/12	**0.802 ⋆**	**0.597**	0.752 ⋆	0.747 ⋆
21/12	0.788 ⋆	0.584	0.696	0.657
05/01	0.767 ⋆	0.561	0.599	0.255

Table 8.3: Average migration success ratios in 2002 and 2004 (combined) for each starting zone and for different starting dates. 2002 and 2004 were years with a weak SPG. For each zone, the best migration success value is highlighted in bold. Stars indicate when the average Ω experienced by individuals is superior or equal to 0.75.

Dates	S-W Norw. Sea	S-E Norw. Sea	N Norw. Sea	Bay of Biscay
21/11	0.726	0.469	0.729	**0.551**
06/12	0.748 ⋆	0.515	**0.745 ⋆**	0.386
21/12	0.762 ⋆	**0.553**	0.714	0.370
05/01	**0.788 ⋆**	0.510	0.603	0.338

uals from the South-East area (tab. 8.2 and 8.3). According to Ω distributions of December and the spawning season in those years, most adults in this area would first be targeting the continental shelf north of Shetland before slowly following the southward shift of the suitable spawning conditions. Both strong northward shelf currents and the shape of the 120 m isobath line might however make a southward migration along the shelf very difficult, which could explain the very low spawning migration success obtained for the South-East Norwegian Sea adults.

Migration success of the Bay of Biscay adults seemed to be much higher in years of strong SPG than of weak SPG, although this was highly dependent on the migration starting date. For both 1992/1994 and 2002/2004 results, the earlier adults started their spawning migration, the higher was their success (tab. 8.2 and 8.3). The fact that the success of a migration starting the 21st of November was very high for 1992/1994 was likely due to the distribution of suitable spawning habitats (fig. 8.2), which tended to be present farther south in those years. Higher success might have been reached in 2002/2004, if the migration started at an earlier date, giving enough time for the southern adults to reach suitable spawning areas. However, the much stronger decrease in success for adults starting later in 1992/1994 compared to 2002/2004 suggested that the timing window for a successful migration in years of strong SPG might be smaller than during years of weak SPG. This could be strongly related to both currents and the changes in Ω distribution between December and March. In 2002/2004, early migrating adults had the advantage of being able to reach the Rockall Plateau, probably thanks to weaker shelf currents (fig. 8.4.b, d and 8.5.h), while later migrating adults were able to detect Ω gradients from farther south thanks to the Ω distribution shifting slowly southward over the season.

Migration timing also affected success of individuals from the Norwegian Sea regions. The highest success was found for earlier migration starting dates in 1992/1994 than in 2002/2004. As explained before, Ω fields tended to change a lot between December and March in the northern areas. As a result, early migrating adults would follow gradients towards areas which might not stay suitable for the spawning season. This effect seemed to be stronger in 2002/2004 than in 1992/1994 resulting in later optimal migration starting dates in 2002/2004 (tab. 8.3). Moreover, according to the migration results for the South-West and North areas, it seemed that the closest from the spawning grounds adults started migrating, the higher was the risk for them to target the wrong areas, thus also resulting in later optimal starting dates for migration.

(a) South-West Norwegian Sea

(b) South-East Norwegian Sea

(c) North Norwegian Sea

(d) Bay of Biscay
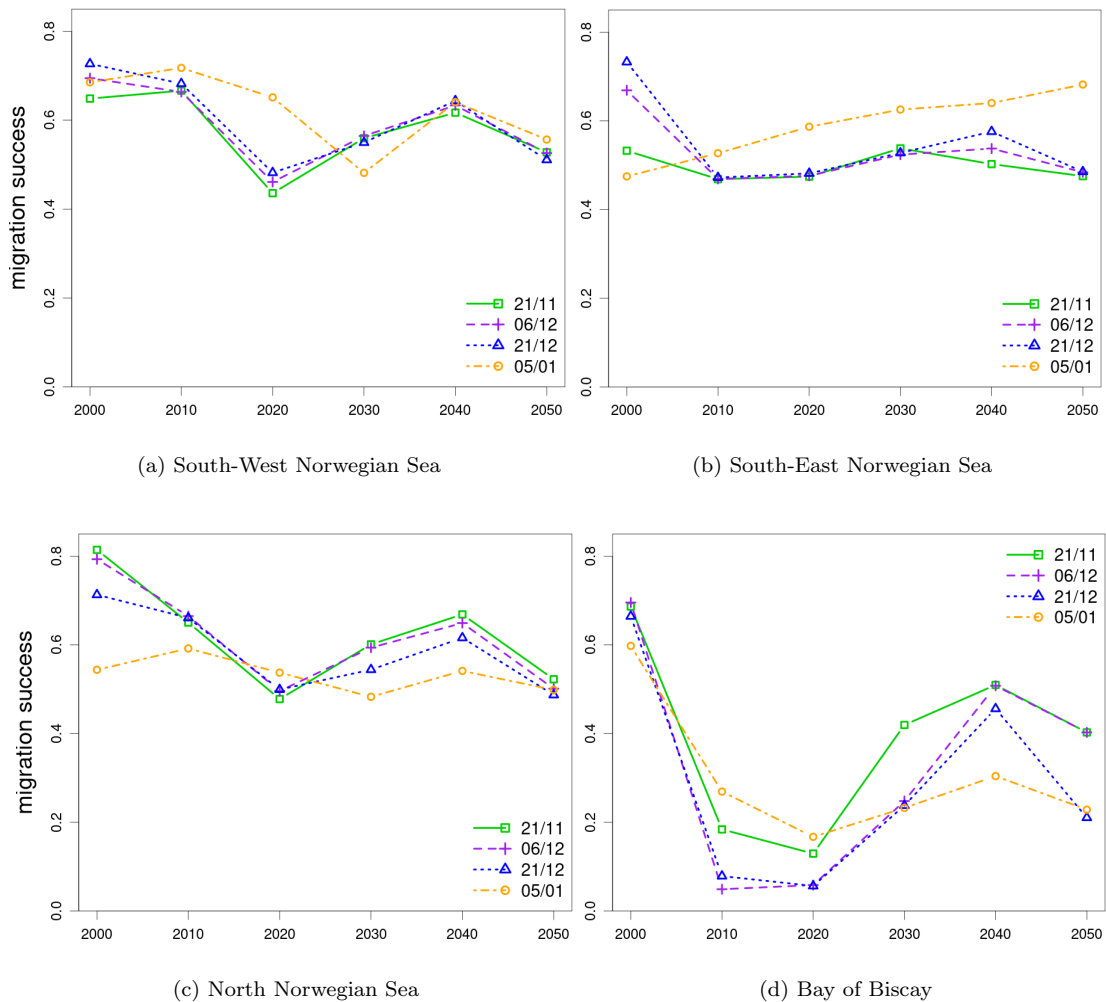
Figure 8.6: Average migration success ratio for each starting zone and for different starting dates in selected years between 2000 and 2050.

Forecasts of spawning migration success varied between starting areas. For adults from both the South-West and the North Norwegian Sea areas, whose migration success was usually among the highest, it seemed to decrease slowly from 2000 to 2050, regardless of the starting date (fig. 8.6.a and c). Except in 2000, adults from the South-East Norwegian Sea area starting their migration before the 5th of January tended to mostly have success values around 0.5, while migration success steadily increased between 2000 and 2050 from 0.48 to 0.68 for those starting the 5th of January (fig. 8.6.b). This supported the previous claim that early migrating adults from the Norwegian Sea had higher risk to end in areas unsuitable to spawning in February-March by wrongly following Ω gradients only present at the start of their migration. The increasing success from adults starting the 5th of January in the South-East Norwegian Sea area was caused by the increase of suitable spawning areas north of Shetland. Finally, adults from the Bay of Biscay had highly variable migration success (fig. 8.6.d), most likely in response to the changes in distribution of suitable spawning habitat from 2000 to 2050 (fig. 8.3), as well as between December and March.

8.3.3 Expected versus predicted spawning distributions

Since the best migration starting date seemed to vary a lot between years and to depend on the starting area, it was decided thereafter to fix this date to the 21st of December for the blue whiting model. This should allow a sufficiently high migration success of adults from any area, while reducing the risk of following early Ω gradients to areas that become unsuitable to spawning before the beginning of the spawning season. Figures 8.7 and 8.8 give the predicted spawning distributions of adults migrating from all the defined areas in sampled years (1992/1994, 2002/2004, 2000-2050).

Compared to the expected spawning distributions for years 1992/1994 and 2002/2004 (fig. 8.2), the Rockall Plateau area was barely covered by the modelled spawning distributions (fig. 8.7). Adults were mostly predicted to finish their spawning migration along the continental shelf off the British Isles, and a lot were not located in suitable spawning areas for most of the spawning season. When suitable spawning areas were present between Iceland and north of Scot-
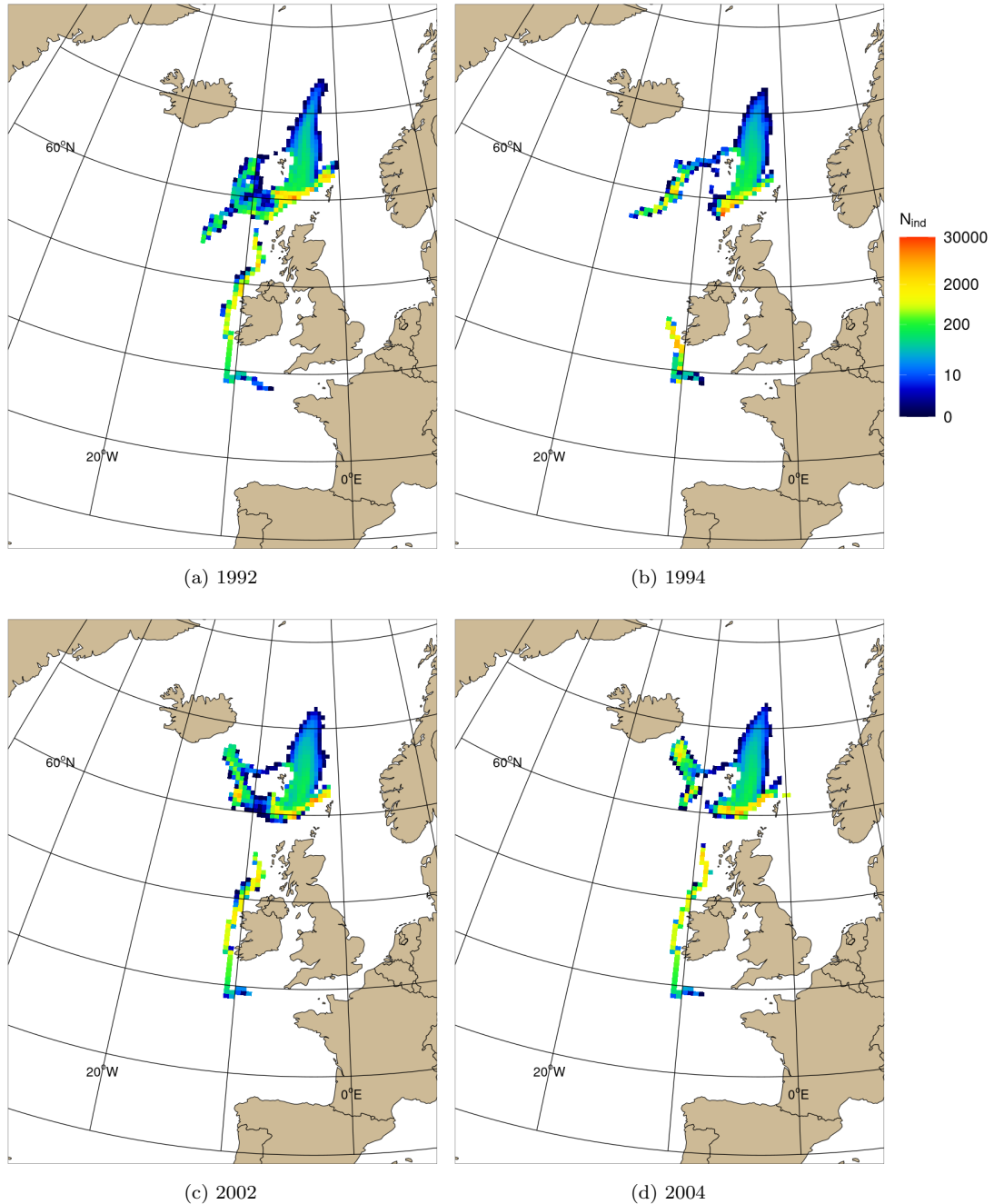
Figure 8.7: Average adult distribution during the spawning season (30/01-16/03) in years with a strong SPG, 1992 (a) and 1994 (b), and in years with a weak SPG, 2002 (c) and 2004 (d), after migration started the 21st of December from every zones (South-West Norwegian Sea, South-East Norwegian Sea, North Norwegian Sea and Bay of Biscay). In total, 120000 individuals were released at the start of each migration.

land (e.g. 2002 and 2004 predictions), almost all individuals from northern areas were predicted to stop there for spawning. As expected, part of the Rockall area was only reached by northern individuals when there were no suitable spawning habitat in the Icelandic and Faroese waters (1992 and 1994).
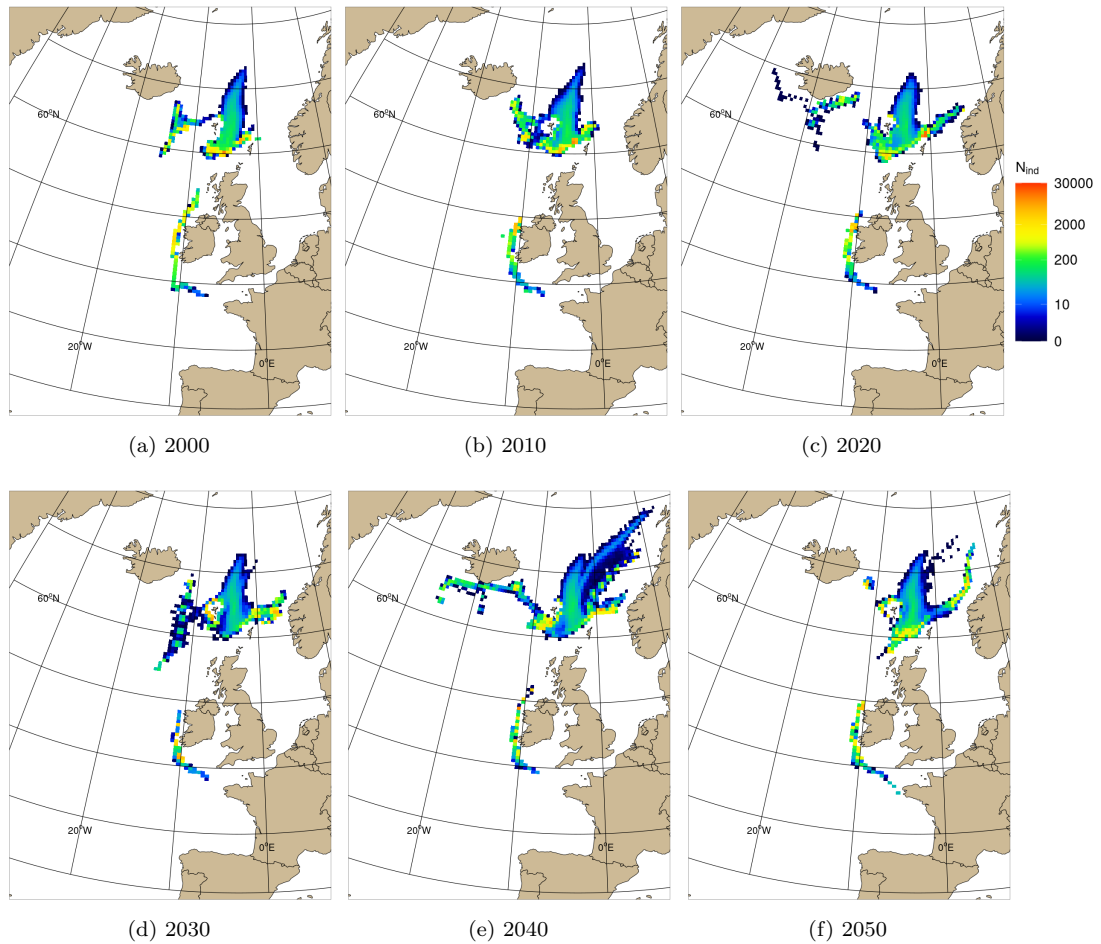
Figure 8.8: Average adult distribution during the spawning season (30/01-16/03) in years 2000 (a), 2010 (b), 2020 (c), 2030 (d), 2040 (e) and 2050 (f) after migration started the 21st of December from every zones (South-West Norwegian Sea, South-East Norwegian Sea, North Norwegian Sea and Bay of Biscay). In total, 120000 individuals were released at the start of each migration.

From 2000 to 2050, the model efficiency at predicting spawning distributions overlapping the expected spawning distribution seemed to decrease (fig. 8.8). Again this was probably caused by the combined effect of the suitable areas moving northward with time and early gradients misleading adults to unsuitable areas during the spawning season. The mean migration success ratio obtained from these simulations was approximately 0.5, which means that, in average, half of the tracked adults were at least located in surrounding areas of optimum spawning habitats.

8.4 Conclusions

Modelling spawning migrations driven by environmental gradients was very challenging. The variable developed for that purpose had to include an 'artificial' gradient describing a linear increase towards the general geographical area of the main spawning grounds, west of British Isles and south of Faroe Islands. Thus gradients of temperature and salinity were only affecting movements of pre-spawning fish, if those were already in this general spawning area, or if suitable spawning conditions were encountered on their migratory route outside of this area. This was the best solution found to ensure that most individuals would move towards suitable spawning grounds. Migration success in the model was indeed quite high for most simulations performed here, except for migrating individuals coming from areas south of the theoretical main spawning area.

Migration starting time and position played a significant role in both migration success and spawning distribution. Individuals always stopped their migration in the first suitable spawning area reached along their way. If these spawning areas were well connected to each other, this could result in dispersion all over them. For these reasons, areas like the Rockall Plateau or the narrow continental shelf between North Scotland and the Porcupine Bank were often ignored by migrating individuals from the Norwegian Sea.

An early or late migration start could be either positive or negative for the migration success depending on an individual initial location and on annual conditions. Thus, migration success could strongly decrease if early migrating individuals were attracted by suitable spawning conditions which disappeared before the spawning period, or if late individuals were located too far away from any suitable spawning area. Sometimes, early migrating individuals were able to reach suitable spawning areas usually dismissed (e.g. Rockall Plateau), thanks to the right conditions of currents and to the fact that other areas were not yet suitable at the time.

Finally, spawning migrations were affected by climate variations. This was to be expected since the spawning suitability gradient was computed from NEMO-Medusa outputs (chap. 4). Nevertheless, strength of currents in the main spawn-

ing area, especially those present in Rockall Trough, had a strong effect on the final shape of the spawning distributions.

According to the literature on the blue whiting population dynamics, the Rockall Plateau was supposed to be favoured in years of weak SPG (Hátún et al., 2009b; Payne et al., 2012). Contradicting results here were likely caused by both the model design and the fact that adults were always initialised in the same areas. In fact, it would be interesting to use the model to also study spawning migrations of individuals from western areas off Greenland (Post et al., 2019), which might then show spawning distributions over the Rockall Plateau that would vary with climate.

Chapter 9

Population dynamics: fishing and climate change effect

The strong fluctuations of the blue whiting stock reported in the past decades (Payne et al., 2012; ICES, 2019b) led to believe that climate variations, in particular the subpolar gyre dynamics, have been in some ways affecting recruitment of the population (chapter 1). However, the important development of the blue whiting fishery between 1980 and 2005, as well as its following years of decreasing fishing activity between 2005 and 2010, could have also resulted in the observed stock variations (chapter 6). It showed that the effect of climate on the blue whiting population might not be as pronounced as suggested by past studies, and that it was important to further investigate the population response to fishing. In this context, a spatial model of the population dynamics presented with the advantage of simulating spatial variations of biogeophysical variables while modelling and testing the effect of different fishing behaviours, as well as studying the population sensitivity to changes of either fishing mortality or climate.

Building such a model was a long and thorough process and in our case, required two modelling stages. The first stage was the building of the length- and life-stage-structured population growth model (chapter 2). The second stage was the modelling of blue whiting population movement, especially adult migrations, that would take the environment into account (chapter 3). In the two previous chapters, the focus was solely on the modelling of the blue whiting migration patterns between feeding and spawning areas. Growth, mortality and reproduction were not included into this stage. Once we were satisfied with both migration behaviours (chapters 7 and 8), transport matrices were computed to be combined with the blue whiting growth model to form the final spatial model of the popu-

lation dynamics.

This was the first time that a model of the blue whiting population integrated population movement influenced by environmental conditions. NEMO outputs of temperature and salinity (chapter 4) and the blue whiting food fields predicted with random forests of CPR data (chapter 5) were directly used in the model for simulating spatial variation of either or both spawning and growth. This ensured that all the population dynamics, not only movement, were affected by environmental changes in both time and space.

The final model was used to make long-term simulations of the blue whiting population. The following chapter describes and explains all the model's main outputs and behaviours. Variations of spatial distributions were this time studied in the context of a changing population, affected by survival and reproduction. The predicted population variations were compared to ICES population estimates. For most sections, the effects of both climate and fishing were investigated. A special emphasis was given to recruitment, as we tried to understand how it was affected by different biological and physical drivers. Finally, the population sensitivity to variation in fishing mortality was studied under different model conditions.

9.1 General model behaviours

9.1.1 Model parameters and fitting

The model was initialised at the beginning of the spawning period with a total of one billion of adults in each length class between 20 and 40 cm, which were equally distributed between all spawning cells of the initial year. This excess of adults at the start of the run ensured the inflow of large quantities of eggs each year until the first eggs released in the system had enough time to hatch into larvae, grow and reach adulthood. This also ensured a faster approach to the model steady state.

As the objective was to run long-term simulations of the blue whiting population dynamics, the model was brought to its steady state before the start of the studied period using a spin-up period. This spin-up period was defined as one single year, usually the first year of the studied period, repeated n times until
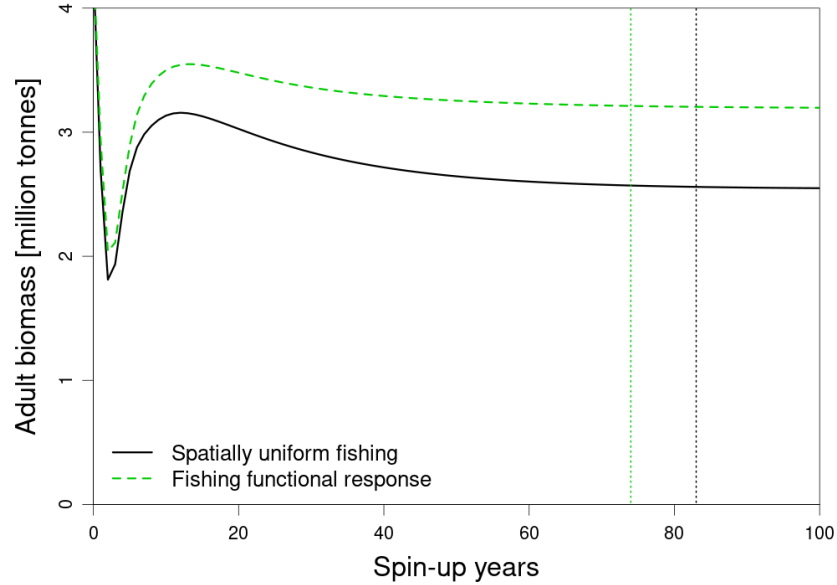
Figure 9.1: Average annual adult biomass (million tonnes) during the spin-up run, showing model steady state approach for the two different fishing models tested: SUF (solid black line) and FFR3 (dashed green line). Parameter values used for both models are given in table 9.1. The two vertical dotted lines indicate the year at which the inter-annual change in adult biomass is less than 1000 tonnes. We consider here that the SUF model reached equilibrium at $t = 83$ years, and the FFR3 model at $t = 74$ years.

the model system approached its steady state. For most model experiments, the steady state was reached in less than 100 years but more than 60 (fig. 9.1). This was very demanding in terms of both computational time and storage space, and therefore, only one spin-up run of 100 years in duration was done for each model setting, using the repeated year 1988. At the end of this spin-up run, only outputs of population abundance in each length class and cell of the spatial domain were saved. Juvenile and adult abundance and distribution of the last spin-up time step were used to initialise all short-term and long-term runs, whether the run period started in 1988 or not. An additional spin-up period of 50 years was then added to those runs to ensure the steady state was always reached before the beginning of the studied period.

Two different fishing models were tested: the spatially uniform fishing model (SUF) and the fishing functional response type III model (FFR3) (chapter 2). Except for the addition of two fishing parameters for the Holling functional response type III equation (B_H and κ) and for the change in parameter value c_0 of

Table 9.1: Parameter values of the fitted models with either spatially uniform fishing (SUF) or fishing functional response type III (FFR3). Values in brackets were used to study the parameter's effect on the model behaviour and outputs. For the spawning/feeding cycle, dates marked with the same number of asterisks were used for the same model run. The end of spawning season also corresponds to the end of the spawning migration. When not specified, the model used was the SUF model with its default set of parameters.

Models			SUF (default)	FFR3
Fishing parameters:				
	B_H	[tonnes/km^2]	-	10.0
	κ	[1]	-	6.0
	f_a	[y^{-1}]	$1.0 \cdot 10^6$	
	f_b	[cm^{-1}]	0.7	
Biological parameters:				
Mortality:				
	δ_E	[y^{-1}]	18.59	
	δ_{D_0}	[y^{-1}]	14.0 (10.0, 12.0)	14.0
	c_0	[g^{-1}]	$3.6 \cdot 10^{-7}$ ($3.0 \cdot 10^{-7}$, $3.3 \cdot 10^{-7}$)	$4.7 \cdot 10^{-7}$
	δ_J	[y^{-1}]	0.2	
	δ_A	[y^{-1}]	0.2	
Life-stage transitions:				
	L_H	[cm]	0.5	
	h	[y^{-1}]	52.14	
	L_R	[cm]	5.0	
	r	[y^{-1}]	36.5	
	L_M	[cm]	21.0 (25.0, 29.0)	21.0
	m	[y^{-1}]	5.0	
Fecundity:				
	e_0	[cm^{-1}]	0.142	
	e_1	[1]	3.742	
Growth:				
	a	[g/cm^3]	$4.875 \cdot 10^{-3}$	
	μ_0	[y^{-1}]	0.207	
	Q_μ	[1]	4.35	
	τ_0	[y/g]	0.364	
	Q_τ	[1]	0.461	
	σ_0	[m^3/y]	$1.52 \cdot 10^3$	
Spawning/feeding cycle:				
Start of spawning migration			21/12	
Start of spawning season			30/01 (24/02*, 05/01**)	30/01
End of spawning season			16/03 (10/04*, 30/04**)	16/03
End of feeding migration			09/07 (03/08*, 23/08**)	09/07

the density-dependent larval mortality, all other parameter values were kept the same between both model settings used to study long-term population dynamics (tab. 9.1).

For some parameters, values were taken directly from the literature. This was

the case for the juvenile and adult mortality rates (ICES, 2019b), fecundity parameters (Bailey, 1982) and life-stage transition lengths and rates of larvae and juveniles (Bailey, 1982; Trenkel et al., 2014; ICES, 2005, 2007). The constant of proportionality a of the weight-length relationship ($W = aL^b$) was estimated so that the relationship would be similar to the one used by Bachiller et al. (2018), while simplified with $b = 3$.

Growth parameters were estimated using values of asymptotic size (L_∞) and growth coefficient (k) of individuals living in different temperature conditions (Raitt, 1968; Kompowski, 1978; Bailey, 1982; Monstad, 1990; Trenkel et al., 2015; Bachiller et al., 2018). It was assumed that the food intake rate (I) at the observed maximum food concentration ($\rho_{\max} \approx 3.44 \cdot 10^{-2}$ g/m^3) approached the maximum food intake rate value ($I_{\max}$) by 0.95. This implied that the half-saturation food concentration was equal to $\rho_H = \rho_{\max}/19$. Then equations 2.10, 2.12 and 2.13 were recast with the different L_∞, k and temperature values to find parameters μ_0, Q_μ, τ_0, Q_τ and σ_0 (tab. 9.1).

Assuming an individual living throughout its life in the same environment with a constant sinusoidal annual cycle of temperature and food, length-at-age values were estimated. This made the ICES estimates of fishing mortalities at age appropriate to use in calculating parameters f_a and f_b of the length-dependent fishing mortality function, so that it reflected fishing age selectivity reported by ICES (2019b).

Migrating and spawning behaviours were controlled by a set of fixed dates. They defined when the adult and juvenile population switched between dispersive and migrating behaviours, when adults switched between spawning and feeding migration, and when the spawning season took place (tab. 9.1). The starting date for the spawning migration was defined based on the conclusions on the migration timing effect on spawning distribution success (chapter 8). The default start and end dates for the spawning season were chosen to represent the main spawning period observed in past studies, as well as to provide a sufficiently high success of the northward feeding migration (chapter 7). As 110 days seemed to be long enough to achieve the feeding migration, this duration was kept constant for all model simulations to define the end date of the feeding migration. After that date, all adults and juveniles were only presenting dispersive behaviours, either

(a)

(b)
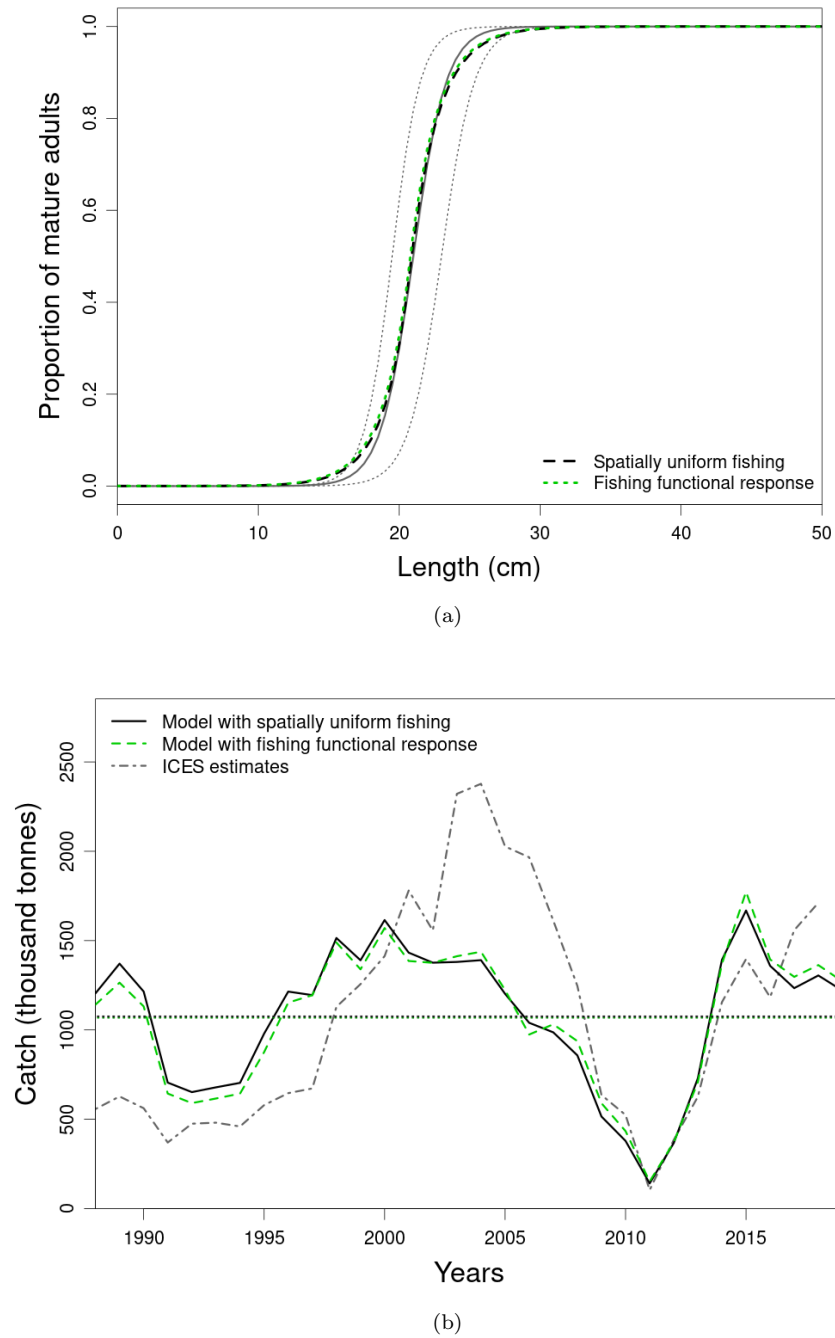
Figure 9.2: Models fitted to (a) the estimated maturity curve (solid grey line) based on ICES data of mature fish proportion by length class with dotted grey lines giving a qualitative confidence interval to represent variability found in ICES data (chapter 1), and to (b) the mean annual total catch recorded in ICES reports (chapters 1 and 6). Comparison between (c) SSB estimated by ICES and by the model, and between (d) First-year recruitment estimated by ICES and annual juvenile recruitment estimated by the model. Results are given for model runs with different fishing models: SUF (black) and FFR3 (green). Horizontal dotted lines in (b), (c) and (d) represent global average values of each model for the period 1988-2019.
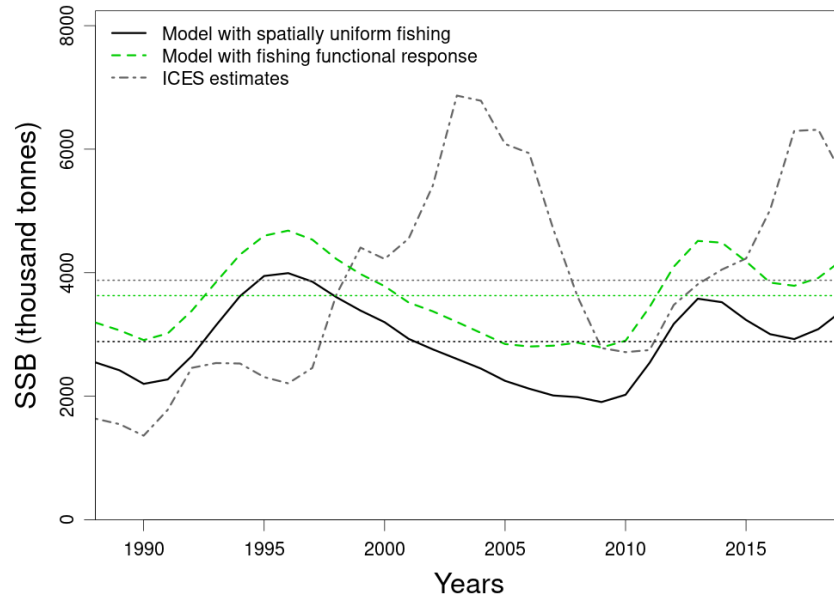
(c)
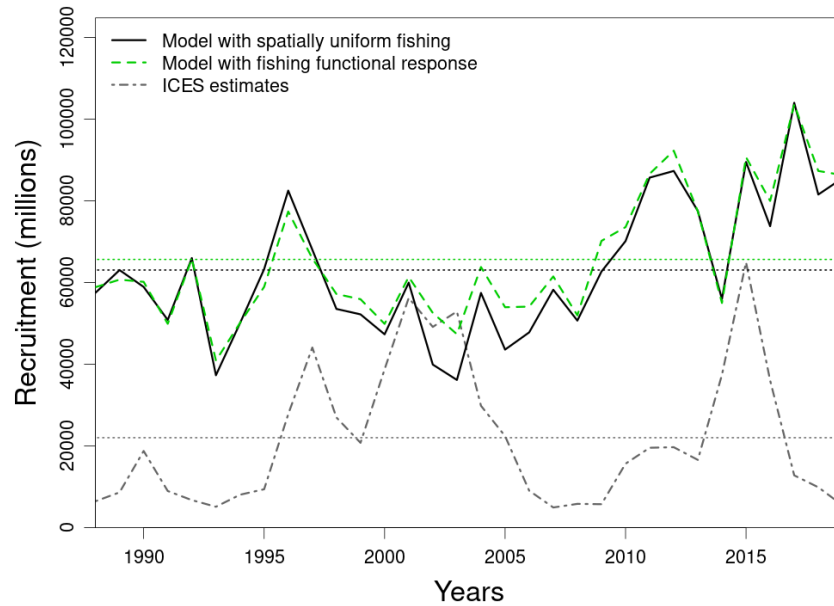
(d)

Figure 9.2: *continued.*

until the next spawning migration started for adults or until the next feeding migration period for juveniles.

At first, spawning was implemented to only take place in areas with suitable temperature, salinity and depth during the spawning season. However, considering how limited those areas could be in some years, the optimal temperature

range for spawning was changed from 9-10°C to 9-14°C, as temperature might not be as important as salinity and because only the 9°C temperature minimum was suggested as a strong limit to the spawning distribution (Hátún et al., 2007; Miesner & Payne, 2018). Thus, while blue whiting adults still undertook spawning migrations modelled by the Ω gradient with the 9-10°C temperature range, they would also spawn in areas with temperatures between 10-14°C, as long as the other optimal conditions were met.

The rest of the parameters were adjusted to fit the model outputs to both the ICES maturity curve (fig. 9.2a) and catch observations from 1988 to 2019 (fig. 9.2b). Since ICES estimated fishing mortality values (ICES, 2019b) were used as maximum annual fishing rates applied to the population (F_Y) from 1988 to 2019, we expected to find a set of parameters that would result in population biomass, recruitment and catch outputs resembling ICES estimates and records over this period. However, an important mismatch was always present between time series of spawning stock biomass (SSB) of the tested models and ICES (fig. 9.2c), while recruitment was in average much higher in the models (fig. 9.2d). Since ICES recruitment and SSB values are also outputs from a model, the average of model catch was fitted to the mean ICES catch value over 1988-2019. This was first done for the SUF model, then repeated for the FFR3 model by only varying the density-dependent larval mortality parameter c_0 (tab. 9.1).

9.1.2 Spatial dynamics

For the following section, both model settings (SUF and FFR3) were used to produce quarterly or annual spatial distributions of each life stage. The models were run from 1988 to 2050 with the model being at equilibrium at the start of 1988. Results from 1992-1994 were compared with those from 2002-2004, to study any variation between different SPG regimes.

Spawners and larvae

In both models, spawning was mostly taking place in the areas north of Scotland, which corresponded to the main spawning areas of the previous spawning

(a) 1992-1994
SUF

(b) 1992-1994
FFR3

(c) 2002-2004
SUF
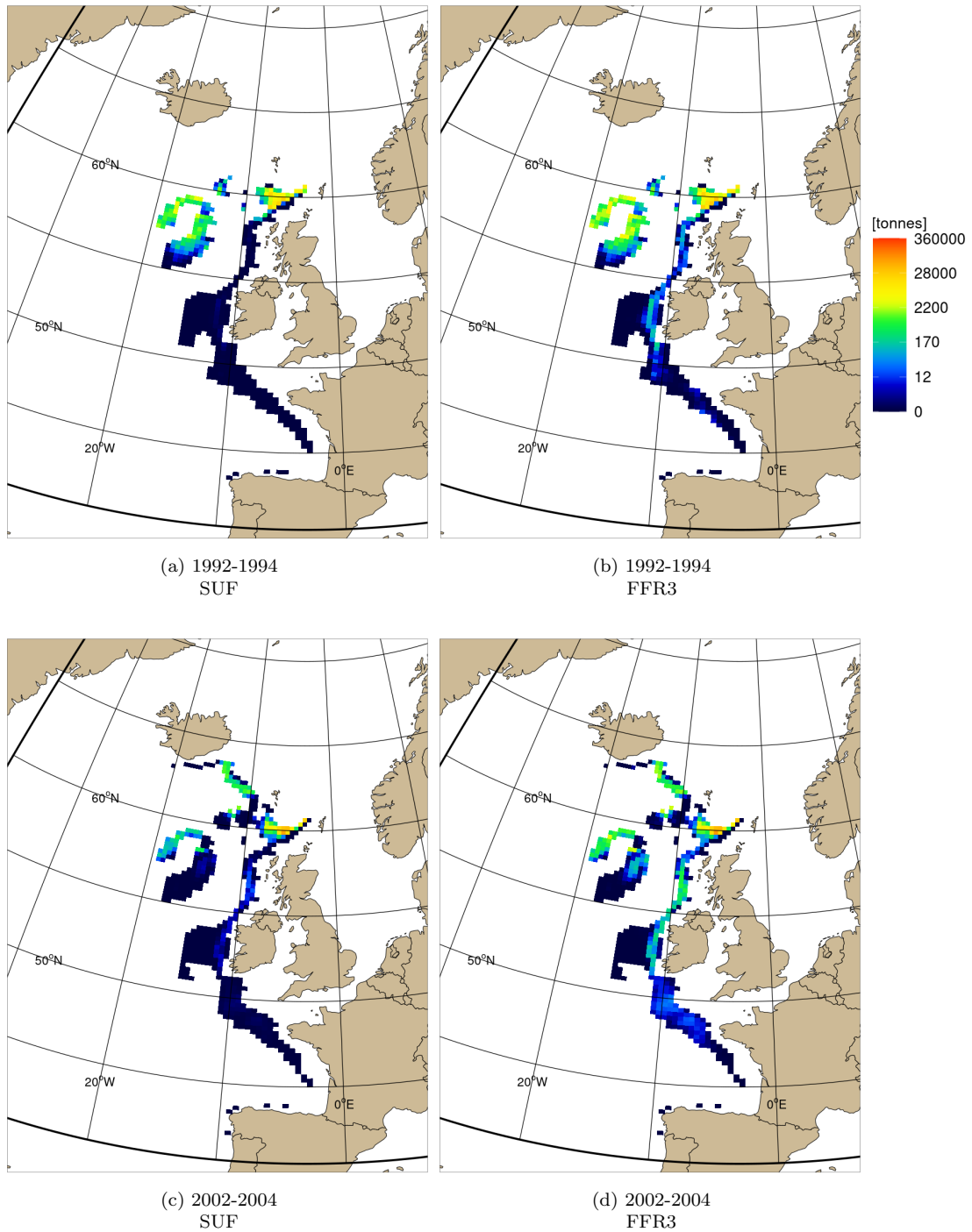
(d) 2002-2004
FFR3

Figure 9.3: Average spawning distributions in 1992-1994 (a,b) and 2002-2004 (c,d) from model runs with different fishing models: (a,c) SUF, and (b,d) FFR3. White areas correspond to areas where no individuals were able to spawn, meaning that those areas' conditions where unsuitable for spawning. In 1992-1994, the subpolar gyre was strong, while in 2002-2004, the subpolar gyre was weak.
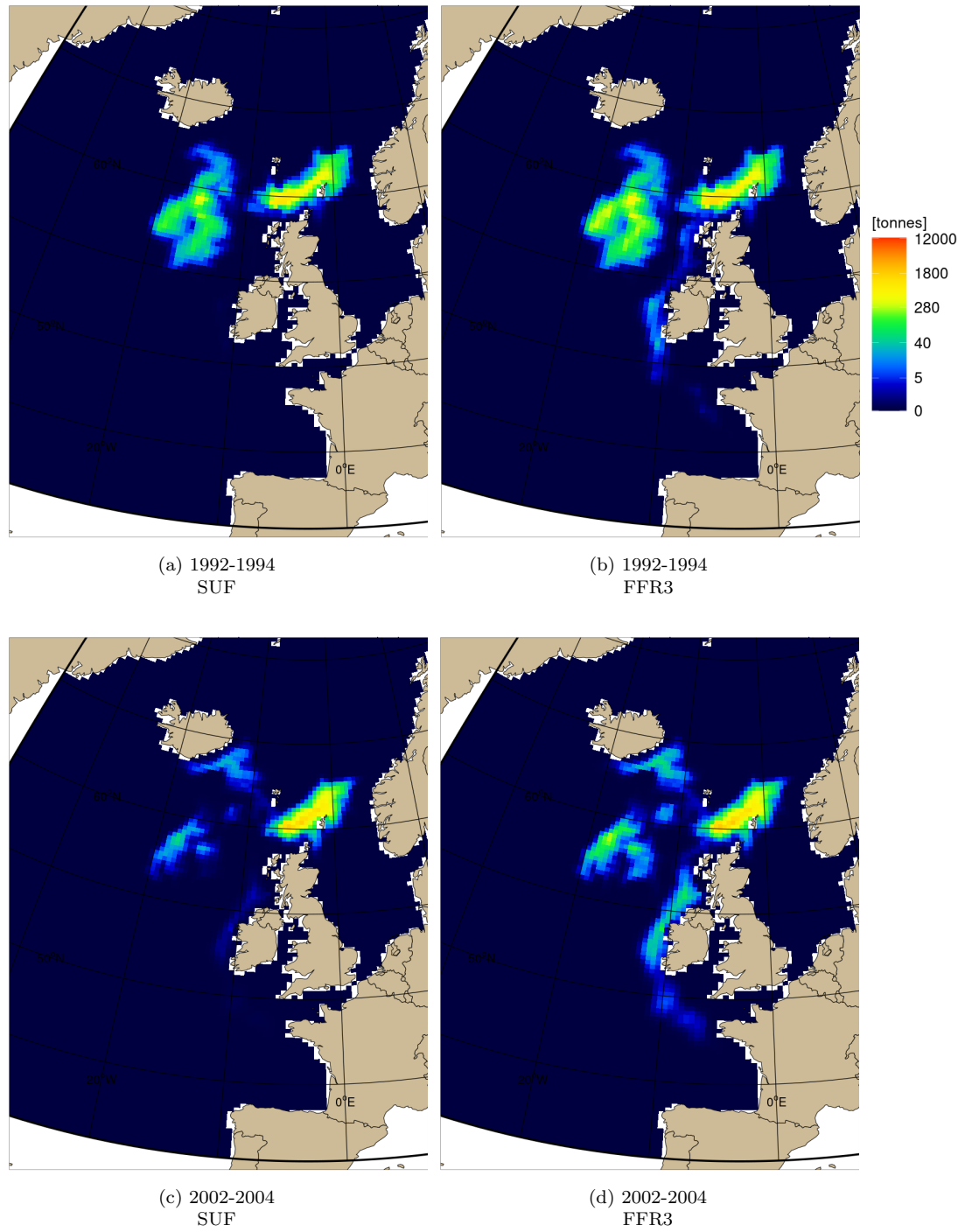
Figure 9.4: Average larval distributions in 1992-1994 (a,b) and 2002-2004 (c,d) from model runs with different fishing models: (a,c) SUF, and (b,d) FFR3. In 1992-1994, the subpolar gyre was strong, while in 2002-2004, the subpolar gyre was weak.

migration results (chap. 8), while the continental shelf of more southern areas, including Porcupine Bank, was mostly deserted by the spawning population. Spawning over the Rockall Plateau was more important in years of strong SPG than in years of weak SPG. In years of weak SPG, spawners were located between Faroe Islands and Iceland (fig. 9.3).

The main difference in spawning distribution between both models was found along the continental shelf, where abundance was higher with the FFR3 model. The functional response type III function reduced considerably the fishing uptake in areas with low fish density. This seemed to mostly affect southern populations. Without the fishing limit dictated by the fishing functional response, spawning was almost non-existent between North Scotland and Brittany in the SUF model (fig. 9.3).

Average larval distributions in February-March reflected spawning distributions (fig. 9.4). The northward larval drift was visible for larvae that were spawned in the area off North Scotland. Since the spawning location was supposed to affect larval drift and juvenile recruitment, this raised the question of whether the presence of spawners in the southern spawning areas was exclusively the result of southward drifting of larvae and southern juvenile recruitment.

Juveniles and recruitment areas

In the model, juveniles followed the same food gradient than adults between mid March and start of July, and were only submitted to dispersion for the rest of the year. As a consequence, mean juvenile distribution in the second quarter revealed migrating behaviours between recruitment areas and feeding grounds, when recruitment did not directly take place in a suitable feeding area (fig. 9.5). In the fourth quarter, mean juvenile distributions were a result of dispersion around both feeding areas and recruitment areas.

Results from the SUF model showed that the majority of juveniles were distributed in the Norwegian Sea throughout the year (fig. 9.5). The second most important population of juveniles were found in the Irminger Sea and South of Iceland. Surprisingly for the SUF model, a small population of juveniles were also present in the South, off Ireland and Brittany, suggesting that a southward larval drift resulting in successful recruitment took place despite the almost non-

(a) 1992-1994
Quarter 2

(b) 1992-1994
Quarter 4

(c) 2002-2004
Quarter 2

(d) 2002-2004
Quarter 4
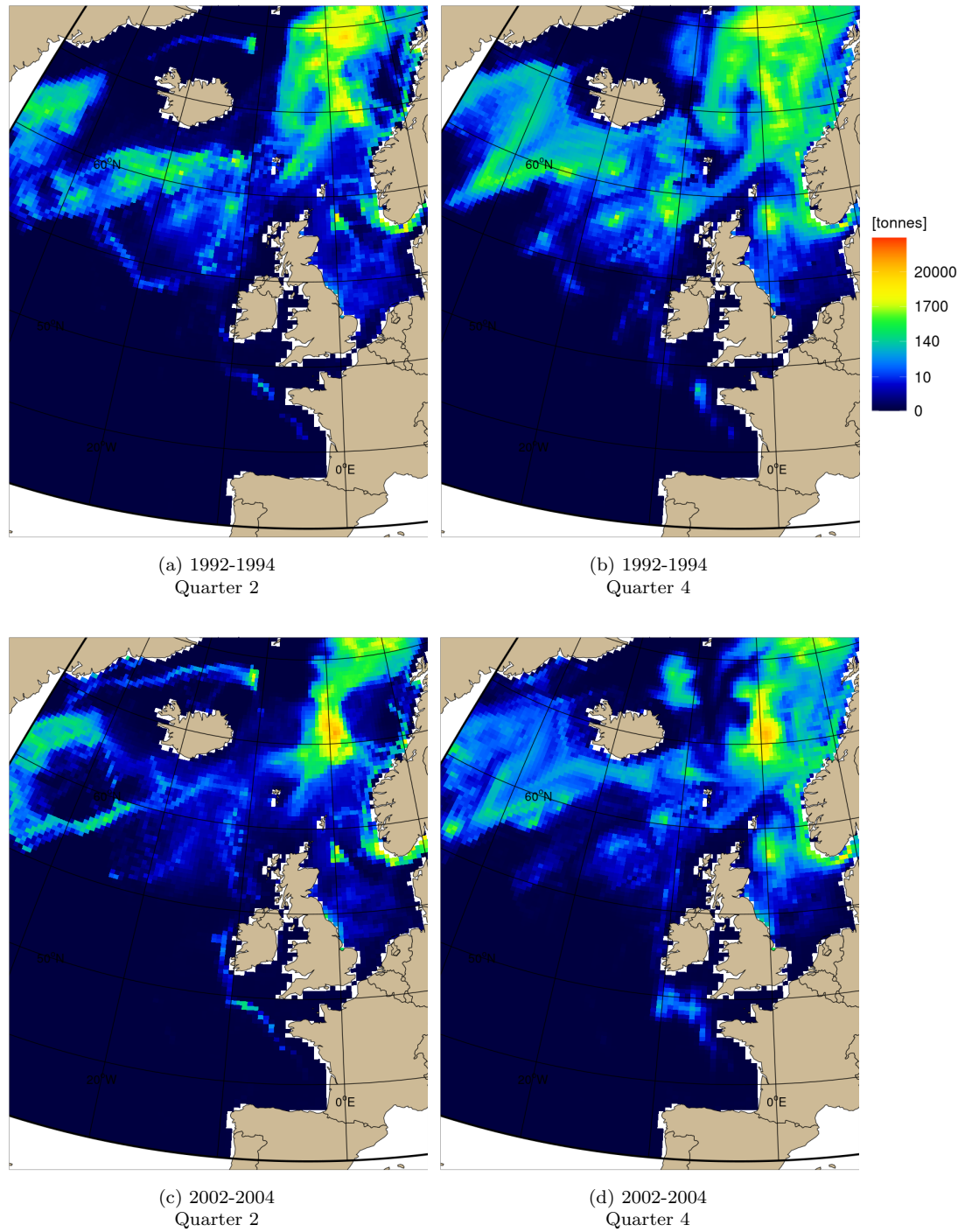
Figure 9.5: Quarterly average juvenile distributions in 1992-1994 (a,b) and 2002-2004 (c,d) for quarters 2 (April-June) and 4 (October-December), from model run with SUF. In 1992-1994, the subpolar gyre was strong, while in 2002-2004, the subpolar gyre was weak.

(a) 1992-1994
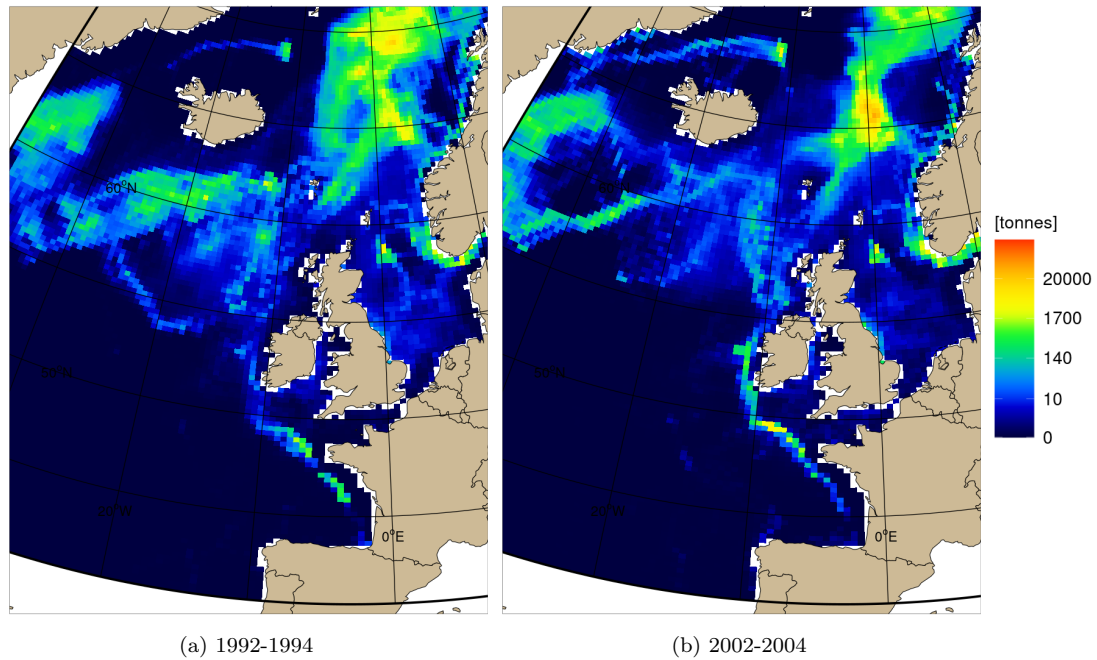
(b) 2002-2004

Figure 9.6: Average juvenile distributions in 1992-1994 (a) and 2002-2004 (b) for April-June (quarter 2), from model run with FFR3. In 1992-1994, the subpolar gyre was strong, while in 2002-2004, the subpolar gyre was weak.

existent or very low spawning observed in the southern spawning grounds (fig. 9.4.a and c). An increase in abundance of juveniles off Ireland and Brittany was observed when using the FFR3 model (fig. 9.6).

Most larvae seemed to grow into the juvenile life stage in the area between Shetland and Norway (fig. 9.7). High recruitment in this area was the result of the northward drift of larvae from the spawning areas North of Scotland. Recruitment of juveniles was also observed above the Rockall Plateau indicating some retention process at work in this area. In the SUF model, recruitment appeared to be again almost non-existent in the southern areas (fig. 9.7.a and c), which suggested that most juveniles observed off Brittany might have reached those areas only after their recruitment in more northern areas, either through migration or dispersion, or both. The FFR3 model however showed a clear recruitment of juveniles all along the continental shelf, between Scotland and Brittany (fig. 9.7.b and d).

(a) 1992-1994
SUF

(b) 1992-1994
FFR3

(c) 2002-2004
SUF
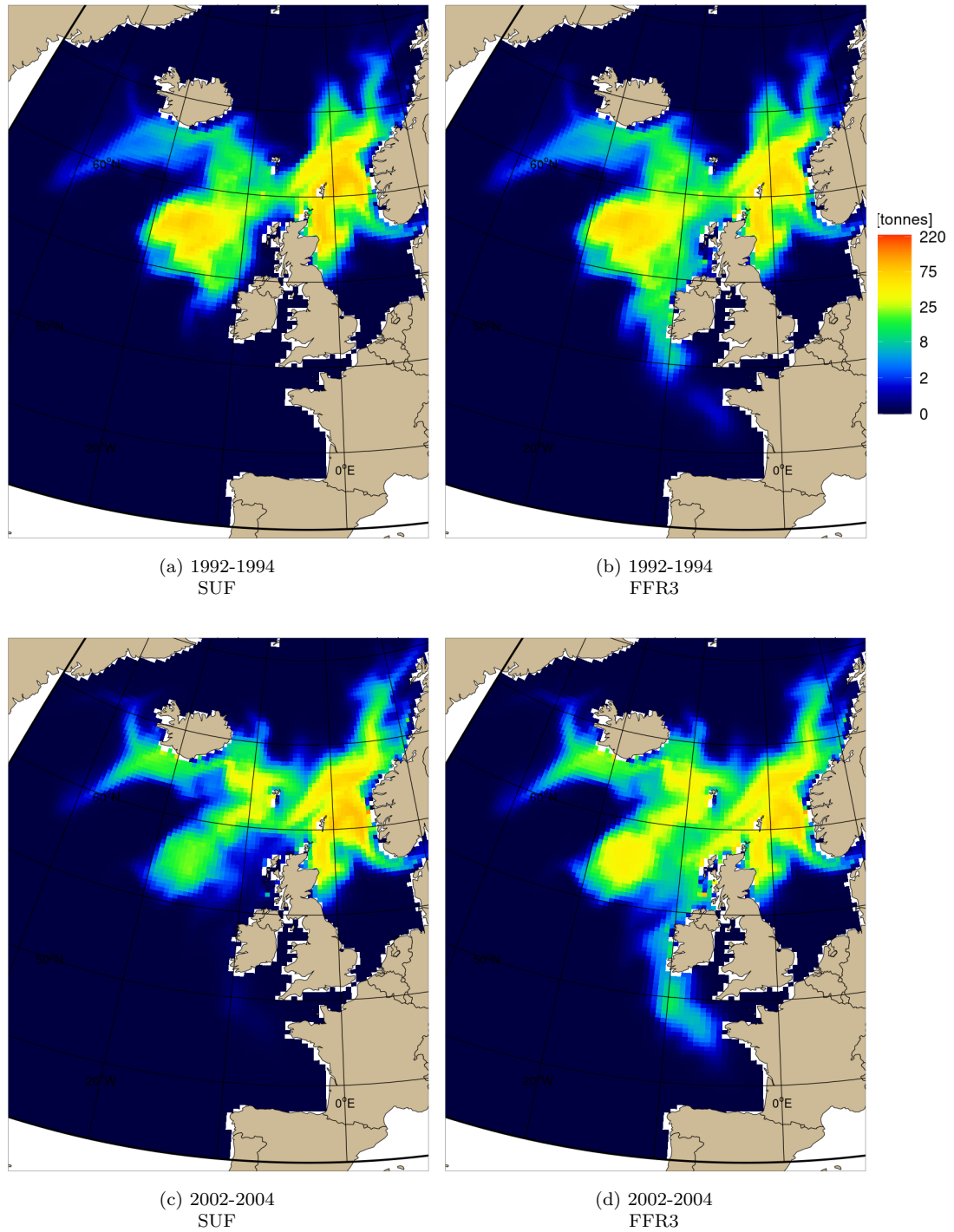
(d) 2002-2004
FFR3

Figure 9.7: Mean annual recruitment of juveniles in 1992-1994 (a,b) and in 2002-2004 (c,d) from model runs with either SUF (a,c) or FFR3 (b,d). Years 1992-1994 were marked by a strong subpolar gyre, while years 2002-2004 were marked by a weak subpolar gyre.

(a) 1992-1994
SUF

(b) 1992-1994
FFR3

(c) 2002-2004
SUF
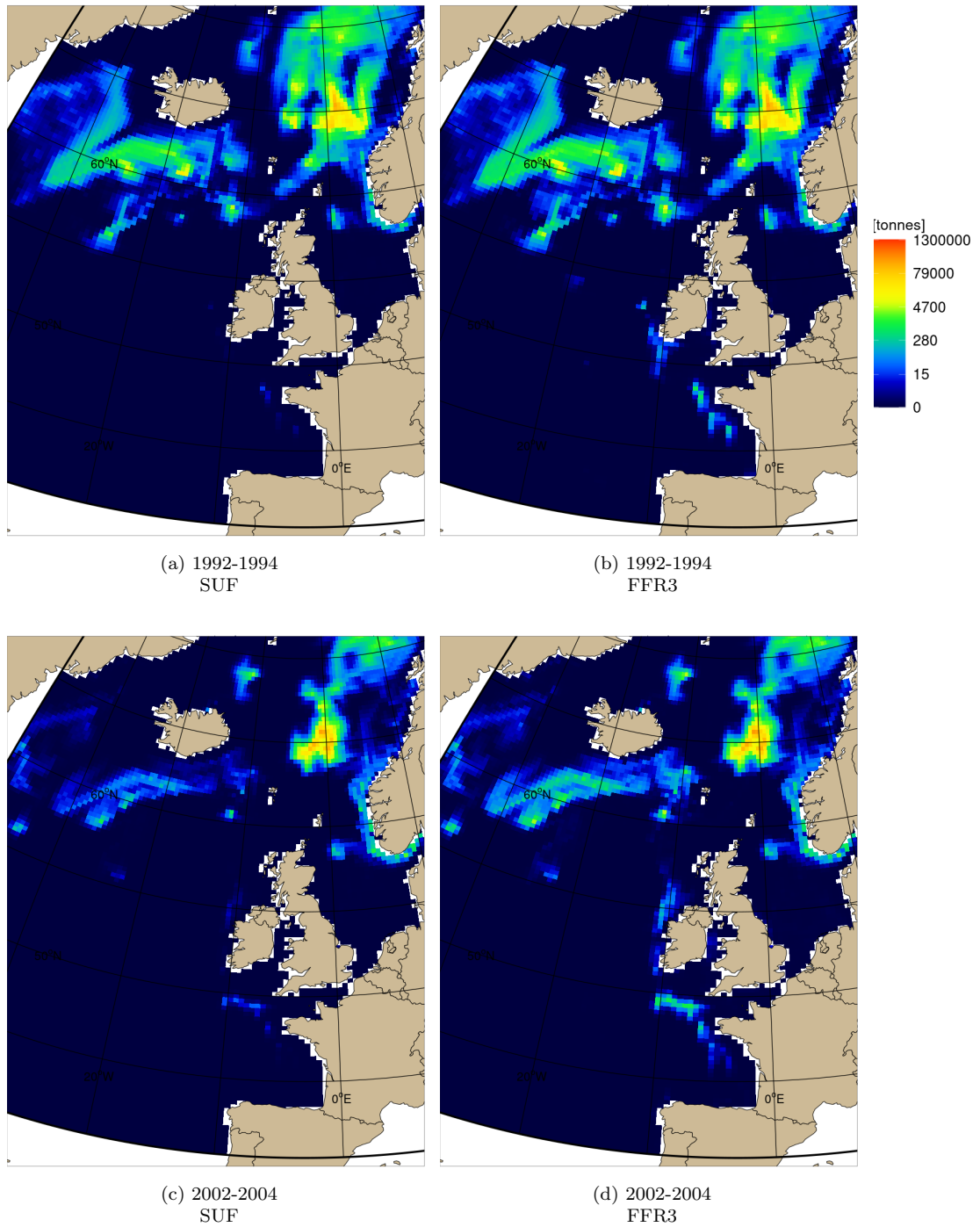
(d) 2002-2004
FFR3

Figure 9.8: Average adult distributions in quarter 3 (feeding season), in 1992-1994 (a,b) and 2002-2004 (c,d), from model runs with different fishing models: (a,c) SUF, and (b,d) FFR3. Years 1992-1994 were marked by a strong subpolar gyre, while years 2002-2004 were marked by a weak subpolar gyre.

(a) 1992-1994
SUF

(b) 1992-1994
FFR3

(c) 2002-2004
SUF
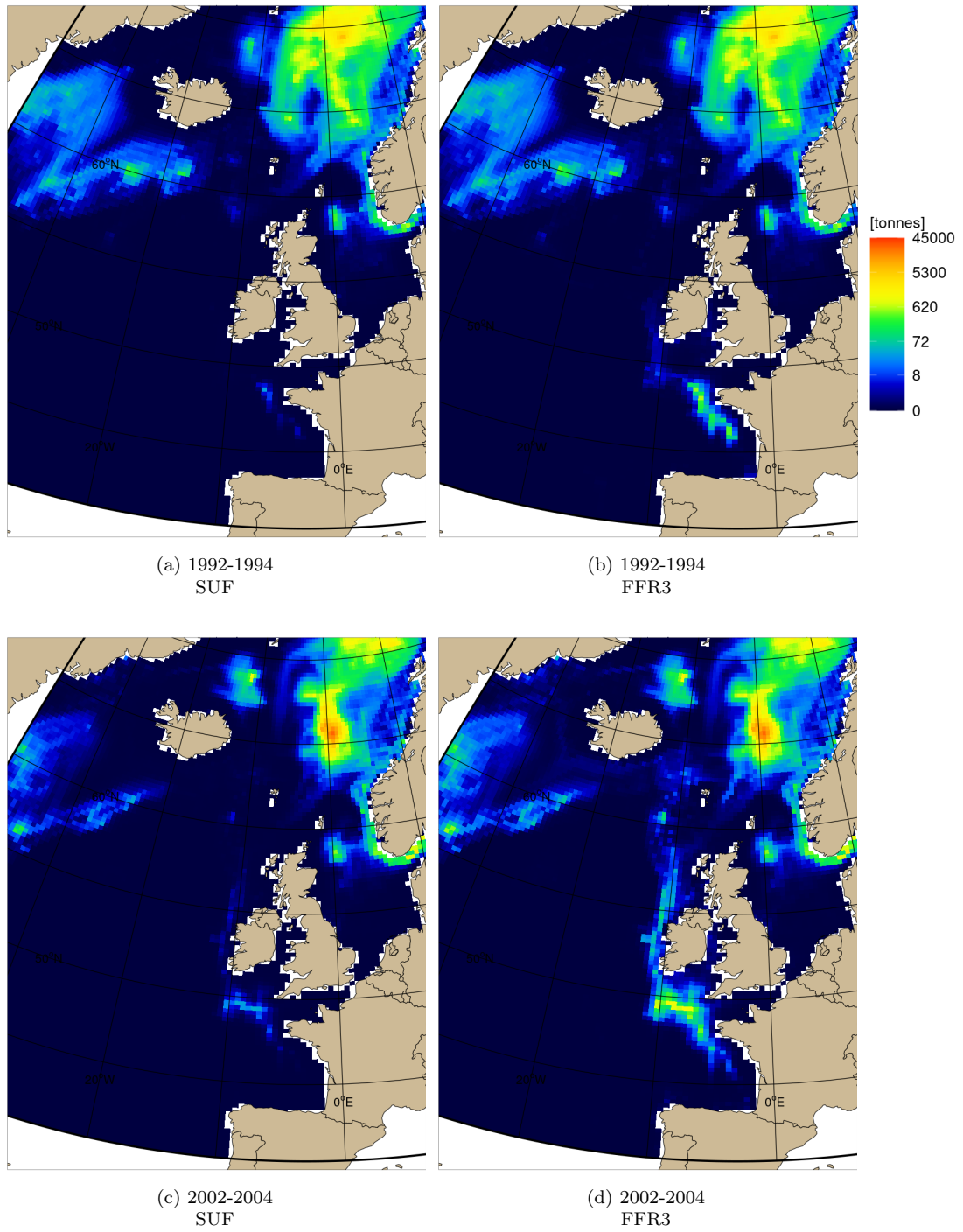
(d) 2002-2004
FFR3

Figure 9.9: Mean annual recruitment of new mature adults in 1992-1994 (a,b) and in 2002-2004 (c,d) from model runs with either SUF (a,c) or FFR3 (b,d). Years 1992-1994 were marked by a strong subpolar gyre, while years 2002-2004 were marked by a weak subpolar gyre.

Adults and maturation

During the feeding season, from July to September (third quarter), the highest abundance of adults were located in the middle of the Norwegian Sea (fig. 9.8). The areas south and south-west of Iceland were also occupied by a relatively large population. While their presence was far less important in the SUF model than in the FFR3 model, some adults resided in the southern areas, along the continental slope.

Maturation of juveniles into adulthood mainly took place in the Norwegian Sea and off the southern coast of Norway (fig. 9.9). In much smaller numbers than in the Norwegian Sea, maturing was also observed in the Irminger Sea region and off Brittany. The FFR3 model differed again from the SUF model with higher numbers of maturing events all along the British continental shelf, especially in the area between South Ireland and Brittany.

(a) Adults - Quarter 1   (b) Adults - Quarter 2   (c) Adults - Quarter 3   (d) Adults - Quarter 4

(e) Catch - Quarter 1   (f) Catch - Quarter 2   (g) Catch - Quarter 3   (h) Catch - Quarter 4
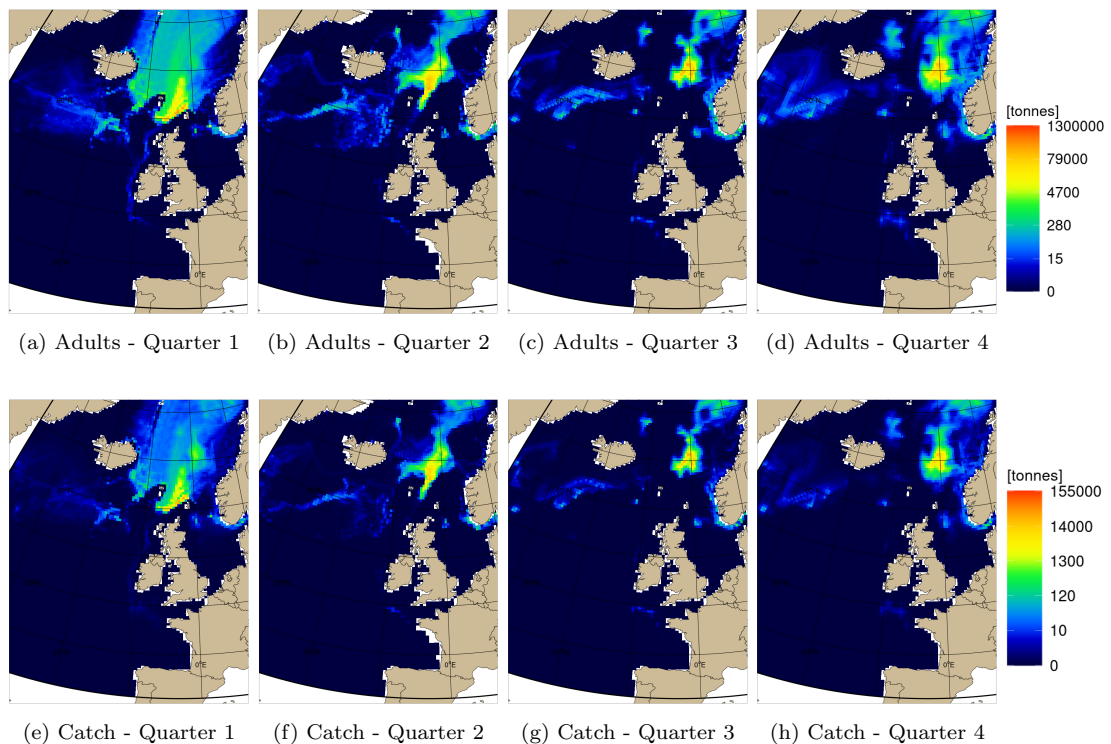
Figure 9.10: Comparison between quarterly averaged distributions of adults (a-d) and Catch (e-h) in 2002-2004 (weak SPG), from model runs with a spatially uniform fishing. In white areas, the adult population and/or catch were null.

(a) Adults - Quarter 1   (b) Adults - Quarter 2   (c) Adults - Quarter 3   (d) Adults - Quarter 4

(e) Catch - Quarter 1   (f) Catch - Quarter 2   (g) Catch - Quarter 3   (h) Catch - Quarter 4
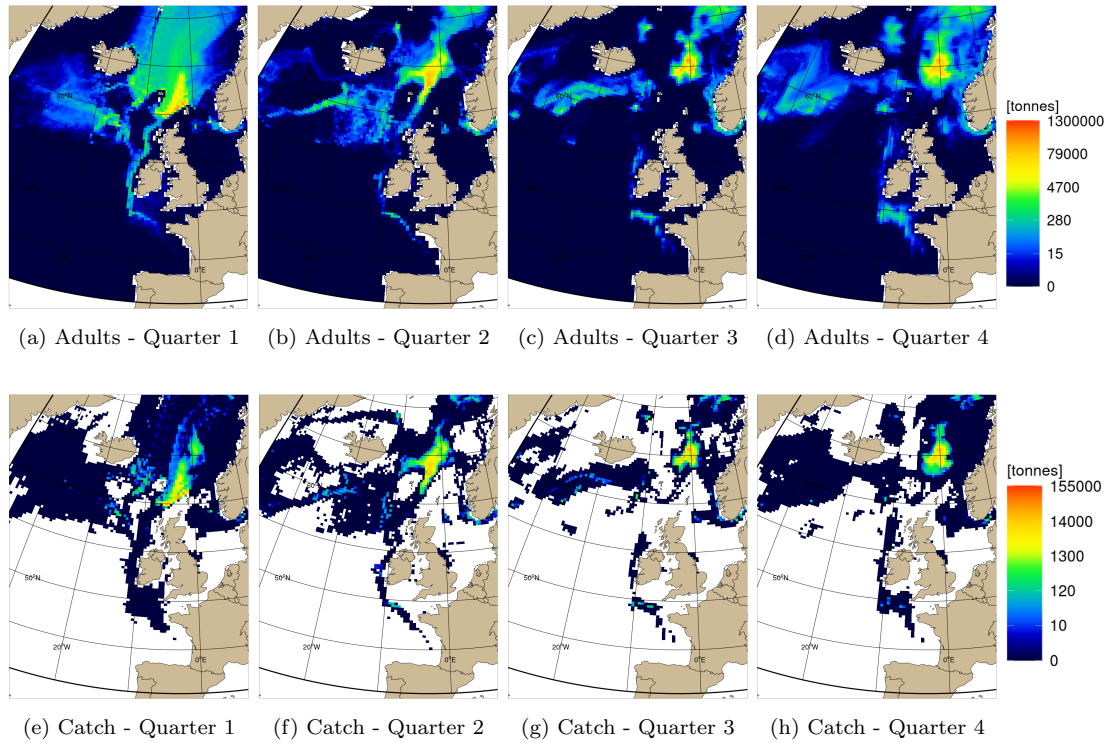
Figure 9.11: Comparison between quarterly averaged distributions of adults (a-d) and Catch (e-h) in 2002-2004 (weak SPG), from model runs with a fishing functional response type III. In white areas, the adult population and/or catch were null.

Fishing

For both models, quarterly catch were strongly following the spatial distribution of adults. In the SUF model, spatially uniform fishing meant that catch occurred quasi proportionally to the adult population in any areas where adult abundance was non-null (fig. 9.10). In the FFR3 model, however, fishing was density dependent, and catch results showed that fishing was then very restrained to the main areas of distribution in the North, especially the Norwegian Sea (fig. 9.11).

9.1.3 Length structure

Population length distributions for juveniles and adults were recorded for the whole 1988-2050 run period. According to the overall mean length distribution for both models (fig. 9.12), the modal length was 6.5 cm for juveniles and 22.5 cm for adults. When combining juvenile and adult length distributions, numbers in each length class decreased continuously and exponentially for length higher than 10 cm. This was most likely due to subjecting both juveniles and adults to
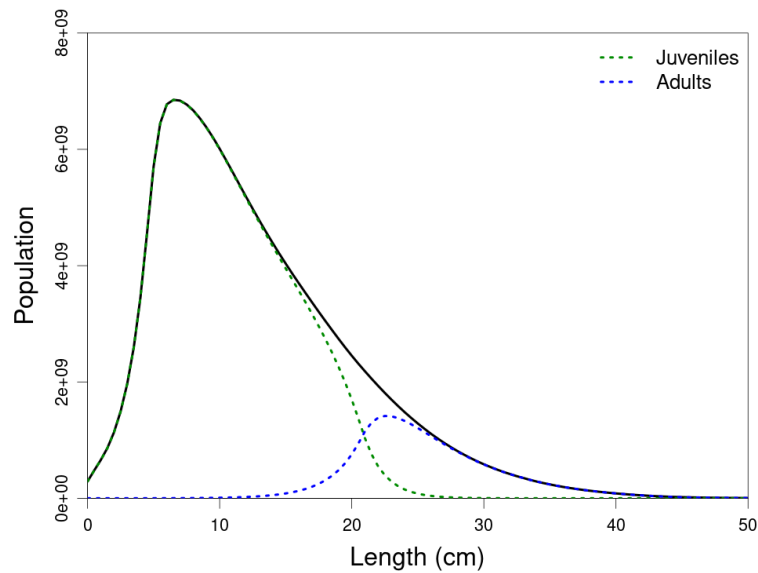
(a) SUF
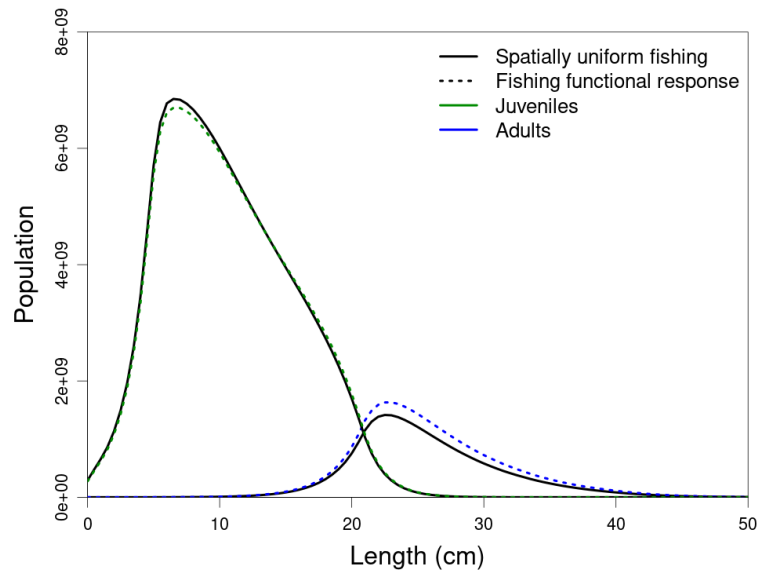
(b) Comparison

Figure 9.12: Average length distributions of both juveniles (green dotted line) and adults (blue dotted line) in the model run with SUF (a), and comparison with average length distributions from the model with FFR3 (b). In (a), the solid black line gives length structure of both juvenile and adult populations combined. In (b), both solid black lines represent juvenile and adult length distributions (separately) for the SUF model, while coloured dotted lines show results from the FFR3 model.

the same constant natural mortality.

While juvenile and adult length structure were very similar between both models, population mean numbers in lengths greater than 13 cm tended to be higher

in the FFR3 model than in the SUF model. Surprisingly, the opposite was observed for smaller lengths, especially around the juvenile modal length value (fig. 9.12.b). This effect can be explained by the density-dependent mortality function for larvae: higher adult abundance values most likely resulted in an increase of larval density in some areas, thus increasing the larval mortality and decreasing the subsequent juvenile recruitment.

Juvenile length distribution varied according to an annual cycle, as expected from the arrival of new recruits into the juvenile population shortly after the spawning season (fig. 9.13). In April, two modal length values were observed in the distribution, marking the start of the recruitment period which seemed to last until July. During this period the recruitment modal length seemed to be around 5-6 cm. After reaching a peak of juvenile abundance around July, the modal length regularly increased from 6 to 11 cm and the number of juveniles in the modal length class decreased exponentially. The drop in juvenile abundance in class lengths greater than 20 cm was caused by maturation.

The effect of climate variation on the population length structure was also studied, either with or without fishing pressure. Only the SUF model was used
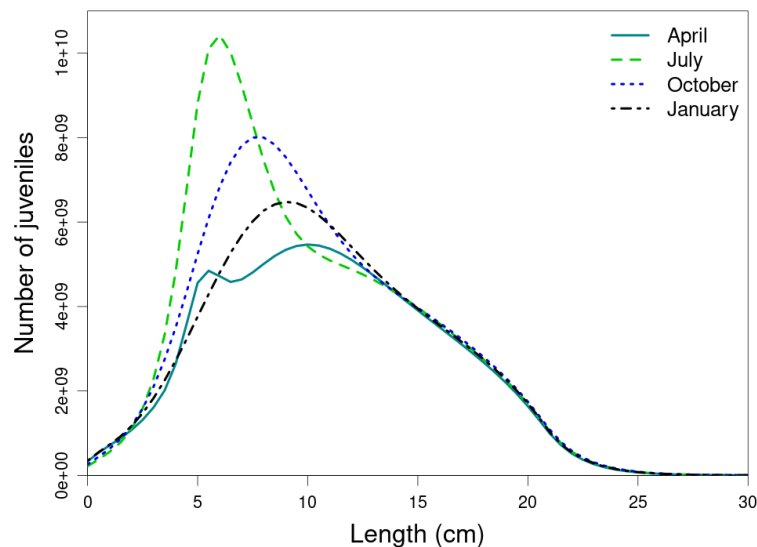
Figure 9.13: Monthly average of juvenile length distribution from model run with SUF. Length distribution are given for April (after spawning period), July, October and January.

for this comparison (fig. 9.14). From 1988 to 2019, fishing mortality values used in the model were those estimated by ICES, and varied between 0.052 and 0.537. Therefore, length distributions from the SUF model were affected by both changes in fishing activity and climate. The modal length seemed to decrease between the
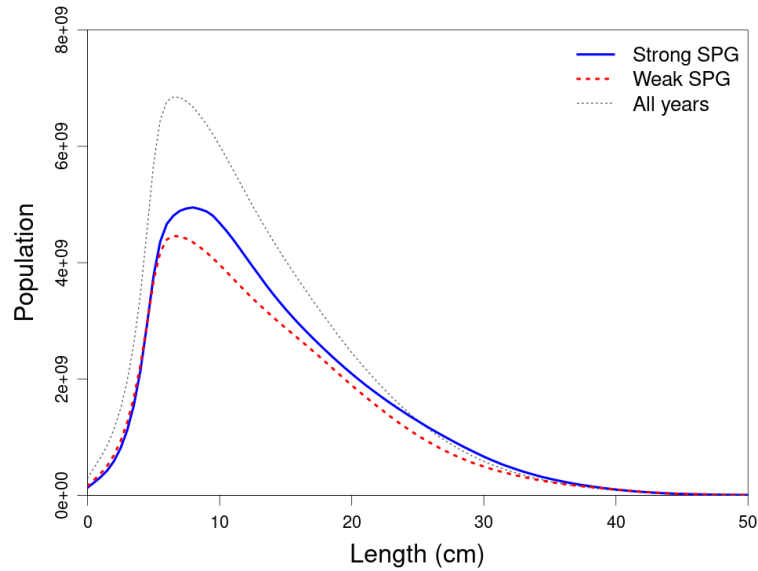
(a) With spatially uniform fishing
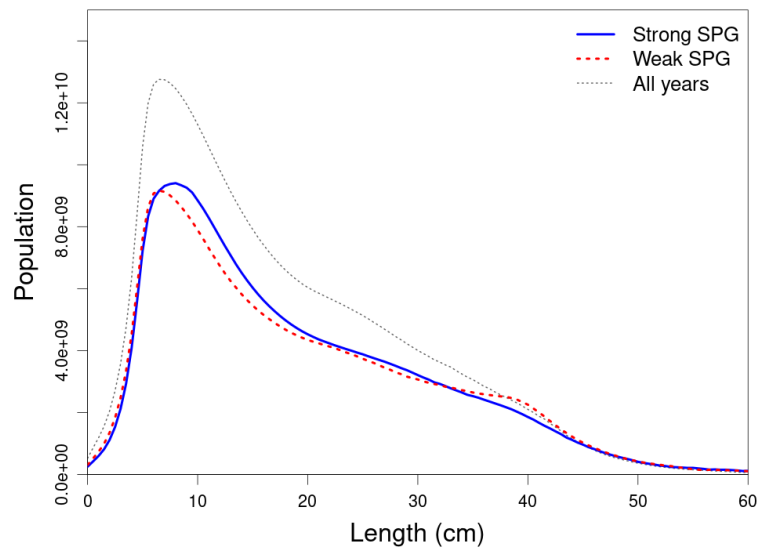
(b) Without fishing

Figure 9.14: Mean population length distribution (juveniles and adults combined) during years of strong SPG (solid blue line), during years of weak SPG (dotted red line), and over the whole 1988-2050 model run (dotted grey line), when fishing was spatially uniform (a) or not included at all in the model (b).

strong SPG regime of 1992-1994 and the weak SPG regime of 2002-2004. In the SUF model, this was also accompanied by a decrease in population abundance. Fishing pressure actually increased between 1992 and 2004, and could partially explain this population decrease. Without fishing, larger proportions of individuals were distributed in lengths between 20 and 50 cm.

9.1.4 Population predictions 1988-2050

Fluctuations of the modelled blue whiting population (using the SUF model) were rather different from the ICES estimated fluctuations of spawning stock biomass (SSB). While using the ICES estimated values of annual fishing mortality from 1988 to 2019 as the maximum fishing mortality that can be applied to an individual (depending on its length) in the corresponding year, the biomass peak observed in the ICES time series around 2003 was absent from the model variations of SSB and TSB (fig. 9.15). In fact, TSB and SSB started a long decrease in 1997 that continued until 2010. Model catch variations seemed to be slightly better at following ICES SSB values. This was due to the ICES fishing mortality values used in the model from 1988 to 2019. After 2019, the maximum annual fishing mortality was kept at a constant value of 0.335, which was also the ICES
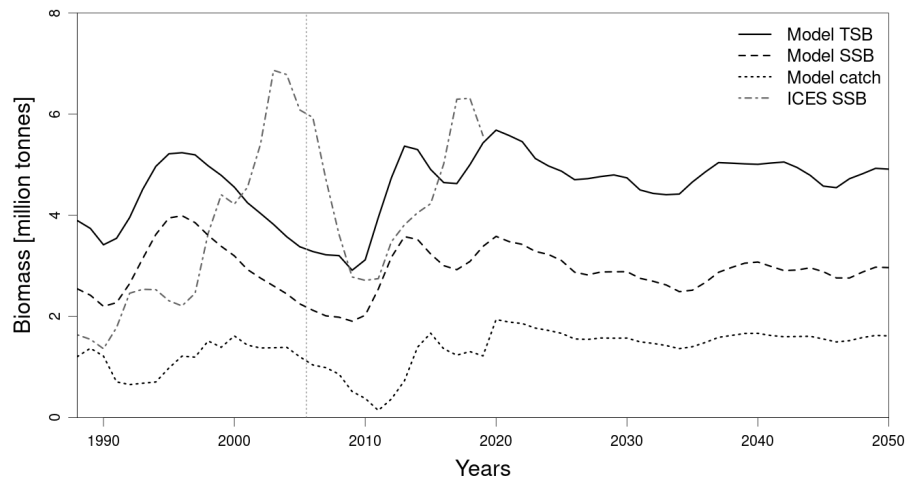
Figure 9.15: Time series of total stock biomass (TSB) including both juvenile and adults population (solid black line), spawning stock biomass (SSB) exclusively composed of adults (dashed black line), and annual catch (dotted black line), from the 1988-2050 model run with SUF. Annual values of SSB estimated by ICES (grey line) for the period 1988-2019 are represented here for comparison with the model results.
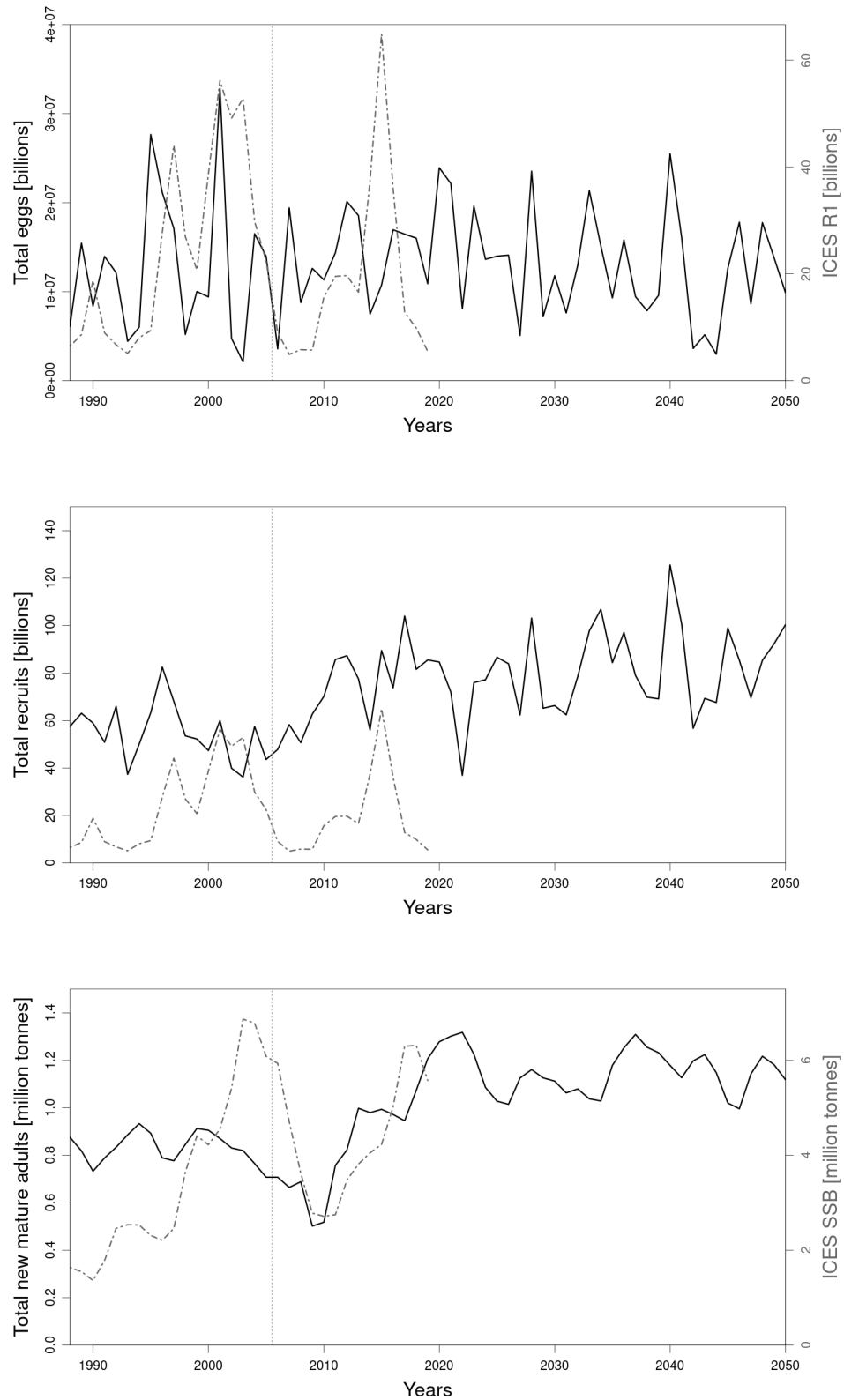
Figure 9.16: Time series of annual egg production (top graph), juvenile recruitment (middle graph) and recruitment of new mature adults (bottom graph). Comparison with ICES time series (grey) of first-year recruitment R1 (top and middle graphs) and SSB (bottom graph).

fishing mortality value estimated for 2019 (ICES, 2019b). We noticed then that biomass fluctuations tended to be far less important when keeping a constant fishing mortality. Nevertheless, biomass seemed to slowly and linearly decrease from 2020 to 2035, before experiencing a period of higher biomass values from 2038 onwards, only interrupted by a small drop around 2046. From 2020 to 2050, small variations observed would exclusively be the result of changes in physical (temperature, salinity, currents) and biological (food) conditions experienced by blue whiting.

Model time series of the total annual number of spawned eggs seemed to vary much more closely with the ICES estimated abundance values for first-year recruits than model juvenile recruitment (fig. 9.16). In the model outputs, the two spawning peaks of 1995 and 2001 seemed to almost coincide with the 1997 and 2001 peaks of recruitment obtained by ICES. However, years of low egg production appeared to affect juvenile recruitment over longer time than sporadic intense spawning events. This could be caused by the density dependent mortality function of larvae, which might reduce the positive effects of very productive spawning grounds, especially if those were limited to small surfaces: high egg production would then result in higher local densities of larvae, increasing mortality and thus cancelling any benefits for recruitment.

Except for the period 2000-2007, the annual abundance of new mature adults seemed to have fluctuations with a similar pattern to the ICES SSB fluctuations (fig. 9.16.c). ICES SSB variable is supposed to describe the population of mature adults with ages between 3 and 7, and thus the variable was very different to our model definition of SSB which encompassed the whole adult population. The fact that the variations in recruitment of mature adults tended to reflect ICES SSB variations more than our model SSB variable suggested that, in the model context, the ICES definition of spawning stock might be more representative to the population of newly mature adults than the whole adult population. When comparing both time series of juvenile recruitment and adult recruitment, a time lapse of three years seemed to exist between the observed population fluctuations, suggesting that the juvenile stage might last around three years in average. This supported the previous claim that the ICES SSB variable corresponded to new mature adults in the model, where adults likely came to maturity at an age between 3 and 5. Finally, the lack of strong population increase between 2000

and 2003 seemed to be the result of poor juvenile recruitment over this period, despite the few years of strong spawning. Causes of these juvenile recruitment variations were further investigated in the next section.

SSB time series were very alike between both SUF and FFR3 models. However, a model run performed without fishing revealed very different fluctuations compared to both models with fishing (fig. 9.17). From 1988 to 2005, SSB was relatively constant, then dropped around 2013, and was followed by an increase of nearly 10 million tonnes in 10 years. From 2025 onwards, the population biomass became quite stable again, only interrupted by a small drop around 2035. While differences between model runs with and without fishing were expected in the period 1988-2019 because of the varying fishing mortality, differences observed over the period 2020-2050 were quite surprising and might indicate that fishing had a strong effect on population recruitment and/or growth.

Comparison of adult mean length time series between the different models seemed to support this claim. From 2020 to 2050, variations in adult mean length followed very similar patterns for all model runs (fig. 9.18). Adult mean length was always significantly greater in the simulation without fishing pressure, implying that the lack of fishing mortality allowed adults to grow into larger
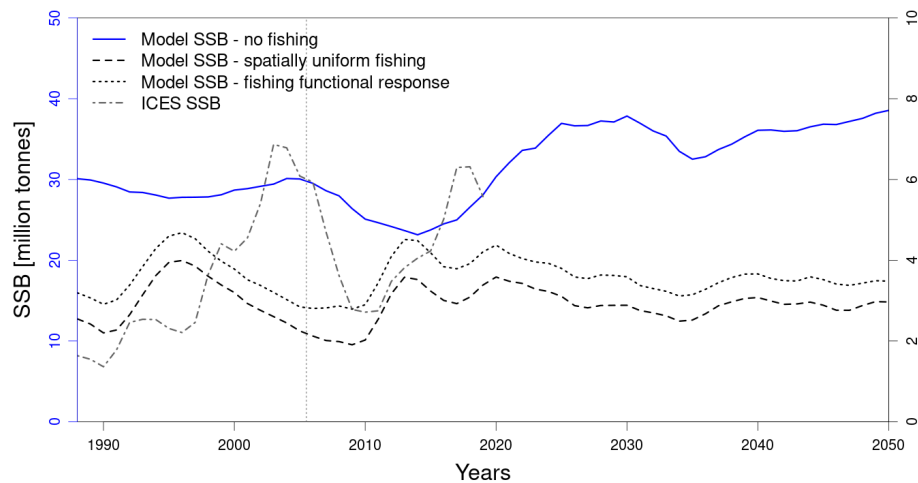
Figure 9.17: Comparison between SSB time series from the model without fishing pressure (solid blue line), the model with SUF (dashed black line), the model with FFR3 (dotted black line), and ICES (dashed grey line). The axis for the black and grey lines are read on the right side of the graph (in million tonnes).
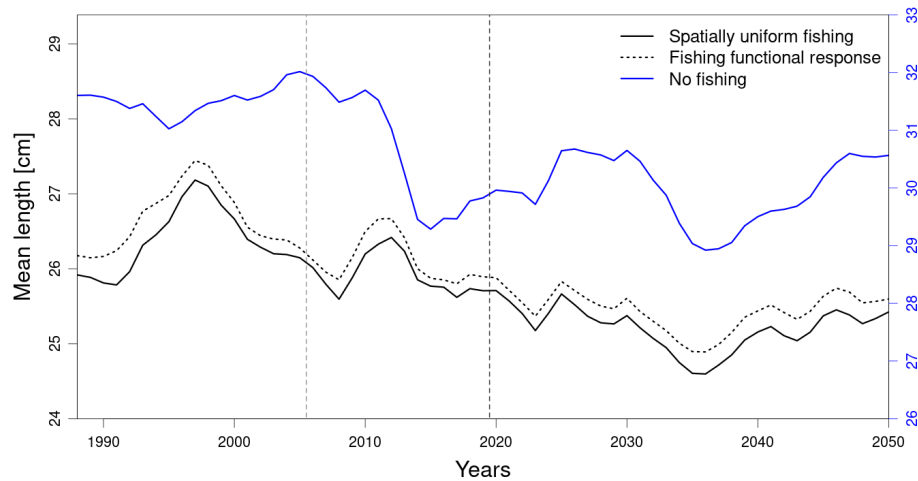
Figure 9.18: Time series of adult mean length (cm) from models with different fishing behaviours. The vertical dashed lines mark first the transition between historical and projection NEMO-Medusa outputs and second the transition between using varying fishing pressure (F_Y) from available ICES estimates (when fishing is activated) and using constant F_Y.

individuals as they lived longer. Thus, differences in SSB fluctuations observed previously were most likely caused by different recruitment response to changes in environmental conditions. As fishing tended to keep adult lengths small, spawning seasons were producing significantly less larvae than in the absence of fishing. Because of this, variations in the density-dependent larval mortality would tend to be weaker in the case of a constant fishing pressure than in the absence of fishing. It was suspected that, in the absence of fishing, any environmental effect on the larval population and subsequently on juvenile recruitment would be amplified by the fact that bigger adults would spawn greater quantities of eggs, because larger population of larvae are more sensitive to environmental changes affecting their spatial distribution.

9.2 Identifying drivers to recruitment

In this section, except for the study of migration timing effect on recruitment (sec. 9.2.2), the model was used without fishing for the whole run period (1988-2050) to try and identify biological and/or environmental drivers to recruitment independently of the fishing activity. The SUF model was used in section 9.2.2

to be able to compare with the results of the default model run.

9.2.1 Relationship between juvenile recruitment and other population indices

Variation in the population biomass seemed to be mostly determined by juvenile recruitment. Both juvenile and adult abundance were highly correlated to recruitment. The annual spawning abundance differed from adult biomass, and suggested that spawning migration success varied inter-annually. Both egg and larval population were strongly correlated to the abundance of spawning adults. However, the relationship between juvenile recruitment and spawning biomass or larval abundance seemed to be explained by a function of the logistic family (fig. 9.19). Considering its resemblance with the Beverton-Holt (BH) recruitment-stock relationship (Beverton & Holt, 1957), a curve of the BH total recruitment function was fitted to the recruitment-spawning biomass and to the recruitment-abundance of larvae scatter-plots. The residual squared error (Rse) value of recruitment for a BH relationship with spawning biomass was 27.5 billions, and
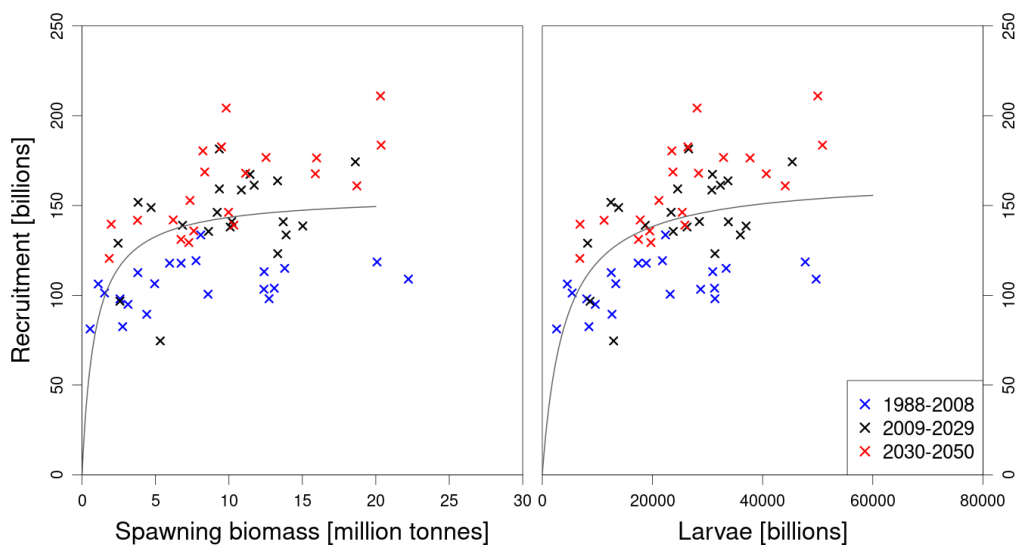
Figure 9.19: Relationship between annual juvenile recruitment and average spawning biomass (average biomass of adults spawning during the spawning period), and between annual juvenile recruitment and the annual average population of larvae. The curves represent a Beverton-Holt total recruitment function fitted to data points ($Rse \approx 27$ billions for both relationships), and colours of data points indicate different periods of the model run: 1988-2008 (blue), 2009-2029 (black), 2030-2050 (red).

it was about 26.6 billions with larval abundance. This variation was most likely caused by the spatial dimension of the model, which resulted in different local values of larval mortality as a function of local population density.

9.2.2 Effect of varying migration parameters

Since spatial dynamics might result in different recruitment response, variations of the spawning season definition were tested in the model to investigate the effect of migration and spawning timing on recruitment. Results suggested that both migration and spawning timing had strong effects on the blue whiting population growth (fig. 9.20). For the same spawning duration, shifting the spawning season about one month forward resulted in different variations of SSB depending on the year, meaning that, depending on the environmental changes experienced by the population, they could probably benefit from changing their spawning period to maximise reproduction success. This was confirmed by looking at the cumulative mean recruitment of juvenile after the beginning of the spawning season, where the later spawning period in March-April resulted in higher recruitment than the
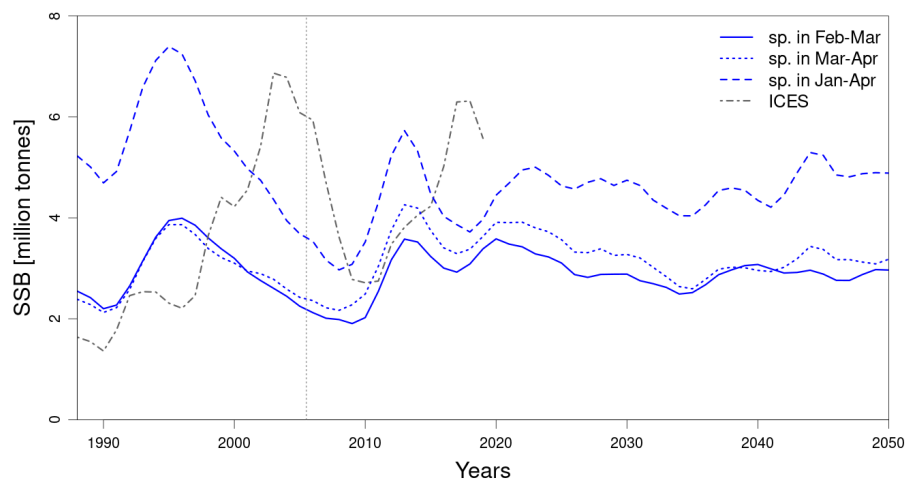
Figure 9.20: Time series of SSB for models with different spawning period definitions: default spawning period, from the 30th of January to the 16th of March (solid blue line) ; same spawning period length but starting about one month later, from the 24th of February to the 10th of April (dotted blue line) ; and a four-month spawning period, from the 5th of January to the 30th of April (dashed blue line). Spawning migration starting date was fixed to the 21st of December for all models, while the end of the feeding migration always took place 120 days after the end of the spawning period. Comparison of model results with ICES SSB estimates from 1988 to 2019 (dashed grey line).
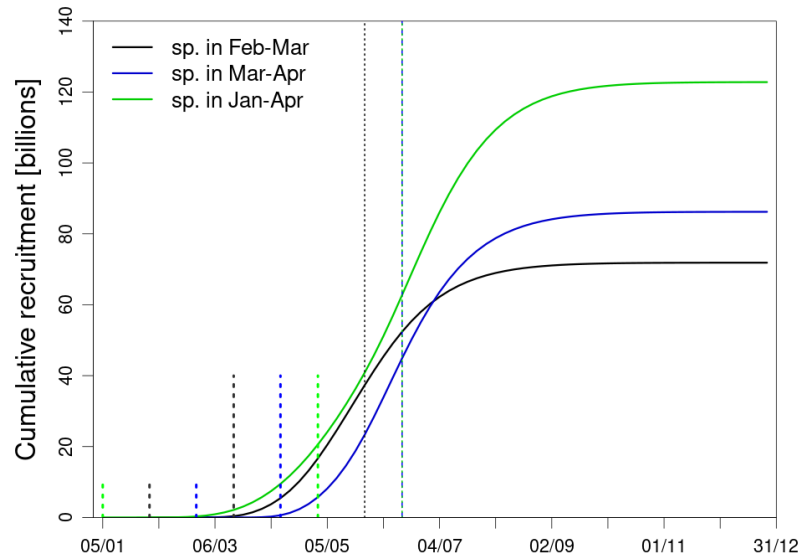
Figure 9.21: Cumulative mean recruitment of juveniles through the year for models with different spawning periods (see fig. 9.20). The shortest vertical dashed lines mark the start of the spawning period for each model, while the second short vertical lines mark the end of spawning. Other vertical lines give the time step at which 50% or more of the total annual recruitment has been reached (blue and green lines overlap each other).

model default spawning period of February-March (fig. 9.21).

Still with the same starting date for the spawning migration, the spawning season was extended this time from January to April. SSB values were much higher than in the previous spawning settings and varied with a greater amplitude (fig. 9.20). According to the fecundity function in the model, the longer was the defined spawning period, the less eggs were spawned in one time step, while the total number of eggs produced over the season stayed relatively the same. Therefore, local density of eggs and larvae were less important when spawning was spread over four months, and so was the density-dependent larval mortality. In average, higher recruitment levels were observed in the simulation with the four-month spawning period (fig. 9.21).

With the January-April spawning season definition, only a small proportion of the adult population was sufficiently close to suitable spawning grounds at the start of their migration to be able to spawn from the start to the end of the spawning season, and so only a small proportion of adults produced the total quantity of eggs corresponding to their size. This means that this spawning setting resulted in a smaller proportion of individuals successfully releasing all

their eggs during one season. However, this also allowed for more flexibility, since individuals were allowed to spawn almost as soon as a suitable spawning habitat was reached, and it improved survival of larvae because of lower local densities.

(a)

(b)
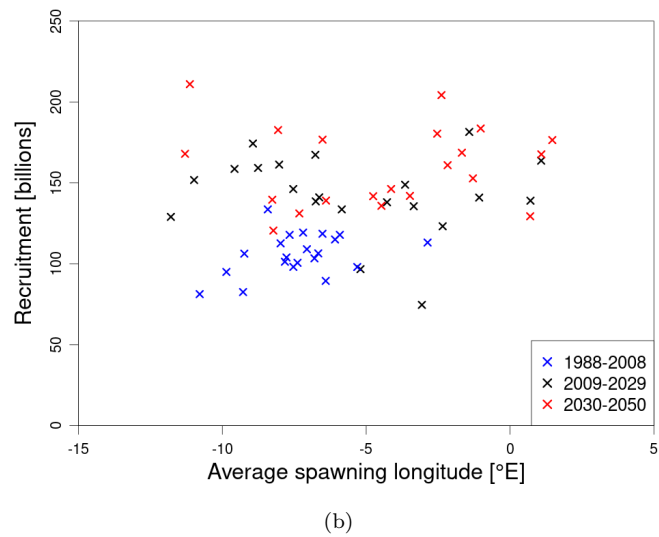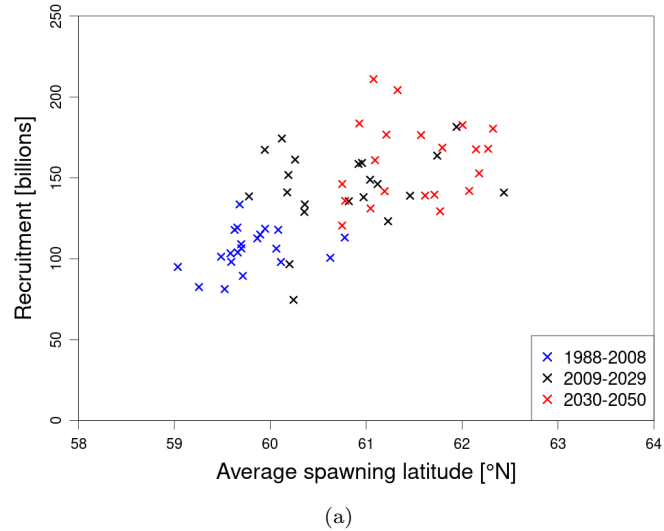
Figure 9.22: Effect of spawning area properties on following juvenile recruitment: (a) effect of spawning latitude ($r = 0.66$), (b) effect of spawning longitude ($r = 0.26$), (c) effect of the size of the spawning area ($r = 0.05$), (d) effect of the longitudinal stretch of the spawning area ($r = 0.47$). Further correlations for each time periods are given in table 9.2.
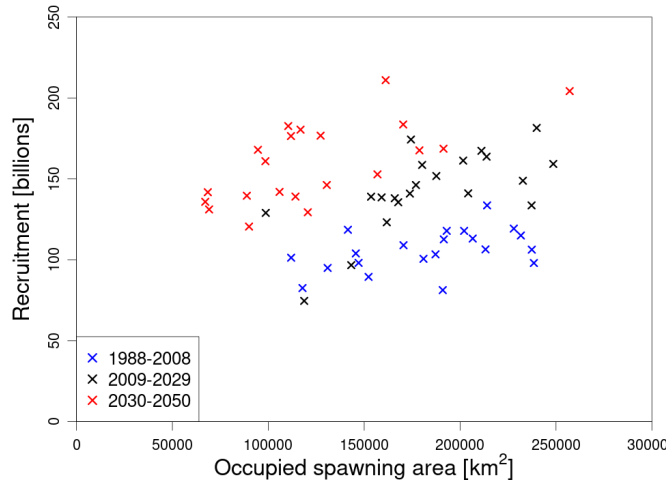
(c)
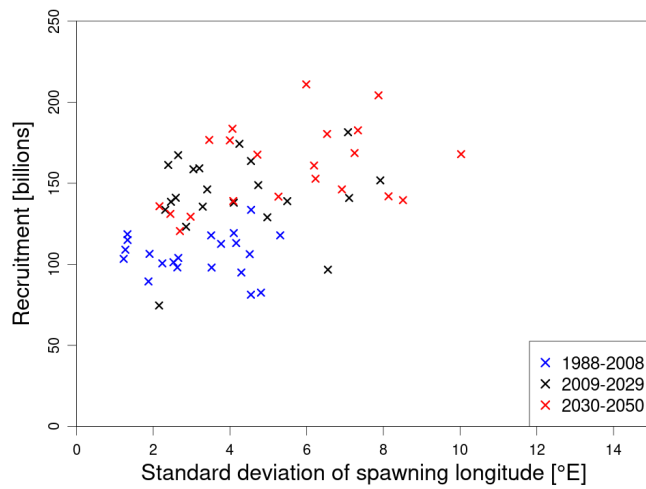
(d)

Figure 9.22: *continued.*

9.2.3 Importance of spawning location and larval drift for recruitment

In the previous section, changing the definition of the spawning season led to changes in population recruitment, and variations in the amplitude of response implied that annual variation of other spawning-dependent variables might also explain recruitment fluctuations. First, we looked for possible relationships between juvenile recruitment and spatial properties of the spawning distribution (fig. 9.22). The number of new juvenile recruits tended to be higher when the spawning distribution was located farther North ($r = 0.66$) and was more spread
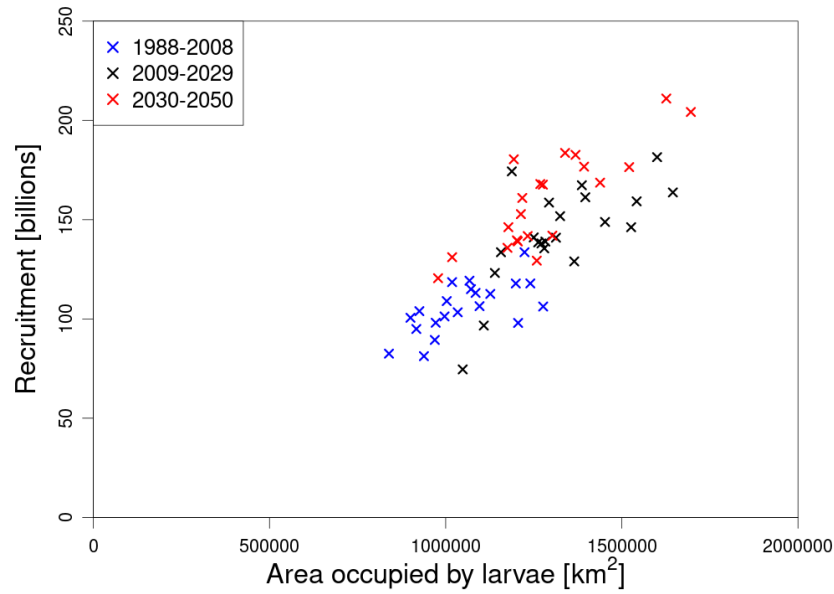
Figure 9.23: Relationship between juvenile recruitment and the average area occupied by larvae in February-March.

longitudinally ($r = 0.47$). Although relationship between recruitment and spawning longitude was weak, they also tended to be positively correlated ($r = 0.26$).

At first, variations in surface occupied by spawning adults seemed to have no clear effect on recruitment (fig. 9.22.c). However, by splitting the model outputs into three time periods (each 21 years long), significantly stronger positive correlations were observed between both variables (tab. 9.2). Similarly, correlations with the mean spawning latitude, longitude and the standard deviation of the spawning longitude tended to be less significant when focusing on each period separately. This suggested that spawning conditions changed drastically between 1988 and 2050 and resulted in a slow increase in juvenile recruitment. Mean spawning latitude, mean and standard deviation of spawning longitude seemed

Table 9.2: Pearson correlations (r) between annual juvenile recruitment and variables describing spatial dynamics of the spawning populations.

Variable	1988-2050	1988-2008	2009-2029	2030-2050
Mean size of spawning area	0.05	0.45	0.65	0.66
Mean spawning longitude	0.26	0.38	-0.14	0.01
Standard deviation of spawning longitude	0.47	-0.01	0.14	0.36
Mean spawning latitude	0.66	0.32	0.23	0.15
Mean size of area occupied by larvae	0.81	0.66	0.70	0.84

to contribute to this long-term increase, while the size of the area occupied by spawning adults seemed to have a relatively more important effect on recruitment, participating in its inter-annual variations.

Since the effect of varying spawning distribution on recruitment seemed to be limited, spatial processes taking place after spawning were also investigated. The average area occupied by larvae from February to March was chosen as index for larval dispersal and compared to juvenile recruitment values (fig. 9.23). A strong positive correlation was revealed between both variables, regardless of the time period (tab. 9.2). Therefore, it was concluded that larval drift was the most determining process for juvenile recruitment.

9.2.4 Effect of varying environmental conditions experienced by larvae on recruitment

Since the larval stage appeared to play an important role in recruitment, we wanted to pinpoint the environmental variables experienced by larvae which might affect recruitment success. With larval population dispersion already identified as a potential driver, we looked for a possible relationship between currents experienced by larvae and juvenile recruitment. Positive correlations with flow velocity ($r = 0.50$) and circular standard deviation of flow direction ($r = 0.38$) suggested that recruitment tended to be higher when larvae were in average transported by faster currents and experienced a wider range of flow directions (fig. 9.24.a and b). This supported the previous claim that larval drift conditions affected recruitment success.

Changes in the environmental conditions experienced by larvae along their drift might also cause recruitment variation. As shown by the distinct groups of data points for each defined periods in the scatter plot 9.24.c, the negative correlation detected with salinity ($r = -0.42$) was most likely due to the slow recruitment increase that took place between 1988 and 2050 as well as the spawning location shift to higher latitudes (fig. 9.22.a), thus bringing earlier in the season most of the larval population into less saline waters. In fact, if the periods 1988-2029 and 2030-2050 are studied separately, no significant relationship seemed to exist between salinity experienced by larvae and recruitment. Correlations with

temperature and food were also calculated. While food concentration experienced by larvae seemed to have a small positive effect on recruitment ($r = 0.36$), temperature alone held no significant relationship with recruitment ($r = -0.13$). However, larval growth was both food and temperature dependent, and thus the average growth experienced by freshly hatched larvae ($L_H = 0.5$ cm) over one time step was calculated and also compared to recruitment levels. Juvenile recruitment seemed to be positively correlated with larval growth ($r = 0.43$). Although the previous observation could also be made here when studying each period separately, a relationship between larval growth and juvenile recruitment was more likely: a faster larval growth would lead to an earlier juvenile recruit-
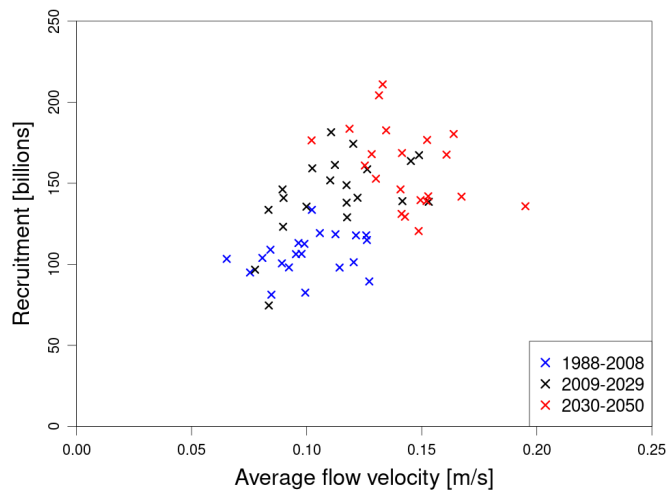
(a)
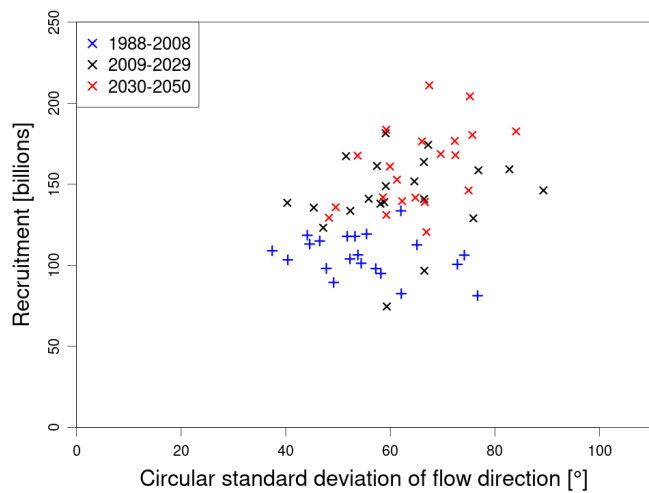
(b)

Figure 9.24: Effect of flow velocity (a), flow dispersion (b), salinity (c) and growth (d) experienced by larvae in February-March on juvenile recruitment.
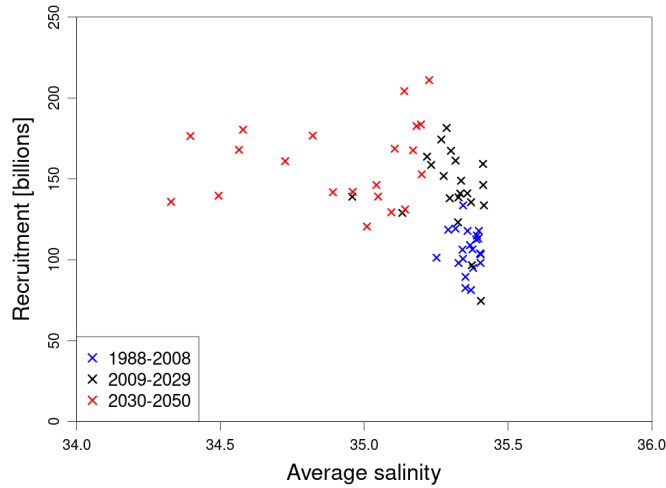
(c)
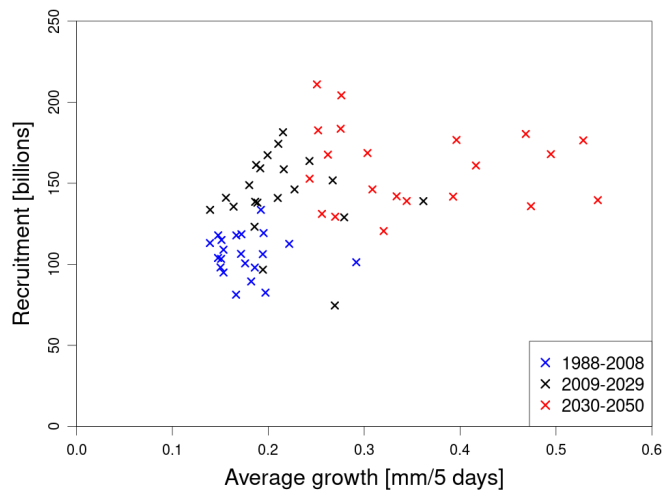
(d)

Figure 9.24: *continued.*

ment, thus reducing the time larvae are subjected to density-dependent mortality.

9.3 Population response to fishing

9.3.1 A density-dependent fishing mortality for the blue whiting stock?

The blue whiting model was tested with two different fishing definitions, either spatially uniform or following a functional response type III which, for the later, depended on local population density. In section 9.1, we already pointed out

some differences between the outputs of the SUF and FFR3 models. When fishing fleets targeted areas with high stock density, it resulted in increasing the total stock biomass, even when larval density dependent mortality parameter c_0 was increased slightly to allow for similar total catch outputs. While time series of population biomass from both models showed very similar variations, we wondered if the population response and resilience to changes in fishing pressure were also the same between models.

First, time series of mean length for each life stage provided some insight to the implication of both model designs for the population structure and its response to changing fishing pressure and environmental conditions (fig. 9.25). A consequence of a density-dependent fishing (FFR3 model) was an increase in the average length of the adult population. As larger adults produce more eggs, the number of larvae hatching simultaneously also increases, together with the local density-dependent mortality rate. This explained the shift of the mean larval lengths towards slightly lower values observed with the FFR3 model. From 1988 to 2019, when fishing pressure varied between years, the mean length of the juvenile population in the FFR3 model varied slightly differently from juvenile mean length in the SUF model. Though, after 2019, when annual fishing pressure was kept constant, juvenile mean length values in the FFR3 model were strictly
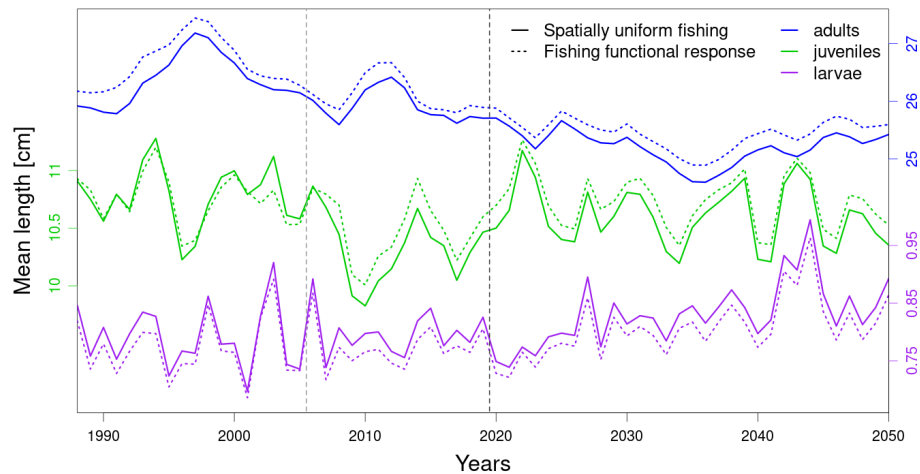
Figure 9.25: Time series of mean length of adults (blue), juveniles (green) and larvae (purple) from models with either SUF (solid lines) or FFR3 (dotted lines). Adult length is read on the right axis in the upper part, juvenile length on the left axis, and larva length at the bottom of the right axis.
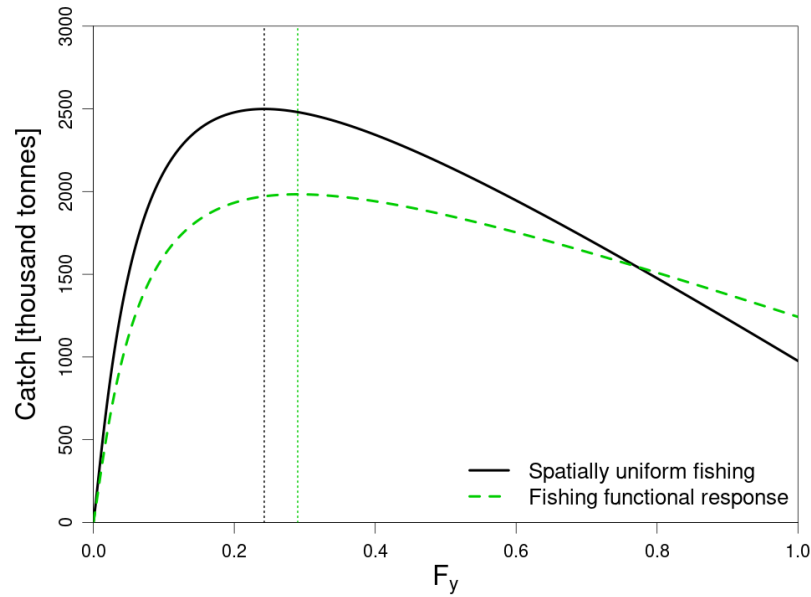
Figure 9.26: Comparison between yield curves computed from model runs with SUF (solid black line) and with FFR3 (dashed green line). For each yield curve, only the year 1992 is used and the model is run for 100 years. The 1992 model steady state is reached. Model runs are repeated for different values of constant fishing pressure F_Y between 0 and 1. In 1992, $F_{MSY} = 0.243$ for the SUF model, and $F_{MSY} = 0.290$ for the FFR3 model (vertical lines).

higher than in the SUF model. This could indicate different recruitment response to varying fishing pressure between both models. Considering that the amplitude of mean length variation between 1988 and 2019 was greater in the SUF model than in the FFR3 model, this suggested that the population response to fishing was more sensitive in the SUF model than in the FFR3 model.

To further investigate this response to fishing pressure, yield curves were computed from model simulations with environmental conditions from one chosen year only, repeated until steady state of the model was reached. For those simulations, the annual fishing pressure F_Y was kept constant. Several constant values of F_Y were tested for each year and a yield curve was inferred from the steady state catch values obtained with each F_Y. As in the example presented in figure 9.26, catch of the SUF model tended towards zero faster with increasing fishing pressure F_Y than in the FFR3 model. The maximum sustainable yield (MSY) was higher for SUF than for FFR3, and was reached at lower F_Y. Those results supported the assumption that the SUF model response to changes in fishing pressure was more sensitive. In the FFR3, the fishing stock seemed to be more

resilient to F_Y variations.

9.3.2 Influence of model parameters

As mentioned in the previous section, both fishing models seemed to have different recruitment response to fishing pressure. Model parameters were fitted so
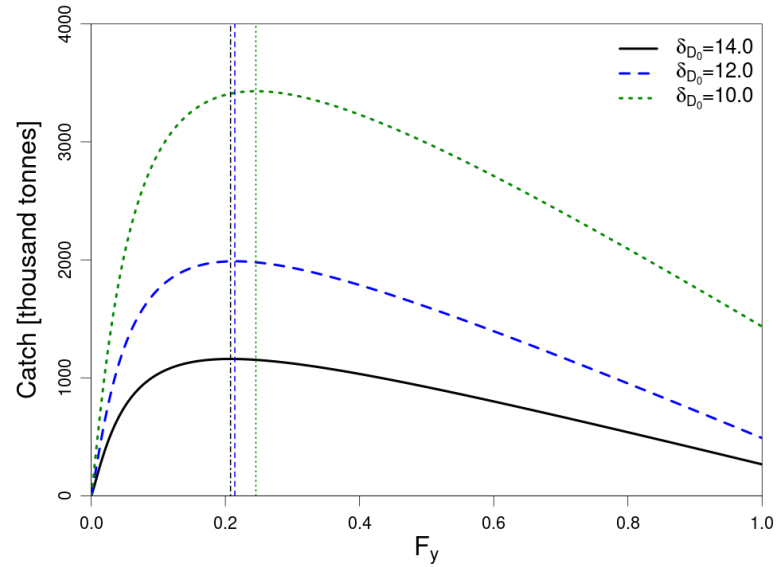
(a)
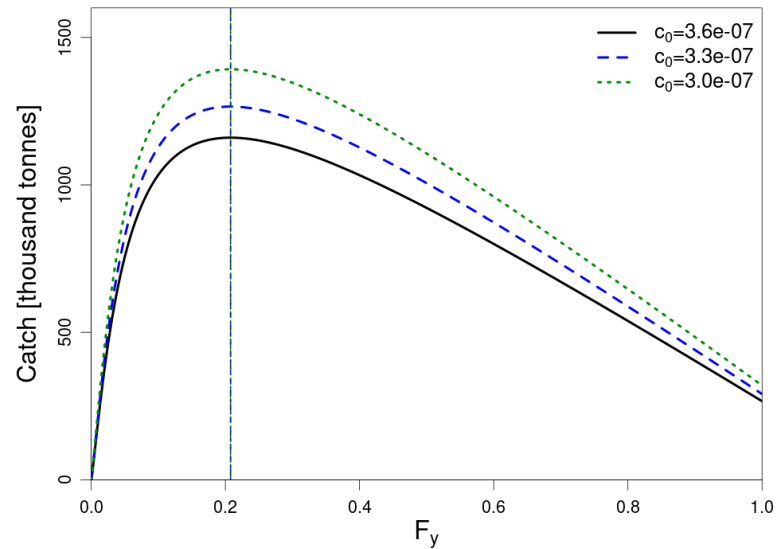
(b)

Figure 9.27: Effect of varying larval mortality parameters (δ_{D_0} and c_0) on yield curves computed with 2000's model steady state outputs. The solid black lines give yield curves in the default model setting ($\delta_{D_0} = 14.0$ and $c_0 = 3.6 \cdot 10^{-7}$). (a) MSY is reached at $F_{\mathrm{MSY}} = 0.208$ for $\delta_{D_0} = 14.0$, at $F_{\mathrm{MSY}} = 0.214$ for $\delta_{D_0} = 12.0$, and at $F_{\mathrm{MSY}} = 0.246$ for $\delta_{D_0} = 10.0$. (b) MSY is reached at $F_{\mathrm{MSY}} = 0.208$ for any c_0 parameter value.
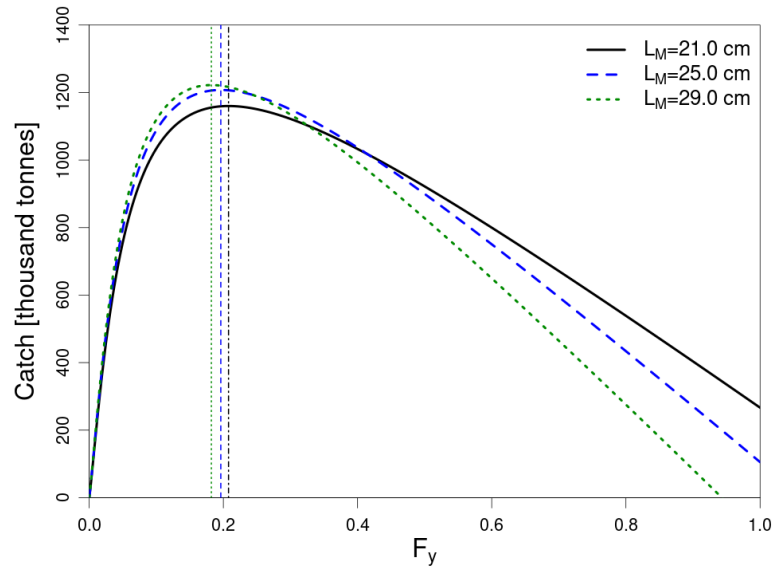
Figure 9.28: Effect of varying maturation length (L_M) on yield curves computed with 2000's model steady state outputs. The solid black line gives the yield curve in the default model setting ($L_M = 21$ cm). $F_{\mathrm{MSY}} = 0.208$ for $L_M = 21$ cm, $F_{\mathrm{MSY}} = 0.196$ for $L_M = 25$ cm, and $F_{\mathrm{MSY}} = 0.182$ for $L_M = 29$ cm.

that the model catch average was approaching the average of reported values from ICES. As a consequence, both models used different values of the parameter c_0 in the larval density-dependent mortality function (tab. 9.1). Therefore, it was wondered how different values of parameters that affect either juvenile recruitment or adult maturation might affect the sensitivity of the population response to fishing pressure. Effect of both larval mortality parameters, δ_{D_0} and c_0, and maturation length L_M on yield curves were here studied. For this section, only the SUF model was used.

Decreasing the value of the intrinsic larval mortality rate δ_{D_0} resulted in a decrease of both catch/yield value and F_{MSY}, the annual fishing pressure at which maximum yield is reached (fig. 9.27.a). While increasing parameter c_0, which controls sensitivity of the larval mortality to density changes, only decreased the yield, neither changing F_{MSY} nor the F_Y value at which the population goes extinct (fig. 9.27.b).

Varying maturation length L_M had the most important effect on the population response to fishing. Increasing L_M caused F_{MSY} to decrease, while MSY increased (fig. 9.28). But most importantly, sensitivity to increasing F_Y was enhanced with

greater L_M values, causing the extinction of the population to happen at lower fishing pressure F_Y.

9.3.3 Climate effect?

Average yield curves for the periods 1992-1994, 1997-1999 and 2002-2004 were computed in an attempt to study the effect of climate on the population response to fishing. The period 1997-1999 was considered as a transitional regime between years of strong SPG (1992-1994) and years of weak SPG (2002-2004). The average yield curves obtained seemed to indicate that the weakening of the subpolar gyre caused a reduction of the maximum average yield that can be harvested, as well as a reduction of the fishing pressure needed to approach this maximum sustainable yield (fig. 9.29).

However, during the investigation of a possible climate effect on population response to fishing, average yield curves for slightly different time period definitions that would still be representative of varying climate regime were also computed. It was then discovered that the results were very sensitive to small variations in
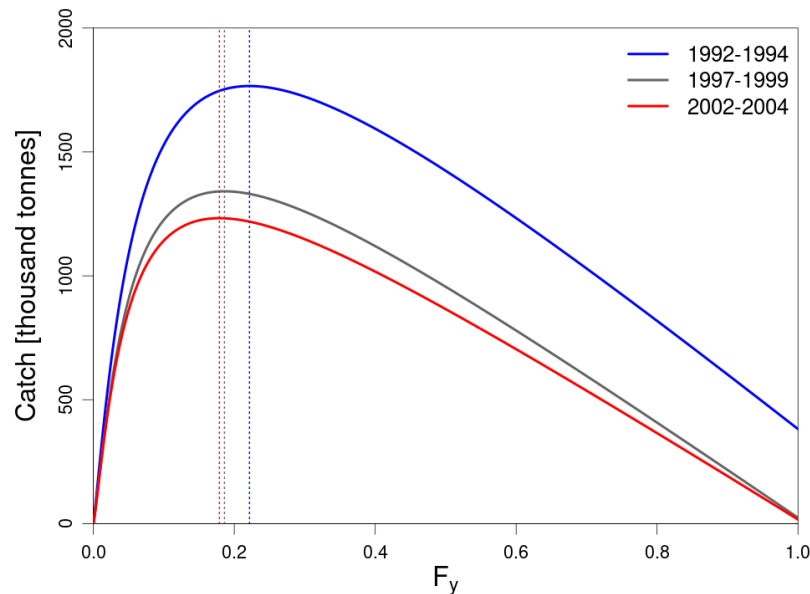
Figure 9.29: Average yield curves for different time periods which are supposed to have different climate regimes: strong SPG in 1992-1994 (blue), weak SPG in 2002-2004 (red), transitional regime in 1997-1999 (grey). $F_{\mathrm{MSY}} = 0.222$ for the period 1992-1994, $F_{\mathrm{MSY}} = 0.186$ for the period 1997-1999, and $F_{\mathrm{MSY}} = 0.179$ for the period 2002-2004.

the defined time periods (e.g. adding one to two years to the original periods, or shifting them one or two years forward or backward in time). This could lead sometimes to completely opposite results to the ones describe here, and suggested that climate was not the driver to these strong changes in response.

9.3.4 Fishery impact on population sustainability

For each year of the studied period (1988-2050), the SUF model was run to steady state for different constant values of F_Y, so as to obtain yield curves for each year. Examples of those yield curves are given in figure 9.30. They showed a wide range of yield curves, suggesting an important effect of varying environmental conditions on the population sensitivity to fishing.

Yearly MSY and F_{MSY} values were inferred from the yield curves to study fluctuations of the population sensitivity to fishing, and to attempt to comprehend the impact of fishery activities on population sustainability. MSY and F_{MSY} values were poorly correlated ($r = 0.26$), although some periods seemed to show similar trends between both variables which suggested that they might have common drivers (fig. 9.31). Unlike F_{MSY}, MSY was strongly correlated with the adult
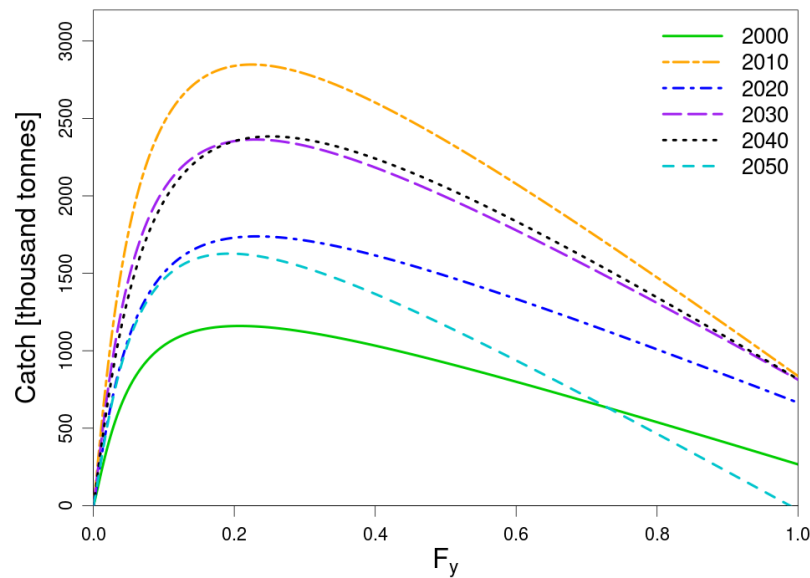
Figure 9.30: Examples of yield curves for years between 2000 and 2050. All model runs used SUF and default set of parameters.
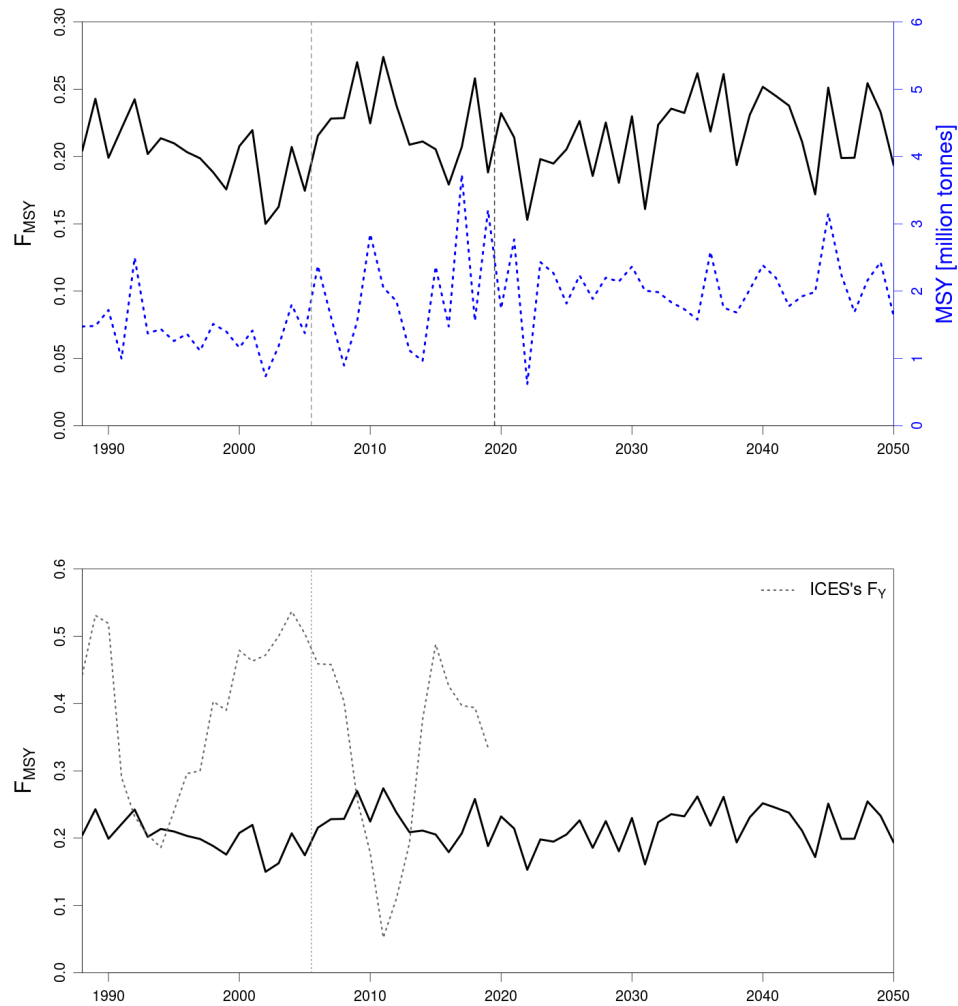
Figure 9.31: Time series of F_{MSY} (solid black line)) and MSY values (dotted blue line) from 1988 to 2050 (a), and comparison between time series of F_{MSY} and ICES F_Y values (dotted grey line) used in long-period model runs between 1988 and 2019 (b). The first vertical dashed line marks the transition between historical and projection NEMO-Medusa outputs, and the second marks the transition between varying F_Y (ICES) and constant F_Y.

and juvenile population biomass when $F_Y = 0$ (tab. 9.3). Relationships between F_{MSY} and indices of individual growth ($\bar{L}_A$, $\bar{L}_\infty$ and $\bar{k}$) suggested that the F_{MSY} value was affected by growth of both adults and juveniles. While Recruitment seemed to mostly affect MSY, it still held a mild positive effect on F_{MSY}, which could explain the similarities observed between MSY and F_{MSY} variations.

The model's F_{MSY} values were compared with the ICES fishing mortality F_Y from 1988 to 2019 (fig. 9.31). Except for a few years around 1993 and 2011, F_Y was always considerably greater than F_{MSY}. In the model context, this means

Table 9.3: Pearson correlations between MSY or F_{MSY} and variables describing the population structure and growth at steady state, when fishing pressure is null ($F_Y = 0$). B_{A+J} is the biomass of juveniles and adults combined (tonnes), R the annual abundance of juvenile recruits (number of individuals), and $\bar{L}_A$ the mean adult length (cm). $\bar{L}_\infty$ and $\bar{k}$ are respectively the mean asymptotic size (cm) and the mean growth coefficient of the VBG equation for the steady state population, computed from the average spatial distribution of both adults and juveniles and the corresponding average food and temperature conditions.

Variables	B_{A+J}	R	$\bar{L}_A$	$\bar{L}_\infty$	$\bar{k}$
MSY	0.97	0.81	0.14	0.08	-0.03
F_{MSY}	0.01	0.40	-0.58	-0.53	0.55

that the blue whiting stock was overexploited for most of the time between 1988 and 2019. The mean F_{MSY} for blue whiting was estimated at 0.21, while the annual fishing pressure was around 0.36 in average. Consequences of over-fishing the stock were suspected to be greater in years of decreasing and/or low MSY (e.g 1995-2005). In long-term simulations, it might result in a decline of the population that would last longer than the overexploitation period, since the system would have been pulled farther away from its steady state than if the theoretical MSY had stayed at high values.

After 2019, the annual fishing pressure applied in the model was constant and equal to F_{2019}. While the value was always slightly higher than F_{MSY}, examples of yield curves in that period (fig. 9.30) showed that values of F_Y between 0.2 and 0.4 would still allowed for catch values approaching MSY, assuming the distance between each year's steady state is not too high.

9.4 Conclusions

While the ICES estimated fishing mortality values were used in the spatial model, our predictions of the blue whiting population abundance differed from the ICES estimated stock fluctuations (ICES, 2019b). Some results suggested that the model's spatial properties might strongly affect recruitment. Larval drift seemed to be among the most important recruitment driving processes. In fact, recruitment was also strongly affected by parameters controlling migration timings, which were known to affect spawning distribution and success of adults (chapter 8). This was likely caused by the larval density-dependent mortality which would be at the highest over the spawning grounds.

Both fishing models tested here produced very similar long-term predictions. The main differences were found in the spatial distributions and in the population response to changes in fishing pressure. The FFR3 model allowed for better recruitment along the French and British continental shelf, while the SUF model seemed to make the population more sensitive to increasing fishing pressure above F_{MSY}. This again emphasised the role played by the population's spatial distribution on its own recruitment.

Finally, the population sustainability response to fishing pressure (yield curves) seemed to be highly dependent on individual and population growth properties, whether those were defined by model parameters (e.g. maturation length in fig. 9.28) or varying according to changes in experienced environmental conditions (e.g. L_∞ and k in tab. 9.3). In contrast, its relationship with climate variations was inconclusive.

Part V

Discussion

Chapter 10

A spatial model for the blue whiting population to understand its response to fishing and climate change

As we saw in the last chapter, the spatial population model which was built for studying blue whiting population dynamics can produce a large range of prediction outputs, from spatial and length distributions to time series of total abundance of each life stage. Considering the complexity, it can prove difficult to assess the model in its whole. However, the many model experiments performed in this work, especially those considering only the spatial component of the model, helped identify a few important drivers which caused the variability observed in the model predictions, in particular currents, food and temperature gradients.

This model incorporated three main innovative aspects. First, the entire life cycle was modelled explicitly. Many other population dynamics models simply statistically parametrize recruitment as a function of spawning stock and a few environmental indices based on historical data (e.g. with the biophysical model for predicting anchovy recruitment by Allain et al. (2007)). However, compared to the model presented here, this approach is not sufficient for future projections where the environment may change outside the envelope of past variability. Secondly, hindcasts and projection of the particular prey species of importance to blue whiting were incorporated into the model. Finally, the most innovative development was a new approach for modelling the spatial migration dynamics of the fish throughout their ocean-scale annual feeding and spawning migration cy-

cle. This was a game-changing development which allowed the impact of oceano-graphic variability on migration routes to be modelled mechanistically for the first time.

In this final chapter, the model performance at simulating blue whiting population dynamics is first discussed, focusing in turn on different aspects of the model. Then, interpretation of the model results is compared with the most recent empirical studies of the blue whiting population dynamics when those are available.

10.1 Model performance

In mechanistic population models, one can not expect to perfectly reproduce recruitment and all other population dynamics seen in nature (O'Brien, 2016). Thus, while the blue whiting model was driven by high resolution hydrodynamics and annual fishing mortality estimates from ICES stock assessment (ICES, 2019b), it resulted in different time series of stock variations than the one estimated by ICES, especially over the period 1990-2010, when the highest stock fluctuations had been recorded. And removing the fishing pressure altogether showed small population fluctuations over this period, a very smooth and slightly mismatched version of the strong increase in recruitment observed around the year 2000 (ICES, 2005), which was assumed to be caused by climate variations (Payne et al., 2012). Here, we looked for a possible explanation for this mismatch between the model and ICES estimates, and so we assessed in turn the model performance at simulating migrations, growth, larval survival, recruitment and fishing.

10.1.1 Migrations

Aspects of the migration model component were considered the most innovative aspects of the model because they represent in a process-based way the motivations for fish to migrate in particular directions and speeds at different stages of their annual cycle. By directly adding velocities of fish movements to the flow velocities used in a particle tracking model (chap. 3), the model still falls into

the category of physical transport models (PTM) while considering some modelling aspects of individual-based models (IBM) (Bauer & Klaassen, 2013). The advantage of such a model was its simplicity in implementing general swimming rules for speed and direction.

Here, direction and speed of migratory movements were completely determined by environmental clues, such as gradients and local values of biogeophysical variables (here currents, temperature, salinity, bathymetry and food). This means that the observed variability of pathways and/or final distributions is exclusively caused by environmental changes in the areas crossed by blue whiting, as it was suggested by several studies (Hátún et al., 2007; Miesner & Payne, 2018). In this context, the effect of climate change on blue whiting migration and distribution can be easily studied.

In general, the model performed well at predicting feeding distributions in summer (chap. 7). Highest population concentrations were mainly found in the central area of the Norwegian Sea around latitude 65°N and longitude 0°E, which seems to mostly agree with past biomass and catch observations in this area (Utne et al., 2012b; Pronyuk, 2019). Compared to the same past studies, a similar variability in distributions was also observed here, with the population spreading occasionally in areas farther North and into the Barents Sea.

Past IBWSS acoustic survey observations (Marine Institute et al., 2013, 2014, 2018, 2019) and other model predictions (Miesner et al., 2022) showed that the spawning population was mostly distributed along the Irish and Scottish continental shelf. In comparison, our modelled spawning population was mainly confined to the area off northern Scotland (chap. 9). Nevertheless, the model still managed to capture the spawning distribution shift towards the more western areas, here Icelandic waters, during years of weak SPG (Hátún et al., 2009b).

A particularly challenging aspect of the migration modelling was in representing arrival at a suitable habitat and the termination of movement (chap. 3, sec. 3.2.4). In the model, dispersive movements take over migratory movements when reaching an area with suitable conditions, which results in the population spreading itself over this area and its close surroundings. In this context, a spatial discontinuity in the distribution of suitable areas was shown to be an obstacle to the population dispersion over the entirety of the habitat. This was espe-

cially visible with the spawning migration, where adults stopped in areas over the Iceland-Faroe Ridge when these were suitable, and dismissed altogether more southern areas like Rockall and the Irish continental shelf (chap. 8).

This limitation in the migration model has consequences for the final model (once population migration and growth are combined), since both spawning and feeding migrations are successively used, together with larval drift. If suitable southern and western spawning areas can not be reached because of the model design, this may result in the wrong dominant feeding migration patterns and in the absence of important larval drift patterns, leading to errors in population recruitment and growth. This could well be one of the main reasons for the difference between the model SSB predictions and ICES estimates.

In the future, an idea of model improvement could be to think of a density-dependent function which would compute a probability of switching to dispersive behaviours around suitable habitats as a function of population density in the area reached. As a consequence, it might enable a part of the migrating population to reach farther suitable habitats and to produce more realistic population distributions.

10.1.2 Juvenile and adult growth

Another important aspect of the model is how individual growth is computed. Growth is represented by the von Bertalanffy function which has two main parameters, the maximum growth rate k and the maximum body length L_∞, often implemented as constants in population models (Speirs et al., 2010; Andrews et al., 2006; Heath & Gallego, 1998). However here, considering first principles, the VBG parameters vary with environmental variables: k is a function of temperature, while L_∞ depends on both temperature and food. This means that the average growth of an individual in one year is highly dependent on successfully reaching suitable feeding habitats between spring and summer, and on the quality of these habitats. Since feeding migrations were specifically designed to lead most juveniles and adults successfully to areas that would maximise their growth, the model variations of individual growth are again very dependent on the performance of the feeding migration model. Therefore, it is unlikely that

changing growth parameters would lead to major changes in the predicted pattern of population fluctuations, and the simplicity of the growth function may be why the model response to environmental variability is smoother than in reality.

Spatial, seasonal and long-term variations of food were predicted by a machine-learning algorithm (random forests) trained on CPR data. While predictions of food distribution were mostly satisfactory (chap. 5), it is important to point out that the random forest performance at predicting plankton distributions will likely drop considerably with time, the more distant the data is from the model training period, especially in a context of climate change (Brun et al., 2016).

Blue whiting prey selectivity was estimated from stomach records from either the British and French continental shelf or Icelandic and southern Norwegian waters (chap. 5). It is possible that the selectivity index values were less consistent with blue whiting diet in areas which were poorly represented in this dataset, especially the Irminger Sea, as it seemed to be one of the most suitable areas for feeding predicted by the random forests.

In a very recent study, Post et al. (2021a) observed that blue whiting in the Irminger Sea would preferably feed on euphausiids, copepods and amphipods in that order. However, copepod species involved were mostly *Calanus hyperboreus* and *Paraeuchaeta* spp., while *C. finmarchicus* was almost absent in the diet, which supported the claim that blue whiting mostly dismiss *C. finmarchicus* as a prey (chap. 5). Although the blue whiting food variable could still be improved by future studies of the blue whiting diet, for example by considering more copepod species, the present variable seemed to be already well adapted to blue whiting feeding behaviours.

10.1.3 Survival in early life stages and recruitment

Population growth was mostly controlled by the larval density-dependent mortality function (chapter 2). Density-dependent mortality functions for other life stages were also tested alone or combined, but they either removed population variability or added too much complexity into the model, and thus they were abandoned. A Beverton-Holt relationship between recruitment and spawning biomass emerged from the long-run outputs of the model, although it was par-

tially hidden in the noise caused by interannual environment variability (chapter 9). By comparison, Ekerhovd (2008) who failed to fit this relationship to ICES data in the past (ICES, 2007), suggested that recruitment was likely affected by numerous environmental factors which might make the detection of such relationship very difficult. In fact, Munch et al. (2018) showed that recruitment variations was not always well explained by changes in stock biomass. According to our model, the success of the spawning migration could well be involved in recruitment variations, since no stock-recruitment relationship could be observed when considering the total adult biomass instead of the spawning biomass.

The larval density-dependent mortality function can describe either competition among larvae or predation which would both increase with larval aggregation. This is the reason why mortality would be at the highest during spawning events, since all larvae would hatch in the same area before being dispersed and transported by currents. Because of this, the fitted model value of the parameter controlling the sensitivity of larval mortality to density variations is mostly explained by how dense the larval population is around the spawning period.

According to the model results, increasing the length of the spawning period can be beneficial for recruitment, since it reduced the number of eggs spawned at the same time, thus reducing considerably the mortality experienced by larvae over the spawning grounds (chapter 9). Moreover, results suggested that recruitment variability was increased, probably due to increased variability in larval drift and in the subsequent quality of nursery habitats. Together with the strong positive correlation observed between recruitment and the average area occupied by larvae over the spawning period, this suggests that recruitment is strongly affected by spatial distribution of larvae.

The fact that recruitment is also strongly affected by spatial dynamics supports the idea of model improvement mentioned at the end of section 10.1.1. This is also consistent with the study from Cadrin et al. (2019), which pointed out the importance of including appropriate spatial dynamics in models to improve recruitment estimates. In the blue whiting case, increasing dispersive behaviours around suitable spawning habitats when those are already occupied by high quantities of adults, and thus increasing the coverage of the spawning distribution, is

likely to result in lower larval densities over the spawning grounds. During the fitting stage of the blue whiting model, it would mean that the parameter of the density-dependent mortality function can be increased to balance with the lower maximum of larval density, which in turn would likely result in a higher amplitude of recruitment variations.

Furthermore, considering the possible strong predation of blue whiting larvae by mackerel (Payne et al., 2012) and blue whiting adults (see chapter 5), it might be interesting to also consider other larval survival functions simulating spatial dynamics of predators, as a way to improve recruitment predictions in the model (Akimova et al., 2019).

10.1.4 Fishing models

Because of the spatial dimension of the model, it was important to consider the spatial distribution of fishing effort and how to implement it in the model. Records of blue whiting catch distribution showed that fishery areas were similar to the population distribution areas, following seasonal migrations (chapter 6). Thus, assuming that fishing fleets follow population movements, we expected that either the blue whiting population was always affected by the same constant fishing pressure (spatially uniform distribution of the fishing rate - SUF model) or fishing pressure was increasing with population density (functional response type III equation - FFR3 model), representing a fishing fleet concentrating their fishing effort in high fish density areas (chapter 2). The different spatial distribution of recruitment observed between the two fishing models tested in this work suggested the importance of the choice of the fishing strategy represented by the model for recruitment (chapter 9). Like with FFR3, a fishing activity pressure that varies in space will likely result in higher recruitment in some areas which are 'connected' to spawning areas with low population densities (e.g. southern continental shelf areas, off Ireland).

Both fishing models assumed that the fishing fleet always knows where to find the stock. However, in reality, fishing fleets will most likely target areas where they fished in the past which resulted in high catch success. Moreover, fishing effort is likely decreasing with the distance to the coast because of the increasing fuel consumption by fishing boats with increasing distance to harbours. Both

fishing effort and experience were ignored in this model. However, some implementation ideas involving those two notions could be tested in the future.

For example, I started implemented a fishing functional response type III equation (chap. 2), whose parameters p and B_H would vary according to the past yield experienced in a local area. We could thus imagine a power p close or equal to 1 when areas have never been experienced in the past or when fishing success has been low for some time. This would switch the functional response type III to a functional response type II, and would then describe a fishing effort which is not targeting specifically areas with high population density - because those are unknown - but is increasing logarithmically with population density since the fishing fleet is 'learning' where to fish.

10.2 Blue whiting population dynamics

10.2.1 Spatial dynamics and recruitment

The fact that recruitment showed a strong positive correlation with the average surface area occupied by larvae but much less so with the spawning surface area implied that larval development success was positively affected by the larval dispersion around the spawning areas (chapter 9). In fact, Vikebø et al. (2007) showed with their model that the fitness of the larval population (growth and survival) would increase when drifting patterns become more variable in response to changes in the environmental conditions experienced by larvae. This supports the importance of larval drift variability for larval development.

Average larval distributions presented in chapter 9 showed that larvae were spawned over the Hatton Plateau, the most western side of the Rockall area, while we know from spawning migration experiments (chapter 8) that northern or southern adults could almost never reach such area during those years, especially in 2002-2004. Therefore, the only explanation for the presence of larvae over the Hatton Plateau is the existence of spawners coming from western areas. In the model, adult maturation events also took place regularly in the Irminger Sea and South of Iceland, which confirmed this spawning origin. Moreover, the presence of a population in these areas has been recently confirmed by the study from Post et al. (2019), who also suggested that adults from west of Greenland

would still come back to the most western areas of the main spawning grounds.

The majority of juvenile recruitment events took place in the area between Scotland and Norway, in the northern North Sea, or over the Rockall Plateau. In years with stronger recruitment, larvae tended to be more spread all over the Rockall area and towards southern Icelandic waters. Results suggest here that western larval drift is positive for blue whiting recruitment, together with repeated spawners from the Irminger Sea. In parallel, according to the FFR3 fishing model outputs, southern recruitment was associated with a larval distribution all over the British continental shelf. However, although our own larval drift experiments (appendix B) and those from Svendsen et al. (1996) showed a strong southward drift, the later suggested that low productivity in the South would probably result in low recruitment. This is probably the reason why recruitment in that area tended to be much lower than in northern or western areas, even with the FFR3 model.

Following the important recruitment in the southern Norwegian Sea, the results suggest that juveniles reached the northern Norwegian Sea and potentially the Barents Sea by doing a combination of dispersive and small feeding migratory movements (chap. 9). The northern Norwegian Sea constituted a pool for new mature adults. In years of strong recruitment, this northward drift and/or migration of larvae and juveniles might be slightly faster. These predictions seem to support observations from Heino et al. (2008) which showed a strong positive relationship between the incidence of young blue whiting fish in the catches performed in the Barents Sea and the total recruitment of the North-East Atlantic stock.

10.2.2 Effect of fishing

As mentioned previously, the different fishing models resulted in different spatial distributions, especially in the southern region, where FFR3 tended to improve juvenile and adult recruitment (chap. 9, fig. 9.6 and 9.9). This shows that using different fishing strategies can significantly affect population recruitment locally. Furthermore, it will have a long-term effect on the population sustainability and its resilience to increasing fishing pressure. This is the reason why the population response to changes in fishing pressure was more sensitive in the SUF strategy

than in the FFR3 strategy (chap. 9, fig. 9.26). Both evidences combined tend to suggest that the presence of a consistent southern recruitment could be essential for the population resilience to overexploitation.

The population response to fishing seems to be also strongly affected by the population growth properties. In particular, increasing either the intrinsic larval mortality rate or the maturation length will result in increasing sensitivity of the population sustainability to changes in fishing pressure. Furthermore, juvenile and adult growth seem to play an essential role in determining the population annual sensitivity to fishing pressure. Thus, a fast growth but a low asymptotic length were favourable to population resilience in response to fishing increase. This was likely due to environmental conditions leading greater numbers of juveniles to become mature at smaller length, potentially reducing the fishing pressure applied to them, while being able to reproduce.

The annual yield curves predicted with the model also suggest that the relationship between recruitment and fishing depends on two factors. First, recruitment directly affects fishing catch success, with annual MSY strongly correlated to annual recruitment. Second, the level of population sensitivity to fishing activity impacts recruitment, which can be dramatic in times of overexploitation ($F_Y >> F_{MSY}$): if F_{MSY} decreases, it will result in an acceleration of the stock decrease over this period, which can last even after F_{MSY} increases again or fishing pressure decreases (low resilience of the stock). In the long-term predictions, this was for example observed over the period 1995-2010 (chap. 9).

10.2.3 Effect of climate variations

In general, climate effect was mostly visible in the variations of feeding migration pathways and spawning distributions (chap. 7 and 8). The feeding and spawning migration experiments were mostly agreeing with past claims of the climate effect on blue whiting spatial dynamics (Hátún et al., 2007, 2009b). In years of strong SPG, successful northward feeding migration pathways were mostly restricted to the Faroese-Shetland Channel and initiated by adults from the continental shelf area, while any individuals present in western areas would tend to migrate westward. The westward migration is also present in years of weak SPG, however it is also joined by a northward migration taking the route west of Faroe Islands.

Pre-spawning migrations from Norwegian Sea adults resulted in more northern spawning distribution and spreading more towards Iceland when the SPG was weakening. The fact that this mechanistic process-based migration model resulted in emergent model behaviours agreeing with empirical assumptions added to its performance success (sec. 10.1.1).

Although most distribution patterns in the final model were similar to those observed in the migration experiments (chapter 9), the population had a more western spawning distribution in years of strong SPG than in years of weak SPG, which seems to contradict observations from Hátún et al. (2009b). This result would probably change once the pre-spawning migration model is improved to give a bit more flexibility to adults in their final choice of spawning areas. Apart from this, other interesting population movement patterns were observed with the full blue whiting model. Thus, it seemed that northward drifting and migrating juveniles were reaching areas farther north in the Norwegian Sea in years of strong SPG than in years of weak SPG. Heino et al. (2008) suggested that climate variation might indeed affect the inflow of young blue whiting fish into the Barents Sea. Furthermore, more adults seemed to be present in the Irminger Sea in years of strong SPG. While Post et al. (2021b) also showed climate variability in distribution and abundance of blue whiting in Greenland waters, opposite trends were observed. This contradiction might be again the result of missed suitable spawning areas in years of weak SPG due to the spawning migration model design.

While recruitment seemed mostly unaffected by temperature or salinity changes, the slow recruitment increase between 1988 and 2050 suggests that the weakening of the subpolar gyre combined with the northward shift of the spawning grounds has a positive effect on recruitment. MSY Catch projections between 2015 and 2050 under the RCP8.5 climate scenario from Fernandes et al. (2020) tended to mostly agree with the trend of SSB modelled without fishing pressure. It was thus inferred from this study that the model would likely show a similar decrease in stock and recruitment after 2050.

Furthermore, according to NEMO-Medusa forecasts to the end of the century, blue whiting spatial distribution is likely to shift northward under the RCP8.5 climate scenario. Martins et al. (2021) already estimated this northward shift of suitable habitat to be around +12.5°N. It would be interesting to make longer

simulations of the blue whiting model to verify these assumptions and compare this last estimation with 2090-2099 forecasts of population distributions.

No clear relationship was observed between the population fishing response and climate variations. However, as discussed in the previous section, population sustainability was strongly affected by individual growth, which is highly dependent on environmental conditions experienced by the population. Thus, while no direct relationship seemed to exist between fishing and climate responses of the population, it is easy to assume that climate change might still indirectly affect the blue whiting population sensitivity to overexploitation.

10.2.4 A separate southern population?

There is a long-standing debate about whether the blue whiting in the North-East Atlantic comprises a single population unit or two discrete units (Brophy & King, 2007; Was et al., 2008; Keating et al., 2014; Pointin & Payne, 2014; Mahe et al., 2016). The recent study of Cadrin et al. (2019) pointed out the necessity of understanding spatial population dynamics for properly defining stock units used in many stock assessment models and for improving recruitment predictions. In the first chapter (section 1.4), we acknowledged the current discussion of whether or not the blue whiting population is in fact constituted of two distinct populations. While this question was not central to this modelling work, we chose on purpose to consider the North-Atlantic population as one single entity. As a consequence, all individuals in the model, whether initiated over southern, northern or western spawning grounds were all subjected to the same environment-dependent growth parameters and the same environmental gradient fields.

In the model, the most important population movements were taking place between the spawning area off Scotland and the Norwegian Sea feeding grounds. Only a very small proportion of the population seemed to be recruited in areas south of Ireland, suggesting that southward larval drift was less frequent than other drifting patterns and that adults tended to keep to the northern areas of the spawning grounds. However, an other important part of the population seem to undertake migrations between the western side of the Rockall area and the Irminger Sea.

Considering the very low densities of the population observed in the South, we assume that the southern recruitment in the model is mostly self-sustained by their first-time spawners, which will then undertake feeding migrations with the rest of the population (mainly northward). The fact that the two different fishing strategies tested here produced very different recruitment intensities of the southern population, suggests that maladapted fishing management strategies will have a greater negative impact on small subpopulations which act as recruitment source for the rest of the population. In that case, when this subpopulation is affected by the same fishing pressure than the main population (SUF model), thus disregarding its health status - local densities (used in the FFR3 model) -, it will result in the depletion and potential permanent disappearance of the subpopulation. This idea is supported by Reiss et al. (2009), who suggested the need to develop different management strategies for these kinds of stocks against the risk to lose a genetic pool of the population. Thus, the model suggests that the southern recruitment of the population might benefit from a blue whiting fishing management plan which considers the southern population as a distinct fishing stock, different from the rest of the stock.

However, the current model performance needs to be taken into account in this interpretation. Indeed, adults migrating from the Norwegian Sea never reach southern spawning regions along the continental shelf, while they are expected to do so in reality (Marine Institute et al., 2013, 2014, 2018, 2019). Once the model is successfully improved and produce more representative spawning distributions, we might observe a better southern recruitment due to northern individuals also participating in spawning southward drifting larvae. This would then contradict the presence of two genetically different population or the need to consider two distinct blue whiting stocks for fishing management plans as suggested by past studies (Svendsen et al., 1996; Skogen et al., 1999; Brophy & King, 2007; Was et al., 2008; Keating et al., 2014; Pointin & Payne, 2014; Mahe et al., 2016). However, our results suggest that the population present in the Greenland waters (Post et al., 2019) might be a better candidate for a second important stock unit, especially since this suggestion is supported by the fourth genetic barrier estimated by Was et al. (2008) along the north-west boundary of the Rockall Plateau.

For further study the population structure of blue whiting in the North-East Atlantic, it would be therefore interesting to compute average length distribution of individuals crossing areas of interest. Currently, these model outputs are not available and need to be added. Among the areas of interest, I propose: south of Ireland, the continental shelf west of Ireland and Scotland, the area between Iceland and Scotland, the Rockall Plateau, the Hatton Plateau, the Irminger Sea, and the Norwegian Sea. Very different length distributions between the most northern, southern and western areas would confirm the three distinct drifting and recruitment patterns, while the comparison with and between the length distributions of the different areas constituting the spawning grounds would tell us whether or not the population mix for reproduction, and whether or not these areas are considered as spawning grounds by repeated spawners, which would mean that the three populations have also distinct migration patterns.

10.3 Conclusions

The project has resulted in a new and innovative approach for modelling ocean migratory fish species such as blue whiting. It has potential for studying effects of varying environmental conditions on population recruitment or for making long-term predictions of spatial distribution and stock biomass. Its spatial, length and life-stage structure offers the opportunity to study population variability from different approach angles (e.g. spatial distributions, length distributions, time series, yield curves...) using the same model simulations.

While the model performance can always be further improved, emergent properties of the model accurately reproduce some of the important features of the population spatial dynamics, namely the blue whiting feeding migration, its summer distribution in the Norwegian Sea, the westward larval and juvenile drift into the Irminger Sea and the subsequent spawning and feeding migrations of the western adult population. Finally, it offers a great opportunity to test different fishing behaviours or fishery management strategies, and to study their consequences for the population over the long term and in a climate change context.

Appendices

Appendix A

CPR predictions using GAMs

At first, attempts at predicting the CPR taxa abundance - needed for estimating the blue whiting food variable - were made using general additive models (GAM). The method was first chosen as it allows for interpretation of the effect and importance of each predictor on the studied variable. However, predictor selection for each model here was very time consuming and some model predictions were not satisfying enough, so we abandoned GAMs for random forests (chap. 5). GAMs results are only presented here for comparison. The 'gam' function from the R package `mgcv` was used (Wood, 2018).

A.1   Predictor selection and importance

Predictors of the studied variables are selected using the forward-stepwise selection method described by Hastie et al. (2009). Starting first with simple models using only one predictor, we progressed towards more complexed models by selecting at each step the predictor that resulted in the lowest Akaike information criterion (AIC) value. A new predictor was only included into the model, if the AIC value of the model with this predictor was reduced by more than 6 compared to the last selected model (Richards, 2008).

For each CPR taxa (euphausiids, hyperiids and *C. finmarchicus*), we considered the following predictor candidates: day of year (yearday), the binary factor Day/Night (daytime), depth, latitude (lat), and NEMO-Medusa variables of sea surface temperature (SST), sea surface salinity (SSS) and mesozooplankton (mezo). For temperature and salinity, both the actual value (t) and the annual average (y) were tested as predictors.

We also attempted to select and include interactions between predictors. However, the time needed to compute each GAM quickly became too considerable and the very low improvement of the model performance was not worth it. For this reason, the GAMs presented here have been stopped before this step and any interaction effect between variables have been ignored.

Euphausiids

Annual average of SST and SSS were selected as predictors to the variations of euphausiid CPR abundance (tab. A.1). The final model with its predictors had 23.78% of its deviance explained, which is the percentage of the model improvement gained by adding all these predictors. SST_y was the first predictor selected for the model, while it was among the less important predictors of the random forests of euphausiids.

Hyperiids

For hyperiids, annual average of SST was also selected for the GAM, but this time it was the time-step value SSS_t which was selected between both salinity variables (tab. A.2). SST_y was again the first predictor to be selected. The Day/Night factor was however among the last predictors selected and only improved lightly the GAM compared to its previous version, while the predictor was considered the most important predictor for the random forest models. The final GAM for CPR abundance of hyperiids had a deviance explained of 26.70%.

C. finmarchicus

The GAM for CPR abundance of *C. finmarchicus* had the best score of deviance explained with 55.456%. Annual average of temperature and salinity were again selected as predictors for this model, and SST_y was still the first selected predictor of the model (tab. A.3). In fact, SST_y alone could explain 39.47% of the deviance present in the CPR data, which is far more than the model improvement obtained for euphausiid and hyperiid GAMs when using all the predictors. SST_y was also the most important predictor of the *C. finmarchicus* random forests.

Table A.1: Predictor selection process for the GAM describing variations in CPR qualitative abundance (accepted numbers) of euphausiids. At each stage, one new predictor is selected if its corresponding GAM's AIC value is the smallest and decreases by more than 6 compared to the previous AIC value. The GAM selected at each stage is represented in bold in the table. The deviance explained (DE) by the model in percent is written in the last column.

Model	AIC	AIC diff.	DE (%)
Euph $\sim$ yearday	543179	2353	6.67
Euph $\sim$ daytime	546218	5392	2.57
Euph $\sim$ SST$_t$	546792	5967	1.82
Euph $\sim$ SST$_y$	**540825**	**0**	**9.68**
Euph $\sim$ SSS$_t$	544510	3685	4.91
Euph $\sim$ SSS$_y$	543849	3024	5.79
Euph $\sim$ depth	544375	3550	5.08
Euph $\sim$ mezo	545072	4247	4.13
Euph $\sim$ lat	546680	5855	1.97
Euph $\sim$ SST$_y$ + yearday	**536579**	**-4247**	**15.08**
Euph $\sim$ SST$_y$ + daytime	538336	-2489	12.89
Euph $\sim$ SST$_y$ + SSS$_t$	539074	-1751	11.98
Euph $\sim$ SST$_y$ + SSS$_y$	538512	-2314	12.69
Euph $\sim$ SST$_y$ + depth	539913	-912	10.89
Euph $\sim$ SST$_y$ + mezo	538220	-2606	13.02
Euph $\sim$ SST$_y$ + yearday + daytime	**532284**	**-4295**	**20.32**
Euph $\sim$ SST$_y$ + yearday + SSS$_t$	534762	-1817	17.35
Euph $\sim$ SST$_y$ + yearday + SSS$_y$	534583	-1995	17.57
Euph $\sim$ SST$_y$ + yearday + depth	535927	-652	15.91
Euph $\sim$ SST$_y$ + yearday + mezo	535881	-698	15.97
Euph $\sim$ SST$_y$ + yearday + daytime + SSS$_t$	530663	-1621	22.26
Euph $\sim$ SST$_y$ + yearday + daytime + SSS$_y$	**530450**	**-1834**	**22.51**
Euph $\sim$ SST$_y$ + yearday + daytime + depth	531630	-654	21.12
Euph $\sim$ SST$_y$ + yearday + daytime + mezo	531585	-699	21.18
Euph $\sim$ SST$_y$ + yearday + daytime + SSS$_y$ + depth	530026	-425	23.03
Euph $\sim$ SST$_y$ + yearday + daytime + SSS$_y$ + mezo	**529853**	**-598**	**23.23**
Euph $\sim$ SST$_y$ + yearday + daytime + SSS$_y$ + mezo + depth	**529392**	**-461**	**23.78**

Table A.2: Predictor selection process for the GAM describing variations in CPR qualitative abundance (accepted numbers) of hyperiids. At each stage, one new predictor is selected if its corresponding GAM's AIC value is the smallest and decreases by more than 6 compared to the previous AIC value. The GAM selected at each stage is represented in bold in the table. The deviance explained (DE) by the model in percent is written in the last column.

Model	AIC	AIC diff.	DE (%)
Hype $\sim$ yearday	377362	812	9.25
Hype $\sim$ daytime	382312	5762	0.29
Hype $\sim$ SST$_t$	381274	4724	2.27
Hype $\sim$ SST$_y$	**376550**	**0**	**10.37**
Hype $\sim$ SSS$_t$	380877	4328	2.98
Hype $\sim$ SSS$_y$	380571	4022	3.54
Hype $\sim$ depth	377361	811	9.13
Hype $\sim$ mezo	377755	1206	8.53
Hype $\sim$ lat	381089	4539	2.60
Hype $\sim$ SST$_y$ + yearday	372086	-4464	17.86
Hype $\sim$ SST$_y$ + daytime	376406	-144	10.62
Hype $\sim$ SST$_y$ + SSS$_t$	375262	-1288	12.74
Hype $\sim$ SST$_y$ + SSS$_y$	374855	-1694	13.42
Hype $\sim$ SST$_y$ + depth	373609	-2941	15.41
Hype $\sim$ SST$_y$ + mezo	**371781**	**-4769**	**18.39**
Hype $\sim$ SST$_y$ + mezo + yearday	370641	-1140	20.33
Hype $\sim$ SST$_y$ + mezo + daytime	371385	-396	19.00
Hype $\sim$ SST$_y$ + mezo + SSS$_t$	369508	-2273	22.10
Hype $\sim$ SST$_y$ + mezo + SSS$_y$	369519	-2263	22.09
Hype $\sim$ SST$_y$ + mezo + depth	**368452**	**-3330**	**23.60**
Hype $\sim$ SST$_y$ + mezo + depth + yearday	367942	-510	24.50
Hype $\sim$ SST$_y$ + mezo + depth + daytime	367963	-489	24.33
Hype $\sim$ SST$_y$ + mezo + depth + SSS$_t$	**367459**	**-993**	**25.23**
Hype $\sim$ SST$_y$ + mezo + depth + SSS$_y$	367618	-834	24.99
Hype $\sim$ SST$_y$ + mezo + depth + SSS$_t$ + yearday	367022	-437	26.01
Hype $\sim$ SST$_y$ + mezo + depth + SSS$_t$ + daytime	**366998**	**-461**	**25.91**
Hype $\sim$ SST$_y$ + mezo + depth + SSS$_t$ + daytime + yearday	**366543**	**-455**	**26.70**

Table A.3: Predictor selection process for the GAM describing variations in CPR qualitative abundance (accepted numbers) of *C. finmarchicus*. At each stage, one new predictor is selected if its corresponding GAM's AIC value is the smallest and decreases by more than 6 compared to the previous AIC value. The GAM selected at each stage is represented in bold in the table. The deviance explained (DE) by the model in percent is written in the last column.

Model	AIC	AIC diff.	DE (%)
Cfin $\sim$ yearday	494669	15165	17.10
Cfin $\sim$ daytime	504414	24910	0.07
Cfin $\sim$ SST$_t$	492032	12528	21.40
Cfin $\sim$ SST$_y$	**479504**	**0**	**39.47**
Cfin $\sim$ SSS$_t$	497831	18327	11.93
Cfin $\sim$ SSS$_y$	496883	17380	13.60
Cfin $\sim$ depth	495634	16131	15.44
Cfin $\sim$ mezo	500956	21452	6.26
Cfin $\sim$ lat	496479	16976	14.34
Cfin $\sim$ SST$_y$ + yearday	**468700**	**-10804**	**52.56**
Cfin $\sim$ SST$_y$ + daytime	479333	-171	39.70
Cfin $\sim$ SST$_y$ + SSS$_t$	478539	-965	40.75
Cfin $\sim$ SST$_y$ + SSS$_y$	478427	-1077	40.89
Cfin $\sim$ SST$_y$ + depth	477760	-1744	41.75
Cfin $\sim$ SST$_y$ + mezo	476905	-2599	42.86
Cfin $\sim$ SST$_y$ + yearday + daytime	468608	-92	52.66
Cfin $\sim$ SST$_y$ + yearday + SSS$_t$	467748	-952	53.61
Cfin $\sim$ SST$_y$ + yearday + SSS$_y$	467796	-904	53.56
Cfin $\sim$ SST$_y$ + yearday + depth	**467438**	**-1262**	**53.97**
Cfin $\sim$ SST$_y$ + yearday + mezo	468293	-407	53.00
Cfin $\sim$ SST$_y$ + yearday + depth + daytime	467365	-73	54.06
Cfin $\sim$ SST$_y$ + yearday + depth + SSS$_t$	466790	-648	54.67
Cfin $\sim$ SST$_y$ + yearday + depth + SSS$_y$	**466768**	**-670**	**54.69**
Cfin $\sim$ SST$_y$ + yearday + depth + mezo	466774	-664	54.69
Cfin $\sim$ SST$_y$ + yearday + depth + SSS$_y$ + daytime	466702	-66	54.77
Cfin $\sim$ SST$_y$ + yearday + depth + SSS$_y$ + mezo	**466134**	**-635**	**55.37**
Cfin $\sim$ SST$_y$ + yearday + depth + SSS$_y$ + mezo + daytime	**466068**	**-66**	**55.45**

A.2 Model performance

Prediction accuracy was already quite low when the model was used on the data subset used for training and most of time even lower when used on the test subset (tab. A.4). We noted here that the model performance of the *C. finmarchicus* was very similar for predicting both the training and test data subsets in both time and space, which seemed to indicate some robustness of GAMs at extrapolating and forecasting that random forests might lack.

Table A.4: GAM performances for each taxa in space and time. In both cases, prediction accuracy was studied first on the train data and then on the test data. For each model assessment, the Root Mean Squared Error (RMSE) is first given, followed by Pearson's coefficient of determination (r^2) in brackets.

GAM	space train	space test	time train	time test
Euph	10.84 (0.09)	9.28 (0.04)	9.46 (0.11)	14.11 (0.03)
Hype	4.69 (0.14)	4.85 (0.03)	4.50 (0.12)	5.57 (0.08)
Cfin	61.84 (0.14)	34.07 (0.10)	58.50 (0.13)	54.77 (0.13)

A.3 GAM predictions

Euphausiids

GAM predictions of euphausiid quarterly distributions showed similar features to the random forests predictions. However, they overestimated abundance values, especially in areas where euphausiid abundance was supposed to be very low according to CPR observations (fig. A.1).

Hyperiids

Predicted abundance of hyperiids also tended to be overestimated, especially in offshore areas of the North Atlantic (fig. A.2). The GAM seemed to predict similar distribution patterns to the random forest.

C. finmarchicus

Predictions of *C. finmarchicus* showed the nearest resemblance to the random forest's predictions of distribution and seasonal variation (fig. A.3). However, density values were overestimated, almost twice more than with the random forest model.

(a) January 2000

(b) April 2000

(c) July 2000

(d) October 2000
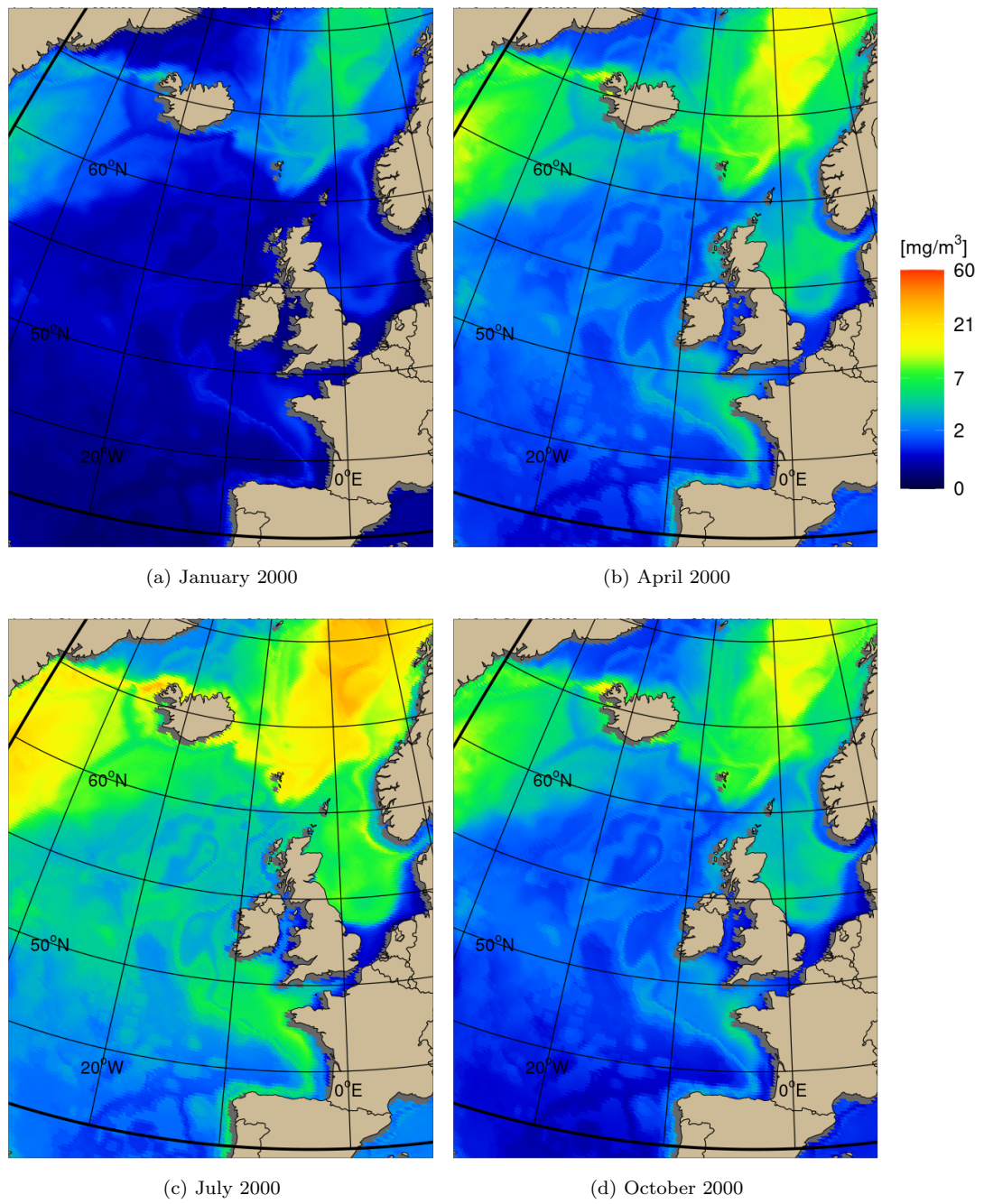
Figure A.1: Examples of GAM predictions of euphausiid concentration (mg/m^3) in year 2000.

(a) January 2000

(b) April 2000

(c) July 2000

(d) October 2000
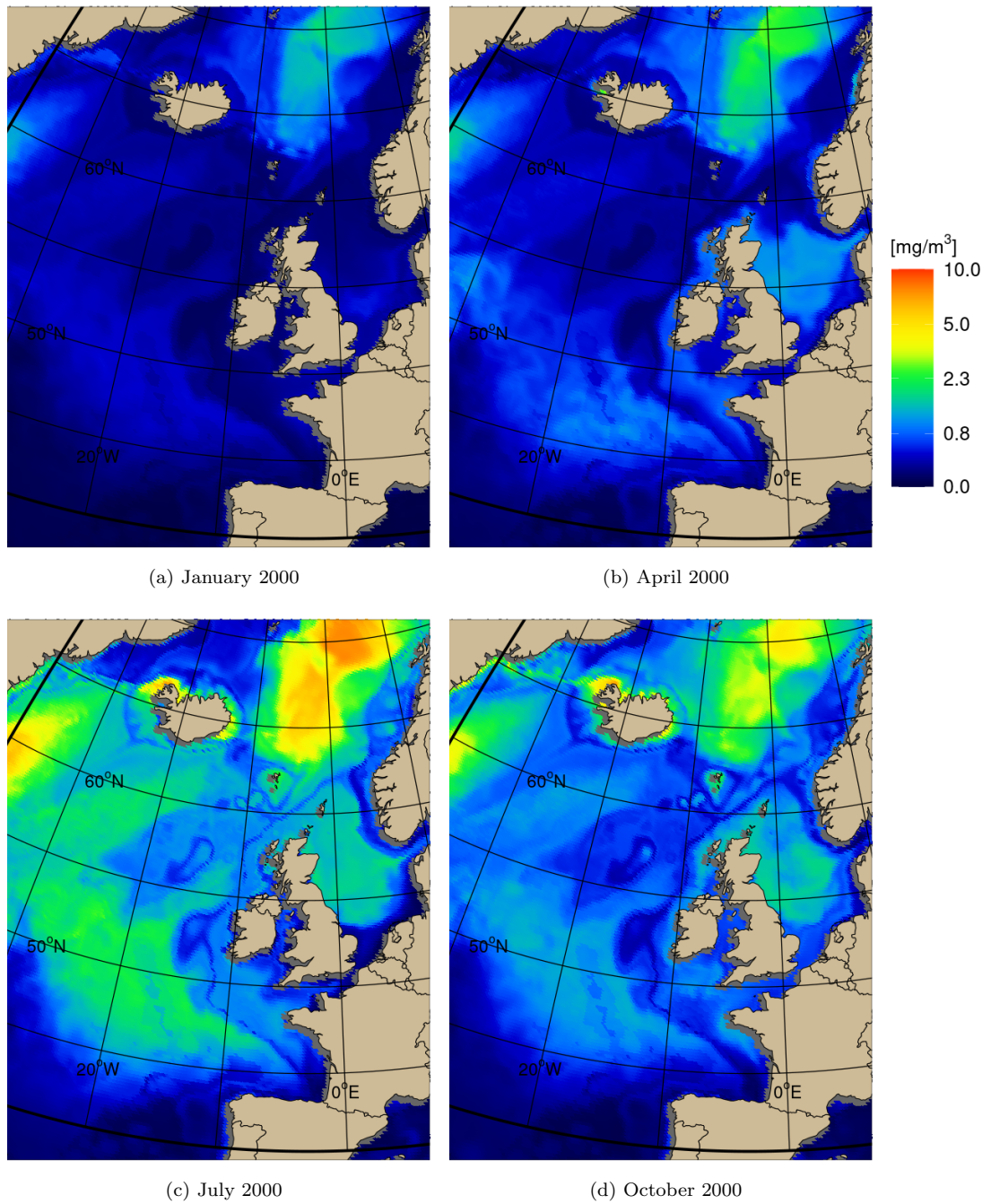
Figure A.2: Examples of GAM predictions of hyperiid concentration $(\mathrm{mg/m^3})$ in year 2000.

(a) January 2000

(b) April 2000

(c) July 2000

(d) October 2000
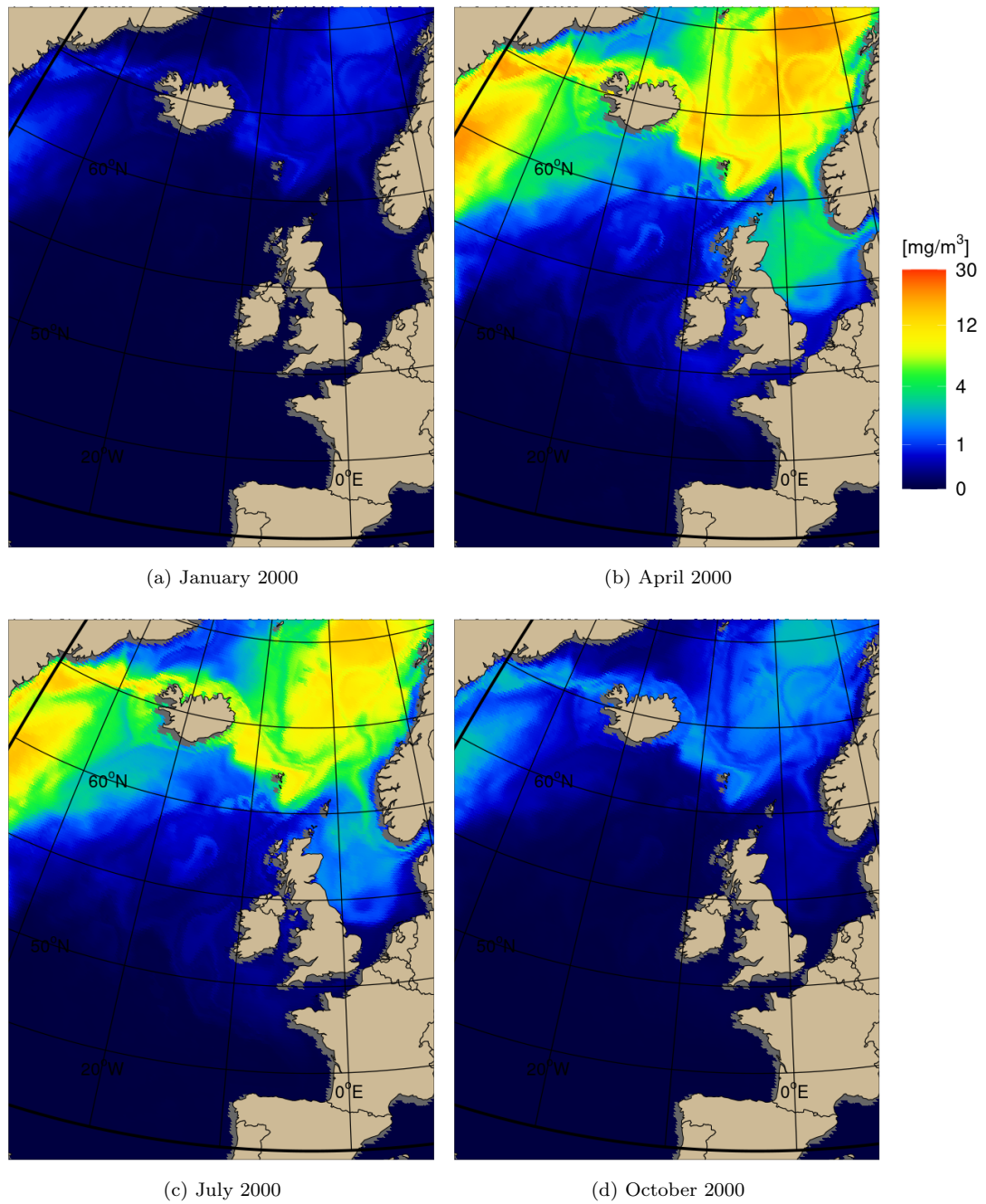
Figure A.3: Examples of GAM predictions of *C. finmarchicus* concentration (mg/m^3) in year 2000.

Appendix B

Larval drift

Passive transport of eggs and larvae were modelled using `Ichthyop`. Before producing time-step transport matrices in the blue whiting model, a short study of the particle tracking performance at simulating larval drift was realised and results were compared with past model studies. We first investigated the overall spreading of larvae from the spawning grounds, at different time after spawning. Then we investigated the effect of the spawning location on drift pattern.

B.1   `Ichthyop` tracking simulations of blue whiting larval drift

Larvae were released all over the suitable spawning areas defined by the NEMO-Medusa temperature and salinity, and by the bathymetry. In the example of larval drift presented in figure B.1, it seemed that the majority of larvae were drifting northward along the continental shelf to reach areas in the northern North Sea or farther north along the Norwegian continental shelf, thus showing the strong effect of the northward continental shelf edge current on larval drift. Some larvae seemed to be transported west from the Rockall area by strong eastern and northern currents of the subpolar gyre towards areas south of Iceland and over the Reykjanes Ridge. In this example, southern larvae seemed to be more affected by dispersion than southward currents. Although not shown here, southward drift could be more important in different years.

These larval distributions after 60 days and 120 days of tracking were very similar to the blue whiting larval drift simulations performed by Bartsch & Coombs

(1997). The use of `Ichthyop` particle tracking model for modelling passive transport of blue whiting larvae was then judged satisfying enough for the purpose of our spatial population model.

B.2 Spawning distribution effect

Like Skogen et al. (1999), we investigated the effect of spawning location on larval drift direction. After 120 days of tracking with `Ichthyop`, we separated the larvae into three categories depending on their total drift direction between their starting position and last position, and considering only larvae that travelled a greater distance than the average in the defined directions : (1) northward drifting larvae, (2) southward drifting larvae and (3) westward drifting larvae.

According to figures B.2 and B.3, northward drifting larvae which were transported towards - and sometimes into - the North Sea and Norwegian Sea were initially distributed along the continental shelf between latitudes 50 and 60°N. Larvae which ended over the Iceland-Faroe Ridge were most likely from areas of the Rockall Plateau.

The southward larval drift seemed to be mostly performed by larvae from the western edge of the Porcupine Bank and from the continental shelf south of the 50°N latitude. Some individuals from the northern part of the Rockall area seemed to be transported to the south-east part of Rockall by anticyclonic currents over the plateau.

Finally, the most important westward larval drift seemed to come from individuals initially located at the very north-east edge of the Rockall Plateau. Spawning locations of blue whiting eggs were definitely influencing larval drift direction, but it seemed here slightly more complicated than just a separation between southern larvae drifting southward and northern larvae drifting northward as suggested by Skogen et al. (1999): westward larval drifts towards the Irminger Sea were also observed with this model.
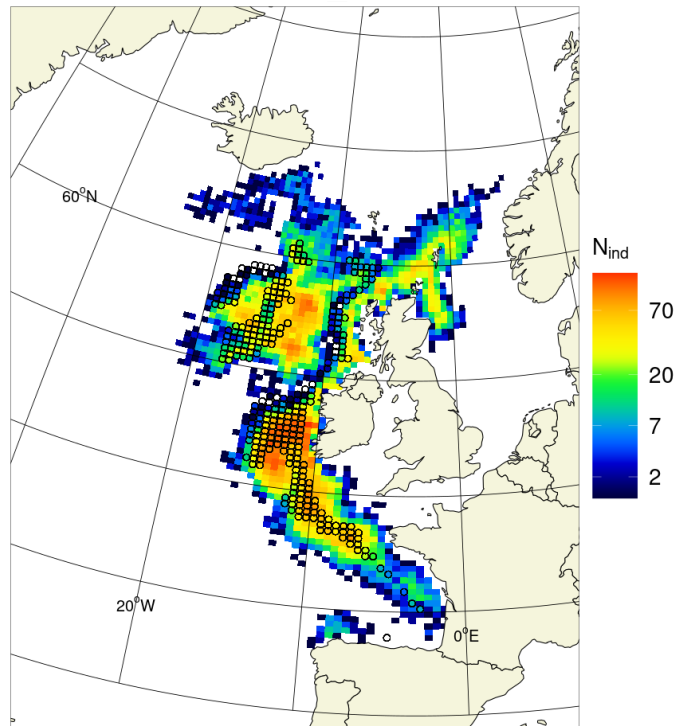
(a) 60 days
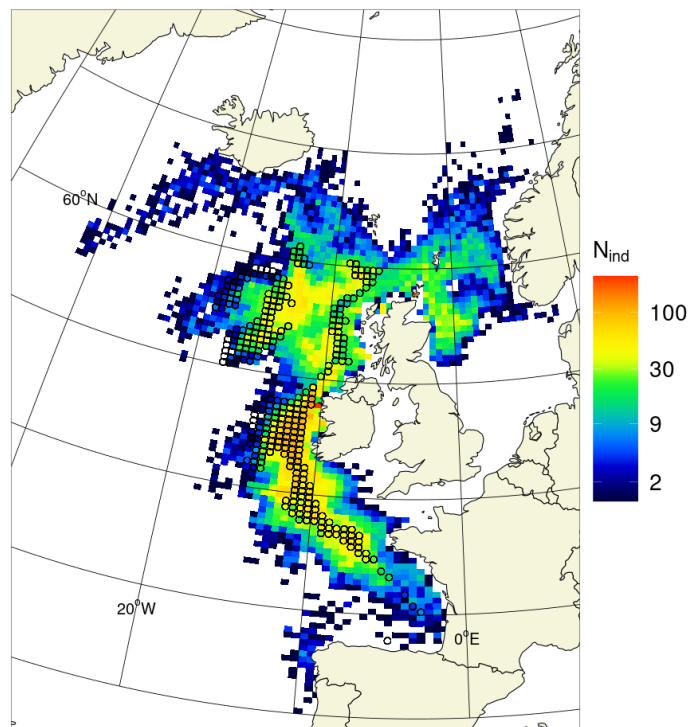
(b) 120 days

Figure B.1: Example of spatial distribution of larvae after 60 days (a) and 120 days (b) of passive transport with diffusion in 1994, modelled by `Ichthyop`. The black circles represent the starting cells of larvae, which correspond to the theoretical spawning area. 100 individuals were released in each of those spawning cells at the start of February (04/02).

(a) North drift

(b) South drift

(c) West drift
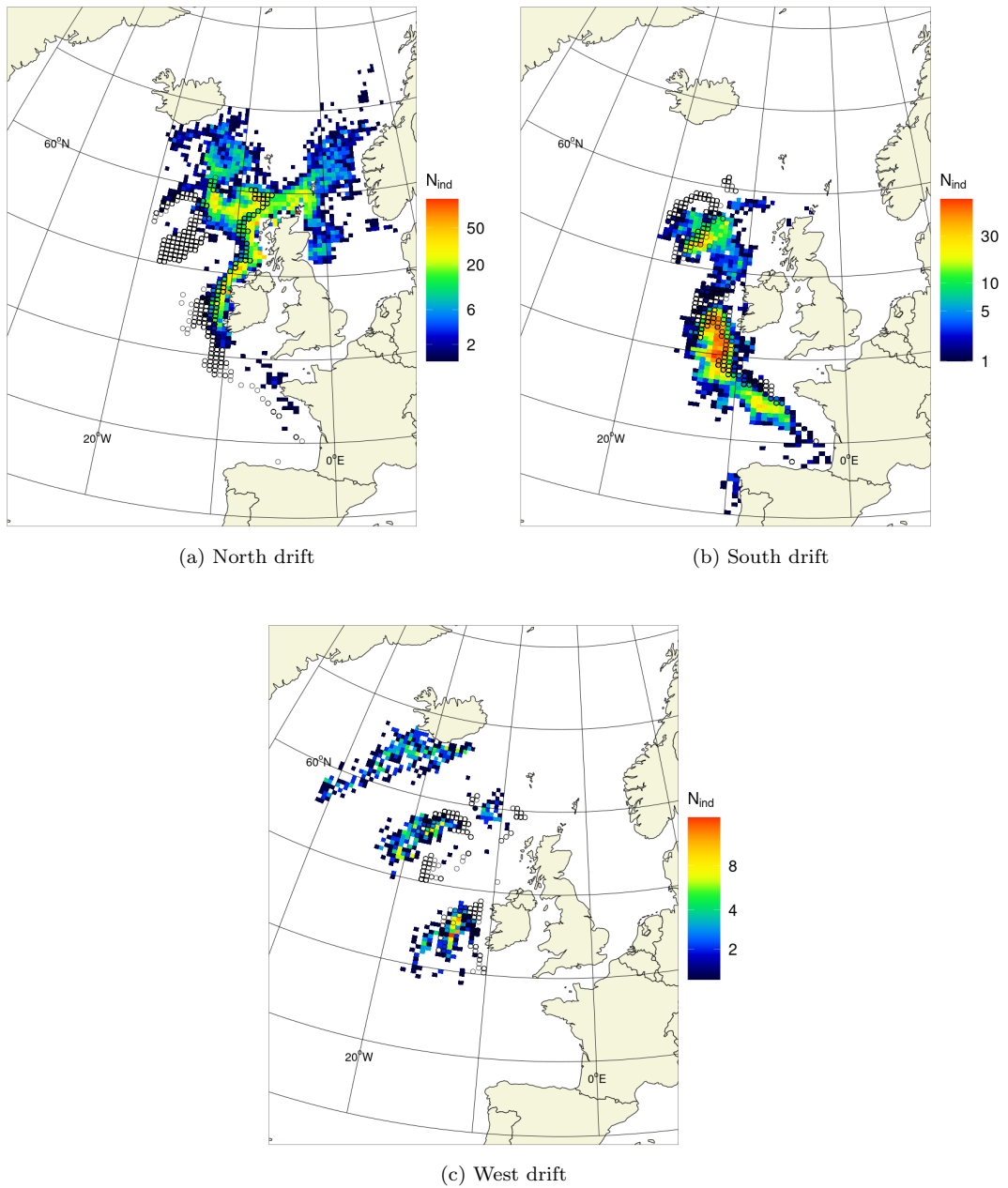
Figure B.2: Example of spatial distribution of larvae drifting northward (a), southward (b) or westward (c) after 120 days in 1994, modelled by `Ichthyop`. As in fig. B.1, the black circles represent the starting cells of larvae. Fading circles mean that less than 100 individuals departing from that position drifted north- or southward (see fig. B.3).

(a) North drift

(b) South drift

(c) West drift
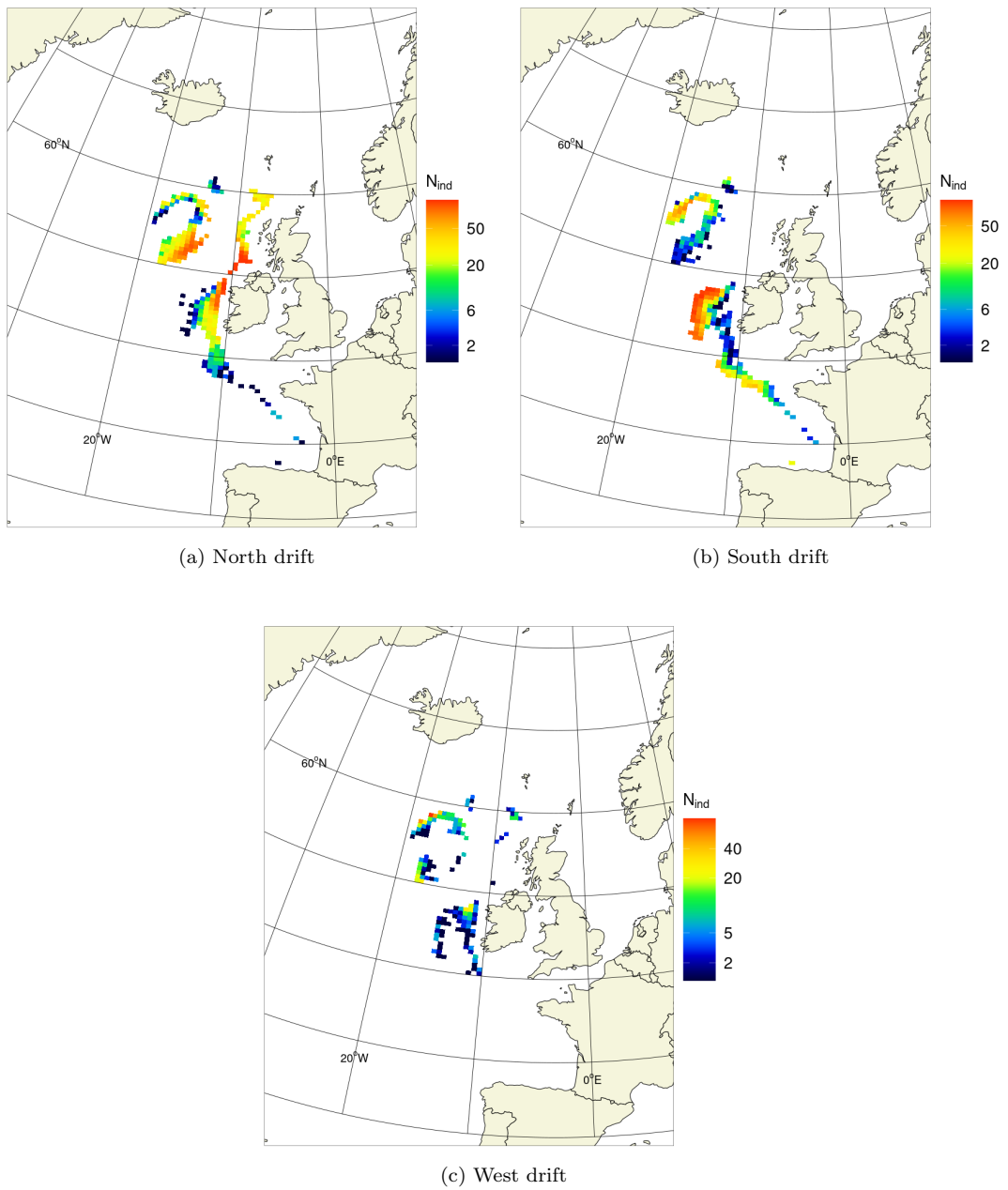
Figure B.3: Example of initial spawning distribution of larvae drifting northward (a), southward (b) or westward (c) after 120 days in 1994 (final distributions in fig. B.2).

Bibliography

Abollo, E., Calvo, M., & Pascual, S. (2001). Hepatic coccidiosis of the blue whiting, *Micromesistius poutassou* (Risso), and horse mackerel, *Trachurus trachurus* (L .), from Galician waters. *Journal of Fish Diseases*, 24, 335–343.

Ådlandsvik, B., Coombs, S., Sundby, S., & Temple, G. (2001). Buoyancy and vertical distribution of eggs and larvae of blue whiting (*Micromesistius poutassou*): observations and modelling. *Fisheries Research*, 50(1-2), 59–72.

Akimova, A., Hufnagl, M., & Peck, M. A. (2019). Spatiotemporal dynamics of predators and survival of marine fish early life stages: Atlantic cod (*Gadus morhua*) in the North Sea. *Progress in Oceanography*, 176(August 2018), 20pp.

Allain, G., Petitgas, P., Lazure, P., & Grellier, P. (2007). Biophysical modelling of larval drift, growth and survival for the prediction of anchovy (*Engraulis encrasicolus*) recruitment in the Bay of Biscay (NE Atlantic). *Fisheries Oceanography*, 16(6), 489–505.

Andrews, J., Gurney, W., Heath, M., Gallego, A., O'Brien, C., Darby, C., Tyldesley, G., & Andrews, J.M. and Gurney, W.S.C. and Heath, M.R. and Gallego, Alejandro and O'Brien, C.M. and Darby, C. and Tyldesley, G. (2006). Modelling the spatial demography of Atlantic cod (*Gadus morhua*) on the European continental shelf. *Canadian Journal of Fisheries and Aquatic Sciences*, 63, 1027–1048.

Anon (1990). Report of the Blue Whiting Assessment Working Group, Copenhagen 13-19 September 1989. *ICES*, C.M(1990/Assess:3), 99pp.

Bachiller, E., Skaret, G., Nøttestad, L., & Slotte, A. (2016). Feeding ecology of Northeast Atlantic Mackerel, Norwegian spring-spawning herring and blue whiting in the Norwegian Sea. *PLoS ONE*, 11(2).

Bachiller, E., Utne, K. R., Jansen, T., & Huse, G. (2018). Bioenergetics modeling of the annual consumption of zooplankton by pelagic fish feeding in the Northeast Atlantic. *PLoS ONE*, 13(1), 1–29.

Bailey, M. C. & Heath, M. R. (2001). Spatial variability in the growth rate of blue whiting (*Micromesistius poutassou*) larvae at the shelf edge west of the UK. *Fisheries Research*, 50(1-2), 73–87.

Bailey, R. S. (1982). The Population Biology of Blue Whiting in the North-Atlantic. *Advances in Marine Biology*, 19, 257–355.

Bartsch, J. & Coombs, S. (1997). A numerical model of the dispersion of blue whiting larvae, *Micromesistius poutassou* (Risso), in the eastern North Atlantic. *Fisheries Oceanography*, 6(3), 141–154.

Bauer, S. & Klaassen, M. (2013). Mechanistic models of animal migration behaviour - their diversity, structure and use. *Journal of Animal Ecology*, 82(3), 498–508.

Beare, D. & McKenzie, E. (1999). Continuous Plankton Recorder data and diel vertical migration in stage V and VI *Calanus finmarchicus*: a statistical analysis. *Fisheries Oceanography*, 8, 126–137.

Bersch, M., Yashayaev, I., & Koltermann, K. P. (2007). Recent changes of the thermohaline circulation in the subpolar North Atlantic. *Ocean Dynamics*, 57(3), 223–235.

Berx, B. & Payne, M. R. (2017). The Sub-Polar Gyre Index - A community data set for application in fisheries and environment research. *Earth System Science Data*, 9(1), 259–266.

Beverton, R. & Holt, S. (1957). On the Dynamics of Exploited Fish Populations. Fisheries Investment Series 2. Vol. 19. *UK Ministry of Agriculture and Fisheries: London.*

Bingman, V. P. & Cheng, K. (2005). Mechanisms of animal global navigation: comparative perspectives and enduring challenges. *Ethology Ecology & Evolution*, 17(4), 295–318.

Biri, S. & Klein, B. (2019). North Atlantic Sub-Polar Gyre Climate Index: A New Approach. *Journal of Geophysical Research: Oceans*, 124(6), 4222–4237.

Bjørndal, T. (2009). Overview, roles, and performance of the North East Atlantic fisheries commission (NEAFC). *Marine Policy*, 33(4), 685–697.

Bjørndal, T. & Ekerhovd, N. A. (2014). Management of pelagic fisheries in the North East Atlantic: Norwegian spring spawning herring, mackerel, and blue whiting. *Marine Resource Economics*, 29(1), 69–83.

Blindheim, J., Bratberg, E., & Dragesund, O. (1971). Fisheries investigations with F/F GO Sars in the Irminger and Norwegian Sea 28 July–21 August 1970. *Fiskens Gang*, 9, 168–73.

Böning, C. W., Scheinert, M., Dengg, J., Biastoch, A., & Funk, A. (2006). Decadal variability of subpolar gyre transport and its reverberation in the North Atlantic overturning. *Geophysical Research Letters*, 33(21), 1–5.

Born, A. & Mignot, J. (2012). Dynamics of decadal variability in the Atlantic subpolar gyre: A stochastically forced oscillator. *Climate Dynamics*, 39(1-2), 461–474.

Boyd, R., Roy, S., Sibly, R., Thorpe, R., & Hyder, K. (2018). A general approach to incorporating spatial and temporal variation in individual-based models of fish populations with application to Atlantic mackerel. *Ecological Modelling*, 382, 9–17.

Breiman, L. (1996). Bagging predictors. *Machine learning*, 24(2), 123–140.

Breiman, L. (2001). Random forests. *Machine learning*, 45(1), 5–32.

Brophy, D. & King, P. A. (2007). Larval otolith growth histories show evidence of stock structure in Northeast Atlantic blue whiting (*Micromesistius poutassou*). *ICES Journal of Marine Science*, 64(6), 1136–1144.

Brun, P., Kiørboe, T., Licandro, P., & Payne, M. R. (2016). The predictive skill of species distribution models for plankton in a changing climate. *Global change biology*, 22(9), 3170–3181.

Cabral, H. N. & Murta, A. G. (2002). The diet of blue whiting, hake, horse mackerel and mackerel off Portugal. *Journal of Applied Ichthyology*, 18(1), 14–23.

Cadrin, S. X., Goethel, D. R., Morse, M. R., Fay, G., & Kerr, L. A. (2019). "So, where do you come from?" The impact of assumed spatial population structure on estimates of recruitment. *Fisheries Research*, 217(December 2018), 156–168.

Carrera, P., Meixide, M., Porteiro, C., & Miquel, J. (2001). Study of the blue whiting movements around the Bay of Biscay using acoustic methods. *Fisheries Research*, 50(1-2), 151–161.

Chapman, J. W., Klaassen, R. H., Drake, V. A., Fossette, S., Hays, G. C., Metcalfe, J. D., Reynolds, A. M., Reynolds, D. R., & Alerstam, T. (2011). Animal orientation strategies for movement in flows. *Current Biology*, 21(20), R861–R870.

Chesson, J. (1983). The estimation and analysis of preference and its relatioship to foraging models. *Ecology*, 64(5), 1297–1304.

Collins, W. J., Bellouin, N., Doutriaux-Boucher, M., Gedney, N., Halloran, P., Hinton, T., Hughes, J., Jones, C. D., Joshi, M., Liddicoat, S., Martin, G., O'Connor, F., Rae, J., Senior, C., Sitch, S., Totterdell, I., Wiltshire, A., & Woodward, S. (2011). Development and evaluation of an Earth-System model - HadGEM2. *Geoscientific Model Development*, 4(4), 1051–1075.

Coombs, S. H., Pipe, R. K., & Mitchell, C. E. (1981). The vertical distribution of eggs and larvae of blue w hiting. *Rapp. P.-v. Réun. Cons. int. Explor. Mer*, 178, 188–195.

Cutler, D. R., Edwards Jr, T. C., Beard, K. H., Cutler, A., Hess, K. T., Gibson, J., & Lawler, J. J. (2007). Random forests for classification in ecology. *Ecology*, 88(11), 2783–2792.

Dale, K., Falk-Petersen, S., Hop, H., & Fevolden, S.-E. (2006). Population dynamics and body composition of the Arctic hyperiid amphipod *Themisto libellula* in Svalbard fjords. *Polar Biology*, 29(12), 1063–1070.

Dolgov, A. V., Johannesen, E., Heino, M., & Olsen, E. (2010). Trophic ecology of blue whiting in the Barents Sea. *ICES Journal of Marine Science*, 67(3), 483–493.

Dormann, C. F., Elith, J., Bacher, S., Buchmann, C., Carl, G., Carré, G., Marquéz, J. R., Gruber, B., Lafourcade, B., Leitão, P. J., Münkemüller, T., Mcclean, C., Osborne, P. E., Reineking, B., Schröder, B., Skidmore, A. K., Zurell, D., & Lautenbach, S. (2013). Collinearity: A review of methods to deal with it and a simulation study evaluating their performance. *Ecography*, 36(1), 27–46.

Edwards, M. (2018). Raw data for total Hyperiidae, total Euphausiidae, total *Calanus finmarchicus*, (35-75N, 50W-20E) 1958-2014 as recorder by the Continuous Plankton Recorder Survey. Plymouth. DOI: 10.7487/2018.242.1.1140.

Ekerhovd, N.-A. (2007). Individual vessel quotas and unregulated species: the Norwegian blue whiting fishery. *NHH Dept. of Economics Discussion Paper*, (5).

Ekerhovd, N.-A. (2008). The blue whiting coalition game.

Ekerhovd, N.-A. (2010). The stability and resilience of management agreements on climate-sensitive straddling fishery resources: the blue whiting (Micromesistius poutassou) coastal state agreement. *Canadian Journal of Fisheries and Aquatic Sciences*, 67(3), 534–552.

Elith, J. & Leathwick, J. R. (2009). Species distribution models: ecological explanation and prediction across space and time. *Annual review of ecology, evolution, and systematics*, 40, 677–697.

Fernandes, J. A., Frölicher, T. L., Rutterford, L. A., Erauskin-Extramiana, M., & Cheung, W. W. (2020). Changes of potential catches for North-East Atlantic small pelagic fisheries under climate change scenarios. *Regional Environmental Change*, 20(4).

Fleming, M. D. & Hoffer, R. M. (1979). Machine processing of Landsat MSS data and DMA topographic data for forest cover type mapping. *Purdue University, LARS Technical Report*, (Publication 062879), 377–390.

Foukal, N. P. & Lozier, M. S. (2017). Assessing variability in the size and strength of the North Atlantic subpolar gyre. *Journal of Geophysical Research: Oceans*, 122(8), 6295–6308.

Garcia-Soto, C. & Pingree, R. D. (2009). Spring and summer blooms of phytoplankton (SeaWiFS/MODIS) along a ferry line in the Bay of Biscay and western English Channel. *Continental Shelf Research*, 29(8), 1111–1122.

Gastauer, S., Fässler, S. M. M., O'Donnell, C., Høines, Å., Jakobsen, J. A., Krysov, A. I., Smith, L., Tangen, Ø., Anthonypillai, V., Mortensen, E., Armstrong, E., Schaber, M., & Scoulding, B. (2016). The distribution of blue whiting west of the British Isles and Ireland. *Fisheries Research*, 183, 32–43.

Geistdoerfer, P. (1983). L'alimentation du merlan bleu *Micromesistius poutassou* (Risso, 1826)(Téléostéens, Gadidae) dans le nord-est de l'océan Atlantique. *ICES Journal of Marine Science*, 41(1), 67–75.

Giæver, M. & Stien, J. (1998). Population genetic substructure in blue whiting based on allozyme data. *Journal of Fish Biology*, 52, 782–795.

Gierz, P., Lohmann, G., & Wei, W. (2015). Response of Atlantic overturning to future warming in a coupled atmosphere-ocean-ice sheet model. *Geophysical Research Letters*, 42(16), 6811–6818.

Gislason, H., Daan, N., Rice, J. C., & Pope, J. G. (2010). Size, growth, temperature and the natural mortality of marine fish. *Fish and Fisheries*, 11(2), 149–158.

González-Quirós, R. & Anadón, R. (2001). Diet breadth variability in larval blue whiting as a response to plankton size structure. *Journal of Fish Biology*, 59, 1111–1125.

Guisan, A., Edwards Jr, T. C., & Hastie, T. (2002). Generalized linear and generalized additive models in studies of species distributions: setting the scene. *Ecological modelling*, 157(2-3), 89–100.

Gurney, W. & Nisbet, R. M. (1998). *Ecological Dynamics*. Oxford University Press.

Häkkinen, S. & Rhines, P. B. (2004). Decline of Subpolar North Atlantic Circulation During the 1990s. *Science*, 304, 555–559.

Hansen, B. & Jákupsstovu, S. H. í. (1992). Availability of blue whiting (*Micromesistius poutassou*) in Faroese waters in relation to hydrography. *ICES mar. Sci. Symp.*, 195, 349–360.

Hastie, T., Tibshirani, R., Friedman, J. H., & Friedman, J. H. (2009). *The elements of statistical learning: data mining, inference, and prediction*, volume 2. Springer.

Hátún, H. (2005). Influence of the Atlantic Subpolar Gyre on the Thermohaline Circulation. *Science*, 309(5742), 1841–1844.

Hátún, H., Arge, J., & Sandø, A. B. (2007). Environmental influence on the spawning distribution and migration pattern of northern blue whiting (*Micromesistius poutassou*). *Ices Cm 2007/B:06*, (1961), 10pp.

Hátún, H., Lohmann, K., Matei, D., Jungclaus, J. H., Pacariz, S., Bersch, M., Gislason, A., Ólafsson, J., & Reid, P. C. (2016). An inflated subpolar gyre blows life toward the northeastern Atlantic. *Progress in Oceanography*, 147, 49–66.

Hátún, H., Payne, M. R., Beaugrand, G., Reid, P. C., Sandø, A. B., Drange, H., Hansen, B., Jacobsen, J. A., & Bloch, D. (2009a). Large bio-geographical shifts in the north-eastern Atlantic Ocean: From the subpolar gyre, via plankton, to blue whiting and pilot whales. *Progress in Oceanography*, 80(3-4), 149–162.

Hátún, H., Payne, M. R., & Jacobsen, J. A. (2009b). The North Atlantic subpolar gyre regulates the spawning distribution of blue whiting (*Micromesistius poutassou*). *Canadian Journal of Fisheries and Aquatic Sciences*, 66(5), 759–770.

Heath, M. R. & Gallego, A. (1998). Bio-physical modelling of the early life stages of haddock, Melanogrammus aeglefinus, in the North Sea. *Fisheries Oceanography*, 7(2), 110–125.

Heino, M., Engelhard, G. H., & Godø, O. R. (2003). Variations in the distribution of blue whiting in the Barents Sea : climatic influences or year class effects ? *Ices Cm*, Q: 03, 11pp.

Heino, M., Engelhard, G. H., & Godø, O. R. (2008). Migrations and hydrography determine the abundance fluctuations of blue whiting (*Micromesistius poutassou*) in the Barents Sea. *Fisheries Oceanography*, 17(2), 153–163.

Heino, M. & Godo, O. R. (2002). Blue whiting - a key species in the mid-water ecosystems of the north-eastern Atlantic. *ICES Council Meeting Papers*, CM 2002/L:.

Henderson, G. (1961). Contribution towards a plankton atlas of the northeastern Atlantic and the North Sea. *Bulletins of Marine Ecology*, 5, 105–111.

Hermanson, L., Eade, R., Robinson, N. H., Dunstone, N. J., Andrews, M. B., Knight, J. R., Scaife, A. A., & Smith, D. M. (2014). Forecast cooling of the Atlantic subpolar gyre and associated impacts. *Geophysical research letters*, 41(14), 5167–5174.

Hillgruber, N. & Kloppmann, M. (1999). Distribution and feeding of blue whiting *Micromesistius poutassou* larvae in relation to different water masses in the Porcupine Bank area, west of Ireland. *Marine Ecology Progress Series*, 187(1996), 213–225.

Hillgruber, N. & Kloppmann, M. (2000). Vertical distribution and feeding of larval blue whiting in turbulent waters above Porcupine Bank. *Journal of Fish Biology*, 57(5), 1290–1311.

Hillgruber, N., Kloppmann, M., Wahl, E., & Westernhagen, H. (1997). Feeding of larval blue whiting and Atlantic mackerel: a comparison of foraging strategies. *Journal of Fish Biology*, 51(sa), 230–249.

Hillgruber, N., Kloppmann, M., & Westernhagen, H. (1995). Distribution of blue whiting *Micromesistius poutassou* larvae in the Porcupine Bank area, west of Ireland, in relation to hydrography and the feeding environment. *ICES Journal of Marine Science*, 73.

Hjøllo, S. S., Huse, G., Skogen, M. D., & Melle, W. (2012). Modelling secondary production in the Norwegian Sea with a fully coupled physical/primary production/individual-based *Calanus finmarchicus* model system. *Marine Biology Research*, 8(5-6), 508–526.

Huse, G., Utne, K. R., & Fernö, A. (2012). Vertical distribution of herring and blue whiting in the Norwegian Sea. *Marine Biology Research*, 8(January 2015), 488–501.

ICES (2004). *Report of the Northern Pelagic and Blue Whiting Fisheries Working Group, 27 April - 4 May 2004, ICES, Copenhagen.* Technical Report CM 2004/ACFM:24.

ICES (2005). *Report of the Northern Pelagic and Blue Whiting Fisheries Working Group (WGNPBW), 25 August - 1 September 2005, ICES Headquarters Copenhagen.* Technical Report CM 2006/ACFM:05.

ICES (2007). *Report of the Working Group on Northern Pelagic and Blue Whiting Fisheries (WGNPBW), 27 August - 1 September 2007, Vigo, Spain.* Technical Report CM 2007/ACFM:29.

ICES (2011a). *ICES WGNAPES REPORT 2011 Report of the Working Group on Northeast Atlantic Pelagic Ecosystem Surveys (WGNAPES).* Technical Report SSGESST:16.

ICES (2011b). Widely distributed and Migratory stocks. Blue whiting in Subareas I–IX, XII, and XIV (Combined stock) - Advice September 2011. In *ICES Advice 2011, Book 9* (pp. 41–52).

ICES (2012a). *Report of the Benchmark Workshop on Pelagic Stocks (WKPELA).* Technical Report ACOM:47.

ICES (2012b). Widely distributed and migratory stocks. Blue whiting in Subareas I – IX, XII, and XIV - Advice September 2012. In *ICES Advice 2012, Book 9* (pp. 1–14).

ICES (2013). Widely distributed and migratory stocks. Blue whiting in Subareas I – IX, XII, and XIV - Advice October 2013. In *ICES Advice 2013, Book 9* (pp. 1–14).

ICES (2014). Widely distributed and migratory stocks. Blue Whiting in Subareas I – IX , XII , and XIV - Advice September 2014. In *ICES Advice 2014, Book 9* (pp. 1–13).

ICES (2016a). *Report of the Working Group on Widely Distributed Stocks (WG-WIDE), 31 August - 6 September 2016, ICES HQ, Copenhagen, Denmark.* Technical Report ICES CM 2016/ACOM:16.

ICES (2016b). *Report of the Workshop on Blue Whiting (Micromesistius poutassou) Long Term Management Strategy Evaluation (WKBWMS), 30 August 2016, ICES HQ, Copenhagen, Denmark.* Technical Report ICES CM 2016/A-COM:53.

ICES (2019a). *Stock Annex: Blue whiting (Micromesistius poutassou) in subareas 1-9, 12, and 14 (Northeast Atlantic and adjacent waters).* Technical Report ICES Stock Annex (WGWIDE, September 2019).

ICES (2019b). Working Group on Widely Distributed Stocks (WGWIDE). *ICES Scientific Reports*, 1(36), 948pp.

IPCC (2013). *Climate Change 2013: The Physical Science Basis. Contribution of Working Group I of the Fifth Assessment Report of the Intergovernmental Panel on Climate Change.* Technical report, Cambridge, United Kingdom and New York, NY, USA.

Johns, T. C., Durman, C. F., Banks, H. T., Roberts, M. J., McLaren, A. J., Ridley, J. K., Senior, C. A., Williams, K., Jones, A., Rickard, G., et al. (2006). The new Hadley Centre climate model (HadGEM1): Evaluation of coupled simulations. *Journal of climate*, 19(7), 1327–1353.

Jones, C. D., Hughes, J. K., Bellouin, N., Hardiman, S. C., Jones, G. S., Knight, J., Liddicoat, S., O'Connor, F. M., Andres, R. J., Bell, C., Boo, K. O., Bozzo, A., Butchart, N., Cadule, P., Corbin, K. D., Doutriaux-Boucher, M., Friedling-stein, P., Gornall, J., Gray, L., Halloran, P. R., Hurtt, G., Ingram, W. J., Lamarque, J. F., Law, R. M., Meinshausen, M., Osprey, S., Palin, E. J., Par-sons Chini, L., Raddatz, T., Sanderson, M. G., Sellar, A. A., Schurer, A., Valdes, P., Wood, N., Woodward, S., Yoshioka, M., & Zerroukat, M. (2011).

The HadGEM2-ES implementation of CMIP5 centennial simulations. *Geoscientific Model Development*, 4(3), 543–570.

Jones, K. H. (1998). A comparison of algorithms used to compute hill slope as a property of the DEM. *Computers and Geosciences*, 24(4), 315–323.

Keating, J. P., Brophy, D., Officer, R. A., & Mullins, E. (2014). Otolith shape analysis of blue whiting suggests a complex stock structure at their spawning grounds in the Northeast Atlantic. *Fisheries Research*, 157, 1–6.

Kloppmann, M., Mohn, C., & Bartsch, J. (2001). The distribution of blue whiting eggs and larvae on Porcupine Bank in relation to hydrography and currents. *Fisheries Research*, 50(1-2), 89–109.

Kloppmann, M. H. F., Hillgruber, N., & Von Westernhagen, H. (2002). Wind-mixing effects on feeding success and condition of blue whiting larvae in the Porcupine Bank area. *Marine Ecology Progress Series*, 235, 263–277.

Kompowski, A. (1978). Growth rate of Iceland and North Sea blue whiting, *Micromesistius poutassou* (Risso, 1810). *Acta Ichthyologica et Piscatoria*, 8, 5–21.

Langøy, H., Nøttestad, L., Skaret, G., Broms, C., & Fernö, A. (2012). Overlap in distribution and diets of Atlantic mackerel (*Scomber scombrus*), Norwegian spring-spawning herring (*Clupea harengus*) and blue whiting (*Micromesistius poutassou*) in the Norwegian Sea during late summer. *Marine Biology Research*, 8(5-6), 442–460.

Lazure, P. & Dumas, F. (2008). An external–internal mode coupling for a 3D hydrodynamical model for applications at regional scale (MARS). *Advances in water resources*, 31(2), 233–250.

Lett, C., Verley, P., Mullon, C., Parada, C., Brochier, T., Penven, P., & Blanke, B. (2008). A Lagrangian tool for modelling ichthyoplankton dynamics. *Environmental Modelling & Software*, 23(9), 1210–1214.

Liaw, A. & Wiener, M. (2002). Classification and Regression by randomForest. *R News*, 2(3), 18–22.

Lindley, J. (1982). Continuous plankton records: geographical variations in numerical abundance, biomass and production of Euphausiids in the North Atlantic Ocean and the North Sea. *Marine Biology*, 71(1), 7–10.

Lindley, J., Robins, D., & Williams, R. (1999). Dry weight carbon and nitrogen content of some euphausiids from the north Atlantic Ocean and the Celtic Sea. *Journal of plankton research*, 21(11), 2053–2066.

Lohmann, K. J. (1991). Magnetic orientation by hatchling loggerhead sea turtles (*Caretta caretta*). *Journal of Experimental Biology*, 155(1), 37–49.

Lohmann, K. J., Lohmann, C. M., & Endres, C. S. (2008). The sensory ecology of ocean navigation. *Journal of Experimental Biology*, 211(11), 1719–1728.

Lopez-Lopez, L., Preciado, I., Muñoz, I., Decima, M., Molinero, J. C., & Tel, E. (2017). Does upwelling intensity influence feeding habits and trophic position of planktivorous fish? *Deep-Sea Research Part I: Oceanographic Research Papers*, 122(February), 29–40.

MacKenzie, K. (1978). Eimeria infection of blue whiting, *Micromesistius poutassou* (Risso). *Ices C.M.*, 54, 4pp.

MacKenzie, K. (1981). The effect of Eimeria sp. infection on the condition of blue whiting, *Micromesistius poutassou* (Risso). *Journal of Fish Diseases*, 4(6), 473–486.

Madec, G., Delecluse, P., Imbard, M., & Lévy, C. (1998). OPA 8.1 ocean general circulation model reference manual. *Note du Pôle de modélisation*, 11, 91pp.

Madec, G. & NEMO-team (2008). NEMO Ocean Engine, Scientific Notes of Climate Modelling Center. Institut Pierre-Simon Laplace (IPSL). *Technical Report No. 27*, ISSN 1288-1619.

Magozzi, S., Yool, A., Vander Zanden, H., Wunder, M., & Trueman, C. (2017). Using ocean models to predict spatial and temporal variation in marine carbon isotopes. *Ecosphere*, 8(5), 20pp.

Mahe, K., Oudard, C., Mille, T., Keating, J., Gonçalves, P., Clausen, L. W., Petursdottir, G., Rasmussen, H., Meland, E., Mullins, E., Pinnegar, J. K.,

Hoines, Å., & Trenkel, V. M. (2016). Identifying blue whiting (*Micromesistius poutassou*) stock structure in the northeast Atlantic by otolith shape analysis. *Can.J.Fish.Aquat.(submitted)*, 73, 1363–1371.

Manly, B., Miller, P., & Cook, L. (1972). Analysis of a selective predation experiment. *The American Naturalist*, 106(952), 719–736.

Marine Institute, Institute for Marine Resources and Ecosystem Studies, Institute of Marine Research, PINRO, Faroe Marine Research Institute, Marine Scotland Marine Laboratory, Johann Heinrich von Thünen-Institut, Danish Institute for Fisheries Research, Birdwatch, & Irish Parks and Wildlife Service (2014). International Blue Whiting Spawning Stock Survey (IBWSS) Spring 2014. *Marine Institute, Galway*, (pp. 1–36).

Marine Institute, Institute for Marine Resources and Ecosystem Studies, Institute of Marine Research, PINRO, Faroe Marine Research Institute, Marine Scotland Marine Laboratory, Johann Heinrich von Thünen-Institut, Danish Institute for Fisheries Research, Irish Whale and Dolphin Group, & Galway and Mayo Institute of Technology (2013). International Blue Whiting Spawning Stock Survey (IBWSS) Spring 2013. *Marine Institute, Galway*, (pp. 1–36).

Marine Institute, Wageningen Marine Research, Institute of Marine Research, PINRO, Faroe Marine Research Institute, Marine Scotland Marine Laboratory, Johann Heinrich von Thünen-Institut, Danish Institute for Fisheries Research, & Galway and Mayo Institute of Technology (2018). International Blue Whiting Spawning Stock Survey (IBWSS) Spring 2018. *Marine Institute, Galway*, (pp. 1–29).

Marine Institute, Wageningen Marine Research, Institute of Marine Research Bergen, PINRO, Faroe Marine Research Institute, Marine Scotland Marine Laboratory, Johann Heinrich von Thünen-Institut, Danish Institute for Fisheries Research, & Spanish Institute of Oceanography (2019). International Blue Whiting Spawning Stock Survey (IBWSS) Spring 2019. *Marine Institute, Galway*, (pp. 1–32).

Martins, M. R., Assis, J., & Abecasis, D. (2021). Biologically meaningful distribution models highlight the benefits of the Paris Agreement for demersal

fishing targets in the North Atlantic Ocean. *Global Ecology and Biogeography*, 30(8), 1643–1656.

Marzocchi, A., Hirschi, J. J.-M., Holliday, N. P., Cunningham, S. A., Blaker, A. T., & Coward, A. C. (2015). The North Atlantic subpolar circulation in an eddy-resolving global ocean model. *Journal of Marine Systems*, 142, 126–143.

Miesner, A. K., Brune, S., Pieper, P., Koul, V., Baehr, J., & Schrum, C. (2022). Exploring the Potential of Forecasting Fish Distributions in the North East Atlantic With a Dynamic Earth System Model, Exemplified by the Suitable Spawning Habitat of Blue Whiting. *Frontiers in Marine Science*, 8(January), 1–23.

Miesner, A. K. & Payne, M. R. (2018). Oceanographic variability shapes the spawning distribution of blue whiting (*Micromesistius poutassou*). *Fisheries Oceanography*, (July 2017), In Press.

Miller, K., Huettmann, F., Norcross, B., & Lorenz, M. (2014). Multivariate random forest models of estuarine-associated fish and invertebrate communities. *Marine Ecology Progress Series*, 500, 159–174.

Monin, A. & Ozmidov, R. (1981). Oceanic turbulence. *Leningrad: Gidrometeoizdat*.

Monstad, T. (1990). *Distribution and growth of blue whiting in the North-East Atlantic 1980-1988*. Technical Report C.M. 1990/H:14, International Council for the Exploration of the Sea (ICES).

Monstad, T. & Blindheim, J. (1986). Relationship in distribution of blue whiting and hydrographic conditions in the Norwegian Sea during summer, 1980-1985. *ICES CM 1986/H:54*, (C.M.1986/H:54), 1–18.

Munch, S. B., Giron-Nava, A., & Sugihara, G. (2018). Nonlinear dynamics and noise in fisheries recruitment: A global meta-analysis. *Fish and Fisheries*, 19(6), 964–973.

Munk, P. (1995). Foraging behaviour of larval cod (*Gadus morhua*) influenced by prey density and hunger. *Marine biology*, 122(2), 205–212.

Nøttestad, L., Giske, J., Holst, J. C., & Huse, G. (1999). A length-based hypothesis for feeding migrations in pelagic fish. *Canadian Journal of Fisheries and Aquatic Sciences*, 56(S1), 26–34.

O'Brien, C. M. (2016). Management: new approaches to old problems. *Fish reproductive biology: implications for assessment and management*, (pp. 395–437).

Pájaro, M. & Macchi, G. (2001). Spawning pattern, length at maturity, and fecundity of the southern blue whiting (Micromesistius australis) in the southwest Atlantic Ocean. *New Zealand Journal of Marine and Freshwater Research*, 35(2), 375–385.

Pálsson, Ó. K. (2005). An analysis of by-catch in the Icelandic blue whiting fishery. *Fisheries Research*, 73(1-2), 135–146.

Payne, M. R., Egan, A., Fässler, S. M. M., Hátún, H., Holst, J. C., Jacobsen, J. A., Slotte, A., & Loeng, H. (2012). The rise and fall of the NE Atlantic blue whiting (*Micromesistius poutassou*). *Marine Biology Research*, 8(5-6), 475–487.

Peliz, A., Marchesiello, P., Dubert, J., Marta-Almeida, M., Roy, C., & Queiroga, H. (2007). A study of crab larvae dispersal on the Western Iberian Shelf: Physical processes. *Journal of Marine Systems*, 68(1-2), 215–236.

Pepin, P., Robert, D., Bouchard, C., Dower, J. F., Falardeau, M., Levesque, K., Llopiz, J. K., Fortier, L., Jenkins, G. P., Meekan, M. G., Murphy, H. M., Ringuette, M., Sirois, P., & Sponaugle, S. (2015). Once upon a larva: revisiting the relationship between feeding success and growth in fish larvae. *ICES Journal of Marine Science*, 72(2), 359–373.

Pinnegar, J. K. (2014). DAPSTOM - An Integrated Database & Portal for Fish Stomach Records. Version 4.7. *Centre for Environment, Fisheries & Aquaculture Science, Lowestoft, UK*, February 2014, 39pp.

Pinnegar, J. K., Goñi, N., Trenkel, V. M., Arrizabalaga, H., Melle, W., Keating, J., & Óskarsson, G. (2015). A new compilation of stomach content data for commercially important pelagic fish species in the northeast Atlantic. *Earth System Science Data*, 7(1), 19–28.

Pitois, S. G. & Fox, C. J. (2006). Long-term changes in zooplankton biomass concentration and mean size over the Northwest European shelf inferred from Continuous Plankton Recorder data. *ICES Journal of Marine Science*, 63(5), 785–798.

Planque, B. & Fromentin, J.-M. (1996). *Calanus* and environment in the eastern North Atlantic. I. Spatial and temporal patterns of *C. finmarchicus* and *C. helgolandicus*. *Marine Ecology Progress Series*, 134, 101–109.

Pointin, F. & Payne, M. R. (2014). A resolution to the blue whiting (*Micromesistius poutassou*) population paradox? *PLoS ONE*, 9(9).

Polonsky, A. (1968). Materials on the biology of Poutassou. In *Rapports et Procès- verbeaux des Réunions. Conseil International pour l'Exploration de la Mer*, volume 158 (pp. 105–108).

Polonsky, A. S. (1969). Some problems of the biology of poutassou - Micromesistius (Gadus) poutassou (Risso). *Trudy atiasnticheskii nauchno-issledovateskii Institut rybnogo khozyaistva i okeanografii*, 23, 61–86.

Post, S., Fock, H. O., & Jansen, T. (2019). Blue whiting distribution and migration in Greenland waters. *Fisheries Research*, 212(May 2018), 123–135.

Post, S., Jónasdóttir, S., Andreasen, H., Ólafsdóttir, A., & Jansen, T. (2021a). Blue whiting *Micromesistius poutassou* diel feeding behaviour in the Irminger Sea. *Marine Ecology Progress Series*, 678, 1–16.

Post, S., Werner, K. M., Núñez-Riboni, I., Chafik, L., Hátún, H., & Jansen, T. (2021b). Subpolar gyre and temperature drive boreal fish abundance in Greenland waters. *Fish and Fisheries*, 22(1), 161–174.

Powers, J. E. (2014). Age-specific natural mortality rates in stock assessments: size-based vs. density-dependent. *ICES Journal of Marine Science*, 71(7), 1629–1637.

Prokopchuk, I. & Sentyabov, E. (2006). Diets of herring, mackerel, and blue whiting in the Norwegian Sea in relation to Calanus finmarchicus distribution and temperature conditions. *ICES Journal of Marine Science*, 63(1), 117–127.

Pronyuk, A. (2019). Distribution of blue whiting in season of feeding 2004–2018. *Trudy VNIRO*, 178, 50–68.

Putman, N. F., Verley, P., Shay, T. J., & Lohmann, K. J. (2012). Simulating transoceanic migrations of young loggerhead sea turtles: Merging magnetic navigation behavior with an ocean circulation model. *Journal of Experimental Biology*, 215(11), 1863–1870.

Raitt, D. F. S. (1968). *Synopsis of Biological Data on the Blue Whiting: Micromesistius Poutassou (Risso, 1810)*. Food and Agriculture Organization of the United Nations.

Reiss, H., Hoarau, G., Dickey-Collas, M., & Wolff, W. J. (2009). Genetic population structure of marine fish: Mismatch between biological and fisheries management units. *Fish and Fisheries*, 10(4), 361–395.

Riahi, K., Grübler, A., & Nakicenovic, N. (2007). Scenarios of long-term socio-economic and environmental development under climate stabilization. *Technological Forecasting and Social Change*, 74(7), 887–935.

Riahi, K., Rao, S., Krey, V., Cho, C., Chirkov, V., Fischer, G., Kindermann, G., Nakicenovic, N., & Rafaj, P. (2011). RCP 8.5—A scenario of comparatively high greenhouse gas emissions. *Climatic change*, 109(1), 33–57.

Richards, S. A. (2008). Dealing with overdispersed count data in applied ecology. *J Appl Ecol*, 45(1), 218–227.

Richardson, A. J., Walne, A. W., John, A. W., Jonas, T. D., Lindley, J. A., Sims, D. W., Stevens, D., & Witt, M. (2006). Using continuous plankton recorder data. *Progress in Oceanography*, 68(1), 27–74.

Ritter, P. (1987). A vector-based slope and aspect generation algorithm. *Photogrammetric Engineering and Remote Sensing*, 53(8), 1109–1111.

Rodriguez-Galiano, V. F., Ghimire, B., Rogan, J., Chica-Olmo, M., & Rigol-Sanchez, J. P. (2012). An assessment of the effectiveness of a random forest classifier for land-cover classification. *ISPRS journal of photogrammetry and remote sensing*, 67, 93–104.

Ryan, A. W., Mattiangeli, V., & Mork, J. (2005). Genetic differentiation of blue whiting (*Micromesistius poutassou* Risso) populations at the extremes of the species range and at the Hebrides-Porcupine Bank spawning grounds. *ICES Journal of Marine Science*, 62(5), 948–955.

Saikia, S. K. (2016). On the methodology of feeding ecology in fish. *European Journal of Ecology*, 2(1), 35–46.

Sgubin, G., Swingedouw, D., Drijfhout, S., Mary, Y., & Bennabi, A. (2017). Abrupt cooling over the North Atlantic in modern climate models. *Nature Communications*, 8.

Shchepetkin, A. F. & McWilliams, J. C. (2005). The regional oceanic modeling system (ROMS): a split-explicit, free-surface, topography-following-coordinate oceanic model. *Ocean modelling*, 9(4), 347–404.

Silva, A., Azevedo, M., Cabral, H., Machado, P., Murta, A., & Silva, M. A. (1997). Blue Whiting (*Micromesistius poutassou*) as a Forage Fish in Portuguese Waters. In *Forage Fishes in Marine Ecosystems. Proceedings of the International Symposium on the Role of Forage Fishes in Marine Ecosystems. Alaska Sea Grant College Program Report No. 97-01* (pp. 127–146).

Skjoldal, H.-R., Sætre, R., Faernö, A., Misund, O., & Røttingen, I. (2004). *The Norwegian Sea ecosystem*. Trondheim: Tapir Academic Press.

Skogen, M. D., Monstad, T., & Svendsen, E. (1999). A possible separation between a northern and a southern stock of the northeast Atlantic blue whiting. *Fisheries Research*, 41(2), 119–131.

Speirs, D. C., Guirey, E. J., Gurney, W. S. C., & Heath, M. R. (2010). A length-structured partial ecosystem model for cod in the North Sea. *Fisheries Research*, 106(3), 474–494.

Stocker, T., Qin, D., Plattner, G.-K., Alexander, L., Allen, S., Bindoff, N., Bréon, F.-M., Church, J., Cubasch, U., Emori, S., Forster, P., Friedlingstein, P., Gillett, N., Gregory, J., Hartmann, D., Jansen, E., Kirtman, B., Knutti, R., Krishna Kumar, K., Lemke, P., Marotzke, J., Masson-Delmotte, V., Meehl, G., Mokhov, I., Piao, S., Ramaswamy, V., Randall, D., Rhein, M., Rojas, M.,

Sabine, C., Shindell, D., Talley, L., Vaughan, D., & Xie, S.-P. (2013). Technical Summary. In T. Stocker, D. Qin, G.-K. Plattner, M. Tignor, S. Allen, J. Boschung, A. Nauels, Y. Xia, V. Bex, & P. Midgley (Eds.), *Climate Change 2013: The Physical Science Basis. Contribution of Working Group I to the Fifth Assessment Report of the Intergovernmental Panel on Climate Change* (pp. 31–116). Cambridge, United Kingdom and New York, NY, USA: Cambridge University Press.

Svendsen, E., Skogen, M., Monstad, T., & Coombs, S. (1996). Modelling the variability of the drift of blue whiting larvae and its possible importance for recruitement. *Ices C.M. 1996/S : 31*, (pp. 12pp).

Timmermann, R., Goosse, H., Madec, G., Fichefet, T., Ethe, C., & Dulière, V. (2005). On the representation of high latitude processes in the ORCA-LIM global coupled sea ice-ocean model. *Ocean Modelling*, 8(1-2), 175–201.

Trenkel, V. M., Huse, G., MacKenzie, B. R., Alvarez, P., Arrizabalaga, H., Castonguay, M., Goñi, N., Grégoire, F., Hátún, H., Jansen, T., Jacobsen, J. A., Lehodey, P., Lutcavage, M., Mariani, P., Melvin, G. D., Neilson, J. D., Nøttestad, L., Óskarsson, G. J., Payne, M. R., Richardson, D. E., Senina, I., & Speirs, D. C. (2014). Comparative ecology of widely distributed pelagic fish species in the North Atlantic: Implications for modelling climate and fisheries impacts. *Progress in Oceanography*, 129(PB), 219–243.

Trenkel, V. M., Lorance, P., Fässler, S. M. M., & Høines, A. S. (2015). Effects of density dependence, zooplankton and temperature on blue whiting *Micromesistius poutassou* growth. *Journal of Fish Biology*, 87(4), 1019–1030.

Utne, K. R., Hjøllo, S. S., Huse, G., & Skogen, M. (2012a). Estimating the consumption of Calanus finmarchicus by planktivorous fish in the Norwegian Sea using a fully coupled 3D model system. *Marine Biology Research*, 8(5-6), 527–547.

Utne, K. R. & Huse, G. (2012). Estimating the horizontal and temporal overlap of pelagic fish distribution in the Norwegian Sea using individual-based modelling. *Marine Biology Research*, 8(5-6), 548–567.

Utne, K. R., Huse, G., Ottersen, G., Holst, J. C., Zabavnikov, V., Jacobsen, J. A., Óskarsson, G. J., & Nøttestad, L. (2012b). Horizontal distribution and overlap of planktivorous fish stocks in the Norwegian Sea during summers 1995–2006. *Marine Biology Research*, 8(5-6), 420–441.

Valletta, J. J., Torney, C., Kings, M., Thornton, A., & Madden, J. (2017). Applications of machine learning in animal behaviour studies. *Animal Behaviour*, 124, 203–220.

van den Berk, J., Drijfhout, S. S., & Hazeleger, W. (2021). Circulation adjustment in the Arctic and Atlantic in response to Greenland and Antarctic mass loss. *Climate Dynamics*, (0123456789).

Varela, M. (1996). Phytoplankton ecology in the Bay of Biscay. *Scientia Marina*, 60(SUPPL. 2), 45–53.

Varpe, Ø., Fiksen, Ø., & Slotte, A. (2005). Meta-ecosystems and biological energy transport from ocean to coast: the ecological importance of herring migration. *Oecologia*, 146(3), 443–451.

Vikebø, F., Jørgensen, C., Kristiansen, T., & Fiksen, Ø. (2007). Drift, growth, and survival of larval Northeast Arctic cod with simple rules of behaviour. *Marine Ecology Progress Series*, 347, 207–219.

Von Bertalanffy, L. (1951). General system theory, a new approach to unity of science. 5. Conclusion. *Human biology*, 23(4), 337–345.

Wallraff, H. G. (2004). Avian olfactory navigation: its empirical foundation and conceptual state. *Animal Behaviour*, 67(2), 189–204.

Ware, D. M. (1975). Relation between egg size, growth, and natural mortality of larval fish. *Journal of the Fisheries Research Board of Canada*, 32(12), 2503–2512.

Was, a., Gosling, E., McCrann, K., & Mork, J. (2008). Evidence for population structuring of blue whiting (*Micromesistius poutassou*) in the Northeast Atlantic. *ICES Journal of Marine Science*, 65(2), 216–225.

Wiltschko, R. (1995). *Magnetic orientation in animals*, volume 33. Springer Science & Business Media.

Wood, S. (2018). Package 'mgcv', v. 1.8-23: Mixed GAM computation vehicle with automatic smoothness estimation.

Wouters, B., Hazeleger, W., Drijfhout, S., Van Oldenborgh, G. J., & Guemas, V. (2013). Multiyear predictability of the North Atlantic subpolar gyre. *Geophysical Research Letters*, 40(12), 3080–3084.

Yool, A., Martin, A. P., Anderson, T. R., Bett, B. J., Jones, D. O., & Ruhl, H. A. (2017). Big in the benthos: Future change of seafloor community biomass in a global, body size-resolved model. *Global Change Biology*, 23(9), 3554–3566.

Yool, A., Popova, E., Coward, A., Bernie, D., & Anderson, T. (2013a). Climate change and ocean acidification impacts on lower trophic levels and the export of organic carbon to the deep ocean. *Biogeosciences*, 10(9), 5831–5854.

Yool, A., Popova, E. E., & Anderson, T. R. (2011). MEDUSA-1.0: A new intermediate complexity plankton ecosystem model for the global domain. *Geoscientific Model Development*, 4(2), 381–417.

Yool, A., Popova, E. E., & Anderson, T. R. (2013b). MEDUSA-2.0: An intermediate complexity biogeochemical model of the marine carbon cycle for climate change and ocean acidification studies. *Geoscientific Model Development*, 6(5), 1767–1811.

Yool, A., Popova, E. E., & Coward, A. C. (2015). Future change in ocean productivity: Is the Arctic the new Atlantic. *Journal of Geophysical Research: Oceans*, 120(12), 7771–7790.

Zarauz, L., Irigoien, X., & Fernandes, J. A. (2008). Modelling the influence of abiotic and biotic factors on plankton distribution in the Bay of Biscay, during three consecutive years (2004–06). *Journal of plankton research*, 30(8), 857–872.

Zhou, Q. & Liu, X. (2004). Analysis of errors of derived slope and aspect related to DEM data properties. *Computers and Geosciences*, 30(4), 369–378.